ASSESSMENTS OF HUMAN LAND USE, EROSION, AND SEDIMENT DEPOSITION IN THE SOUTHEASTERN AUSTRALIAN TABLELANDS

Eric W. Portenga

University of Vermont, MS
University of Michigan, BS

Submitted in fulfilment of the
requirements for the Degree of
Doctor of Philosophy

School of Geographical and Earth Sciences
College of Science and Engineering
University of Glasgow

&

Department of Environmental Sciences
Faculty of Science and Engineering
Macquarie University

February, 2015

ABSTRACT

Humans have interacted with their surroundings for over one million years, and researchers have only recently been able to assess the geomorphic impacts indigenous peoples had on their landscapes prior to the onset of European colonialism. The history of human occupation of Australia is noteworthy in that Aboriginal Australians arrived ~50 ka and remained relatively isolated from the rest of the world until the AD 1788 when Europeans established a permanent settlement in Sydney, New South Wales. The southeastern Australian Tablelands landscape, west of Sydney, has seemingly undergone drastic geomorphic change since European arrival. The introduction of European grazing practices reportedly led to the occurrence of deep erosional incisions, gullies, into valley bottoms and hillslopes, releasing sediment, which is subsequently deposited over downstream wetland environments – swampy meadows. This sediment is often called post-settlement alluvium (PSA); however, the age and genesis of PSA in Australia are debated. Questions regarding the geomorphic features and processes in the Tablelands remain unanswered because few studies quantify the timing of gully incision, PSA deposition, or the pre-human rate of landscape change.

Erosion rates inferred from concentrations of *in situ* ^{10}Be measured in fluvial sediment (n = 11) and bedrock outcrops (n = 6) range from 2.9–11.9 mm/kyr and 5.2–13.8 mm/kyr, respectively. The two sample populations are statistically indistinguishable, suggesting no relief has been generated since 600–110 ka. The overall erosion rate in the Tablelands is 7.5 mm/kyr, equal to long-term denudation rates integrated since ~20 Ma. Aboriginal Australians have been present in the Tablelands for at least 30 kyr, ~12–26% of the cosmogenic integration time, yet widespread Aboriginal fire use did not measurably affect landscape erosion until ~5.5 ka, in sync with increased charcoal in the sediment record.

Portable optically stimulated luminescence (OSL) reader data from poly-mineral and poly-grain size samples collected from gully wall profiles of PSA and swampy meadow sediment show that swampy meadow environments were buried by PSA and that PSA is alluvium derived from upstream gully erosion. No relationships between bulk OSL and sample grain size or mineralogy exist, and inferences about bulk sediment mineralogy or

grain size cannot be determined from portable OSL reader data. Large variability in adjacent PSA sample replicates, however, reveals incomplete sediment bleaching conditions during PSA deposition during floods. Greater bleaching efficiency is inferred from the small variability of bulk OSL data in the uppermost 10s of cm of PSA profiles.

Measured concentrations of meteoric ^{10}Be and bulk OSL in two PSA deposits in Birchams Creek show that initial gully incision eroded into weathered sandstone regolith and not swampy meadow environments, as previously believed. Initial gully incision was shallow (<15 cm) and PSA filled ponds in the lower reaches of the catchment. Continued erosion upstream led to a second depositional episode of PSA before headward gully incision from the mouth of Birchams Creek eroded through PSA deposits. Headward erosion of this gully created the continuous gully present at the site today. Initial gully incision was likely the result of livestock trampling in valley bottoms during droughts, creating localised slopes greater than the critical slope threshold required to erode the valley bottom.

OSL burial ages of six PSA deposits collected throughout the Tablelands range from 195.1 ± 17.8 to 90.4 ± 8.9 a, corresponding to AD 1800–1932. The OSL burial ages are younger than European arrival in the Tablelands, and the term, PSA, is redefined as post-European settlement alluvium in Australia, recognising the earlier settlement of the region by Aboriginal Australians whose land use did not lead to PSA deposition. PSA burial ages agree with existing quantitative and anecdotal gully incision data. Contrary to previous assertions that gully incision began asynchronously in the Tablelands, three periods of synchronous gully erosion in localised areas within the Tablelands are recognized: 185 a, 158 a, and 94 a (AD 1828, 1855, and 1919, respectively) – in the southern, northern, and central Goulburn Plains, respectively. The AD 1828 and AD 1919 periods of gully incision correspond to the transition from drought-dominated climate regimes to flood-dominated regimes, and the AD 1855 period of gullying corresponds to a flood-dominated regime. Gully incision in the Tablelands is thus a result of European-introduced grazing practices, which primed the landscape for further erosion and degradation during climatic shifts.

PSA deposits in the southeastern Australian Tablelands are some of the most recent examples of anthropogenic sedimentation in human history. The earliest preserved examples of PSA-type sediments are ~8,000 years old and found throughout the world. The establishment of an onset date for the Anthropocene is currently debated, and I believe the oldest PSA and PSA-type sediments around the world can define this modern epoch.

DEDICATION

Living so far away from family
is not an easy thing to do.

Dad, Lizzie, Ryan, Britta, Sarah, and Rob,
without your unconditional support,
I would never have been able to leave Michigan
in pursuit of geomorphic curiosity.

In particular, I dedicate this Thesis
to my nephew and niece, Baker and Aubrey,
with whom I have not had nearly enough Uncle-time!

I also dedicate this Thesis in loving memory
of my mother, Ann,
and my grandparents
who are always with me in spirit.

To my extended family:
Thank you for the on-line Christmas "Hellos!"
I promise I will be home for the holiday next year.

To my second family:
Brennen, Barb, Steve, Alissa, and Cyndy.
I wish I could see you more often.

TABLE OF CONTENTS

LIST OF FIGURES

LIST OF TABLES

ACKNOWLEDGEMENTS

I am often asked how a guy from Michigan, managed to secure a doubly-international joint-PhD at the University of Glasgow and Macquarie University. The sequence of events that eventually led to my moving to Glasgow began with a series of side projects for my former advisor, Paul Bierman, at the University of Vermont. Paul invited me, along with Dylan Rood, a current PhD supervisor, to do some fieldwork in Greenland, and during long hikes out to glaciers, there was a lot of time to chat about career paths.

It was Dylan who eventually convinced me to visit the University of Glasgow to give a talk and interview for the PhD. Visiting Glasgow was the last unknown factor about the logistics of the PhD as I had visited Macquarie University the year before while working on one of P. Bierman's projects, and while in Sydney met Paul Hesse, Tim Ralph, and David Fink, so I already had an idea for what life in Australia would be like during that half of my degree. Coincidentally, I previously met Paul Bishop, my Glasgow supervisor, at the University of Vermont when he visited to give a research seminar, and after spending nearly every day in his office during my visit to Glasgow, discussing the PhD, I felt like taking this step was actually something I could do and wanted, if not needed, to do.

Tackling a PhD and living in three countries in as many years is beyond stressful, and I literally would not have been able to finish without good physical and mental health and close ties to friends and family, new and old. For these reasons, this section may be longer than normal, but I truly would not have made it through, nor would I have felt at home in both Glasgow and Sydney, without the following people.

Alessa and Andy were exactly the right first people to meet from the University of Glasgow, and both have since become good friends and conference compadrés. Two months after my first visit, I arrived in Glasgow with my suitcases to start the PhD, and I was immediately welcomed into my new home, the Gregory Building, by an office full of great people who have been so kind to wait to finish their PhDs until my return from Australia! Heather, Rebecca, Penne, Jill, Callum, and Daisy, have all become very good friends as well as my UK family, the kind that introduces you to Six Nations Rugby, St. Patrick's Day in Belfast, music festivals in Inverness and Oban, and all of the coffee breaks and summer barbecues Glasgow has to offer! Heiko, Heidi, and Fiona have offered many words of advice over the years.

But six months was all I had before heading south to Sydney, a much bigger city, and more dramatic. The drama started before I even arrived as fog shrouded the Sydney airport, diverting my flight to Brisbane, while I sat on board with extreme tonsillitis. I had no means of getting in touch with Damian, my Macquarie supervisor, whom I had not yet met in person and who sat at the airport for four hours waiting for me, without any word! Eventually, I borrowed a passenger's phone and got in touch with Damian who organised a taxi for me upon my arrival from the airport to the university and has since always found ways to help me through tricky situations.

Once settled in, I quickly became close friends with two great women, Danielle and Louise, who are now like sisters to me, with whom I have shared some wonderful trips to the Blue Mountains, Tasmania, and Prague. I met Stacy, my third Sydney-sister, shortly thereafter, and Stacy became my partner-in-crime on campus, in the lab, in class, and in the courtyard with our coffees. My time at Macquarie would not have been nearly as memorable if it were not for these three women. I reunited with Tim R. and Paul H. who I thank for helping me out when I had some car trouble, and I met Kira Westaway, my co-supervisor who went well above and beyond her duties to teach me about optically stimulated luminescence and even baked me a birthday cake on a field trip! The entire Macquarie staff became valued mentors for me, and I truly appreciate the communal rapport between staff and students.

Of course, I was not always on campus, and I would not have learned as much about life in Australia, its music, culture, and politics, nor would I have had as many amazing experiences if it were not for my friends in the city, Rick, Quazi, Mohammed, Harry, Andrew, Grant, Dan, Ben, Sandy, Craig, and Paul, with whom I shared numerous curry dinners and holiday parties, went skiing, abseiled cliffs and canyons, hiked beaches, and attended festivals (not to mention the excursions on Big Red around Sydney Harbour). To Mark for dutifully always being up for a chat and for introducing me to Mudgee, Andrew for being a fellow Michigander in Sydney, and Carter for showing me the best food spots in Sydney, but more for sharing a passion for travel and introducing me to Portlandia. I could not have asked for better friends who made Sydney feel like a home for me, especially Owen and Michelle who shared my actual home in Sydney! I thank Jess and Amy for putting up with me in the office, and Lani, Adam, Marek, Nate, Zacc, and Ben are some of the most brilliant people in the world, and I can't wait for our paths to cross again!

After a year and a half Down Under, it was time to go back to Glasgow where familiar faces greeted me, along with new faces, including Crystal, Charlotte, Ruth, Ben, and Hazel who all quickly became good friends and better hillwalking buddies! I am sure our time is not quite done! And I especially want to thank Kevin for letting me get my work done, but also reminding me what it is like having a social life away from campus, for the first real Christmas I have had in three years, and for all the Sunday drives!

Though I did not get to see my friends from home that often, their support and constant contact helped remember where I am from and keep sight of who I am. I am lucky to have such incredible brothers from other mothers and sisters from other misters, but especially Nick, Jared, Drew, Abe, Drew, Derek, Dan, Jon, and Jeremy, Monica, Margo, Rachel, Lauren, Erica, JoJo, Jessie, Meika, Beth, Claire, Renise, and Beth. I want to thank Jess, Slim, Kristen, Molly, and Nicole who made the effort to visit me in Glasgow, Martin and Lydia for hosting me in Vermont and New Years in New Zealand, Caitlyn for watching Michigan Football in Sydney and driving the Great Ocean Road, and Arianne, my high school friend who welcomed me to Sydney!

Finishing a PhD in three countries would never have been possible without the incredible administrative support of Jane, Heather, Farhana, and Paula. I need to thank Meredith, Olivia, Therese, and Adam for their incredible help in the field, and Tom, Lee, Veronica, Ben, Zacc, Rory, Lani, Stacy, and Russell, without whom I would still be stuck doing lab work!

More than anyone, I need to thank the hard work that Paul Bishop and Damian Gore put into making this PhD possible and to Kira Westaway and Dylan Rood for helping make its completion a reality. Specifically, I want to thank Paul for supporting me on every step of this unusual joint-PhD process and his belief in my ability to succeed, Damian for helping me rediscover my confidence when I needed it the most and helping me to understand the nuances of working in and writing about rural Australia, Kira for working with me to develop new skills in the field, laboratory, and classroom, and Dylan for being an incredibly supportive academic coach, helping me navigate the ins and outs of early career academics. I sincerely thank each and every one of them for the time spent mentoring me, tutoring me, listening to me, helping me when it was wanted, being frank when it was needed, and letting me explore this project independently. I know that I am a better geomorphologist, academic, teacher, and person because of their mentorship. I can only hope working with me was as enjoyable for them as working with them was for me.

DECLARATION OF ORIGINALITY

I hereby declare
that the work presented in this thesis has been carried out by myself,
except where due acknowledgement is made,
and has not been submitted for any other degree.

Eric W. Portenga

DEFINITIONS, UNITS, & ABBREVIATIONS

a – Annum/years ago (date)

ACT – Australian Capital Territory

AD – Anno Domini

Al – Aluminium

AMS – Accelerator mass spectrometry

B – Boron

Be – Beryllium

BIRC – Birchams Creek, NSW

BL – Blue light LED

BLSL – Blue light LED stimulated luminescence

C – Carbon

CAM – Central age model

cm – Centimetre

cm^2 – Square centimetres

CRONUS – Cosmic-Ray Produced Nuclide Systematics (on-line erosion rate calculator)

Cs - Caesium

D_{50} – Average grain size

DC – Dark count

D_e – Equivalent Dose (in units of Gy)

DGEM – Discontinuous gully erosion model

Fe – Iron

FENW – Fenwick Creek, NSW

g – Grams

GOOR – Gooromon Ponds Creek, NSW

GRAB – Grabben Gullen Creek, NSW

GROV – Groves Creek, NSW

Gy – Grays

ICP-OES – Inductively-coupled plasma optical emission spectroscopy

IR – Infrared

IRSL – Infrared stimulated luminescence

IUGS – International Union of Geological Sciences

IUPAC – International Union of Pure and Analytical Chemistry

K – Potassium

ka – Thousands of years ago (date)

km – Kilometres

kyr – Thousands of years (time duration)

LED – Light emitting diode

LGM – Last glacial maximum

m – Metres

Ma – Millions of years ago (date)

MAM – Minimum age model

mL – Millilitres

mm – Millimetres

MULW – Mulwaree River, NSW

Myr – Millions of years (time duration)

n – Sample population

Nb – Niobium

Nd – Neodymium

NIST – National Institute of Standards and Technology

NSW – New South Wales

O – Oxygen

OSL – Optically stimulated luminescence

Pb – Lead

PHIL – Phils River, NSW

PRIM – Primrose Valley Creek, NSW

PSA – Post-settlement alluvium; Post swampy-meadow alluvium; Post-European settlement alluvium

Ra – Radon

RYRI – Ryries Creek, NSW

SAR – Single aliquot regenerative dose protocol

SM – Swampy meadow

SRM – Standard Reference Materials

SSEM – Single site erosion model

SUERC – Scottish Universities Environmental Research Centre

TAS – Tasmania

Th – Thorium

Ti – Titanium

TL – Thermoluminescence

U – Uranium

UVM – University of Vermont

V – Vanadium

VIC – Victoria

XRD – X-ray diffraction

Y – Yttrium

yr BP – Calibrated radiocarbon years before present

μg – Micrograms

TIME NOTATION IN THIS THESIS

In a Groundwork Perspective, published in the Geological Society of America's monthly magazine, *GSA Today*, Nicholas Christie-Blick (2012) summarises the disagreement in the Earth Sciences community over the use of time notation in Geological writing. A joint task force between the International Union of Geological Sciences (IUGS) and the International Union of Pure and Applied Chemistry (IUPAC) concluded that:

> *"We neither accept nor reject the IUGS-IUPAC Task Group's recommendation to apply Ma, generally, as the unit of deep time. We accept the argument for Ma as a single unit for time but would recommend flexibility, allowing for the retention of Ma as specific notation for points in time (i.e., dates) and myr* [sic] *as a unit of time denoting duration..."*

Thus, unless otherwise noted, all time-units in this Thesis will abide by the following convention:

1. **Duration** of time: yrs (years), kyr (thousands of years), Myr (millions of years)
   Example: Uplift rates were consistent for 20 Myr.
2. **Rates** of geological processes: m/Myr (metres per millions of years), mm/kyr (millimetres per thousands of years)
   Example: The erosion rate for outcrop sample, SAMP-01, is 5 mm/kyr, much lower than neighbouring outcrops.
3. **Specific dates** in time, "years before present" is implicit: years ago (a), thousand years ago (ka), million years ago (Ma).
   Example: Humans arrived to Australia ~50 ka.
4. **Specific dates** easily expressed in calendar notation: AD 18xx–18xx
   Example: Incision began in AD 1890–1910.
5. **Ranges** of specific dates: 2–1 ka (between 2,000 and 1,000 years ago)
   Example: Sediment deposition occurred from 1,000–700 a.
6. **Radiocarbon years**: calibrated years before present (yr BP; present being 1950)
   Example: Evidence of cohabitation is given by charcoal dated to be 10 kyr BP.

CHAPTER

INTRODUCTION

The relationships between humans, land use, and landscape change are complex and dynamic. For centuries, Europeans wrongly believed that indigenous people of New World lands (i.e. the Americas, Australia, New Zealand) lived as part of their environments without much impact on their surroundings, but research over the last few decades has shown that pre-European cultures around the world intensively altered their surroundings, leading to drastic, if not catastrophic, environmental change. Increased soil erosion often develops into deep incisions into the landscape – erosional gullies – and sediment removed by erosion is implicated in the destruction of downstream environments, often leaving a legacy of environmental change preserved in the geological record for hundreds, if not thousands, of years. Over the last few centuries, changes in land use practices of New World lands by European colonists led to widespread landscape alteration. This thesis examines landscape change in one of the most recently-colonised lands in the world, Australia, in order to better understand the effects of human-induced landscape change around the world and through time, the culmination of which leads me to define what I believe will be our collective anthropogenic signature in the annals of geological time.

1.1 A BRIEF HISTORY OF THE GLOBAL RISE AND SPREAD OF AGRICULTURE

Modern humans have only existed for the most recent 1.8 Myr of our planet's 4,500 Myr history (Dalrymple, 2001; Johanson et al., 1987; Leakey et al., 1964; Patterson et al.,

1955). In a geological blink-of-the-eye, humans began the exodus out of Africa (Agusti and Lordkipanidze, 2011), arriving in central Asia by1.7 Ma (Gabunia et al., 2000; Vekua et al., 2002), Europe by 1.2 Ma (Carbonell et al., 1995; Carbonell et al., 2008), Australia by ~50 ka (Miller et al., 2005; Olley et al., 2006), and North America by ~15.5 ka (Waters et al., 2011a; Waters et al., 2011b). After a little less than 1.8 Myr, the human diaspora was complete with the occupation of southern South America by 14.4 ka (Dillehay et al., 2008, 2012).

Environmental change occurred along with the spread of the human population. Hunting tools dating back to the earliest Pleistocene have been uncovered in Tanzania (Blumenschine et al., 2003) – perhaps the first record of human-induced environmental change. Hunting and the use of fire have been implicated in the demise of megafaunal species throughout the Pleistocene and Holocene (Barnosky and Lindsey, 2010; Bird et al., 2013; Dodson et al., 1993; Holdaway and Jacomb, 2000; Johnson, 2005; Miller et al., 1999; Roberts et al., 2001; Waters et al., 2011b), though some of these claims have been contested (Gill et al., 2009; Guthrie, 2004; Stuart et al., 2004; Wroe and Field, 2006). Whether caused by climatic changes or by humans, there is no question that some megafauna were hunted (Holdaway and Jacomb, 2000; Waters et al., 2011b) and that megafaunal loss had profound ecological implications (Gill et al., 2009; Johnson, 2009).

Nearly 1.8 Myr passed before agricultural practices became ubiquitous, as early as ~10 ka (Liu et al., 2009; Smith, 1997; Sokal et al., 1991; Zhao, 2010) with the exception of three regions of the world: the Arctic, Australia, and Antarctica. In southern Greenland and Australia, indigenous peoples continued hunting and gathering practices until the arrival of Vikings to Greenland in AD 1000 (Massa et al., 2012; Sandgren and Fredskild, 2008) and European colonists to Australia in AD 1788 (Yen, 1995; Zhou, 2013); agriculture has not yet been introduced to Antarctica. Shortly after the rise of agricultural practices around the world, gas trapped in ice cores began recording higher levels of CO_2 and CH_4 than were expected (Ruddiman, 2003). Since then, the natural biotic, atmospheric, hydrologic, and geomorphic processes that shaped the world humans evolved into relinquished their dominance to a new geomorphic process, anthropogenic change.

1.2 ANTHROPOGENIC GEOMORPHOLOGY

1.2.1 LOSS OF NATURAL LAND

Humans have now become the dominant and most efficient movers of sediment and Earth material on our planet (30 Gt/yr), more than rivers and glaciers combined (27.3 Gt/yr, Hooke, 1994); this estimate, however, does not include agricultural land as it mostly occupies low-relief terrain in which soil is displaced, but not always lost. While mining and construction projects move the majority of human-displaced material, further investigations of agricultural land show that agricultural land releases three times more sediment than all of the world's rivers combined (FIGURE 1.1) (Wilkinson and McElroy, 2007), and erosion often increases after agricultural ploughing, even when sustainable techniques are employed (Montgomery, 2007b). The continued and increasing use of agriculture throughout the world has resulted in a total loss of natural land – that is, forested and non-agricultural land – of 53.5% of the portion of Earth's surface not covered by ice sheets or water (Hooke et al., 2012).

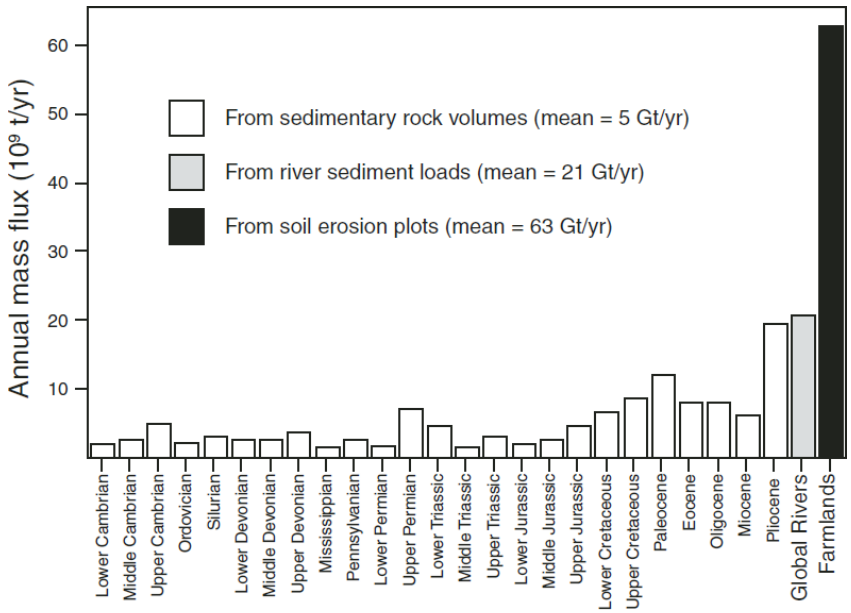

FIGURE 1.1
Wilkinson and McElroy (2007) demonstrate that three times more sediment is transported away from agricultural sources than the global total annual sediment delivery of rivers to the ocean.

1.2.2 SOIL EROSION AND POST-SETTLEMENT ALLUVIUM

The rate of pre-human soil erosion is consistent with the rate of soil production over geological timescales (FIGURE 1.2) (Montgomery, 2007b), and often much lower than

modern sediment yields (e.g. Brown et al., 1998; Reusser et al., 2015); the rate of modern soil erosion is significantly higher than natural soil production, a rate that is quickly diminishing our planet's potential to sustain the growing population (Hooke et al., 2012), making it one the greatest environmental issues in the world (Toy et al., 2002). Much of the world's eroded soil is never delivered to the ocean, but is trapped behind dams or held in other reservoirs (Merritts et al., 2011; Walter and Merritts, 2008; Wilkinson and McElroy, 2007), stored as colluvium on hillslopes (Fuchs et al., 2004; Lang, 2003; Lang and Hönscheidt, 1999; Trimble, 1983), or stored within river basins as aggradational stream deposits, often referred to as post-settlement alluvium (PSA) (Brannstrom and Oliveira, 2000; Knox, 2006; Richardson et al., 2014; Starr, 1989; Wilkinson and McElroy, 2007). Because PSA is typically deposited near its source (Trimble, 1983), it compounds the effects of upland soil erosion by burying downstream agricultural land, filling wetland and fluvial ecosystems, and silting estuaries, leading Wilkinson and McElroy (2007) to conclude that its erosion and deposition is one of the most concerning geomorphic processes in the world. Montgomery (2007a) even implicates soil erosion and post-settlement alluvium deposition as a primary cause in the rise and fall of civilisations around the world through time.

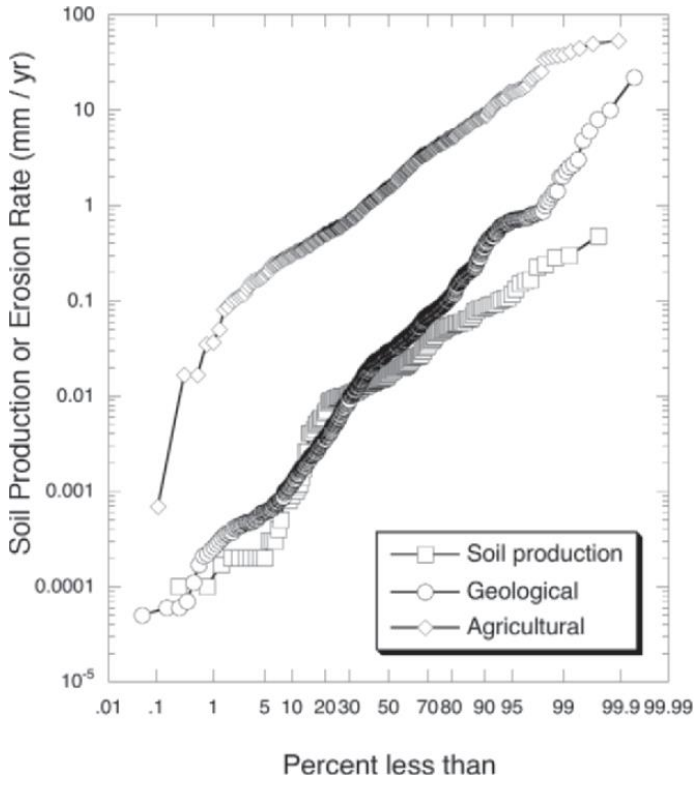

FIGURE 1.2
Montgomery (2007b) illustrates that over geological timescales, pre-agricultural soil loss was of a similar magnitude to geological soil production and that modern agricultural practices are currently operating at unsustainably high levels.

The term post-settlement alluvium has become synonymous with sediment deposition resulting from land clearance after the arrival of Europeans to New World lands in the AD 1600s–1800s. In the United States (FIGURE 1.3), eroded topsoil was deposited in the Chesapeake and San Francisco Bays shortly after European or American movement into the respective drainage catchments, clearing land for agriculture (Helz and Valette-Silver, 1992; Valette-Silver et al., 1986; van Geen et al., 1999), suggesting a much more intensive and widespread land use regime than used by Native Americans. Also, stream aggradation rates increased dramatically after American agriculture began in the upper Mississippi River basin (Knox, 1977; Kreznor et al., 1990; Magilligan, 1985). In South America, pressure to increase grazing and agricultural production led to widespread gully erosion, resulting in the deposition of PSA across valley bottoms and in lakes (Brannstrom and Oliveira, 2000; García-Rodríguez et al., 2002). Similar agricultural pressures led to alluvial aggradation in Mexico (Beach et al., 2006), South Africa (Damm and Hagedorn, 2010), New Zealand (Richardson et al., 2014), and Australia (Eyles, 1977b; Rustomji and Pietsch, 2007). Sediments akin to PSA are found in the Old World as well. In post-Industrial Revolution Great Britain, for example, land clearance for mining resulted in sediment filling valley bottoms (Foulds et al., 2013; Passmore and Macklin, 1994), and Lang et al. (2003a) note the presence of PSA-type sediments in the Rhine River of Germany following 19th century infrastructure projects.

Recently, numerous studies have found PSA-type sedimentary deposits throughout the New and Old Worlds, the ages of which demonstrate that indigenous peoples had widespread geomorphic effects on their landscapes well before the European colonial era. For instance, Richardson (2013) observed sedimentation increases in New Zealand shortly after the arrival of the Maori people to the islands. Increases of sediment deposition rates in Mexican wetlands increased multiple times shortly before the Maya civilisation collapsed (Beach et al., 2006; Beach et al., 2009). Land clearing and hillslope agriculture as far back as the Bronze Age and Neolithic led to downstream sedimentation in Greece (Fuchs et al., 2004; Lespez, 2003), Ethiopia (Nyssen et al., 2004), Germany (Lang et al., 2003b), China (Kidder et al., 2012), the British Isles (Foulds and Macklin, 2006), and in Bolivia (Coltorti et al., 2010), to name but a few.

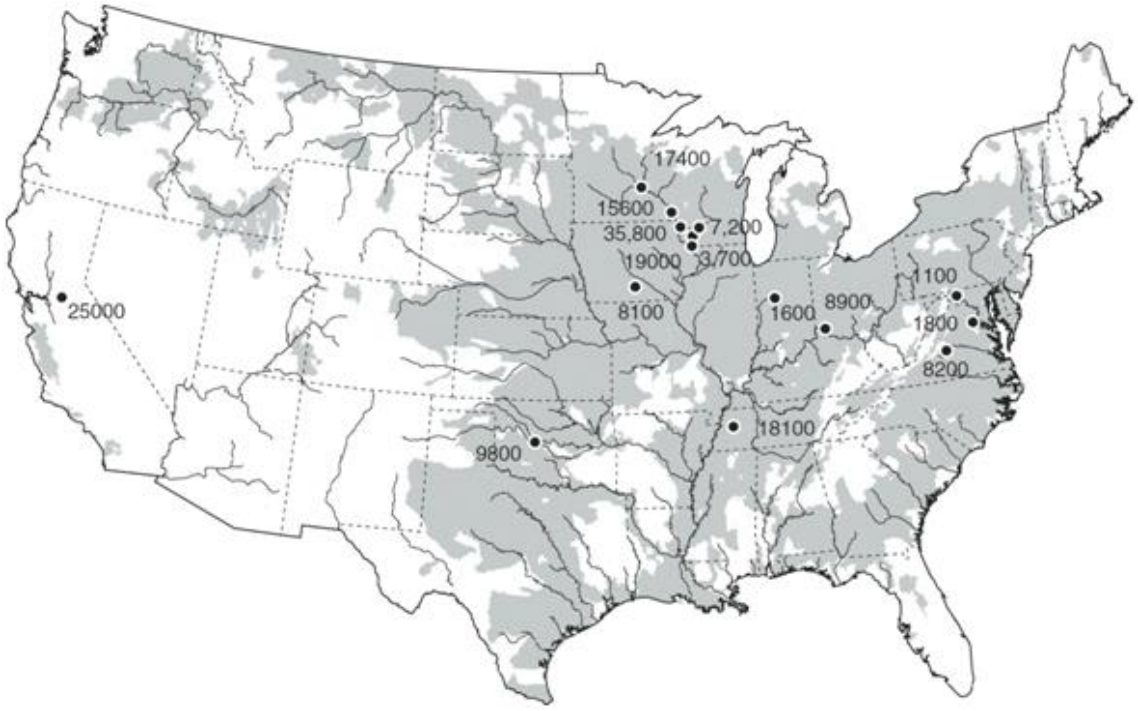

FIGURE 1.3
Agricultural erosion rates throughout the conterminous United States and rates of post-settlement alluviation from Wilkinson and McElroy (2007). Grey shaded regions are cropland erosion rates >100 mm/kyr. Labelled black dots are sites where PSA has accumulated and the numbers are PSA accumulation rates (mm/kyr). Background erosion rates of the eastern seaboard, compiled by Portenga and Bierman (2011), are nearly one order of magnitude lower than modern agricultural erosion rates.

1.2.3 THE AUSTRALIA CONUNDRUM

As evidence builds for a global argument that all peoples and cultures through time are responsible for the loss of over half of the world's natural lands, Australia stands out as an exception. The austral continent was seemingly inhabited throughout by ~50 ka (Bowler et al., 1970; Roberts et al., 1994; Turney et al., 2001), 35 kyr before humans set foot in the Americas, but Aboriginal Australians never adopted agriculture (Yen, 1995). Aboriginal Australians undoubtedly used fire to modify their surroundings (Gammage, 2011), but the only evidence of widespread sediment deposition resulting from land clearing seems to be PSA deposited after the arrival of Europeans (Gore et al., 2000; Rustomji and Pietsch, 2007; Wasson et al., 1998). Aboriginal Australians are argued to be the cause of Australian megafauna extinction (Johnson, 2005; Miller et al., 2005; Roberts et al., 2001), yet the evidence for this argument is circumstantial and strongly debated (Field et al., 2008; Wroe and Field, 2006). Recent suggestions of active neotectonics aside (Sandiford, 2003), the combination of Australia's geological stability (Bishop, 1985; Veevers, 2006), its long human history, geographic isolation, and the relative recency of European arrival provide

an ideal setting in which to study the complex relationships between humans and land use changes from before the dawn of agriculture through to the modern world.

1.3 THESIS FORMAT AND STRUCTURE

This thesis presents a series of interrelated studies, which taken together, investigate sediment erosion, transport, and deposition processes, the relationships between humans and land use, the change from Aboriginal to European land use, and the timing and scale of environmental change. In this thesis, I aim to provide background erosion rates in the Tablelands over geologic timescales, resolve outstanding discussions regarding the genesis and age of PSA deposits throughout the Tablelands, and determine the geographical location of initial gully incision sites in Tablelands valley bottoms, as well as the depth of initial incision that supplied sediment to PSA deposits.

CHAPTER 2.0 provides a geological and geomorphic description of the Tablelands.

The primary objective of each subsequent chapter differs, and so the methods vary. Each chapter is presented with its own introduction covering the background literature followed by the methods germane to that chapter. Details of the primary techniques employed for this thesis are given at the beginning of the first chapter in which they appear.

Specifically, this thesis focuses on the geomorphic processes and chronology of the Tablelands of southeastern Australia by addressing the following topics and questions:

CHAPTER 3.0 analyses the background erosion rate in the Tablelands using cosmogenic ^{10}Be. What is the background, or pre-human, erosion rate of the Tablelands? How does erosion and sediment generation in the Tablelands respond to bushfire? Are erosion rates integrated over tens of thousands of years more consistent with erosion rates integrated over millions of years? Or have they been perturbed by Aboriginal Australian fire regimes since 50 ka?

CHAPTER 4.0 reassesses evidence over the debate of the origin of sandy sediment deposits throughout the Tablelands. Is a portable OSL reader able to discern whether sediment

deposits in valley bottoms are derived from the weathering of granite or alluvial packages deposited during high-magnitude floods? Are portable OSL reader data of buried sediment interpreted to be of swampy meadow origin consistent with data from modern swampy meadows? What relationships, if any, are there between portable OSL reader data and bulk sediment mineralogy, bulk sediment grain size, or adjacent sample replicates?

CHAPTER 5.0 explores the suitability of meteoric ^{10}Be and bulk OSL reader data in identifying initiation sites of gully erosion using Birchams Creek as an example. Do erosional gullies incise into swampy meadow valley bottom soils or into weathered regolith? Where is the geographic location of initial gully incision at Birchams Creek? What is the initial depth of incision? What conditions led to gully incision at Birchams Creek and does its topography make it more susceptible to erode than other creeks?

CHAPTER 6.0 reconstructs a chronology of PSA deposition in the Tablelands. Were PSA deposits throughout the Tablelands deposited before or after European arrival? Are single-grain OSL burial ages for PSA sediment consistent with quantitative and anecdotal evidence of gully erosion and sediment deposition? Are PSA depositional ages in the Tablelands synchronous? What can PSA burial ages tell us about the likely drivers of gully incision and sediment deposition in the Tablelands?

CHAPTER 7.0 closes the thesis with an overview of individual chapter conclusions and an assessment of how the chronology of landscape change in Australia relates to human-land use interactions elsewhere in the world through time.

CHAPTER

THE TABLELANDS OF SOUTHEASTERN AUSTRALIA

2.1 GEOLOGICAL SETTING

Subduction along what is now eastern Australia occurred 450–340 Ma, which led to the accretion of terranes composed of oceanic arc volcanics and turbidite sequences (Gray and Foster, 2004). Formation of the Lachlan Fold Belt occurred during the culminating phase of orogenesis that formed the supercontinent, Pangaea. Australia rifted apart from Pangaea in the Mesozoic between 160–99 Ma (Veevers, 2006). Rifting of the Lord Howe Rise and Challenger Plateau microplates from continental Australia occurred in the early Cainozoic between 83–52 Ma (Gaina et al., 1998), forming the Tasman Sea.

Cainozoic rifting associated with the separation of Antarctica from Australia was accompanied by basaltic eruptions throughout eastern Australia (Weissel and Hayes, 1978), including in the southeastern Australian Tablelands, which occupy the eastern headwaters of the main tributaries of the Murray-Darling River catchment (FIGURE 2.1). Early Miocene basalts sporadically flowed along the continental divide of the northern Goulburn Plains ~20 Ma and filled palaeovalleys of the Upper Lachlan River catchment, in the upper parts of the Murray-Darling network that drains the southeastern Australian Tablelands (Bishop et al., 1985; Young and McDougall, 1993). Slow, long-term erosion rates since the Early Miocene (1–10 m/Myr) have locally inverted the landscape such that the basalt now crops out along the tops of narrow hilltop plateaux (Bishop, 1985; Bishop et al., 1985). Further evidence for long-term landscape stability in the study area is the

unchanged position of the Australian continental divide, which follows the Great Dividing Range (Bishop, 1986). The continental divide separates the coastal rivers (e.g. Hunter, Hawkesbury, Shoalhaven) from the Murray-Darling River, which empties to the Southern Ocean >1,000 km to the southwest.

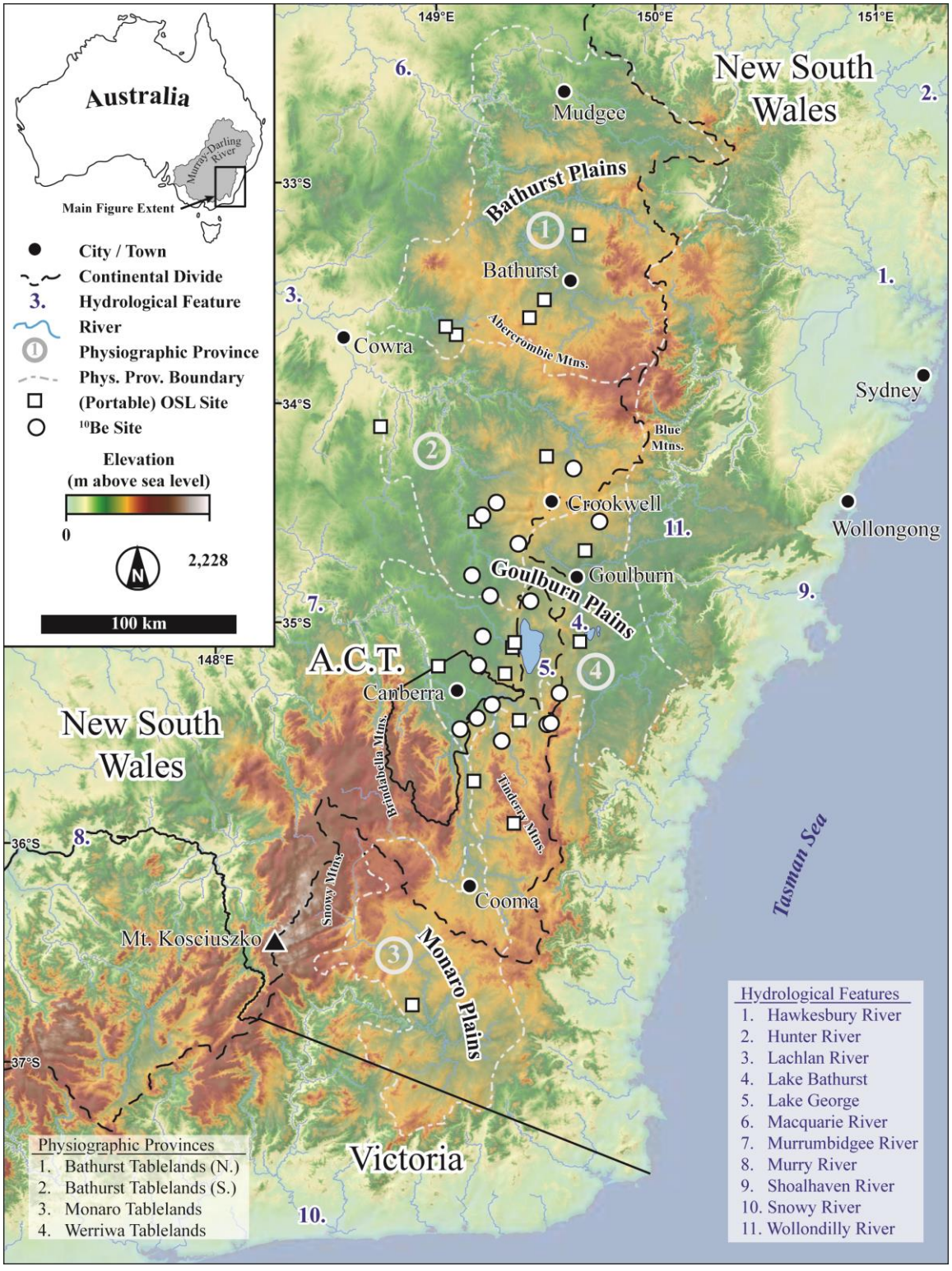

FIGURE 2.1
Physiographic map of southeastern Australia and the greater Tablelands region. Boundaries of physiographic provinces are from Pain et al. (2011). ACT: Australian Capital Territory.

2.2 LATE QUATERNARY CLIMATIC AND GLACIAL HISTORY

Despite Australia's size, only a very small area of the continent was glaciated during the Last Glacial Maximum (LGM); however, much of the Tablelands were subject to periglacial (e.g. cold climate) geomorphic processes during the zenith of Pleistocene glaciations in Australia (Barrows et al., 2004). The extent of Pleistocene glaciations in Australia are well recorded in Tasmania (Barrows et al., 2002) (FIGURE 2.2), and Late Pleistocene glaciers in the Snowy Mountains in southern New South Wales grew and shrank through multiple episodes of ice advance (Barrows et al., 2001) through to the LGM (32–16 ka) (Barrows et al., 2004; Barrows et al., 2001, 2002; Williams et al., 2009). LGM periglacial activity was likely present throughout southeastern Australia at elevations >600 m above sea level, which includes much of the Tablelands (Barrows et al., 2004; Bowler et al., 1976; Costin, 1972; Coventry, 1976; Williams et al., 2009). Lake George on the central southeastern Tablelands experienced its largest extent and greatest depth, ~37 m above the current lake bottom, between 27–21 ka, coinciding with LGM glaciation (Barrows et al., 2004; Coventry, 1976). Glacial conditions were all but absent by 9 ka (Costin, 1972) though periglacial activity temporarily resumed around 3–2 ka causing water levels in Lake George to rise (Costin, 1972; Coventry, 1976). The modern Tablelands climatic conditions and Lake George water levels have existed since 2 ka and have remained relatively consistent (Bowler et al., 1976; Coventry, 1976).

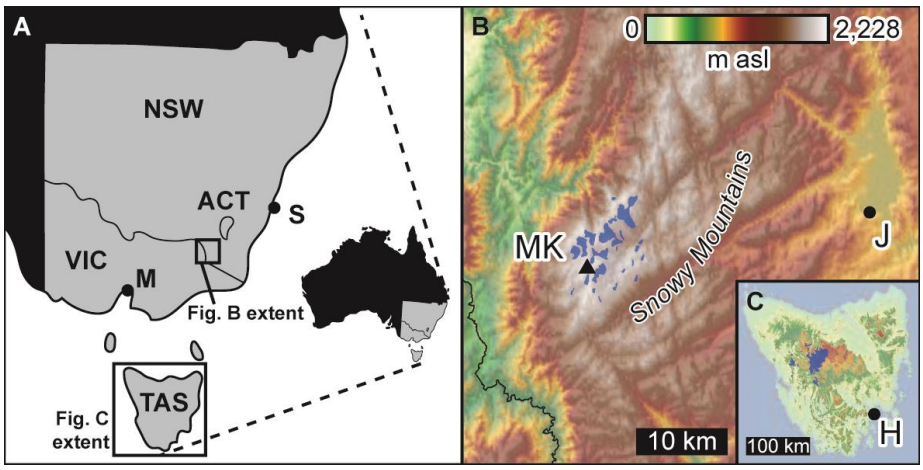

FIGURE 2.2
A. *Regional map of the southeastern states of Australia. NSW: New South Wales; ACT: Australian Capital Territory; VIC: Victoria; TAS: Tasmania; S: Sydney; M: Melbourne.* ***B.*** *Local map of the Snowy Mountains in New South Wales with LGM glacier extents (blue shapes), after Barrows et al. (2004). MK: Mount Kosciuszko, Australia's highest mountain at 2,228 m above sea level. J: Jindabyne, New South Wales. Colour scale same as for FIGURE 2.1.* ***C.*** *Topographic map of Tasmania with the extent of LGM glaciation, after Colhoun et al. (1996). H: Hobart. Colour scale same as for FIGURE 2.1.*

The modern Tablelands experiences a temperate climate (Peel et al., 2007) where mean annual rainfall ranges between 600 and 1,000 mm/yr and mean annual temperatures range from 9–15°C (BOM, 2015). Climatic shifts affecting the Tablelands are strongly related to El Niño Southern Oscillation events and changes in atmospheric circulation patterns (Suppiah and Hennessy, 1998), and like coastal New South Wales, the Tablelands are influenced by alternating drought- and flood-dominated precipitation regimes (Erskine and Warner, 1988; Erskine and Warner, 1998). The cyclicity between flood- and drought-dominated regimes has been questioned (Kirkup et al., 1998) and defended (Erskine and Warner, 1998). Bushfires are common in southeastern Australia, especially during periods of drought, and their occurrence on millennial scales is highly correlated with interglacial and glacial cycles, respectively, in the northern hemisphere (Mooney et al., 2011).

2.3 MODERN TABLELANDS GEOGRAPHY

The southeastern Australian Tablelands mostly occupy elevations between 500–1,000 m above sea level. The southeastern Tablelands boundary, as defined for this thesis, is a division and recombination of physiographic provinces described by Pain et al. (2011). Pain et al.'s (2011) Bathurst Tablelands are separated into a northern and southern unit, split by the Abercrombie Mountains, and the southern unit is then combined with the Werriwa Tablelands as seen in FIGURE 2.1. The southeastern Tablelands are then divided into three sections: (1) The northern Bathurst Plains inland of the Blue Mountains to the east and the Abercrombie Mountains to the south, (2) the central Goulburn Plains bounded by the Abercrombie, Blue, and Brindabella Mountains to the north, east, and south, respectively, and (3) the southern Monaro Plains within the Snowy Mountains (FIGURE 2.1).

Prior to the arrival of Europeans to the Tablelands in the early AD 19th century, the hillslopes were covered by open eucalypt forests (FIGURE 2.3) (Eyles, 1977b; Scott, 2001), but valley bottoms were treeless and unchannelised. Instead, water in valley bottoms filtered through wetlands called swampy meadows (FIGURE 2.4) (Mactaggart et al., 2008), which often featured ponds, or chains of ponds (Eyles, 1977b; Scott, 2001); however, the exact distribution of forests, grassland, and swampy meadows is not well understood (Butzer and Helgren, 2005).

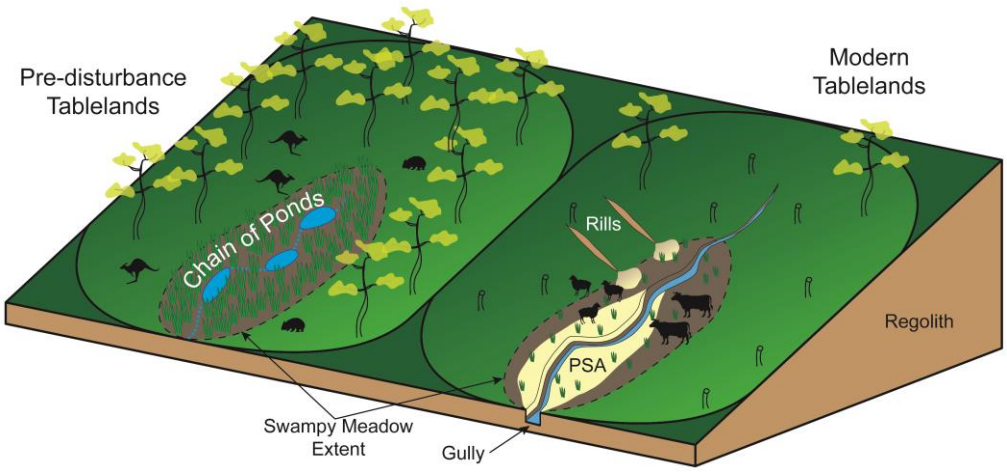

FIGURE 2.3
*Schematic diagram of a typical Tablelands stream basin before European settlement of the region (**left**) and after the land was modified for European grazing practices (**right**). In the pre-disturbance diagram, the dashed blue line only represents a potential water drainage path, when in reality, pre-disturbance swampy meadows were not channelised.*

FIGURE 2.4
*Swampy meadow landscapes in Neville State Forest (**left**) and in the Shoalhaven River catchment (**right**). Chains of ponds are shown in the Shoalhaven River valley bottom. Both photos are from Mactaggart (2008).*

The development of rills and gullies – deep erosional features – in the Tablelands landscape (FIGURES 2.3, 2.5) has occurred naturally numerous times throughout the Holocene (Coventry and Walker, 1977; Eriksson et al., 2006; Prosser, 1991; Scott, 2001). Though gullies have replaced swampy meadows in valley bottoms in the present-day Tablelands landscape (Eyles, 1977b), the cause of their development is debated, as is their relationship to thick packages of sandy sediment that buried many of the lower valley bottom wetlands, traditionally interpreted to be PSA (Butzer and Helgren, 2005; Johnston and Brierley, 2006; Muñoz-Salinas et al., 2011; Rustomji and Pietsch, 2007).

FIGURE 2.5
Extensive, metres-deep erosional gully along Groves Creek, west of Lake George, in the Goulburn Plains.

2.4 HUMAN HABITATION OF THE TABLELANDS

Humans first arrived to and spread throughout Australia by ~50 ka (Bowler et al., 2003; Olley et al., 2006; Roberts et al., 1990; Roberts et al., 1994; Turney et al., 2001); however, evidence of continuous Aboriginal Australian occupation of the Tablelands began ~30 ka (Field et al., 2008; Kohen et al., 1984; Lampert and Hughes, 1974; Megaw, 1965; Stockton and Holland, 1974). Since Aboriginal Australians migrated across the Bass Straits to Tasmania by ~40 ka (Cosgrove, 1999; Gillespie et al., 2012), it is likely that human habitation of the Tablelands is older than current archaeological evidence suggests.

Europeans arrived to Sydney, Australia, in AD 1788, though government-sanctioned explorations of the Tablelands region did not occur until the early AD 1800s (Mitchell, 1839a, b; Oxley, 1820). During the first two decades of the AD 1800s, more and more explorers were reaching the Tablelands (Blaxland, 1870; Evans, 1916; Lawson, 1813; Wentworth, 1813), and by AD 1820 legal settlement of the Tablelands was allowed. The Tablelands were nearly completely settled and claimed by European land holders by AD 1830 (Scott, 2001). European settlers made drastic changes to the Tablelands landscape, all in order to "improve" upon the land by reducing native vegetation through deforestation, ringbarking trees, cutting into and draining swampy meadows, and encouraging grass growth for livestock consumption (Butzer and Helgren, 2005; Eyles, 1977b; Scott, 2001), all of which laid the foundation for a lucrative agricultural industry that still thrives.

CHAPTER

WHAT IS THE BACKGROUND EROSION RATE IN THE TABLELANDS?

3.1 GLOBAL INDIGENOUS LAND USE IN THE PRE-HISTORIC ERA

The extent to which indigenous people of New World lands modified their environmental surroundings has been debated for decades, often focusing on the archaeological and biological impacts with little consideration for the geomorphic response to land use changes.

Indigenous land use often went unnoticed by the first Europeans to settle in the New World lands, likely because disease brought by European explorers killed indigenous populations before settlers arrived (Denevan, 1992). Prior to European exploration of the Americas, fire was frequently used to clear native vegetation for farming and hunting grounds (Armesto et al., 2010; Delcourt and Delcourt, 1997; Delcourt et al., 1998; McLauchlan, 2003; Shaw, 2003), and earthen enclosures, effigy mounds, and pyramids clearly demonstrate the capability of native peoples to move large amounts of Earth material (McLauchlan, 2003; Pauketat, 1998; Reed et al., 1968). Even swaths of land that had previously been considered untouched rainforests in South America were once home to villages and large populations (Heckenberger et al., 2003). In Australia, though, Captain James Cook observed smoke from Aboriginal fires set in northern Queensland in AD 1770, and multiple explorers commented on the continent's park-like landscape (Gammage, 2011), suggesting the obvious use of fire by Aboriginal Australians.

Fire has always been integral to pre-European cultures and even small populations could modify, either directly or indirectly, their landscapes (Delcourt and Delcourt, 1997; Pinter et al., 2011; Shaw, 2003). Not only did indigenous peoples alter their landscapes with fire, but burning vegetation had profound effects on local microclimates (Armesto et al., 2010; Pinter et al., 2011; Shaw, 2003) and possibly led to the extinction of various megafauna – most notably the flightless moa of New Zealand (Anderson, 1989; Holdaway and Jacomb, 2000).

Just as there are examples of landscape degradation, megafaunal extinction, climate change, and vegetation change in New World lands, there are important counterexamples that point equally to relatively low indigenous environmental impact. For instance, the abandonment of settlements in Chaco Canyon, New Mexico was not because of excessive deforestation (Wills et al., 2014); most Pacific islands recovered from the same Polynesian land use that ruined Rapa Nui (Hunt and Lipo, 2006), whose geographic position made it more susceptible to degradation following Polynesian arrival (Rolett and Diamond, 2004); and Malagasy megafauna coexisted with the first islanders for over 2,000 years, even into the period of French colonisation (Burney et al., 2004).

Central to many discussions of indigenous land use around the world is the fate of Pleistocene megafauna. Though global faunal extinctions tend to follow human arrival (Burney and Flannery, 2005), evidence for human overkill is often circumstantial and in many cases megafauna became extinct before humans arrived (Gill et al., 2009; Grayson and Meltzer, 2003). Anthropogenic megafaunal overkill hypotheses (Holdaway and Jacomb, 2000; Martin, 1973) have been scrutinised as there is very rarely direct evidence of overkill (Barnosky et al., 2004; Grayson and Meltzer, 2003). Kill sites are preserved in North America (Reeves, 1978; Waters et al., 2011b), but of extinct species, only mammoths and mastodons are found (Grayson and Meltzer, 2003). The contemporaneity of climate change with human arrival often gives the appearance of overkill when it is more likely that mass extinctions in the northern hemisphere were caused by climate change (Barnosky et al., 2004; Gill et al., 2009; Guthrie, 2004). Indeed, it has been suggested that, without climate change, northern hemisphere species would have survived longer (Barnosky et al., 2004), although eventual extinction was inevitable (Grayson and Meltzer, 2003) and was only accelerated by the use of fire (Pinter et al., 2011).

3.2 AUSTRALIAN ABORIGINAL LAND USE IN THE PRE-HISTORIC ERA

Nowhere is the debate over the timing of human arrival, cause of megafaunal extinction, and effects of fire practices on the landscape more intense than in Australia. The ages of the oldest occupation sites across Australia are consistent at ~50 ka (Bowler et al., 2003; Olley et al., 2006; Roberts et al., 1990; Roberts et al., 1994; Turney et al., 2001) with occupation of Tasmania shortly thereafter at ~40–35 ka (Cosgrove, 1999; Gillespie et al., 2012). The arrival of Aboriginal Australians and their burning practices to the continent is argued to be the principal cause for Australian megafaunal extinction (Gillespie, 2008; Gillespie et al., 2012; Johnson, 2005; Miller et al., 2005; Miller et al., 1999; Roberts et al., 2001; Rule et al., 2012). These claims are hotly contested (Cupper and Duncan, 2006; Field et al., 2008; Price and Webb, 2006; Wroe and Field, 2006; Wroe et al., 2004), and summaries of the current evidence conclude that neither climate change nor Aboriginal arrival can be resolved as the driver of megafauna extinction (Field and Wroe, 2012; Grün et al., 2010; Wroe et al., 2013). The debate continues in southeastern Australia where an apparent co-habitation of megafauna and Aboriginal Australians at Cuddie Springs is contested (Dodson et al., 1993; Gillespie and Brook, 2006). In South Australia, new data suggests former evidence of recent (~16 kyr BP) human-megafaunal coexistence at the Seton Rock Shelter (Hope et al., 1977) is the result of site disturbance (Grün et al., 2006; Grün et al., 2008). Cloggs Cave in eastern Victoria, however, provides evidence of human-megafaunal coexistence at ~23–21 ka (Flood, 1974), well after initial arrival of Aboriginal Australians. Further evidence against human-induced megafauna extinction is the lack of megafaunal remains in shell mounds and no known kill sites or tools used for processing hunted animals (Field et al., 2008; Wroe et al., 2004), though it is possible evidence does exist but is rare or has a low preservation potential. These lines of argument imply that either megafauna were extinct before humans arrived in Australia, that humans did not hunt megafauna, or that megafaunal remains preserved at archaeological sites are exceedingly rare.

Less debated is when Aboriginal Australians used fire on the landscape to create hunting grounds, as there are many European observations of these actions (Gammage, 2011). Aboriginal fire use is implicated in megafaunal extinction (Kershaw et al., 1993) and widespread landscape change (McIntosh et al., 2009; Miller et al., 1999; Roberts et al., 2001). A growing body of evidence suggests that Aboriginal fire use did not increase until the mid-Holocene (Black and Mooney, 2006; Black et al., 2008; Black et al., 2006; Cupper

and Duncan, 2006; Hughes and Sullivan, 1981; Mooney et al., 2011), calling into question the extent of human impact on the landscape relative to that resulting from climate change early in the continent's history (Bird et al., 2013; Price and Webb, 2006).

There is no consensus as to the extent to which anthropogenic burning has changed the Australian landscape over the last few dozen millennia, although the extent of burning must be considerable if fire is to be integral to the megafaunal overkill hypothesis. Assertions that Aboriginal fire use drove megafauna to extinction and set wide tracts of land uncontrollably ablaze (Butzer and Helgren, 2005) ignore the reality that such intensive landscape modification over tens of thousands of years would have had a noticeable geomorphic response, perhaps increased erosion and sediment deposition, and an observable signal in fluvial sediment. Despite claims that light and even moderate intensity burns have no long-lasting effect on sediment yield from catchments (Prosser, 1990; Prosser and Williams, 1998; Tomkins et al., 2006), recent literature highlights the multi-year duration of post-fire landscape recovery of both hillslopes and of whole catchments, even after low intensity controlled burns (Cawson et al., 2013; Lane et al., 2006; Leitch et al., 1983; Noske et al., 2010; Sheridan et al., 2007; Smith et al., 2011; Wilkinson et al., 2009). Post-fire data from southeast Australia over the last few decades show that post-fire sediment flux is derived from topsoil stripping with contributions from deep rill and gully erosion (Atkinson, 1984; Brown, 1972; Nyman et al., 2011; Sheridan et al., 2007) and in some cases even debris flows (Nyman et al., 2011). Though the timing of intense rainfall after a burn is important (Leitch et al., 1983; Sheridan et al., 2007), higher than average sediment fluxes have been observed in burned catchments years after burns, no matter when the rainfall occurred (Cawson et al., 2013; Smith et al., 2011); what may be more important is the combination of rainfall intensity and rainfall duration (Lane et al., 2006).

In this chapter, I look to the geomorphic record to add a new perspective to the discussion of pre-European land use in Australia. To do so, I use the cosmogenic isotope, ^{10}Be, which monitors the residence time of rock and soil in the uppermost few metres of Earth's surface, and when measured from bedrock outcrops and fluvial sediment, ^{10}Be can be used to infer erosion rates integrating over 10^2–10^6 year timescales (Bierman and Steig, 1996; Brown et al., 1995; Granger et al., 1996; Lal, 1991; Nishiizumi et al., 1986). ^{10}Be production by cosmic ray bombardment is well-understood (see below), enabling me to model expected isotopic concentrations in both rock and sediment under different erosional

and burning regimes (FIGURE 3.1). I propose that if Aboriginal Australians used even low intensity burns throughout Australia since 50 ka, its imprint on measured ^{10}Be concentrations will be detectable. This effect will be most noticeable in a stable and slowly eroding landscape setting, which can be assessed by comparing ^{10}Be erosion rates from bedrock outcrops and fluvial sediment (Dethier et al., 2014; Matmon et al., 2003).

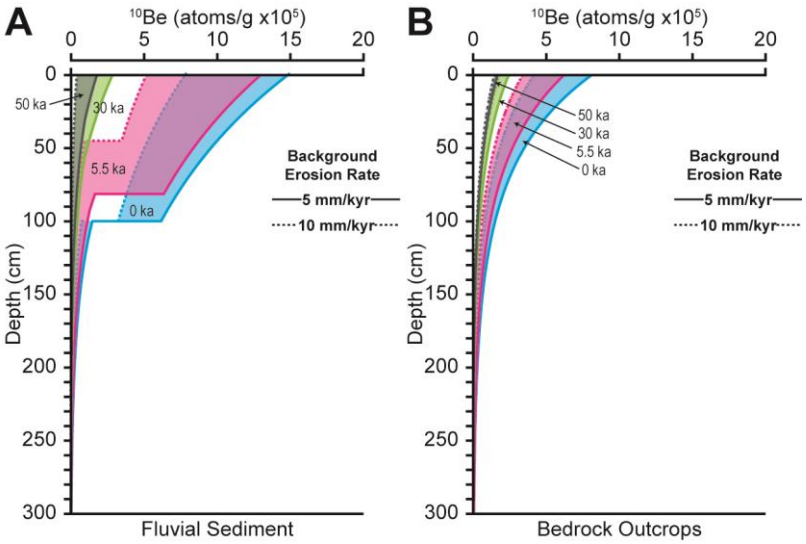

FIGURE 3.1

*Modelled cosmogenic ^{10}Be production for sediment profiles (**A.**) and bedrock outcrop profiles (**B.**) under low intensity fire regimes beginning at 0 ka (no burning, blue), 5.5 ka (increase of charcoal in the sediment record, pink), 30 ka (oldest archaeological dates of Aboriginal settlement of the Tablelands, green), and 50 ka (date of Aboriginal occupation throughout the continent, grey). Long-term background erosion rate boundary conditions of 5–10 mm/kyr are integrated since the Late Paleogene. See Section 3.4.2 for further details and references.*

3.3 GEOMORPHIC STABILITY OF THE TABLELANDS

The geology of the southeastern Tablelands of New South Wales is described in CHAPTER 2.1; however, its long-term landscape erosion rates of ~5–10 m/Myr (Bishop, 1985, 1986; Bishop et al., 1985; Young and McDougall, 1993), integrated since the Late Paleogene (~20 Ma) must be emphasised. The consistently low denudation rates imply continued geomorphologic stability, albeit recent research in neotectonics suggests otherwise (Sandiford, 2003). More importantly, the Late Paleogene-integrated denudation rates provide the context of a constant background rate, which is necessary when assessing presumed impacts of human land use activity. The effects of human land use in the Tablelands should be even more apparent and noticeable in the short-term geomorphic record because the background rates are exceptionally low when compared to other erosion rates around the world (Portenga and Bierman, 2011).

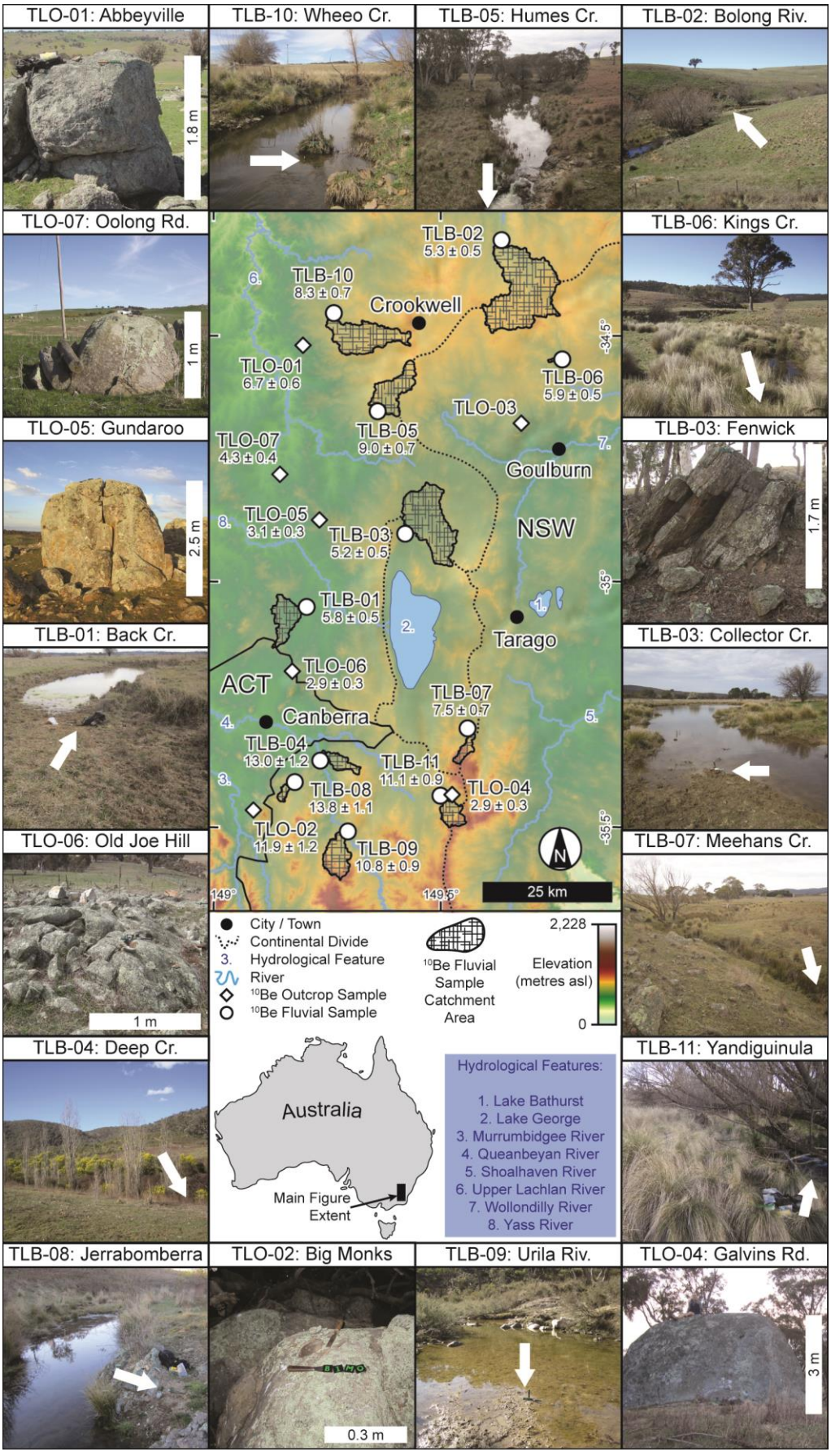

FIGURE 3.2

Locations of samples collected for in situ ^{10}Be erosion rate analysis. Numbers under sample names are the erosion rate (mm/kyr); uncertainties are 1σ. White arrows point to sediment collection location.

3.4 COSMOGENIC ^{10}BE

The isotope, ^{10}Be, is a radioactive cosmogenic nuclide ($t_{1/2}$ = 1.36 Myr) (Korschinek et al., 2010), meaning that it is not produced naturally on Earth but produced by the bombardment of secondary particles (primarily high energy neutrons, but also muons, and others) originating from cosmic rays from space (Lal and Peters, 1962). Meteoric ^{10}Be is primarily produced through spallation reactions with O and N atoms in the atmosphere (FIGURE 3.3) (see CHAPTER 5.0), whereas *in situ* ^{10}Be is produced in the first few metres of the Earth's surface by spallation reactions; spallation reactions occur at lower production rates by muons to much greater depths. The Earth's magnetic field shields much of the planet from cosmic radiation, but since the magnetic field is weaker at the poles, the ^{10}Be production rate is greater at high latitudes. ^{10}Be production is well-constrained (Lal and Peters, 1967; Masarik and Beer, 2009) and can be systematically scaled to any elevation and latitude (Lal, 1991; Stone, 2000). Scaling ^{10}Be production for elevation is exceedingly important as cosmic rays have less atmospheric mass to penetrate before bombarding rock or sediment at Earth's surface.

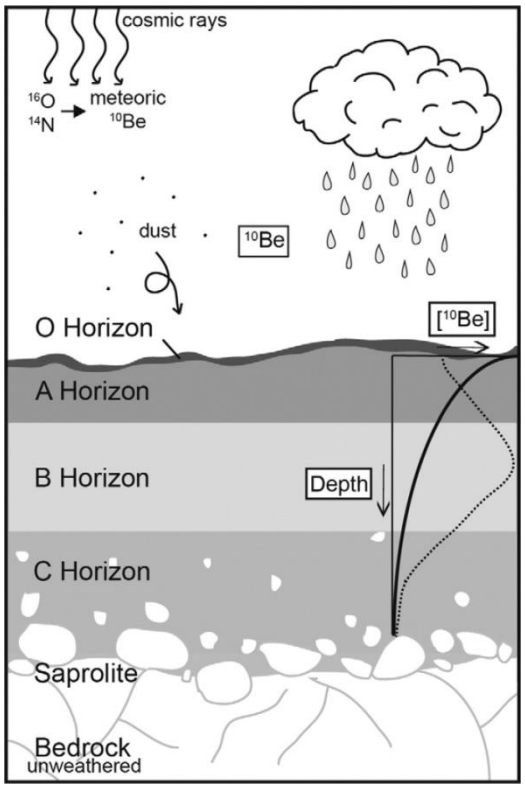

FIGURE 3.3
Schematic diagram of meteoric ^{10}Be in the atmosphere and in situ ^{10}Be in the uppermost few metres of Earth's surface. Characteristic depth profiles of meteoric ^{10}Be (stippled line) and in situ ^{10}Be (solid line) are shown to the right. Figure from Wyshnytzky et al. (2015).

3.4.1 *IN SITU* ^{10}BE

Cosmic rays interacting with Earth surface material (e.g. rock, sediment) produce *in situ* ^{10}Be within the mineral crystal structures where it accumulates and is retained at Earth's surface conditions with time. *In situ* ^{10}Be has proved to be an excellent geochronometer for exposed rock surfaces that have experienced minimal erosion since being exposed to cosmic radiation (Nishiizumi et al., 1991) such as those in glaciated terrain (Corbett et al., 2011), fault scarps (Hippolyte et al., 2006), or those in slowly-eroding landscapes (Bierman et al., 2014). Quartz is typically used as the target mineral for *in situ* ^{10}Be studies because of its resistance to physical and chemical weathering and its near ubiquity in continental lithologies. *In situ* ^{10}Be can be used to measure soil production rates (Heimsath et al., 1997), and in actively eroding landscapes, its measured concentrations in bedrock surfaces can be used to model surface erosion rates integrated over thousands to hundreds of thousands of years (Nishiizumi et al., 1986) using the following equation:

$$N = \frac{P}{\left(\lambda + \left(\frac{\rho\varepsilon}{\Lambda}\right)\right)}$$

where N is the measured nuclide abundance of ^{10}Be (atoms/g), P is the site-specific production rate of ^{10}Be at Earth's surface (atoms/(g/yr)) (Lal, 1991) scaled from a high latitude and sea level elevation production rate of 4.49 ± 0.39 atoms/(g/yr) (Balco et al., 2008), λ is the disintegration constant of ^{10}Be (1/yr), ρ is the sample density (g/cm^3), ε is the steady state erosion rate (cm/yr), and Λ is the attenuation length for neutron spallation (160 g/cm^2) (Gosse and Phillips, 2001). ^{10}Be concentrations in fluvial sand can be used to model an average erosion rate for the upstream contributing river basin area if it can be reasonably assumed that all portions of the catchment are quartz-bearing, that alluvium in a stream bed is a representative mixture of upstream sediment, and that sediment transport time from erosion to sample collection is minimal (Bierman and Steig, 1996; Brown et al., 1995; Granger et al., 1996).

3.4.2 THE ^{10}BE LAND USE MODEL

Expected ^{10}Be concentrations in fluvial sediment are modelled for hillslopes and bedrock outcrops under low intensity fire use regimes, against which measured ^{10}Be concentrations can be compared to assess the purported effects of Aboriginal Australian land use on background erosion rates (FIGURE 3.1). Four models are compared, each with fire use starting at important times in Australian history: 50 ka, the time of Aboriginal Australian occupation throughout the continent (Turney et al., 2001); 30 ka, the oldest archaeological dates of Aboriginal settlement of eastern Australia (Field et al., 2008); 5.5 ka, the moment in the climate-human-fire nexus (Black and Mooney, 2006) when charcoal becomes significantly more abundant in the sedimentary record; and 0 ka, a control scenario in which fire was never used to modify the landscape. ^{10}Be production is modelled at 0.2 mm depth intervals down to 500 cm using the following equation:

$$N = \frac{\left(P_0 e^{\frac{-d\rho}{\Lambda}}\right)}{\left(\frac{\rho\varepsilon}{\Lambda} + \lambda\right)}$$

where N is ^{10}Be concentration (atoms/g), d is depth (cm), and ε is erosion rate (cm/yr). The ^{10}Be surface production rate (P_0) is 7.19 atoms/g, scaled from sea level at high latitude to an average Tablelands elevation of 750 m above sea level at -35°S, using the CRONUS online cosmogenic calculator (Balco et al., 2008). For bedrock models, a bulk rock density of 2.7 g/cm^3 is assumed; for fluvial sediment models, a soil density of 1.4 g/cm^3, an average of sandstone-derived soil (1.6 g/cm^3) (Fifield et al., 2010) and granitic soil (1.2 g/cm^3) (Heimsath et al., 2006), is incorporated into the models, assuming an initial soil-bedrock depth of 1 m (Fifield et al., 2010; Heimsath et al., 2002). Soil production rates of 20 mm/kyr are also incorporated into the models (Heimsath et al., 2006).

End-member erosion boundaries are applied to each model, using a background erosion rate of 5–10 mm/kyr, integrating since the Late Paleogene, and determined independently of this study (Bishop, 1985). Prosser's (1990) 30× increase of hillslope runoff after a light burn are incorporated into the models – a conservative estimate considering that increases of 50–1,000× the background erosion rates are measured more often (Cawson et al., 2013; Noske et al., 2010; Prosser, 1990; Sheridan et al., 2007). In each model, the background erosion rates are increased 30× for 2 years out of every 10 years, even though most

landscapes take longer to recover (Atkinson, 1984; Smith et al., 2011), even from low intensity fires (Blong et al., 1982; Cawson et al., 2013; Leitch et al., 1983; Smith et al., 2011; Wilkinson et al., 2009). None of the models incorporate the potential delivery of sub-surface sediment by gully or rill erosion, or by debris flows (Atkinson, 1984; Nyman et al., 2011; Sheridan et al., 2007). Each model is run using 100 years time steps for 50 kyr. Expected ^{10}Be concentrations derived from these models are shown in FIGURE 3.1.

3.4.3 *IN SITU* ^{10}BE SAMPLE COLLECTION

Fluvial sediment was collected from modern streams throughout the Tablelands (FIGURE 3.2) that exhibited no gully erosion in the upstream contributing area, evidenced from aerial imagery or inspection from the ground. Fluvial sediment was collected from across active channels, point bars, and channel bars to ensure that each sample represents a mixture of sediment from all upstream portions of the drainage basin. Bedrock lithologies of stream catchments varied; however, all lithologies were quartz-bearing. Bedrock samples, typically a few centimetres thick, were removed from the tops of prominent outcrops away from vertical outcrop surfaces, with a hammer and chisel (FIGURE 3.2). Outcrop samples were mostly granitic as non-granite outcrops were difficult to find in the field or were close to the ground, potentially having been buried by sediment after initial exposure.

3.4.4 *IN SITU* ^{10}BE EXTRACTION AND MEASUREMENT

Bedrock samples were crushed, ground down using a plate grinder, and sieved to the 250–850 µm grain size fraction to obtain monomineralic particle sizes; fluvial sediment samples were wet-sieved to the 250–850 µm grain size fraction. All samples were processed at the University of Vermont (UVM) Cosmogenic Nuclide Laboratory in Burlington, Vermont, USA. The 250–850 µm grain size fraction of both crushed bedrock and fluvial sediment were magnetically separated and processed further in order to isolate quartz grains following standard methods and procedures presented by Kohl and Nishiizumi (1992) (FIGURE 3.4). In essence, each sample was treated to a series of weak-acid etches to

remove carbonates and non-quartz minerals, as well as strip away the outermost layer of quartz grains including any adsorbed meteoric ^{10}Be (see CHAPTER 5.0). A 250 µg aliquot from each sample was then tested for cation concentrations using inductively coupled plasma-optical emission spectroscopy (ICP-OES, samples analysed by P. Bierman). If levels of Al, Ti, and Fe were >150 ppm or total cation abundances were >300–400 ppm, the entire sample was treated with another week of weak-acid etches and tested again until the desired cation concentrations were met.

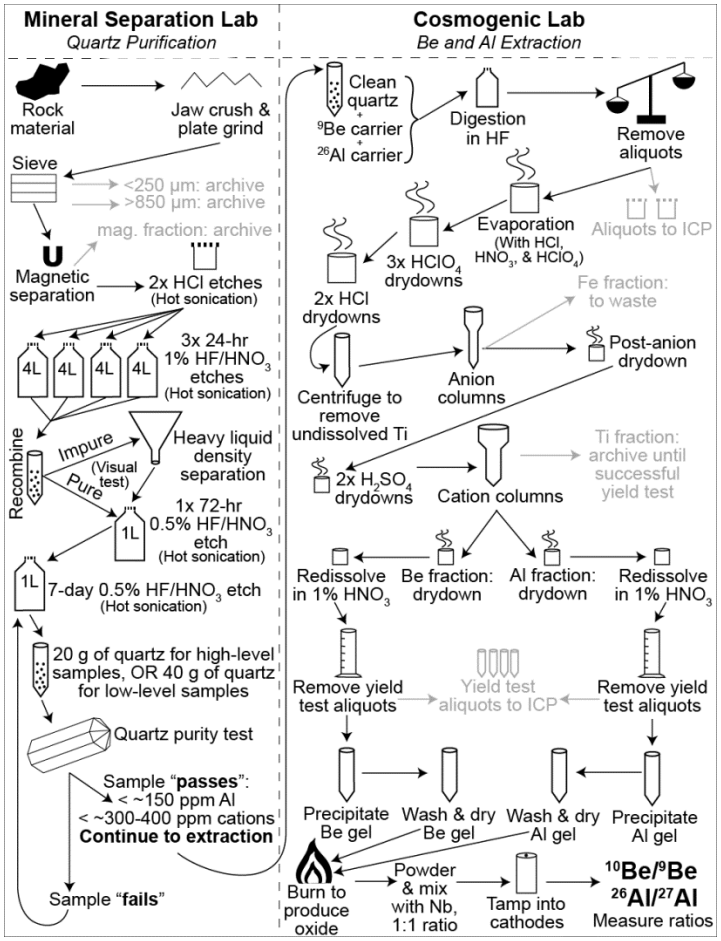

FIGURE 3.4

Schematic diagram of quartz sample processing at the University of Vermont Cosmogenic Nuclide Laboratory. ***Left panel*** *illustrates steps taken to obtain pure quartz, that is, quartz-minerals only though quartz may have inclusions of other minerals.* ***Right panel*** *illustrates steps taken to digest quartz samples and extract ^{10}Be, isolating it from any remaining Fe, Ti, and Al. FIGURE design by L. Corbett (pers. comm., 04 January 2015).*

Isolated quartz separates from each sample were weighed and ~250 µg of naturally-occurring ^{9}Be was added as an analytical carrier to each sample before quartz dissolution (^{9}Be carrier, 285-2A was created at the UVM Cosmogenic Laboratory; [^{9}Be] = 322 µg/mL; ρ = 1.012 g/mL). Be was extracted following procedures outlined in Corbett et al. (2011)

(FIGURE 3.4). Measured $^{10}Be/^{9}Be$ ratios are measured by accelerator mass spectrometry (AMS, see below); thus, the presence of undetected native ^{9}Be in samples – more than was added as a carrier – can result in overestimations of erosion rates (Portenga et al., 2015). Therefore, aliquots from each sample were measured using ICP-OES to demonstrate that the only ^{9}Be in each sample was that added as a carrier (TABLE 3.1). Be was separated from Fe using anion exchange resins and from Al and Ti by cation exchange resins, oxidised, mixed with Nb at a 1:1 molar ratio, and packed into copper cathodes to be measured by AMS.

$^{10}Be/^{9}Be$ ratios were measured using AMS at the Scottish Universities Environmental Research Centre (SUERC) (Xu et al., 2010) in April 2014. $^{10}Be/^{9}Be$ measurements were normalised to the NIST SRM4325 standard material, which has a nominal ratio of 2.79×10^{-11} and blank corrected using two process blanks (avg. = $3.67 \pm 0.085 \times 10^{-15}$), from which concentrations of ^{10}Be were determined for each sample (TABLE 3.1). $^{10}Be/^{9}Be$ ratios shown in TABLE 3.1 include AMS measurement uncertainties and a 1.5% additional uncertainty was propagated throughout.

3.4.5 CALCULATING EROSION RATES

Erosion rates were calculated using the CRONUS online erosion rate calculator (Balco et al., 2008) incorporating Lal's (1991) and Stone's (2000) polynomials to scale ^{10}Be production from high latitude and sea level. Bedrock erosion rates were calculated with no horizon shielding factors; however, shielding factors for fluvial sediment erosion rates were calculated using the weighted mean basin slope for each catchment (TABLE 3.2) using equations in Dunne (1999), derived from 30-meter digital elevation models (Gallant et al., 2011). The effective elevation for drainage basins – the elevation at which the average ^{10}Be production rate for the basin is expected (Portenga and Bierman, 2011) – was used along with the mean latitude and longitude of drainage basins as CRONUS inputs for fluvial erosion rate samples.

Table 3.1: Beryllium Data

UVM Batch	Sample ID	SUERC No.	Blank Corrected[a] $^{10}Be/^{9}Be \times 10^{-13}$	Sample mass (g)	Carrier ^{9}Be (µg)[b]	Aliquot ^{9}Be (µg)[b]	Excess ^{9}Be (µg)[b]	$[^{10}Be]$[c] (atoms/g) × 10^5	Uncertainty
Fluvial sediment samples									
530	TLB-01	b8002	9.625 ± 0.380	17.392	219.7	215.0	-4.7	7.951 ± 0.314	4.0%
530	TLB-02	b8003	13.880 ± 0.536	19.9571	220.9	217.8	-3.1	10.122 ± 0.391	3.9%
530	TLB-03	b8004	12.901 ± 0.472	19.9851	221.9	217.5	-4.4	9.382 ± 0.343	3.7%
530	TLB-04	b8005	3.158 ± 0.180	10.6158	221.8	217.3	-4.5	4.319 ± 0.247	5.7%
532	TLB-05	b8017	8.757 ± 0.192	20.1082	220.1	213.2	-6.9	6.204 ± 0.136	2.2%
530	TLB-06	b8007	11.732 ± 0.369	19.9382	221.8	217.1	-4.7	8.536 ± 0.268	3.1%
530	TLB-07	b8008	10.897 ± 0.484	20.0049	221.4	217.2	-4.2	7.906 ± 0.351	4.4%
532	TLB-08	b8021	5.825 ± 0.138	20.3274	220.5	214.6	-5.9	4.109 ± 0.097	2.4%
532	TLB-09	b8022	8.213 ± 0.185	20.0325	222.8	204.7	-18.1	5.608 ± 0.126	2.3%
532	TLB-10	b8023	8.029 ± 0.234	20.0092	258.8	248.9	-9.9	6.674 ± 0.195	2.9%
532	TLB-11	b8024	7.895 ± 0.179	20.2169	221.7	214.7	-7.0	5.603 ± 0.127	2.3%
Outcrop samples									
530	TLO-01	b8009	9.977 ± 0.398	19.8917	222.1	219.0	-3.1	7.340 ± 0.293	4.0%
530	TLO-02	b8010	3.761 ± 0.235	10.9515	221.9	219.5	-2.4	5.036 ± 0.315	6.2%
530	TLO-04	b8011	23.793 ± 1.090	19.9824	221.6	218.3	-3.3	17.368 ± 0.796	4.6%
530	TLO-05	b8014	1.914 ± 0.388	20.1039	221.4	217.7	-3.7	13.853 ± 0.281	2.0%
532	TLO-06	b8020	7.985 ± 0.179	7.4278	223.4	219.3	-4.1	15.752 ± 0.353	2.2%
530	TLO-07	b8015	13.241 ± 0.577	19.6634	221.1	218.6	-2.5	9.836 ± 0.428	4.4%

[a] $^{10}Be/^{9}Be$ were measured using accelerator mass spectrometry (AMS) at the Scottish Universities Environmental Research Centre (SUERC) and normalised to NIST SRM4325 with a nominal ratio of 2.79×10^{-11} and blank-corrected using two process blanks (avg. = $3.67 \pm 0.85 \times 10^{-15}$) from which ^{10}Be concentrations are derived. Uncertainties shown are AMS measurement uncertainties and a 1.5% additional uncertainty, propagated in quadrature.

[b] We added ~220-260 µg of ^{9}Be standard material, made at UVM (285-2A, $[^{9}Be]$ = 322 µg/mL, ρ = 1.012 g/mL), to each sample before quartz dissolution.

Table 3.2: Location Information & Erosion Rates

Sample	Sample Location	Latitude (°S)[a]	Longitude (°E)[a]	Elevation (m)[a]	Shielding Factor[b]	Thick. (cm) (cm)	Erosion Rate (mm/ky)[c]	Area (km^2)	Sed. Flux (tonnes/km/yr)	Lith.[d]	Weighted Mean Basin Slope (°)[b]
Fluvial sediment samples											
TLB-01	Spring Flat Creek	35.0618	149.2132	585	1	---	5.8 ± 0.5	45.0	8.11	Sa, Si, Ig	3
	(trib. to Back Cr.)	35.0780	149.1770	644							
TLB-02	Bolong River	34.2979	149.6259	754	1	---	5.3 ± 0.5	186.6	7.42	Gr, Si, Sa	3
	(Golspie Rd.)	34.3954	149.6704	908							
TLB-03	Collector Creek	34.9014	149.4334	692	1	---	5.2 ± 0.5	125.2	7.22	Si	2
		34.8823	149.4711	745							
TLB-04	Deep Creek	35.3719	149.2552	589	1	---	13.0 ± 1.2	16.4	18.14	Sa	6
		35.3850	149.2921	809							
TLB-05	Humes Creek	34.6394	149.3744	782	1	---	9.0 ± 0.7	53.1	12.56	Si, Sa, Ba	3
	(Biala-Gurrundah Road)	34.6062	149.4027	873							
TLB-06	Kings Creek	34.5386	149.7427	753	1	---	5.9 ± 0.5	0.8	8.26	Si, Sa	3
	(trib. to Tarlo R. at Backarm Rd.)	34.5416	149.7335	788							
TLB-07	Meehans Creek	35.3197	149.5620	813	1	---	7.5 ± 0.7	11.9	10.54	Gd	8
		35.3559	149.5531	983							
TLB-08	Tributary to Jerrabomberra	35.4320	149.1868	712	1	---	13.8 ± 1.1	5.4	19.29	Rh	6
	Creek (at Swan Dr.)	35.4474	149.1726	817							
TLB-09	Urila Creek	35.5355	149.2991	718	1	---	10.8 ± 0.9	37.4	15.12	Gd, Sa	9
		35.5817	149.2841	951							
TLB-10	Wheeo Creek	34.4525	149.2756	762	1	---	8.3 ± 0.7	78.9	11.63	Si, Sa, Ba	3
	(Narrawa Road)	34.4928	149.3400	881							
TLB-11	Yandyguinula Creek	35.4595	149.5080	809	1	---	11.1 ± 0.9	21.9	15.60	Gd, Sa	9
	(Galvins Cr. Rd.)	35.4914	149.5244	997							
					Average ± Std Err =		**8.7 ± 0.9**				
					Area-weighted Average =		**7.0**				
Outcrop samples											
TLO-01	Abbeyville	34.5108	149.2122	722	1	3	6.7 ± 0.6	---	---	Gr	---
	(along Bevendale Rd.)										
TLO-02	Big Monks Hill	35.4832	149.1081	907	1	1	11.9 ± 1.2	---	---	Ig	---
TLO-04	Galvins Creek Road	35.4598	149.5188	891	1	1	2.9 ± 0.3	---	---	Gd	---
TLO-05	Gundaroo Road	34.8769	149.2470	712	1	7	3.1 ± 0.3	---	---	Gr	---
TLO-06	Old Joe Hill	35.1939	149.1908	808	1	5	2.9 ± 0.3	---	---	Ig	---
TLO-07	Winrock Estate	34.7818	149.1647	614	1	4	4.3 ± 0.4	---	---	Gr	---
	(along Oolong Rd.)										
					Average ± Std Err =		**5.3 ± 1.4**				

[a] For TLB samples, average basin coordinates and effective basin elevation are shown in gray. The elevation is an effective elevation derived by summarising ^{10}Be production for the whole basin at the mean coordinates and solving for the elevation required to yield the calculated ^{10}Be production (Portenga and Bierman, 2011).

[b] Shielding factors are estimated using shielding correction factors by Dunne (1997) using the mean weighted basin slope derived from 30-meter digital elevation models (Gallant et al., 2011).

[c] Erosion rates are calculated using the CRONUS on-line cosmogenic erosion rate calculator (Wrapper script vers. 2.2, main calculator vers. 2.1, objective function vers. 2.0, constants vers. 2.2.1, muons vers. 1.1) (Balco et al., 2008), accessed on 10 September 2014 using Lal's (1991) and Stone's (2000) scaling factors for spallogenic ^{10}Be production. CRONUS uses reference sea-level and high latitude spallogenic production rates of 4.49 ± 0.39 atoms/g/yr (±1σ) and uses Heisinger (2002a,b) for muogenic production. For CRONUS data-entry purposes bulk rock density of 2.7 g cm^{-3} were assumed and sample thicknesses of 1 cm were used for calculating basin-averaged erosion rates. Standard pressure flags and NIST_27900 standardisation for 10Be were used.

[d] Lithologic abbreviations: Ba - Basalt, Gr - Granite, Gd - Granodiorite, Ig - Ignimbrite, Rh - Rhyolite, Sa - Sandstone, Si - Siltstone

[e] Mean annual precipitation calculated as the sum of monthly means of each basin. Precipitation data from Hijmans et al. (2005).

3.5 EROSION RATE RESULTS

Erosion rates inferred from ^{10}Be concentrations in outcrop samples range from 2.9–11.9 mm/kyr (average = 5.3 ± 1.4 mm/kyr, standard error, n = 6), and erosion rates from fluvial sediment range from 5.2–13.8 mm/kyr (average = 8.7 ± 0.9 mm/kyr, standard error, n = 11); an area-weighted average erosion rate for fluvial samples is 7.0 mm/kyr. The total population of erosion rates has a normal distribution (FIGURE 3.5), and bedrock outcrop and fluvial erosion rates are indistinguishable at the 95% confidence interval (Students t-Test: p = 0.0576, FIGURE 3.5). The southeastern Australian Tablelands are thus eroding, on average at 7.5 ± 0.6 mm/kyr (standard error). Erosion rates are integrated over the time required to erode through two cosmic-ray attenuation lengths of Earth surface material (160 cm) (Gosse and Phillips, 2001), and the integration time is given by Λ/ε. Thus, the integration time for the slowest erosion rate, 2.9 mm/kyr (TLO-06), is ~600 kyr; the integration time for the fastest erosion rate, 13.8 mm/kyr (TLB-08), is ~110 kyr.

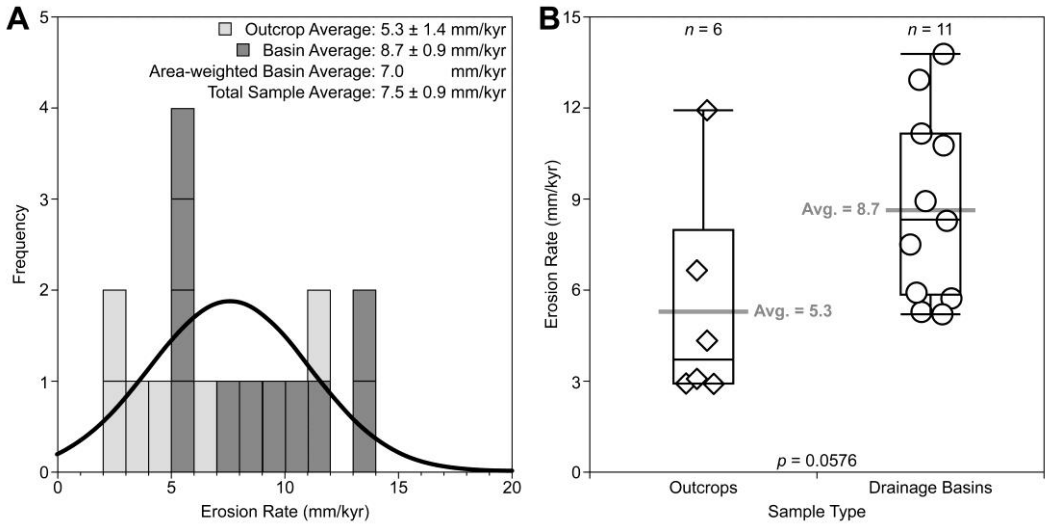

FIGURE 3.5
A. *Histogram showing outcrop and basin-averaged erosion rates (light and dark grey boxes respectively). Black curve shows a normal distribution fit, which passes the Shapiro-Wilk test (p = 0.25).* ***B.*** *Box and whisker plot comparing outcrop erosion rates to basin-averaged erosion rates in the Tablelands.*

The largest and smallest catchments in this study (TLB-02 and TLB-06, respectively) erode at similarly low rates, and fluvial erosion rates from all catchments are within 2 standard deviations of the regional average (FIGURE 3.6). Fluvial erosion rates were converted to sediment fluxes using a sediment density of 1.4 g/cm^3 (TABLE 3.2). Area-normalised sediment fluxes are also all within 2 standard deviations of the regional

average, demonstrating that sediment is well-mixed and representative of the entire upstream area.

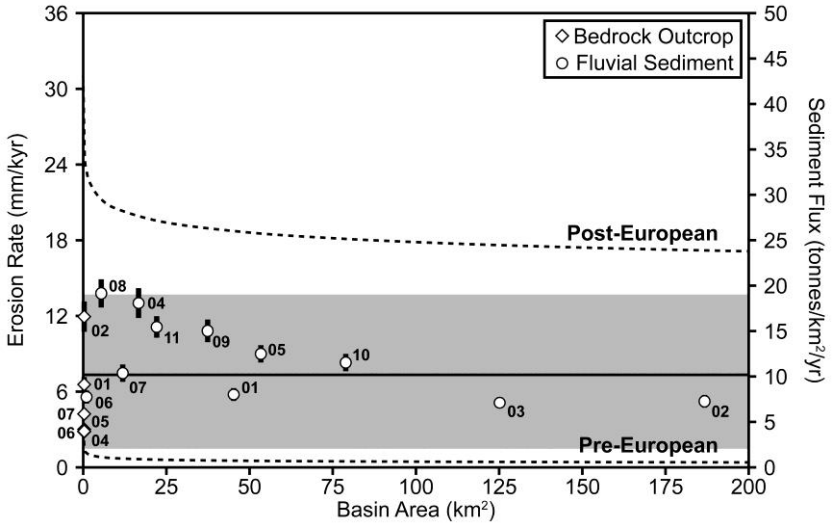

FIGURE 3.6

Sediment fluxes and erosion rates for outcrop and fluvial sediment samples (diamonds and circles, respectively) compared to upstream catchment area. Upper and lower dashed black lines are the estimated post-European and pre-European sediment yields for the Tablelands (Wasson, 1994). Solid black line is the average for all fluvial sediment samples and the solid grey lines represent ±2 standard deviations.

3.6 DISCUSSION OF RESULTS

Artefacts of Aboriginal occupation of the Tablelands and neighbouring Blue Mountains range in age from 30–6 ka (Field et al., 2008; Kohen et al., 1984; Lampert and Hughes, 1974; Megaw, 1965; Stockton and Holland, 1974). The 30 ka arrival date of Aboriginal Australians to the Tablelands is likely to be a minimum age considering the oldest continent-wide occupation sites converge on 50 ka. Based on the average of outcrop and fluvial erosion rates (7.5 ± 0.9 mm/kyr), the 30 ka human occupation of the Tablelands coincides with at least 12–16% of the cosmogenic integration time, 21–26%, if occupation began 50 ka. In either case, Aboriginal habitation of Australia is longer than indigenous human occupation of any other New World land, allowing significantly more time for anthropogenic landscape disturbance. Yet, Pleistocene-integrated cosmogenic erosion rates in this study are consistent with Paleogene-integrated denudation rates (Bishop, 1985; Bishop et al., 1985).

3.6.1 LIKELIHOOD OF A 50 KA ONSET OF ANTHROPOGENIC BURNING REGIMES

Modelled ^{10}Be concentrations indicate that had Aboriginal Australians used even low intensity fires on the Tablelands landscape since 30 ka, much less 50 ka, all soil would have been stripped from the landscape and ^{10}Be measured from fluvial sediment would appear to be derived only from bedrock erosion (FIGURE 3.7). This is clearly not the case, however, as measured ^{10}Be concentrations from fluvial sediment are much greater than those predicted for a 50 ka or 30 ka onset of fire use. Moreover, the Tablelands are mantled in soil, albeit thin (~1 m) that supports a lucrative pastoral industry. When did widespread fire begin if not 50 ka or 30 ka? Measured ^{10}Be concentrations of fluvial sediment are comfortably within the limits of fire becoming more prevalent in the Tablelands 5.5 ka, a key time in Australia's climate-human-fire history, which coincides with increased charcoal in the southeastern Australian sedimentary record (Black and Mooney, 2006; Black et al., 2008; Black et al., 2006; Hughes and Sullivan, 1981; Mooney et al., 2011), though these authors are unable to disentangle Aboriginal fire use from climate-induced fire.

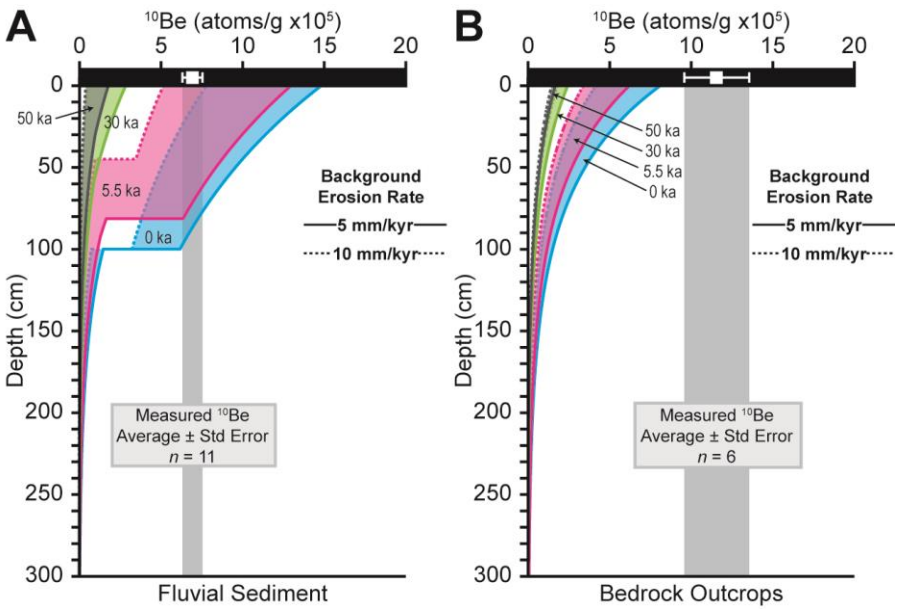

FIGURE 3.7
*Expected model-derived ^{10}Be concentrations for **A.** fluvial sediment samples and **B.** outcrop samples under burning regimes with modelled onset dates of 50 ka (grey), 30 ka (green), 5.5 ka (pink), and 0 ka (blue). White box-and-whisker plots show the average measured ^{10}Be concentrations from each sample type and its associated standard error based on individual ^{10}Be measurements (vertical grey bars).*

Captain Cook and other Europeans first observed fire use in Australia in the late AD 1700s and commented on how well Aboriginal Australians were able to control the burns (Gammage, 2011). Fire use must, therefore, have been in practice for many generations prior to European arrival. Measured ^{10}Be data concur with the supposition of fire use being used for some duration before European arrival as the average ^{10}Be concentration and its uncertainties lay outside the bounds of the 0 ka model (FIGURE 3.7). Measured ^{10}Be data from fluvial sediment, instead, offer strong support for anthropogenic fire use beginning ~5.5 ka as they are strikingly similar to modelled ^{10}Be concentrations derived from estimates of known Aboriginal fire use practices. The average measured ^{10}Be concentration from outcrops (FIGURE 3.7) is greater than any of the predicted models, an indication that outcrops are wholly insensitive to the effects of fire in the Tablelands and are very resistant to erosion once exposed.

The ^{10}Be model is sensitive to fire intensity, landscape recovery time, and the magnitude of increased erosion after fires. Though exact burn intensities of Aboriginal fires can only be estimated, incorporating less conservative estimates of landscape recovery time (Atkinson, 1984; Blong et al., 1982; Cawson et al., 2013; Leitch et al., 1983; Smith et al., 2011; Wilkinson et al., 2009) and the magnitude of increased post-fire erosion (Cawson et al., 2013; Noske et al., 2010; Prosser, 1990; Sheridan et al., 2007) would result in a upwards vertical shift of the modelled ^{10}Be depth profiles seen in FIGURE 3.7. Any upward shift of the ^{10}Be depth profiles would be accompanied by a downward shift of the expected ^{10}Be concentrations and measured ^{10}Be concentrations would thus lie further within the limits of the 5.5 ka background erosion rate envelope set by the 5 mm/kyr and 10 mm/kyr background erosion rates, further supporting my interpretations presented here. Thus, when fire was administered to the Tablelands landscape, it was likely infrequent, localised, and low-impact – surely not enough to alter the geomorphology of a continent and unlikely to drive multiple species of megafauna to extinction.

3.6.2 LONG-TERM SEDIMENT FLUX

Wasson (1994) suggests sediment yields from large basins are not as significantly affected by land use as smaller headwater catchments and that most alluvium in the Tablelands is sourced in these small catchments – a relationship I do not observe (FIGURE 3.6). Long-

term sediment fluxes from the Tablelands are higher than those hindcasted for a pre-European Tablelands (Wasson, 1994); thus, Wasson's pre-European Tablelands sediment flux estimates more aptly estimate an Early Holocene sediment flux following conclusions of a mid-Holocene onset of Aboriginal burning. Nevertheless, all fluvial erosion rates shown here, which come from ungullied catchments, exhibit erosion rates less than those associated with post-European land use change (FIGURE 3.6).

3.6.3 COMPARISON WITH AUSTRALIAN COSMOGENIC STUDIES

Results from this study disagree with conclusions of a nearby cosmogenic nuclide study based on fluvial sediment from the Nattai River in the Blue Mountains (Tomkins et al., 2006) that suggests post-fire sediment flux is so much lower than the ^{10}Be erosion rates that fire-induced sediment flux is not noticeable over millennia. To this end, the Nattai River is seaward of the Great Escarpment and drains deep, narrow catchments that have high potential to supply sediment that was shielded from cosmic-ray bombardment or sediment eroded from boulders plucked from below the cosmic-ray attenuation depth. Sampling fluvial sediment generated by either scenario would produce erosion rates apparently high (they measure ~20 mm/kyr). Rather, the erosion rates determined for the Nattai River catchment are likely monitoring the passage of escarpment retreat as Tomkins et al.'s (2006) erosion rates are similar to Heimsath et al.'s (2001; 2006) rates from the Great Escarpment ~300 km to the south. Cosmogenic erosion rates from the Atherton Tablelands in Queensland (Nichols et al., 2014) and Arnhem Land in the Northern Territory (Heimsath et al., 2009) support this notion, demonstrating fluvial sediment erosion rates along the escarpments are higher than erosion rates from those above the escarpments.

3.7 CHAPTER CONCLUSIONS

Cosmogenic erosion rates from fluvial sediment and bedrock outcrops demonstrate the continued stability of the Tablelands landscape of eastern New South Wales from the Late-Paleogene through to the Holocene. The low rate of landscape change on the central

Tablelands of eastern New South Wales since the Pleistocene is consistent with the pace of landscape change since the Late Paleogene. Data from this chapter suggest either that Aboriginal Australians living in this region since 30 ka did not use fire or burning as intensively as previously thought, that the adoption of fire modification of the landscape came only recently, perhaps mid-Holocene, or the population was not large enough to generate the large amounts of charcoal observed in the sedimentary record since the mid-Holocene. Long-term sediment fluxes from catchments in the Tablelands are lower than post-European sediment fluxes and likely reflect Early Holocene sediment fluxes prior to the onset of mid-Holocene burning. ^{10}Be data cannot resolve whether the intensity of fire use was significantly low for a long duration or as intense as European colonists reported for a short duration. The lack of evidence for fire use in the geomorphic record is even more pronounced if the Tablelands were inhabited 50 ka when the remainder of the continent seems to have been occupied. Finally, no evidence is observed for the type of fire activity that is the suspected cause of direct, or indirect, extinction of Australian megafauna. These data are among the first geomorphic lines of evidence to suggest Aboriginal Australians and their land use practices were drastically less invasive or destructive to their environmental surroundings than previously thought, and much less than the first peoples of many of the other New World lands.

Knowing now that Aboriginal Australian land use is unlikely to have altered the background erosion rates, I shift focus to the sedimentary deposits at the heart of the European versus pre-European erosion debate in the Tablelands.

CHAPTER

THE "A" OF PSA: WHAT IS IT?

4.1 A TABLELANDS STRATIGRAPHY EXPOSED IN GULLY WALLS

Gully erosion – deep incisions on hillslopes and valley bottoms – exposes stratigraphies that reflect the histories of hillslope processes and of sediment transport and deposition (Poesen et al., 2003; Poesen et al., 2002; Valentin et al., 2005). In the southeastern Australian Tablelands, gully erosion has revealed what appears to be a near ubiquitous stratigraphy of lighter coloured sandy sediments overlying darker fine-grained sediments (FIGURE 4.1, 4.2), the traditional geomorphic interpretation of which is that swampy meadow wetland environments (Mactaggart et al., 2008) that occupied valley bottoms before Europeans arrived in the early AD 1800s were buried by sandier sediments eroded from gullies triggered by European grazing and farming practices upstream (Eyles, 1977b; Scott, 2001). Packages of sandier sediment covering valley bottom swampy meadow sediments have thus been widely referred to as post-settlement alluvium (PSA) (Starr, 1989).

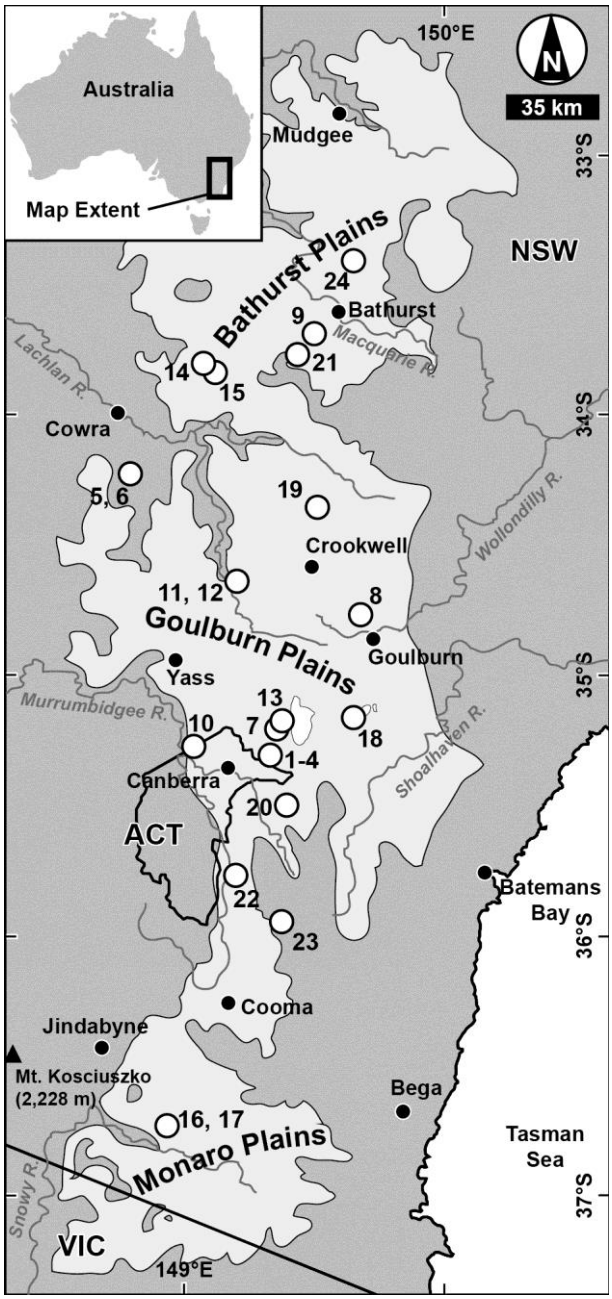

FIGURE 4.1

Location of study sites (white circles) throughout the southeastern Australian Tablelands (light grey region). Photographs of field sites are in APPENDIX A. Inset map shows study location on the Australian continent. Elevations range from 0 m at sea level to 2,228 m at Mt. Kosciuszko in the Snowy Mountains. The Tablelands region is mostly between 500 m and 1,000 m above sea level. State boundaries (black lines) and towns (black circles) are shown for geographic reference. ACT: Australian Capital Territory; NSW: New South Wales; VIC: Victoria. Sampled sites are numbered and specific locations are in TABLE 3.2. 1–4: Birchams Creek; 5–6: Breakfast Creek; 7: Brooks Creek tributary; 8: Fenwick Creek; 9: Georges Plains Creek; 10: Gooromon Ponds Creek; 11–12: Grabben Gullen Creek; 13: Groves Creek; 14: Grubbenbun Creek; 15: Mandurama Ponds Creek; 16–17: Matong Creek; 18: Mulwaree River; 19: Phils River; 20: Primrose Valley Creek; 21: Queen Charlotte's Creek; 22: Ryries Creek; 23: Wangrah Creek; 24: Wyagnon Creek.

FIGURE 4.2
*Photographs of extensive gully erosion at **A.** Groves Creek and **B.** Queen Charlotte Creek. Common stratigraphy of swampy meadow sediments overlain by sandier post-swampy meadow sediments at **C.** Fenwick Creek (field assistant for scale) and **D.** Primrose Valley Creek (gully exposure ~1.5 m). **E.** Cross bedding at Fenwick Creek. **F.** Cross bedding at Matong Creek. **G.** Coarse sand lenses at Mulwaree River. **H.** Swampy meadow clay mixed and deposited along with sand at Phils River; fine grained bedding in lower left of photograph.*

The term "post-settlement alluvium" has been discussed almost as much as the sediment itself has been studied, without much resolution. European land use change in western New South Wales (NSW) led to stream aggradation; yet the incorporation of large amounts of aeolian sand and dust in deposits and the burial of fence posts led Pickard, Gore, and colleagues (Crighton and Gore, 2001; Gore et al., 2000; Pickard, 1994) to refer to these deposits as post-European material, not alluvium. European artefacts incorporated into sandy deposits in western NSW and the Tablelands (including cloth, glass bottles, fencing wire, etc.) indicate that these deposits post-date European arrival to Australia (Erskine and Melville, 1984; Rustomji and Pietsch, 2007; Starr, 1989; Wasson et al., 1998); however, gullying occurred naturally before Europeans arrived (Eriksson et al., 2006; Johnston and Brierley, 2006; Muñoz-Salinas et al., 2014), and the synchroneity of recent episodes of gullying has led to disagreement over the timing and cause of erosion and sediment

deposition. Aboriginal Australians have occupied the Tablelands region since at least 22 ka (Stockton and Holland, 1974) so the term "post-settlement" is perhaps poorly chosen if these sediment deposits are related to European land use change. Finally, calling these sediments alluvium has even been debated by those who argue that gully-exposed stratigraphies are the result of naturally weathered granitic soils (Butzer and Helgren, 2005). In this chapter, I thus seek to identify and define these sandy sediments throughout the Tablelands using laboratory methods in conjunction with field observations.

4.2 ORIGIN OF PSA: THEORETICAL BACKGROUND AND HYPOTHESES

In Australia, Muñoz-Salinas et al. (2011; 2014) assumed the sandy deposits exposed in gully walls of Grabben Gullen Creek were PSA and that the underlying dark sediment represented a former swampy meadow environment. The authors used samples collected from multiple profiles through putative PSA and swampy meadow sediments to conclude that PSA was derived from the erosion of granitic soil upstream rather than from soils formed on the meta-sedimentary bedrock adjacent to the PSA sites. The authors observed marked changes in bulk OSL measurements above and below the visual sedimentary boundary between swampy meadow sediments and overlying PSA, interpreting the increase in bulk OSL at the base of PSA deposits to reflect the PSA's provenance and incomplete sediment bleaching during transport and deposition. This interpretation contrasts with that of Butzer and Helgren (2005) who maintain sediment profiles exposed in gully walls resulted from soil formation of underlying granodiorite bedrock, the swampy meadow textures being derived from feldspars weathering to clay and the PSA being derived from the quartz remaining after feldspar weathering and migration into the subsoil.

Muñoz-Salinas et al. (2011) suggest sediment is well bleached under low energy conditions in a swampy meadow setting and interpreted the increase of bulk OSL in swampy meadow sediments with depth to be a result of post-depositional accumulation of luminescence with age. If this interpretation is correct, modern swampy meadow sediments should likewise exhibit increasing stored dose with depth, with zero luminescence in the shallowest swampy meadow sediments. Furthermore, if the overlying sandy deposits are alluvial, evidence of sediment deposition by flowing water should be preserved in the sandy stratigraphy. Bulk OSL measurements may also be able to distinguish between

fluvial sediments constantly being deposited by regular stream flow such as those trapped behind mill dams in Scotland (Bishop et al., 2005) or by irregular flow dominated by floods such as those of the Mekong River in Cambodia (Muñoz-Salinas et al., 2011). Conversely, if PSA is granitic soil weathered in place, it should only be found in catchments with granitic bedrock and depth profiles of bulk OSL should be similar to those observed in uneroded soil profiles (Muñoz-Salinas et al., 2014; Wilkinson and Humphreys, 2005) with a systematic decrease in luminescence toward the surface.

4.3 METHODS

4.3.1 OPTICALLY STIMULATED LUMINESCENCE (OSL)

OSL is an optical phenomenon of minerals related to the time that has passed since sediment was last eroded, exposed to the sun, and reburied (Aitken, 1998) and is used to determine accurate and precise burial ages of sediment (see CHAPTER 6.0). Buried mineral grains receive natural ionising radiation from surrounding soil that excites electrons within a mineral's crystal structure to a higher-energy state, which are then trapped in defects of the mineral structure (Aitken, 1998). The number of displaced electrons builds up over time until the mineral grain is exposed to sufficient amounts of light or heat, which stimulate electrons, releasing them from their traps, and allowing them to return to a stable energy state, emitting photons (i.e. luminescence) in the process (FIGURE 4.3). If stimulated by heat, thermoluminescence (TL) is emitted, and when stimulated by light, optically stimulated luminescence (OSL) is emitted. The loss of luminescence during stimulation is called bleaching. In most cases, bleaching the OSL signal in sediment with sunlight only takes a few seconds (Godfrey-Smith et al., 1988); thus, the degree to which complete luminescence bleaching occurs can be indicative of the duration and nature of sediment erosion, transport, and deposition. Well-bleached sediment provides the most precise burial ages, and as OSL procedures have become more uniform and widely used (Wintle, 2008a, b), even aeolian deposits less than five years old can be dated (Olley et al., 1998) assuming the sediment was completely bleached. Fluvial and glacial systems are often not ideal for complete bleaching, however, and sediment can be deposited with an inherited accumulated luminescence (Duller, 1994; Huntley and Berger, 1995; King et al., 2014; Li, 1994). Though inherited luminescence is problematic for burial age dating, bulk OSL data

from incompletely bleached sediment can provide important geomorphic information as well.

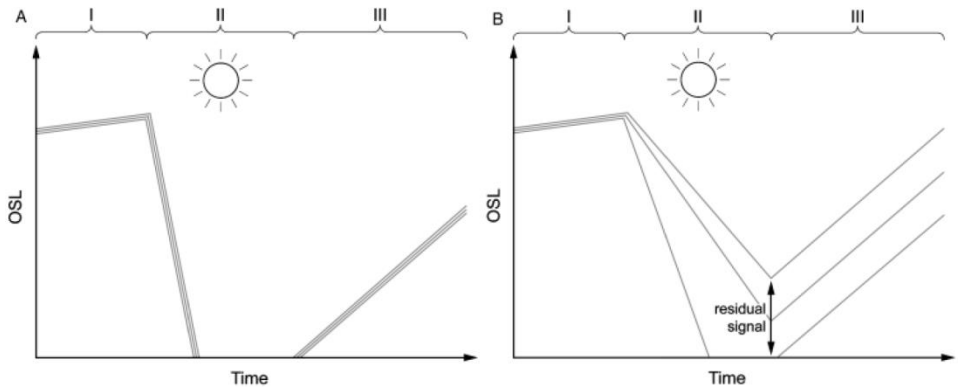

FIGURE 4.3
A. *Phase I: Luminescence accumulates in buried sediment. Phase II: Sediment is eroded and transported under effective bleaching conditions and all luminescence is emitted before reburial. Phase III: Luminescence accumulates after sediment deposition.* ***B.*** *Phase I: Luminescence accumulates in buried sediment. Phase II: Sediment is eroded and transported under ineffective bleaching conditions and many sediment grains retain residual luminescence signal before reburial. Phase III: Luminescence accumulates after sediment deposition.* FIGURE *from Duller (2008).*

4.3.2 LUMINESCENCE PROFILING WITH A PORTABLE OSL READER

Since traditional sedimentological observations and interpretations can be subjective, important stratigraphic boundaries may go unnoticed in the field if there are no observable physical demarcations by, for example, colour or texture; therefore, it is useful to utilise a quantitative, rather than qualitative, approach when describing sediment. Optically stimulated luminescence (OSL) is one such technique used to observe sequential changes of environmental conditions in sedimentary profiles and is different from OSL's more common use as a sediment burial age dating technique in that OSL profiling does not derive ages, but only measures the total luminescence from a sediment sample. OSL profiling has been used previously (Burbidge et al., 2007; Sanderson et al., 2003) and portable OSL instrumentation has existed for several decades (Poolton et al., 1994), but the capability of measuring bulk luminescence from a sediment profile quickly, without sample preparation and while still in the field, has only recently been developed (Sanderson and Murphy, 2010).

Though portable OSL readers have been used to understand changes in sediment transport and deposition processes in coastal, glacial, aeolian, and fluvial settings (Bishop et al., 2011; Bishop et al., 2005; King et al., 2014; Muñoz-Salinas et al., 2014; Muñoz-Salinas et

al., 2011; Munyikwa et al., 2012; Sanderson and Murphy, 2010), portable OSL reader data must be interpreted with caution. Firstly, contributions to bulk luminescence measurements by different grain size abundances in bulk sediment are unknown. Secondly, bulk luminescence measurements do not account or correct for mineralogies mixed in sediment samples. Many minerals emit luminescence (Aitken, 1998; Clark and Sanderson, 1994), and it may be unclear how different mineral phases contribute to the bulk luminescence measurements from portable readers. How the bleaching rates of different minerals (Godfrey-Smith et al., 1988) affect bulk luminescence measurements is not well constrained, and not all mineral phases maintain their stored luminescence over time, even if they are not being stimulated – such as with anomalous fading in feldspar minerals (Wintle, 1973). As neither the dose rate nor the mineral sensitivity can be constrained by the portable OSL reader, bulk OSL data only provide a snapshot of measured emitted luminescence from any given sediment sample.

4.3.3 PORTABLE OSL SAMPLE COLLECTION

Samples were collected from sediment profiles throughout the Tablelands using 18 mm diameter × 30 mm length aluminium tubes (photos of field sites are in APPENDIX A). Duct tape was used to cover the outer end of each tube so that profile sediment in the tube did not slump, minimising the amount of bleached material in each sample. Upon removal of each tube from the sediment, the end of the tube inserted deepest into the sediment was also covered with duct tape. The use of duct tape to cover both ends of the sampling tubes provides a basic sample purification service as the outermost grains at either end of the tube – those most likely to have been exposed to sunlight – adhere to the tape and thus were not incorporated into the measurement of profile samples. All portable OSL samples mentioned in this thesis were collected at 3 cm depth intervals throughout sediment profiles, unless otherwise noted. The reproducibility of bulk luminescence measurements is tested in Grabben Gullen Creek (as noted above), and also at Fenwick Creek and Mulwaree River where sets of replicate samples were collected every 9 cm, spaced laterally ~5–15 cm from the main profile. Standard deviations for sample replicates (2σ; $n = 3$) are calculated at each 9 cm interval.

4.3.4 PORTABLE OSL SAMPLE MEASUREMENT

The portable OSL reader used for this thesis was developed by the Scottish Universities Environmental Research Centre (SUERC; Sanderson and Murphy, 2010) and detects the bulk luminescence emitted from poly-mineral, poly-grain size sediment samples when stimulated with infrared (IR) and blue LED (BL) light sources.

Luminescence laboratories were set up in field accommodation and filtered red light lamps were used under otherwise blackout conditions during sample analysis with the portable OSL reader. Samples were unloaded, one at a time, from the sampling tubes and spread across 5 cm petri dishes, thereby normalising portable OSL data to an equal area; no other sample treatment was performed before measurement. A seven-step stimulation method was applied to measure each sample (TABLE 4.1). During stimulation, the infrared and blue-light stimulated luminescence (IRSL and BLSL, respectively) is measured by a photomultiplier where the total photon counts are quantified. In all analyses, each sample was exposed to IR stimulation before BL stimulation as feldspar phases are sensitive to blue-light stimulation (Sanderson and Murphy, 2010) and if these are not fully bleached during IR stimulation, their luminescence could add to BL measurements (Duller and Bøtter-Jensen, 1993). Following IR stimulation, samples were exposed to BL stimulation to measure luminescence primarily from quartz. Structuring analyses in this way allowed the ratio of IRSL to BLSL to be used to assess whether it is possible to broadly distinguish non-quartz generated luminescence from quartz-generated luminescence and hence to assess for mineralogical changes throughout sediment profiles. Dark counts – luminescence measured in the absence of light stimulation – before and after each IRSL and BLSL provide background luminescence levels of the instrument chamber. Corrections for dark counts are factored into (i.e. subtracted from) analytical results.

Table 4.1: Portable OSL Reader Stimulation Steps

Step	Abbreviation	Description	Duration (s)	Net Photon Counts
1	DC1	Dark count	15	
2	IRSL1	Infrared stimulation	30	IRSL = IRSL1 + IRSL2 - (2 × DC1) - (2 × DC2)
3	IRSL2	Infrared stimulation	30	
4	DC2	Dark count	15	
5	BLSL1	Blue-light stimulation	30	BLSL = BLSL1 + BLSL2 - (2 × DC2) - (2 × DC3)
6	BLSL2	Blue-light stimulation	30	
7	DC3	Dark count	15	

4.3.5 USING AN UPDATED PORTABLE OSL READER

Muñoz-Salinas et al.'s (2014) and Butzer and Helgren's (2005) interpretations of the genesis of sedimentary deposits exposed in gully walls throughout the Tablelands were evaluated by conducting a regional campaign to sample sediment for analysis using a portable OSL reader. I returned to Grabben Gullen Creek to ensure that Munoz-Salinas et al.'s (2014) portable OSL reader data were reproducible with an upgraded portable OSL reader. The new reader allows for automatic switching between stimulation sources, so updated instrumentation is more sensitive to OSL detection and new data from this study appear to be one order of magnitude higher than Muñoz-Salinas et al.'s reader (pers. comm. David Sanderson, 25 April 2014). This one order of magnitude difference was factored into previous data from Grabben Gullen Creek before comparing it to new data measured with the upgraded reader. Muñoz-Salinas et al.'s (2014) interpretation that dark sediment exposed in gully walls below the sandy sediment is from swampy meadow environments was then assessed by collecting three cores and two profiles from known modern swampy meadows. Finally, sixteen profiles through swampy meadow-sandy sediment deposits were collected and compared to weathered bedrock profiles and flood deposits.

4.3.6 X-RAY DIFFRACTOMETRY

As part of the assessment of the sensitivity of portable luminescence data to changes in bulk sediment mineralogy, I quantified mineral phase proportions in a selected subset of sediment samples from four field sites using X-ray diffraction (XRD). XRD measures the scattering of X-rays incident on pulverized mineral crystals, with each mineral phase's mineral structure scattering X-rays at unique angles, which are measured by a moving detector (Warren, 1969). An aliquot of sediment from the subset sample was ground down to a fine powder using a mortar and pestle and mounted on X-ray diffractometer sample platforms. Constituent minerals were detected using a PANalytical X'Pert Pro MPD X-ray diffractometer using conditions of 5–95° 2θ, 45 kV, 40 mA, CuKα radiation, an X'Celerator detector, Bragg Brentano geometry, and a slew rate of 5° 2θ per minute. Minerals present in samples were identified from ICDD PDF2 and PAN-ICSD databases,

and their relative abundances were generalised using Rietveld refinement using Highscore Plus software (vers. 2.2.4).

4.3.7 GRAIN SIZE ANALYSIS

The degree of luminescence bleaching of sediment in transport is inversely related to turbidity (Sanderson et al., 2003), with the latter increasing in high flow velocity streams capable of transporting a variety of grain sizes. The refraction and dimming of light passing through deep water reduces the bleaching of sediment as well. Conversely, fluvial flows with low stream power are less capable of transporting coarser grain size fractions, such as medium and coarse sand, and the shallowness of such flows are also more likely to have increased sun-exposure time before grain reburial and thus a higher likelihood of complete bleaching. Relationships between grain size and bulk luminescence may hypothetically be used to infer relative magnitudes of past sediment-transporting flows as well as perhaps the rapidity of deposition and burial. Sediment samples from the same subset of four field sites used for mineralogical analyses were analysed for their grain size distributions five times using a Malvern MasterSizer optical bench with a Hydro 2000g accessory. Particle refractive indices of 1.544 (quartz) and 1.330 (water) were used. The average grain size (D_{50}) is reported in all analyses and, following Wentworth (1922), grain size fractions are defined as thus: clay (0.01–2 μm), silt (2–62.5 μm), fine sand (62.5–250 μm), medium sand (250–500 μm), and coarse sand (500–2000 μm).

4.4 PORTABLE OSL RESULTS

Multiple lines of evidence were found supporting the traditionally held interpretation that thick surficial sandy sediment deposits throughout the Tablelands are alluvial and not weathered granitic soils (most notably for the latter being that sandy sediment deposits are observed in stream catchments underlain by a variety of granitic and non-granitic lithologies) (TABLE 4.2). The preservation of fluvial bedding features, lenses of coarse sand and gravel, and thinly laminated clay from underlying swampy meadow sediment interbedded with fine sand alluvium (FIGURE 4.4a–d; APPENDIX A) are consistent with the

thick surficial sandy sediment deposits being the result of sediment erosion and transport by fluvial processes. While preserved bedding features are common, they are not ubiquitous.

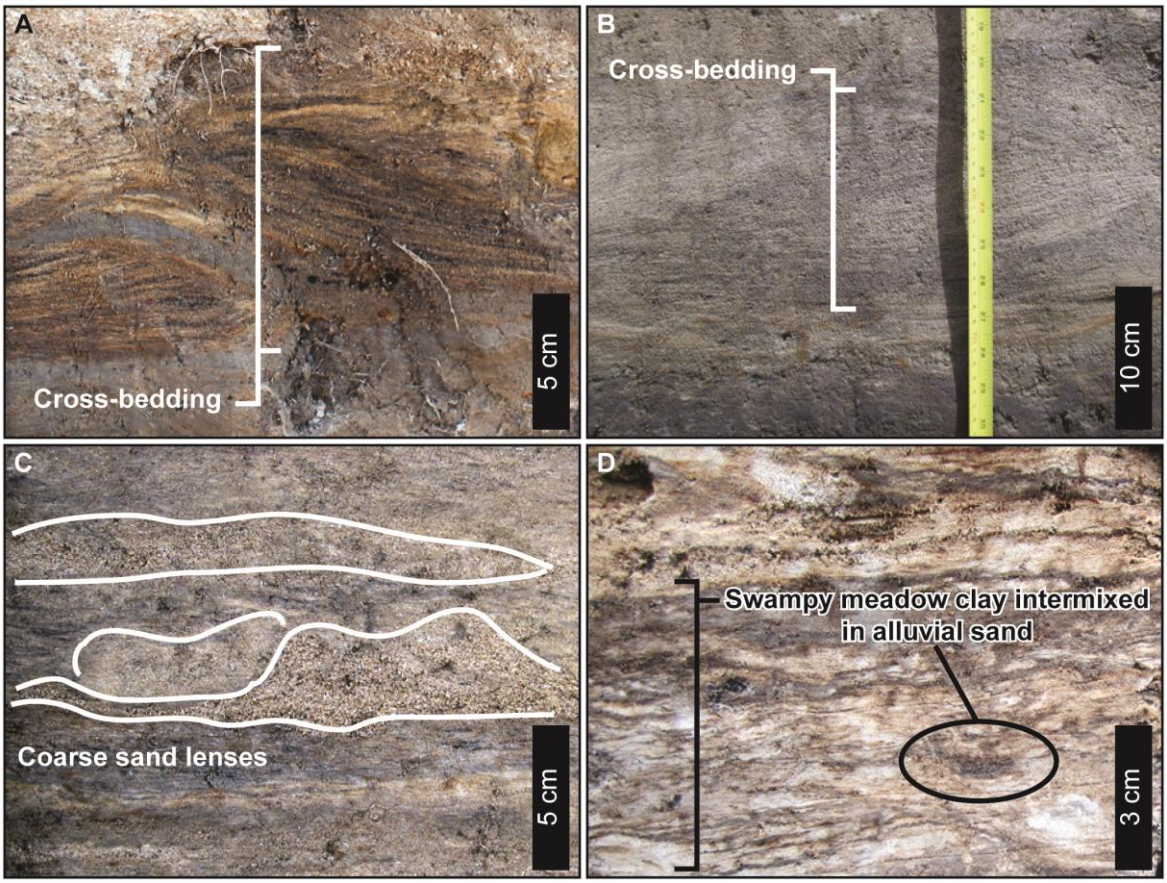

FIGURE 4.4
*Photographs of **A.** cross bedding at Fenwick Creek, **B.** cross bedding at Matong Creek, **C.** coarse sand lenses at Mulwaree River, and **D.** swampy meadow clay mixed and deposited along with sand at Phils River in thinly laminated bedding structures.*

4.4.1 PORTABLE OSL DATA REPRODUCIBILITY

Evidence of Muñoz-Salinas et al.'s (2014) profile, GGC-P3, originally sampled in 2009 along Grabben Gullen Creek had been washed away by a flood in December 2010 (pers. comm. Phillip McGaw, 04 August 2012) that also washed out a farm bridge 5 m above the normal low water level on Grabben Gullen Creek. Data from the resampled Grabben Gullen Creek profile thus come from the same sandy deposit, ~10 m downstream of the GGC-P3 profile. Both bulk IRSL and BLSL measurements increase significantly across the transition from what Muñoz-Salinas et al. interpret as swampy meadow deposits to overlying sandy sediment at 87 cm depth (FIGURE 4.5a). Like Muñoz-Salinas et al. (2014),

resampled bulk OSL data indicate that sandy sediment contains drastically more inherited luminescence than the underlying swampy meadow deposits.

Table 4.2: Portable OSL Reader Sample Site Descriptions

Fig. 1 ID	Sample Site	Latitude (°S)	Longitude (°E)	Upstream Lithologies[a]	Sample Use (*n* =) Bulk OSL	Grain Size	XRD
1	Birchams Creek 1	35.2329	149.3139	Sa	38		
2	Birchams Creek 2	35.2291	149.3156	Sa	30		
3	Birchams Swampy Meadow	35.2313	149.3143	Sa	56		
4	Birchams Regolith	35.2278	149.3174	Sa	34		
5	Breakfast Creek	34.1032	148.7437	Tu, Un	20		
6	Breakfast Flood Deposit	34.1032	148.7437	Tu, Un	27		
7	Brooks Creek (trib.)	35.1141	149.3464	Sa, Gr	29		
8	Fenwick Creek	34.6703	149.6768	Mu, Si, Gr, Ba	31	10	10
9	Georges Plains Creek	33.5239	149.4886	Gr, Mm	20		
10	Gooromon Ponds Creek	35.1981	149.0071	Tu, Mu	32		
11	Grabben Gullen Creek	34.5362	149.1752	Gr, Ms, Ba	120	10	10
12	Grabben Gullen Flood Deposit	34.5378	149.1718	Gr, Ms, Ba	24		
13	Groves Creek	35.0912	149.3533	Sa	24		
14	Grubbenbun Creek	33.6503	149.0425	Gr, Ms	20		
15	Mandurama Ponds Creek	33.6871	149.0874	Gr	30		
16	Matong Creek	36.7383	148.8906	Gr, Ms	37		
17	Matong Hillslope Soil	36.7367	148.8936	Gr	26		
18	Mulwaree River	35.0827	149.6483	Ms, Tu	30	10	10
19	Phils River	34.2397	149.5026	Ms, Gr, Ig, Ba	28		
20	Primrose Valley Creek	35.4403	149.3781	Sa, Mu, Sc	30	10	10
21	Queen Charlotte's Creek	33.6092	149.4222	Un, Gr	20		
22	Ryries Creek	35.7195	149.1699	Sa, Gr, Ig	30		
23	Wangrah Swampy Meadow	35.9113	149.3533	Sa, Gr, Ig	22		
24	Wyagnon Creek	33.2368	149.6478	Sa, Gr	17		

[a] Ba - Basalt; Gr - Granite; Ig - Ignimbrite; Ms - Mixed sedimentary; Mm - Mixed Metamorphics; Mu - Mudstone; Sa - Sandstone; Sc - Schist; Si - Siltstone; Tu - Tuff; Un - Undifferentiated

The most noticeable difference between the resampled profile and the original Grabben Gullen profile is in the uppermost 20 cm of the resampled profile. The highest bulk OSL values measured from resampled sediment (20.7×10^6 and 44.4×10^6 photon counts for IRSL and BLSL, respectively) were at a depth of only 9 cm and constituted a five-fold increase from the bulk OSL measurements at 12 cm. Bulk OSL maxima of an overbank deposit known to be associated with the December 2010 flood (FIGURE 4.5a) are equally as high (17.7×10^6 and 38.8×10^6 photon counts for IRSL and BLSL, respectively), suggesting that the near-surface spike in bulk OSL at the resampled Grabben Gullen Creek site is attributed to the overbank deposition of poorly bleached sediment during the flood. When Muñoz-Salinas et al.'s (2014) data are shifted down-profile to account for the 20 cm of alluvium deposited between sampling years and plotted alongside data from this study, a near-identical profile emerges (FIGURE 4.5a). Unlike the profiles in Muñoz-Salinas et al.

(2014), however, higher resolution sampling in this study reveals more detail in the portable OSL reader data, with data minima being more evident between maxima in resampled data than is apparent in Muñoz-Salinas et al.'s.

4.4.2 PORTABLE OSL DATA FROM FLOOD DEPOSITS

Floods of the scale that inundated Grabben Gullen Creek in 2010 are not rare in the Tablelands region. Bulk OSL was measured from sediment deposited during a flood in February 2012 at Breakfast Creek (FIGURE 4.5b), which exhibits depth profiles similar to those of the swampy meadow-sandy sediment profile in Grabben Gullen Creek. Bulk OSL data from Wyagnon Creek, north of Bathurst, which floods regularly, draining a westward flowing catchment off the Great Dividing Range (FIGURE 4.5c) is also presented. The Wyagnon Creek OSL data show evidence of flood-deposited sediment that carries increasing inherited luminescence as it is deposited, much like the flood deposit at Grabben Gullen Creek.

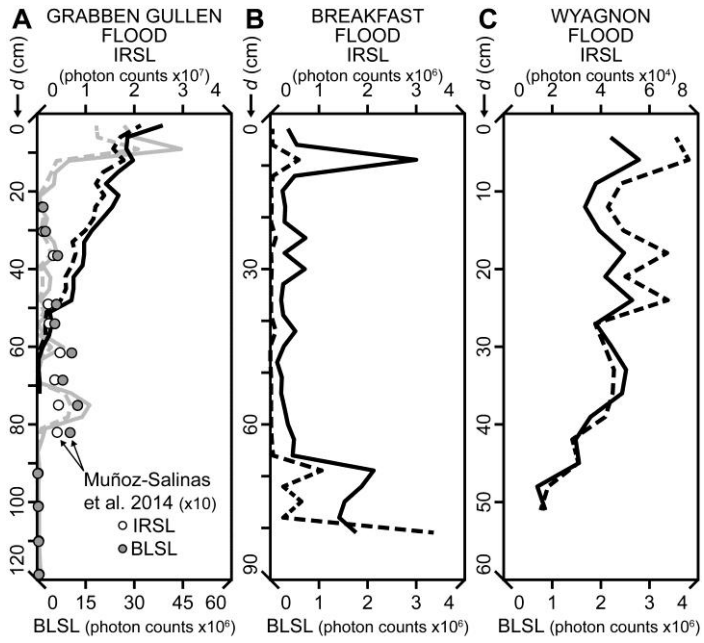

FIGURE 4.5

Bulk IRSL and BLSL data (dashed and solid black lines) from three flood deposits; bulk IRSL and BLSL data tables are found in APPENDIX B. ***A.*** *Bulk luminescence measurements from the December 2010 Grabben Gullen Creek flood deposit collected for this study. Grey dashed and solid lines respectively refer to bulk IRSL and BLSL data from the new Grabben Gullen Creek swampy meadow-PSA profile compared to Muñoz-Salinas et al.'s (2014) IRSL and BLSL data (white and grey circles, respectively), adjusted for an instrumental 10-fold offset (see text).* ***B.*** *Flood deposit associated with the February 2012 flood at Breakfast Creek. Plant roots were found at 80 cm, which is likely the pre-February 2012 flood floodplain surface.* ***C.*** *Uppermost 50 cm of a series of flood deposits at Wyagnon Creek.*

4.4.3 PORTABLE OSL DATA FROM MODERN SWAMPY MEADOWS

Three short cores (~20 cm) were extracted from modern swampy meadow wetlands in Wangrah Creek (FIGURE 4.6a) (Prosser, 1991) to test Muñoz-Salinas et al.'s (2011; 2014) interpretations that the dark sediment exposed in the basal horizons of gully wall stratigraphies at Grabben Gullen Creek are indicative of well-bleached sediments deposited under low energy conditions in swampy meadow environments. The BLSL data from each core (FIGURE 4.6b–d) generally increase systematically with depth with little interruption. The IRSL also generally increases with depth, but is more variable in Cores 1 and 2 than in Core 3. Similar bulk OSL trends were observed over greater depths at Birchams and Mandurama Ponds Creeks (FIGURE 4.6e, f) where swampy meadows have been incised by gullies, but not buried by sandy sediment. Bulk OSL measurements at both of these sites are low at the surface and increase systematically with depth. Surficial sediments in the cores contain almost no luminescence, and the long profiles at Birchams and Mandurama Ponds Creeks likewise exhibit decreasing luminescence upwards to virtually zero luminescence at the swampy meadow surfaces.

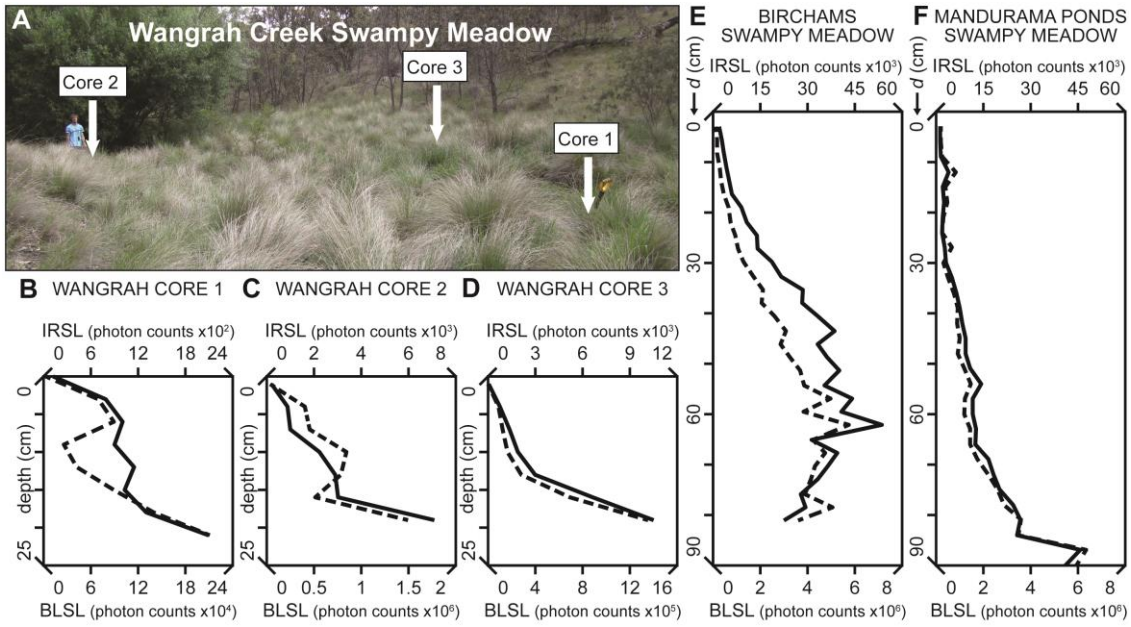

FIGURE 4.6

A. *Photograph of a modern swampy meadow site in the headwaters of Wangrah Creek (person for scale) and the locations of three short cores. Bulk IRSL and BLSL data (dashed and solid black lines, respectively) of* ***B–D.*** *Wangrah Creek Cores 1, 2, and 3, respectively, as well as long profiles of incised but intact swampy meadow exposures at* ***E.*** *Birchams Creek and* ***F.*** *Mandurama Ponds Creek. Bulk IRSL and BLSL data tables are found in APPENDIX B.*

4.4.4 PORTABLE OSL DATA FROM SWAMPY MEADOW–SANDY SEDIMENT DEPOSITS

Each of the sixteen profiles analysed for bulk OSL across the transition from swampy meadow to sandy sediment units exposed in gully wall stratigraphies exhibits a dramatic increase in bulk luminescence (FIGURE 4.7). At some sites, such as Fenwick or Matong Creeks, the increase in luminescence values is immediate whereas at other sites the bulk OSL measurements in the alluvial units increase more gradually to peak values, such as at Birchams 1 or Grubbenbun Creeks, which also exhibit more gradual sedimentary and visual changes from swampy meadow to coarser alluvium. The more abrupt the transition between swampy meadow and overlying alluvium, the closer the bulk OSL maximum is to the lowermost horizon of alluvium (e.g. Georges Plains and Groves Creeks). Sites where the sedimentary boundary between swampy meadow sediments and sandy sediment is distinct, such as at Fenwick, Matong, and Ryries Creeks and Phils River, exhibit bulk OSL profiles that spike immediately at the sedimentary change. However, the visible sediment boundaries at Mulwaree River and Primrose Valley Creek are sharp, yet the underlying swampy meadow sediments do not exhibit systematically decreasing bulk OSL values as would be expected of a swampy meadow; perhaps an example of poorly bleached alluvium mixing with well-bleached swampy meadow sediments or mineralogical changes.

The IRSL:BLSL ratio was examined to assess whether or not this ratio reflects a sample's mineralogy. The IRSL:BLSL ratio at nearly every site also exhibits a marked change at or near the visible sedimentary transition (FIGURE 4.7). IRSL:BLSL ratio measurements from drainage basins underlain by single lithologies (e.g. tributary to Brooks, Fenwick, and Matong Creeks) tend to change the least throughout the swampy meadow-sandy sediment profiles, but this is not always the case. For instance, even though the bedrock in Birchams Creek is monolithologic, the IRSL:BLSL values at Birchams Creek 1 range from ~0.00–0.04 and change quickly over short depth intervals whereas the IRSL:BLSL values at Birchams Creek 2 consistently yields values of ~0.01 at all sampled depths. Though Gooromon Ponds Creek is monolithologic, its ratios change often while the ratios from Georges Plains Creek are fairly consistent even though its catchment area is multilithologic.

4.4.5 PORTABLE OSL DATA AND BULK SEDIMENT MINERALOGY

Rietveld refinement of X-ray diffractograms from every third sample at Fenwick, Grabben Gullen, and Primrose Valley Creeks and Mulwaree River provides an approximation of mineral phase abundance in each sample. The IRSL:BLSL ratios should be positively correlated to the non-quartz:quartz ratios because the BLSL component from feldspars is bleached during the IRSL measurement, which comes before BL stimulation in the portable OSL reader stimulation steps (TABLE 4.1); thus, all measured BLSL should be derived from quartz. No such correlations are observed, however (FIGURE 4.8), except for a weak but significant negative correlation in sediment from Grabben Gullen Creek, which is counterintuitive to expectations. Individual non-quartz mineral phases were examined to assess whether the IRSL signal is coming from only one non-quartz mineral phase (FIGURE 4.9) and find that the IRSL:BLSL ratio at Primrose Valley Creek is strongly and positively correlated with the albite:quartz ratio. Primrose Valley Creek is the only site where an individual non-quartz mineral phase improves the correlation; albite is present at Fenwick Creek and Mulwaree River, but it does not strengthen the correlation between the IRSL:BLSL and non-quartz:quartz ratios.

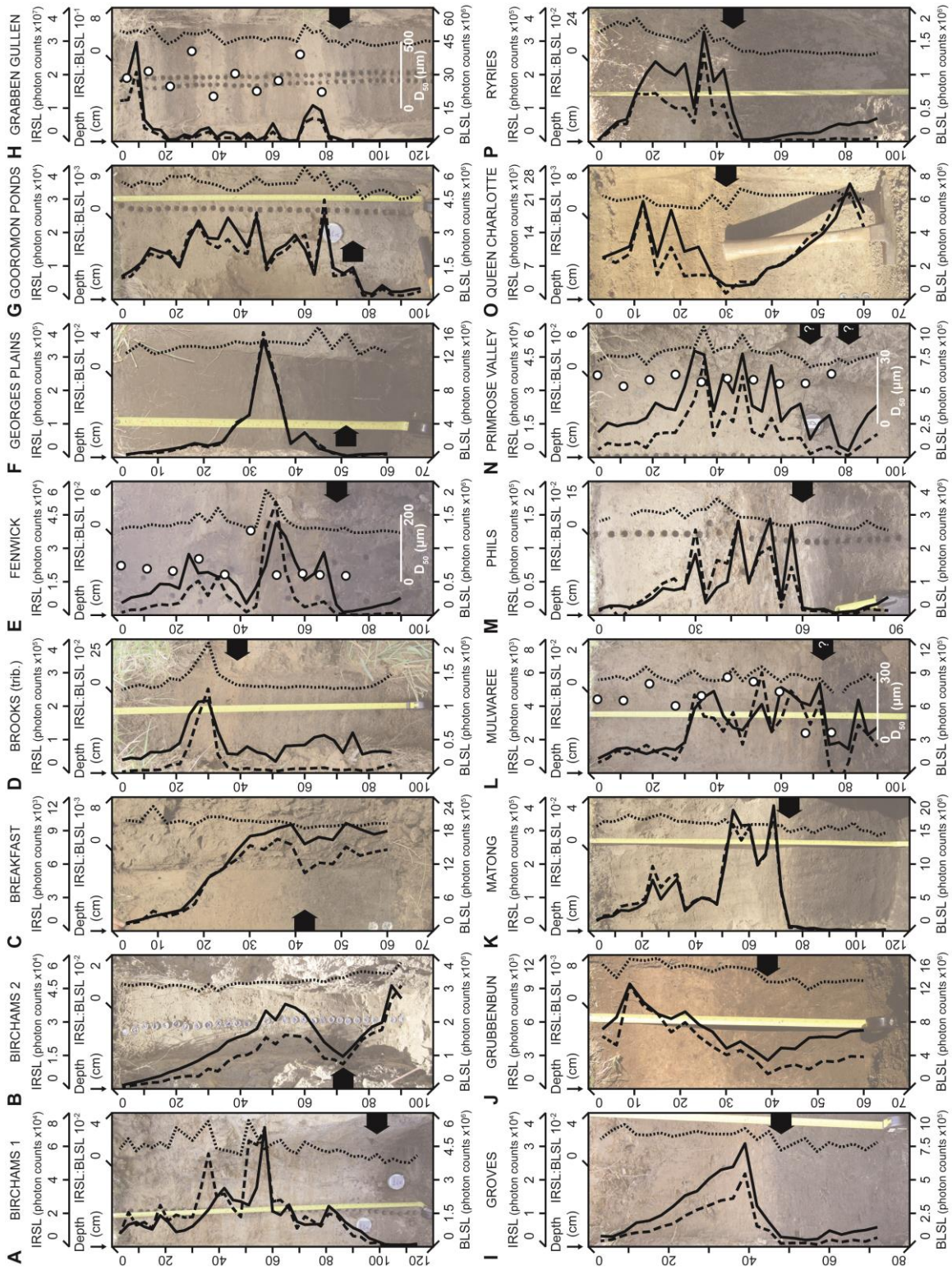

FIGURE 4.7

Bulk IRSL and BLSL measurements (dashed and solid black lines) and the IRSL:BLSL ratio (dotted black line) at each of the sixteen gully exposures of swampy meadow sediments overlain by sandy post-swampy meadow sediment. Field photos of each profile are shown in the background to scale so the transition from dark swampy meadow sediments to lighter post-swampy meadow sediments (thick black arrows) as indicated by bulk luminescence measurements can be observed. Black arrows with question marks at Mulwaree River and Primrose Valley Creek indicate potential, but uncertain, swampy meadow-PSA transition depths. Results from grain size analysis (white circles) are shown at Fenwick Creek, Grabben Gullen Creek, Mulwaree River, and Primrose Valley Creek. White axes show the range of D_{50} values at these four sites. Bulk IRSL, BLSL, and grain size data tables are found in APPENDIX B.

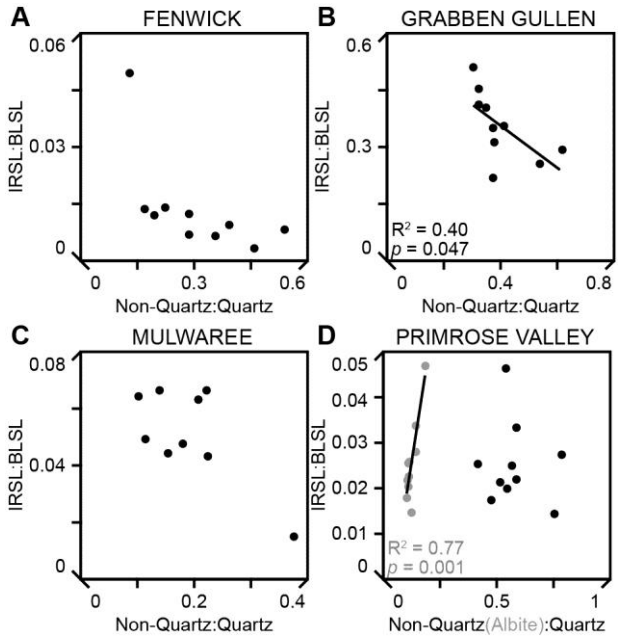

FIGURE 4.8

*A subset of samples from **A.** Fenwick Creek, **B.** Grabben Gullen Creek, **C.** Mulwaree River, and **D.** Primrose Valley Creek highlighting the lack of positive correlations between bulk IRSL:BLSL ratios and non-quartz:quartz ratios. At Primrose Valley Creek, the expected positive correlation is only observed when IRSL:BLSL ratios are compared to the albite:quartz ratio. Bulk IRSL, BLSL, and XRD data tables are found in APPENDIX B*

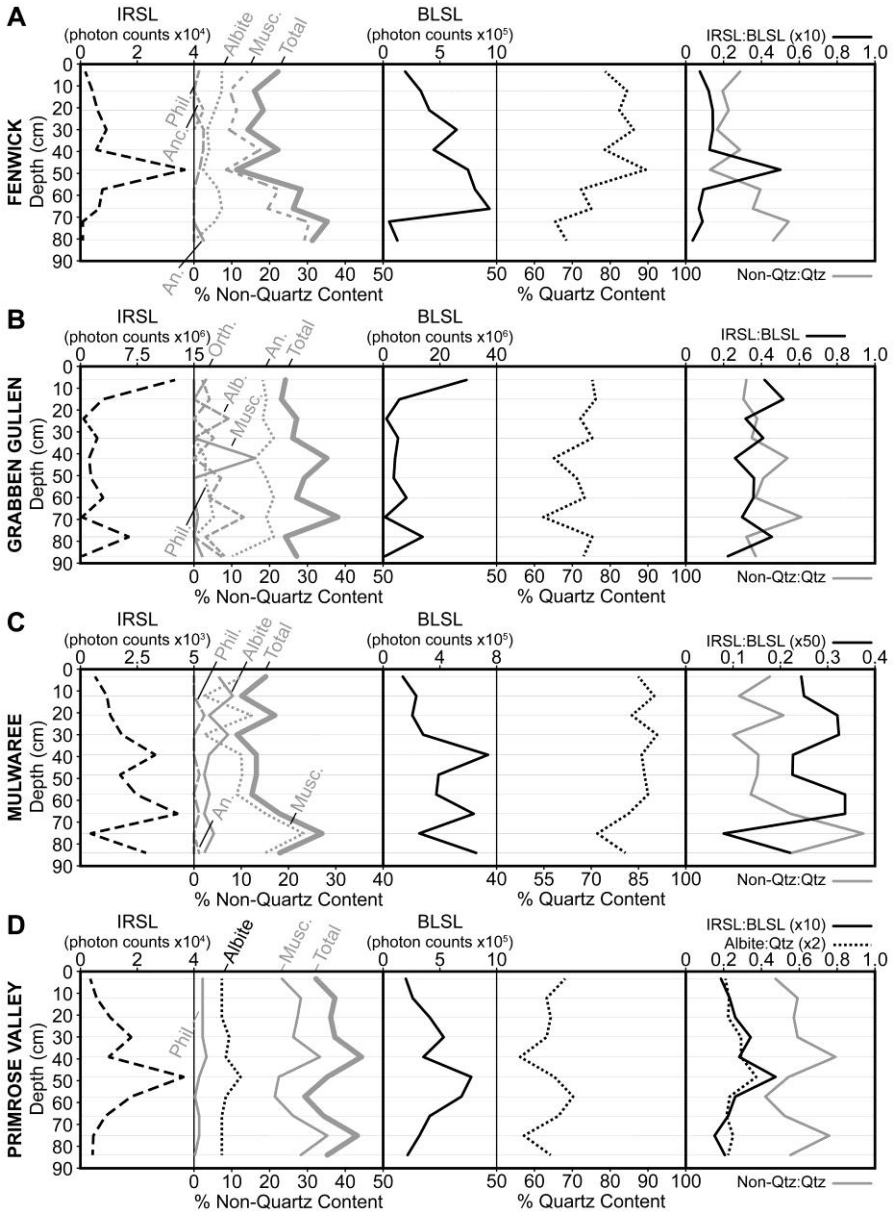

FIGURE 4.9

*X-ray diffraction results for **A.** Fenwick Creek, **B.** Grabben Gullen Creek, **C.** Mulwaree River, and **D.** Primrose Valley Creek. Abbreviated bulk IRSL and BLSL depth profiles are shown (dashed and solid black lines, first and third panels, respectively). At no site does any non-quartz mineralogy resemble the bulk IRSL depth trend, except albite at Primrose Valley Creek. Bulk IRSL, BLSL, and XRD data tables are found in APPENDIX B*

4.4.6 PORTABLE OSL DATA AND BULK SEDIMENT GRAIN SIZE

At some sample sites, changes in IRSL and BLSL values correspond to distinct sedimentary boundaries (e.g. Birchams 1 and Grabben Gullen Creeks), which suggests that bulk OSL measurements may be indicators of dominant grain size. However, there is no correlation between the average grain size (D_{50}) of each sample used for mineralogical determinations and bulk OSL data (FIGURE 4.10), though depth plots of D_{50} (FIGURE 4.7)

indicate that increases in the D_{50} value might be associated with increases in the bulk OSL data at Fenwick and Grabben Gullen Creeks and Mulwaree River (FIGURE 4.7e, h, l), though there is some offset between the two profiles. There is little change in D_{50} values at Primrose Valley Creek throughout the profile (FIGURE 4.7n) even though there are large changes in bulk OSL values with depth. Nevertheless, it seems clear that no specific information on grain size can systematically be inferred from portable OSL data, nor is grain size an indication of bulk OSL.

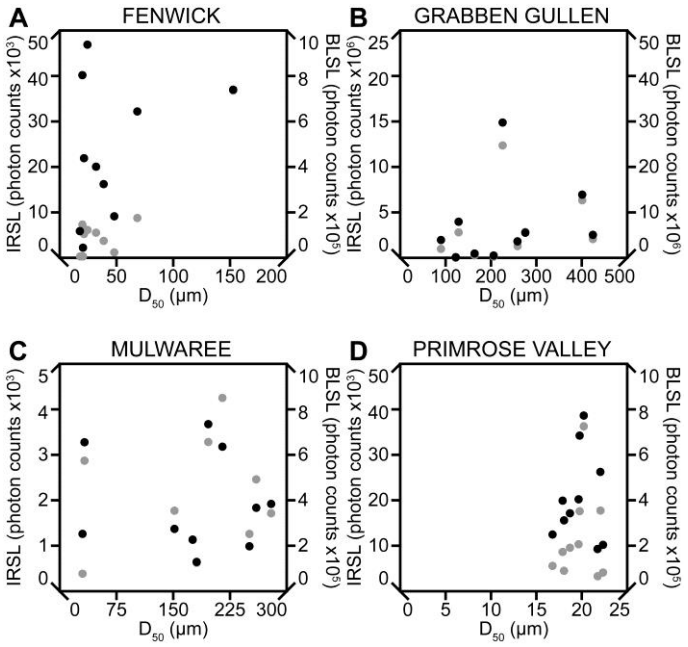

FIGURE 4.10
No relationships between average grain size (D_{50}) and either bulk IRSL (grey dots) or BLSL (black dots) at ***A.*** *Fenwick Creek,* ***B.*** *Grabben Gullen Creek,* ***C.*** *Mulwaree River, or* ***D.*** *Primrose Valley Creek.*

4.4.7 ADJACENT PORTABLE OSL SAMPLE REPLICATE MEASUREMENTS

To further investigate the causes of maxima and minima in bulk OSL profiles, sample replicates adjacent to bulk OSL profiles at Fenwick Creek were collected. Swampy meadow replicates at depths >70 cm at Fenwick Creek closely agree in both bulk IRSL and BLSL measurements, probably reflecting complete pre-depositional bleaching in these low energy environments (FIGURE 4.11a). Between 70 cm and 20 cm depth at Fenwick Creek, IRSL and BLSL measurements are highly variable, which is consistent with the expectation that the alluvium in this depth interval is not well bleached during floods. BLSL measurements converge on similar values in the top 20 cm of the Fenwick Creek profile; IRSL measurements also converge on similar values in the top 20 cm of Fenwick

Creek except at 12 cm depth. Since there are no mineralogical changes in the upper 20 cm of the Fenwick Creek profile, and since constant D_{50} values indicate that stream flow velocity did not diminish at these depths, changes in bulk OSL measurements must reflect an increase in bleaching effectiveness. Sample replicate measurements at Mulwaree River do not demonstrate the same results as at Fenwick Creek. Few of the IRSL replicates converge on the mean IRSL value at any given depth, and only BLSL replicates in the uppermost 30 cm of the profile show little variability (FIGURE 4.11b). However, like Fenwick Creek, the D_{50} value of the uppermost 30 cm of Mulwaree River profile is greater than for depths >65 cm meaning that the tightness of BLSL replicates at the top of the profile represents a return to more effective quartz bleaching conditions than changes in stream flow velocity.

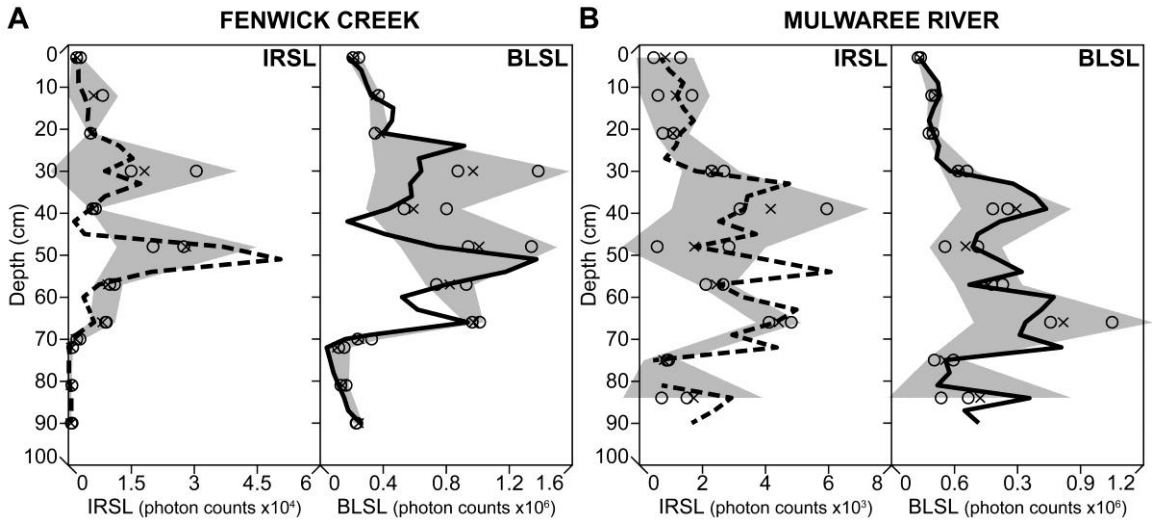

FIGURE 4.11

*Main profile bulk IRSL and BLSL measurements (dashed and solid black lines, respectively) for **A.** Fenwick Creek and **B.** Mulwaree River. Replicate samples collected at every 9 cm (open circles) and the average of replicates (x) are plotted with depth alongside the main profile. Grey shaded region represents the 2σ standard deviation of replicate samples at each depth they were collected and may be an indicator of good (small standard deviations) or poor (large standard deviations) bleaching conditions. Bulk IRSL and BLSL data tables are found in APPENDIX B.*

4.4.8 PORTABLE OSL DATA FROM UNERODED HILLSLOPES AND VALLEY BOTTOMS

A bulk OSL profile was collected through granitic hillslope soils at Matong Creek and weathered sandstone valley bottom soils at Birchams Creek (FIGURE 4.12). Like modern and uneroded swampy meadow profiles (FIGURE 4.6), the hillslope profile from Matong Creek has little luminescence at the surface and increases systematically with depth to the

soil-saprolite boundary (FIGURE 4.12b) (Wilkinson and Humphreys, 2005). The Matong hillslope profile also resembles hillslope soil profiles from various lithologies in Grabben Gullen Creek (Muñoz-Salinas et al., 2014), a consistency expected of sandy valley bottom deposits throughout the Tablelands if they were soils formed from weathered bedrock. The uneroded valley bottom profile from Birchams Creek does not decrease toward zero-luminescence at the profile surface, but instead bulges in the uppermost 20 cm (FIGURE 4.12); however, neither of the bulk OSL profiles at Birchams 1 nor Birchams 2 exhibit a similar depth trend, and thus their genesis is different from that of the uneroded valley bottom soil.

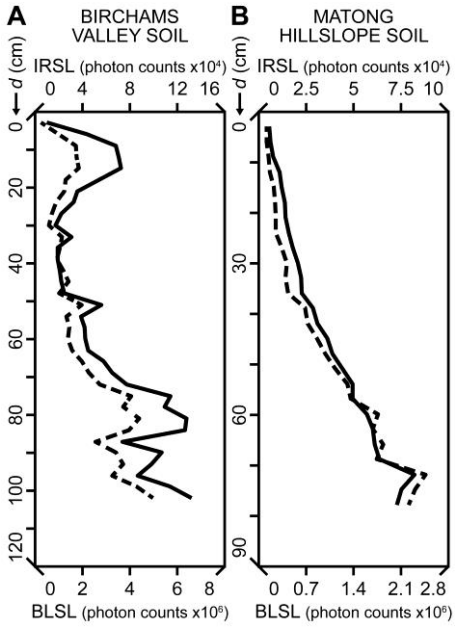

FIGURE 4.12
Bulk IRSL and BLSL (dashed and solid black lines, respectively) collected from uneroded soil profiles at ***A.*** *Birchams Creek sandstone valley bottom soil and* ***B.*** *Matong Creek granite hillslope soil.*

4.5 DISCUSSION OF RESULTS

4.5.1 THE "A" OF PSA

Muñoz-Salinas et al. (2014) identified Grabben Gully Creek valley bottom sediments as alluvium because it was shown that the underlying meta-sedimentary bedrock could not produce the bulk OSL measurements observed in sandy sediment deposits; only the upstream granite soils could produce sediment with similarly high bulk OSL measurements. Though bulk OSL measurements were not used to identify source lithology, the widespread similarity of bulk OSL depth profiles throughout the Tablelands

suggests that the hydrological phenomena that produced these sediments are regional and not unique to Grabben Gullen Creek. Data from this study confirm Muñoz-Salinas et al.'s (2014) interpretation that these sedimentary packages are alluvium and not weathered granitic soils as proposed by Butzer and Helgren (2005). The evidence for the alluvial nature of these sedimentary deposits is not only drawn from field observations of preserved fluvial structures, but also through comparison of bulk OSL measurements with known alluvial deposits, modern swampy meadow accumulations, hillslope soil profiles, and valley bottom soil profiles. Had even a few of the analysed alluvial packages been weathered soils, they would have demonstrated a profile with zero luminescence at the surface and a systematic increase of bulk IRSL and BLSL with depth, such as at all swampy meadow and hillslope profiles, but not a single profile fits this description.

Pickard and Gore and colleagues (Crighton and Gore, 2001; Gore et al., 2000; Pickard, 1994) studied similar deposits in western New South Wales, opting to call those sediments post-European materials since the deposits incorporated sizeable amounts of aeolian sand and dust. While there is almost certainly an aeolian component in these Tablelands deposits (Rowe, 1994), the sediments studied are alluvial and exhibit fluvial sedimentary structures and so 'alluvium' is a suitable description for these materials. The timing of alluvial deposition, pre- or post- European arrival to the Tablelands, is still debated (Johnston and Brierley, 2006; Muñoz-Salinas et al., 2014; Rustomji and Pietsch, 2007; Starr, 1989); thus, for the time being, sediment deposited over swampy meadow sediments in the Tablelands will be referred to as post swampy-meadow alluvium, but the PSA acronym is maintained to remain as consistent as possible with geomorphic studies focused on similar sediment deposits elsewhere in the world (e.g. Booth et al., 2009; Brannstrom and Oliveira, 2000; Kreznor et al., 1990; Magilligan, 1985; Merritts et al., 2011; Wilkinson and McElroy, 2007; Yan et al., 1988).

4.5.2 SWAMPY MEADOWS PRESERVED UNDER PSA

The lack of luminescence at the surface of each swampy meadow site confirms that sediment transport in these low-energy environments must be slow enough to expose transported sediment to sunlight long enough to completely bleach sediments before deposition. Bulk OSL data from modern swampy meadow environments are thus entirely

consistent with Muñoz-Salinas et al.'s (2011; 2014) interpretations. The near complete lack of swampy meadow environments throughout the modern Tablelands and the ubiquity of incised streams – a seemingly new feature to the Tablelands (see Eyles, 1977b; Scott, 2001) – is testament to the degree of geomorphic alteration of the region, whether it was anthropogenically or climatically forced, triggered by some other external drivers, or a combination of all of these. That fossilised relics of swampy meadows are preserved under PSA highlights the observational prowess of the first European explorers, surveyors, and graziers, and their ability to document their surroundings in detail (e.g. Blaxland, 1870; Evans, 1916; Lawson, 1813; Mitchell, 1839a, b; Wentworth, 1813). Furthermore, the ability for quantitative instrumentation like the portable OSL reader to produce and reproduce data, which supports traditionally-held geomorphic notions gives credibility to the technique and its continued use, though there is still much work to be done in understanding what physical sediment characteristics or environmental factors contribute to the observed bulk OSL profile.

4.5.3 RELATIONSHIPS BETWEEN PORTABLE OSL AND BULK GRAIN SIZE

Bishop et al. (2011) reported significant positive correlations between mean grain size and bulk IRSL and BLSL in sediment deposited behind a Scottish mill dam. They suggested that sand, being typically transported as bedload, has a lower chance of being bleached completely and thus carries more inherited luminescence, whereas finer grain sizes are carried higher in the water column and are more exposed to light before reburial. This is a reasonable interpretation, and the lack of similar correlations in Tablelands data is perplexing. Most likely, sediment samples had an insufficient range of grain sizes to produce meaningful correlations, or perhaps the fact that most grain size samples came from flood-deposited alluvium precluded the sort of correlation observed by Bishop et al. (2011). Australian quartz may be more sensitive than Scottish quartz if it has been exposed to stimulation more frequently (Pietsch et al., 2008), and increased sensitivity may lead to the smaller range of observed inherited luminescence. Furthermore, Australian flood waters may just be more turbulent and turbid than Scottish stream flow, and varying sunlight intensity and cloud cover at Scottish and Australian latitudes may preclude any true comparison between the two sites. Widespread flooding of the Mekong River across the Cambodian floodplain, for instance, did not produce systematic relationships between

grain size and bulk OSL measurements (Muñoz-Salinas et al., 2011), so it is likely that the size of the river, flood duration, sediment history, and landscape setting all contribute to relationships between bulk OSL and grain size.

4.5.4 RELATIONSHIPS BETWEEN PORTABLE OSL AND BULK SEDIMENT MINERALOGY

The hypothesis that IRSL would be a proxy for non-quartz minerals and that BLSL would largely come from quartz minerals is inconsistent with the lack of relationship between mineralogy and bulk OSL measurements. This was surprising considering the analytical procedures used should have bleached non-quartz minerals before quartz. The parallelism between the albite and IRSL depth profiles at Primrose Valley Creek is what was expected at all sites; however, not even the grouping all feldspars together as the main contributor to IRSL measurements could reproduce the relationship as albite at Primrose Valley Creek. Muscovite was present in samples from each site and dominated the non-quartz mineralogy, yet the muscovite depth profile did not resemble the IRSL depth profile at any site. Muscovite is known to emit luminescence under blue light conditions (Kortekaas and Murray, 2005), and it might be argued that muscovite contributes more luminescence to the BLSL measurement than to the IRSL measurement. The depth profile of muscovite at all sites resembled the BLSL depth profile just as poorly as it represented the IRSL profiles – that is to say, muscovite does not appear to exert any control of measured bulk OSL data.

4.5.5 PORTABLE OSL OF ADJACENT SAMPLE REPLICATES

The variability of adjacent sample replicates seems to be much more related to bulk OSL depth trends than either grain size or mineralogy. Luminescence variability in adjacent replicate samples at any given depth also provides a good indication of sediment transport conditions and bleaching effectiveness. The small standard deviations in IRSL and BLSL measurements of Fenwick Creek swampy meadow sediment are consistent with Muñoz-Salinas et al.'s (2014) interpretation that swampy meadow sediment is well bleached and the measured bulk OSL is solely from post-depositional accumulation of luminescence.

Though similarly small standard deviations are determined for the uppermost 20 cm of the Fenwick Creek profiles and the top 30 cm of the Mulwaree River BLSL profile, grain sizes in these PSA sediments are greater than in swampy meadow sediments, indicating that high velocity flow continued to the top of the PSA. The decrease in bulk BLSL at the shallowest depths in both profiles and in bulk IRSL at the shallowest depths at Fenwick Creek must reflect the following, perhaps in combination: more complete sediment bleaching, shallowing or declining turbidity of flows in a previous flood, or an increase in post-storm sunlight intensity. The uppermost portion of nearly all sampled profiles exhibit the same general decrease in bulk OSL with decreasing depth, signalling that enhanced post-flood bleaching conditions are a regional phenomenon.

4.5.6 CRYPTOSTRATIGRAPHIC BOUNDARIES ILLUMINATED BY PORTABLE OSL DATA

Mulwaree River and Primrose Valley Creek are examples of how a visual inspection of a sediment profile in the field alone might lead to misinterpreted depositional histories if not supplemented with quantitative data like bulk OSL. Profiles at both creeks appear to have abrupt transitions from swampy meadow sediments to PSA (72 cm and 69 cm depth at Mulwaree River and Primrose Valley Creek, respectively), but swampy meadow sediments below each depth are variable as evidenced by data from sets of replicate samples at Mulwaree River. Whether the transition from swampy meadow to PSA depositional conditions at Primrose Valley Creek (FIGURE 4.7n) is marked by the visible colour transition at 69 cm depth, the cessation of upwardly decreasing bulk OSL measurements at 81 cm depth, or at a depth below the deepest sample cannot be determined. Though the colour transition at 72 cm depth in Mulwaree River sediment (FIGURE 4.7l) seems to mark the change from swampy meadow to PSA depositional conditions, replicate samples at depths >72 cm do not agree nor does the bulk OSL decrease upwardly between 90 cm and 72 cm deep to the colour transition, which suggests that the onset of PSA depositional conditions lies at a depth >90 cm. Rustomji and Pietch (2007) used OSL dating techniques at Mulwaree River and the portable OSL reader Mulwaree River profile for this study is within 1 m of their profile, WP5, whose sample holes were still visible during the October 2012 field campaign. Rustomji and Pietch's sample, WP5-85, was collected below the visible colour transition and yields a single-grain OSL burial age of AD 1841–1881, which

is more similar to the ages determined for PSA at depths <72 cm than of the swampy meadow age at ~110 cm depth, suggesting that while the burial age of this sample is valid, it was likely collected from sediment falsely inferred to be from a swampy meadow environment.

4.5.7 SWAMPY MEADOW EROSION DURING PSA DEPOSITION

Profiles where the underlying swampy meadow sediment bulk IRSL and BLSL measurements are near zero (i.e. completely bleached) at the onset of alluvial deposition likely represent an uneroded valley bottom surface (e.g. Georges Plains, Matong, and Ryries Creeks, and Phils River). Sites where the uppermost swampy meadow sediment has significant non-zero bulk OSL measurements (e.g. Birchams 2, Breakfast, Grubbenbun, and Queen Charlotte Creeks) may be attributed to erosion of swampy meadow before PSA deposition, a cessation of swampy meadow sedimentation before PSA deposition, considerable post-depositional accumulation of luminescence, or a heightened dose rate relative to PSA dosimetry. If a site with non-zero luminescence in the uppermost swampy meadow horizon can be shown to have had minimal post-depositional accumulation of luminescence and an insignificantly distinct dosimetry from the overlying PSA, the depth of swampy meadow erosion may be estimated by finding the y-intercept on the depth axis of a line fitted through the swampy meadow bulk OSL data. I interpret sites where near-zero bulk luminescence measurements are observed (e.g. Birchams 1 and Groves Creeks, Phils River) to represent a mixing layer of eroded swampy meadow sediment and some PSA without significant loss of swampy meadow sediment.

4.5.8 LIMITATIONS OF PORTABLE OSL READERS

Of all possible factors contributing to the observed depth trends in each bulk OSL profile, the most important are the duration and the dose rate of ionising radiation from surrounding sediment. Alpha, beta, and gamma radiation account for the dosimetry of measured sediment samples over different distances (Aitken, 1998), and is difficult to constrain for each sample at such close sampling intervals. Moreover, the cosmic ray dose

contribution at each site (Prescott and Hutton, 1988, 1994) is difficult to determine, or even estimate, without knowing or reasonably being able to infer sediment accumulation and erosion histories for each profile. Analysing OSL data to such an extent is beyond the scope of this study, and counterintuitive to the intended use of the portable OSL reader as a quick, field-based estimation of bulk luminescence. A full analysis of PSA burial ages using OSL dating techniques is presented in CHAPTER 6.0.

4.6 CHAPTER CONCLUSIONS

The utility of a portable OSL reader as a field-based quantitative instrument is demonstrated and used to identify swampy meadow and PSA deposits throughout the southeastern Australian Tablelands. Portable OSL reader data are reproducible on the same sedimentary deposit at Grabben Gullen Creek even after three years and after a large flood inundated parts of the catchment with channel migration eroding the original profile. PSA deposits throughout the region are in fact alluvial, likely eroded, transported, and deposited under similar conditions, and bury swampy meadow sediments that previously blanketed valley bottoms throughout the region. These sandy sediment deposits are not weathered soils as some have postulated. While portable OSL readers, on the basis of the data presented here, do not provide insight to sediment mineralogy, associations between blue-light stimulated luminescence and quartz content are observed, and in some cases individual non-quartz mineral phases may supply the majority of infrared stimulated luminescence. There appear to be no relationships between bulk OSL data and mean sediment grain size; however, observations of changing luminescence measurements at depths where grain size remains constant can be used to make inferences about overall bleaching effectiveness in a stream at the time of sediment deposition. Bleaching effectiveness appears also to be closely related to the variability of bulk OSL measurements from sample replicates. The portable OSL reader is indeed useful, especially in making field-based interpretations of the nature of sediment transport and deposition that are not clearly evident in a sediment profile. The portable OSL reader shows particular promise in identifying sediment horizons that are more completely bleached than others and can aid in locating the more appropriate profile depths for collecting burial age OSL samples (see CHAPTER 6.0).

Sedimentary deposits in the Tablelands are clearly alluvium, but where did they come from? And what erosional process led to their deposition?

CHAPTER

HOW DO GULLIES IN THE TABLELANDS FORM? BIRCHAMS CREEK: A CASE STUDY

5.1 THE ROLE OF LAND USE CHANGE IN GULLY DEVELOPMENT

Erosional gullies are caused by natural (Cox et al., 2010; Eriksson et al., 2006; Voarintsoa et al., 2012) and anthropogenic processes often involving land use changes that reduce native vegetation cover, such as deforestation, trampling, overgrazing, and agro-farming (Eyles, 1977b; Knox, 2006; Mieth and Bork, 2005; Molina et al., 2009; Nyssen et al., 2004; Reusser and Bierman, 2010; Stankoviansky, 2003; Turkelboom et al., 2008). Landscape recovery in gully-affected terrain is not easily or cheaply facilitated (Booth et al., 2009; Merritts et al., 2011; Valentin et al., 2005), though revegetation of degraded areas can often bring erosion rates down to pre-disturbance levels (Dlapa et al., 2012; Prosser et al., 1995; Vanacker et al., 2007; Zierholz et al., 2001). Existing topographic threshold models attempt to predict where gully incision might initiate (Poesen et al., 2003 and references therein; Vandaele et al., 1996), and many studies have shown gully walls and beds to be the source of the majority of sediment produced from landscapes already affected by gullies (Krause et al., 2003; Olley et al., 1993; Whitford et al., 2010). Being able to identify where present gullies initiated would be useful in deciding what erosion prevention measures might be used in an erosion prone landscape and where to apply these

measures, but no studies demonstrate a procedure to retrospectively identify where gullies originally initiated in historical times.

The causes, timing, and processes of gullying have been extensively studied on the southeastern Australian Tablelands (e.g. Gillespie, 1981; Olley et al., 1993; Prosser and Slade, 1994; Wasson et al., 1998) along with the relationship between gullying and mantles of alluvium downstream (see CHAPTER 4.0) (Muñoz-Salinas et al., 2014; Rustomji and Pietsch, 2007; Starr, 1989). The processes of continued headward and lateral expansion of existing gully systems and the resultant higher sediment yields are also well understood (Adamson, 1974; Crouch, 1987; Eyles, 1977a; Neil and Fogarty, 1991; Olley et al., 1993; Olley and Wasson, 2003); however, catchment conditions leading to initial gully incision are often overlooked (Prosser and Slade, 1994; Prosser and Winchester, 1996), though they typically involve vegetation disturbance along valley sides and bottoms (Eyles, 1977a; Prosser, 1991; Zierholz et al., 2001). Such disturbances were likely introduced by European settlers in the early- to mid- AD 1800s (Eyles, 1977b; Scott, 2001; Warner, 1984) (see CHAPTER 6.0), though this is not yet confirmed.

Overland flow is often cited as the main driver of gully incision (Prosser and Abernethy, 1996). The impermeable, water-saturated condition of swampy meadow landscapes has the potential to increase rainfall runoff, producing the shear stress required to overcome the shear strength of the ground cover, thus initiating incision (Prosser, 1991). However, field-based flume experiments on swampy meadow plots in the headwaters of Murrumbateman Creek near Canberra, Australia (Prosser and Slade, 1994), show that swampy meadow soils are resistant to incision and that only a combination of heavy degradation of vegetation and increased discharge is associated with gully incision, whereas the increased light to moderate fire activity since the mid-Holocene (Hughes and Sullivan, 1981; Mooney et al., 2011) or increased grazing activity could not. The observation that newly-established swampy vegetation in modern gully beds can withstand modern floods, thereby aiding in landscape recovery (Zierholz et al., 2001), supports the argument that swampy meadows are not likely to be the site of initial gully incision in the Tablelands. Moreover, Wasson et al. (1998) suggest that alluvium is more likely derived from previously-deposited valley fill such as weathered regolith or hillslope colluvium, but this has not been tested.

Gully incision often occurs within five years of landscape disturbance (Prosser and Soufi, 1998), and while gully-derived alluvium can be transported kilometres downstream (Muñoz-Salinas et al., 2014; Rustomji and Pietsch, 2007), the majority of eroded sediment remains close to its source (Melville and Erskine, 1986). In this chapter, I seek to retrospectively identify the initiation point of gully erosion in a small catchment on the southeastern Australian Tablelands by analysing bulk optically stimulated luminescence (OSL) and measuring concentrations of meteoric ^{10}Be – both of which have characteristic profiles with depth (Graly et al., 2010; Wilkinson and Humphreys, 2005) – in proximal downstream alluvial deposits and in potential upstream source locations, each situated in a different valley bottom substrate. In doing so, potential gully initiation scenarios for Birchams Creek, and likely gullies throughout the Tablelands, will be validated or refuted. Methods presented in this chapter have the potential to be easily used in gullied landscapes around the world as a way to identify erosion-prone hotspots within drainage basins and to help focus effective soil erosion prevention and maintenance efforts on these hotspots.

5.2 BIRCHAMS CREEK

5.2.1 SITE DESCRIPTION

Birchams Creek is a headwater tributary of the Yass River at the locality of Wamboin, NSW, about 15 km northeast of Canberra in the Australian Capital Territory (FIGURE 5.1a). Eyles (1977a) studied a chain of ponds in Birchams Creek and its evolution into a continuous gully system (FIGURE 5.1b) – a process that is thought to occur in creeks throughout the Tablelands region. The first surveys of the creek in AD 1880 show swampy meadows and chains of ponds existing within the lower reaches of the creek before trees were ringbarked and cleared in the early AD 1900s (Eyles, 1977a). The timing of initial gully incision throughout the southeastern Australian Tablelands is constrained in CHAPTER 6.0, and single-grain OSL ages for swampy meadow sediment (SM) and post swampy-meadow alluvium (PSA; see CHAPTER 4.0) deposition in Birchams Creek (samples BIRC-A and BIRC-B in CHAPTER 6.0) indicate continued swampy meadow accumulation in the catchment until AD 1902–1919 while PSA was deposited along the valley bottom between AD 1914–1932.

Birchams Creek drains a 3.8 km^2 catchment, completely underlain by the Adaminaby Group – a turbiditic sandstone sequence. The lithologic homogeneity within Birchams Creek is useful in that variations in the luminescence properties and meteoric ^{10}Be concentrations of sediment within the catchment are more likely to result from environmental changes, not lithology. Birchams Creek has a single main channel that eliminates the need to be concerned with sediment from two sources being mixed before being deposited as PSA; in this way, the extent of alluvium deposition is known and potential sediment source locations are limited.

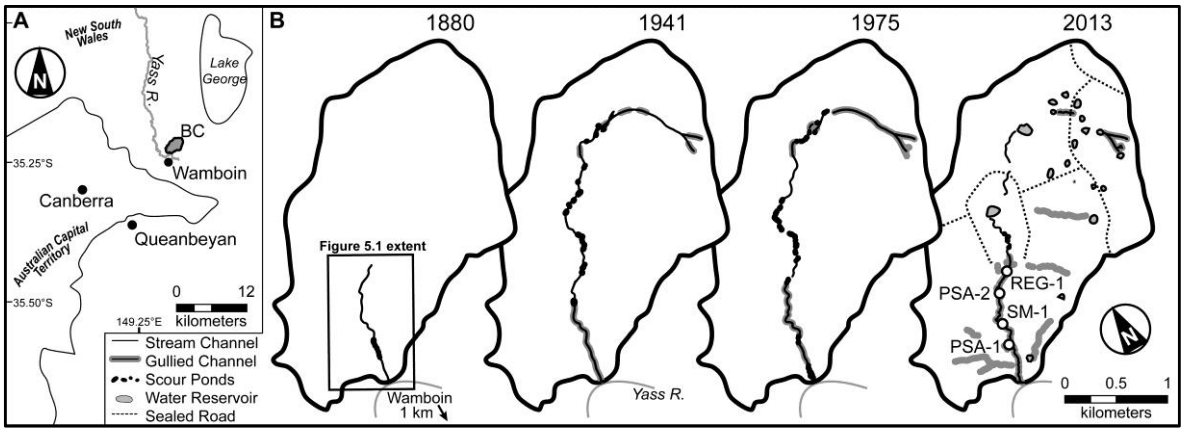

FIGURE 5.1

A. *The Birchams Creek watershed (BC, shaded grey) is a tributary of the Yass River, located halfway between Canberra in the Australian Capital Territory (ACT) and Lake George. Locations of Queanbeyan and Wamboin, New South Wales (NSW) are given for geographic reference.* ***B.*** *Four-step time series illustrating the development of Birchams Creek from a chain of ponds to a gullied watercourse. The AD 1880, 1941, and 1975 time-steps are adapted from Eyles (1977a) and the AD 2013 time-step is drawn from satellite imagery and field site visits. The trapping of sediment by farm dams (reservoirs) and sealed roads across the valley bottom is evidenced by the decrease in gully connectivity during AD 1975–2013.*

5.2.2 A TIMELINE OF GULLY EROSION

Local landowners described a headward migrating gully at the mouth of Birchams Creek as early as AD 1910 (Eyles, 1977a), though the gully head's position at that time is unclear. The lower 1.4 km of the creek is presently one continuous gully; chains of ponds and swampy meadows are present above the modern gully's head. For much of the length of the gully, dark, clay-rich swampy meadow sediment is exposed in gully walls (FIGURE 5.2) from the creek bed, on bedrock in places, to the present ground surface (e.g. at site SM-1, FIGURE 5.1b). PSA is a sandy loam with lenses of gravel exposed unconformably on top of swampy meadow sediments in the lower and middle reaches of Birchams Creek (e.g. sites PSA-1 and PSA-2, respectively, FIGURE 5.1b, 5.2) and can be >1 m thick. PSA

deposits cover 570 m^2 at PSA-1 and 270 m^2 at PSA-2 (approximated from DEM tiles with basin slopes ≤1° using 1-arcsecond SRTM elevation data) (Gallant et al., 2011). Because both the SM and PSA are incised by the gully at PSA-1, PSA deposition must have occurred before the main gully head reached this portion of the catchment. Thus, there must have been gully erosion upstream in order to produce the PSA. Swampy meadow sediments are not found upstream of the upper PSA depositional area (PSA-2); rather, the upper-valley is underlain by weathered regolith of the Adaminaby Group and by older hillslope deposits at and upstream of site REG-1 (FIGURE 5.1b).

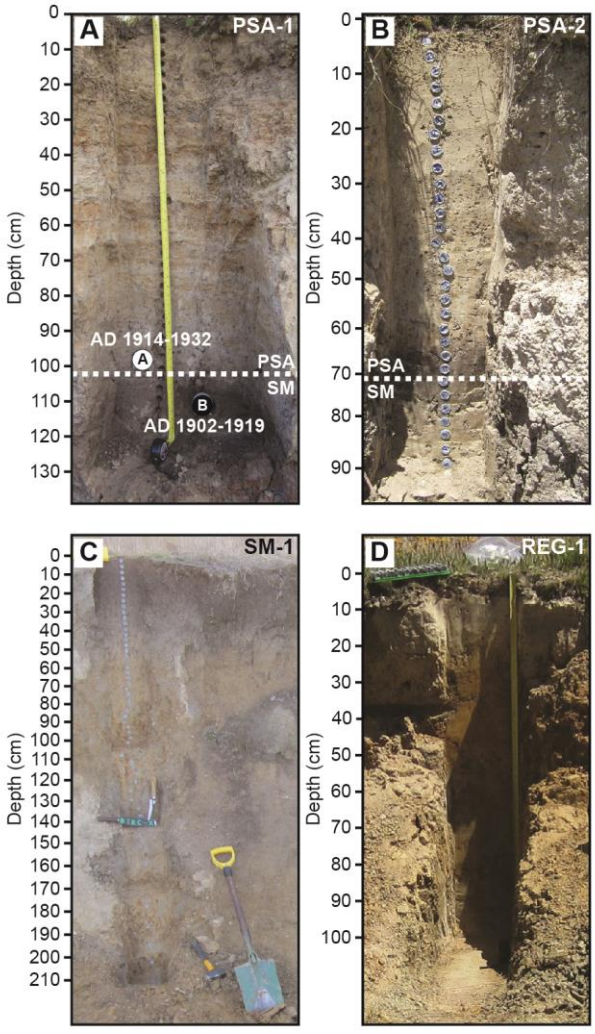

FIGURE 5.2
*Photos of sediment profiles for **A.** PSA-1, **B.** PSA-2, **C.** SM-1, and **D.** REG-1. Vertical axes are not to scale due to oblique photograph angles. Single-grain OSL burial ages of post-European settlement alluvium and swampy meadow sediments at PSA-1 are from CHAPTER 6.0. Dashed white lines at PSA-1 and PSA-2 indicate the bulk OSL transition depth from swampy meadow to post-European settlement alluvium sediment accumulation.*

5.2.3 HYPOTHETICAL GULLY FORMATION SCENARIOS

The distribution of PSA, swampy meadow sediments, and regolith in Birchams Creek provides a natural laboratory to test whether PSA is derived from SM sediment or regolith and addresses the question of where initial gully erosion within the creek began. The majority of sediment transported out of modern gully systems comes from gully bed and gully bank erosion with minimal sediment being derived from hillslopes (Neil and Fogarty, 1991; Olley et al., 1993). Assuming, then, that all PSA comes from valley bottom erosion, and not hillslopes, there are two possible PSA deposition histories at Birchams Creek:

In the discontinuous gully erosion model (DGEM), gully erosion could have initiated at SM-1 and deposited alluvium at PSA-1 at the same time that gully erosion initiated at REG-1 and deposited alluvium at PSA-2 (FIGURE 5.3a). Alternatively, in the single site erosion model (SSEM), gully erosion could have initiated at REG-1 and deposited alluvium at PSA-1 and PSA-2 (FIGURE 5.3b). In the DGEM, eroded sediment is transported along the modern stream channel and incised by headward erosion of the AD 1910 gully. In the SSEM, eroded sediment from REG-1 is deposited down the middle of the valley and headward erosion of the AD 1910 gully erodes away from PSA-1 into SM sediments and then back into PSA-2. Prosser's (1991; 1994) theories of gully development in the Tablelands would be most closely represented by the DGEM in that this is the only scenario tested here where PSA could be derived from erosion of swampy meadow soils.

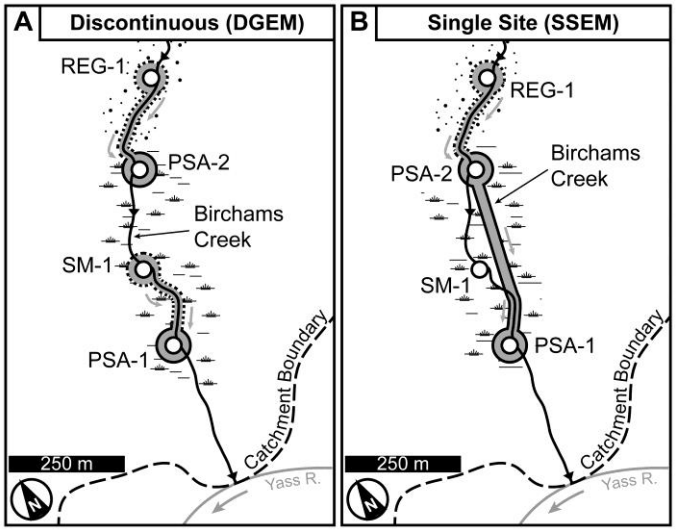

FIGURE 5.3
Schematic diagrams of profile locations and initial gully erosion scenarios at Birchams Creek. ***A.*** *Discontinuous gully erosion model, and* ***B.*** *Single site erosion model. Stippled black lines represent areas of erosion while solid black lines represent deposition. Continuous black line is Birchams Creek with black arrows indicating flow direction.*

5.3 METHODS

5.3.1 PORTABLE OSL READER DATA AS A SEDIMENT TRACER

Muñoz-Salinas et al. (2014) demonstrated the capability of portable OSL reader data to be used in sediment provenance studies. The primary concept behind using portable OSL reader data as a sediment tracer is the assumption that very little of the luminescence signal in quartz grains gets bleached during transport in turbid and turbulent stream flow. Thus, once redeposited, the buried sediment retains its characteristic bulk luminescence from its source. This chapter builds upon Muñoz-Salinas et al.'s work by measuring bulk OSL data in PSA sediment and comparing the results to characteristic bulk OSL profiles of uneroded swampy meadow and weathered regolith valley bottom substrates to identify the geographic location of the source of PSA as well as the initial erosion depth. Detailed portable OSL reader methods can be found in CHAPTER 4.0.

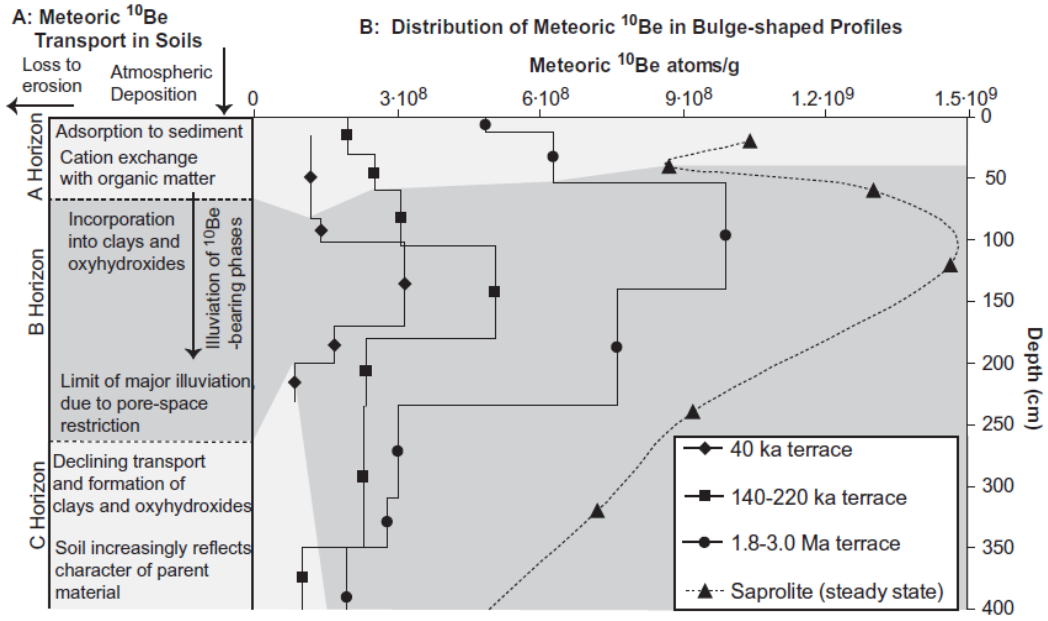

FIGURE 5.4
Selected meteoric ^{10}Be profiles in selected soil profiles with depth from Graly et al. (2010). Meteoric ^{10}Be accumulates in the B-horizons because of the increased surface area of adsorption of clay mineral grains.

5.3.2 METEORIC ^{10}BE DATA AS A SEDIMENT TRACER

The meteoric variety of cosmogenic ^{10}Be (see CHAPTER 3.0) is produced in the atmosphere through spallogenic interactions between secondary cosmic ray-derived particles and O and N target nuclei. Meteoric ^{10}Be is delivered via precipitation and dry fallout to Earth's

surface where it strongly adsorbs to sediment grains, and accumulates in soil profiles (FIGURES 3.3 [page 21], 5.4) (Graly et al., 2010; Willenbring and von Blanckenburg, 2010). Because the delivery of meteoric ^{10}Be varies with precipitation rate, its delivery rate must be determined from global production rate models (Graly et al., 2011; Monaghan et al., 1986) or constrained in the field (Heikkilä et al., 2008; Reusser et al., 2010). Meteoric ^{10}Be strongly adheres to mineral grains and can thus be used as a sediment tracer in a number of geomorphic settings (Brown et al., 1988; Jungers et al., 2009; Reusser and Bierman, 2010; Valette-Silver et al., 1986). Characteristic depth profiles of meteoric ^{10}Be provide a secondary assessment of PSA sediment provenance and initial erosion depth; this study is the first time these disparate but complementary techniques (bulk OSL and meteoric ^{10}Be) have been applied together in a geomorphic context.

5.3.3 PORTABLE OSL AND METEORIC ^{10}BE SAMPLE COLLECTION

Sediment samples for both bulk OSL and meteoric ^{10}Be measurements were collected at each of the four sites in Birchams Creek: PSA-1, PSA-2, SM-1, and REG-1 (photos in APPENDIX A). Bulk luminescence samples were collected at 3 cm depth intervals to a depth of ~1 m at all sites and sediment profile descriptions were recorded (TABLE 5.1); deeper sampling at SM-1 continued at 5 cm intervals. Meteoric ^{10}Be samples were collected as point samples at 9 cm depth intervals at PSA-1, PSA-2, and REG-1, to depths of 102 cm, 75 cm, and 81 cm, respectively, and at 12 cm depth intervals at SM-1 to a depth of 112 cm.

Table 5.1: Birchams Creek Sediment Profile Descriptions

Site	D (cm)	Description
PSA-1	0-3	Fine sandy loam with sandy structure. Dark, loose incipient A-horizon with many roots. pH = 5.5. Munsell Colour = 10YR 3/3 (m).
	3-21	Fine sandy clay loam with earthy structure. <2% charcoal. No bedding features. Roots growing throughout. pH = 6. Munsell Colour = 10YR 6/4 (m).
	21-27	Sand with loose gravel layer consisting of clasts ranging from 12-40 mm (avg. = 20.9 mm; n = 10). Larger roots growing throughout with ~2% charcoal. pH = 7. Munsell Colour = 7.5YR 6/6 (m).
	27-30	Loam, fine sandy with earthy structure. Individual coherent and platy fine-laminae preserved. ~2% charcoal. pH = 6.5. Munsell Colour = 2.5Y 5/6 (m).
	30-33	Sandy clay loam, similar to above but without platy structure. ~5% charcoal. pH = 6. Munsell Colour = 10YR 5/6 (m).
	33-39	Sandy loam with earthy structure with no coherence. Sandy throughout with no bedding features. ~5% charcoal. pH = 6. Munsell Colour = 10YR 5/6 (m).
	39-48	Sandy clay loam. Homogeneous unit with earthy structure and no bedding features. Mottled gray and orange colouring. 10% charcoal. pH = 6.5. Munsell Colour = 10YR 5/8 (m).
	48-54	Sandy loam with earthy structure and alternating horizons of fine-medium sand though distinct bedding not observed. 10% charcoal. pH = 7. Munsell Colour = 10YR 5/6 (m).
	54-96	Fine sandy clay loam with earthy structure and no bedding features though there is banding/mottling due to iron-staining. 15% charcoal. pH = 7. 10YR 5/4 (m).
	96-102	Medium clay unit with angular blocky pedal structure. Bottom of post-swampy meadow sediments. 10% charcoal. pH = 7. Munsell Colour = 10YR 2/2 (m).
	102-114	Medium clay with angular blocky pedal structure and reddish-gray mottling. Top of swampy meadow sediments. Base of unit was not determined. ~15% charcoal. pH = 7. Munsell Colour = 7.5YR 2.5/2 (m).
SM-1	0-3	Loam, fine sandy and very dark in colour. Root growth throughout. Apedal structure. pH = 5.5. Munsell Colour = 10YR 3/3 (m).
	3-21	Clay loam with abundant root growth. Apedal structure. Gradual transitions with over- and underlying units. pH = 6. Munsell Colour = 10YR 4/2 (m).
	21-54	Medium clay of lighter colour but with more iron-staining/mottling than unit above. Some root growth throughout and coarse sand present. pH = 6. Munsell Colour = 2.5Y 5/3 (m).
	54-90	Silty clay loam with orange mottling. Apedal structure with few small gravels throughout. pH = 6. Munsell Colour = 2.5Y 6/6 (m).
	90-102	Sandy clay loam with dark orange mottling and gravels ranging 2-20 mm (avg. = 7.7 mm, n = 15). Very coarse sand size. pH = 7. Munsell Colour = 10YR 6/6 (m).
	102-107	Gravel layer of quartz clasts ranging from 6-53 mm (avg. = 16 mm; n = 15).
	107-142	Medium clay with iron-stained orange mottling throughout. No plant growth and sand size is very fine. pH = 7. Munsell Colour = 2.5Y 6/4 (m).
	142-172	Sandy clay unit with light orange mottling and apedal structure. Some coarse sand throughout but mostly medium sand. pH = 6.5. Munsell Colour = 2.5Y 5/6 (m).
	172-187	Silty clay unit. Crumbly with gravels ranging 3-12 mm (avg. = 7 mm, n = 5). pH = 6.5. Munsell Colour = 2.5Y 5/6 (m).
	187-197	Sandy clay with some orange mottling. pH = 7. Munsell Colour = 2.5Y 6/4 (m).
	197-207	Layer of large gravels ranging from 8-33 mm (avg. = 20, n = 8).
	207-212	Sandy clay with some orange mottling but few gravels ranging 3-10 mm (avg. = 6 mm, n = 3). pH = 7. Munsell Colour = 2.5Y 6/4 (m).
PSA-2	0-3	Light sandy clay loam with earthy structure. Some roots present. pH = 6. Munsell Colour = 10YR 5/4 (m).
	3-27	Sandy clay loam with earthy structure. Roots mostly nonexistant. pH 6.5. Munsell Colour = 2.5Y 5/3 (m).
	27-63	Medium clay with diffuse transition to overlying unit. No roots. Some iron-stained mottling. pH = 6.5. Munsell Colour = 10YR 4/3 (m).
	63-72	Heavy clay including diffuse boundary between uppermost limit of swampy meadow sediments and post-settlement alluvium. Apedal structure. pH = 6.5. Munsell Colour = 10YR 3/3 (m).
	72-90	Heavy clay lighter in colour than overlying unit with very gradual transition. Some iron-stained mottling. pH = 7. Munsell Colour = 10YR 5/3 (m).
REG-1	0-6	Sandy loam with earthy structure and plentiful root abundance. Distinctly separate from underlying unit. Gravels range 5-18 mm (avg. = 6.8 mm; n = 6). pH = 7. Munsell Colour = 10YR 4/3 (m).
	6-18	Fine sandy clay loam with gradual transition to underlying unit. No vegetation growth. pH = 6.5. Munsell Colour = 10YR 4/3 (m).
	18-57	Light clay with varied orange iron mottling. Generally coarser than overlying unit. Earthy structure. pH = 6.5. Munsell Colour = 10YR 5/6 (m).
	57-87	Light medium clay with more coherent structure and finer-grained than overlying unit, though still apedal. No root growth. pH = 7. Munsell Colour = 10YR 5/8 (m).
	87-102	Medium clay similar to unit above. Depth is nearly same as gully depth. Representative of weathered regolith. pH = 7. Munsell Colour = 2.5Y 6/4 (m).

5.3.4 METEORIC ^{10}BE EXTRACTION AND MEASUREMENT

Meteoric ^{10}Be samples were processed at the UVM Cosmogenic Nuclide Laboratory. Meteoric samples were milled to a fine powder and ~0.5 g of powder was mixed with ~0.4 g of ^{9}Be standard solution (SPEX 1000 ppm). Stone's (1998) fusion methods were used to produce beryllium-hydroxide gels, which were then burned to produce beryllium-oxide and mixed with Nb powder at a 1:1 molar ratio before being packed into copper cathodes

to be analysed using AMS at the Scottish Universities Environmental Research Centre (Xu et al., 2010). Measured $^{10}Be/^{9}Be$ ratios were normalised to NIST SRM4325 standard material with a $^{10}Be/^{9}Be$ ratio of 2.79×10^{-11} and blank-corrected using three process blanks (avg. = $1.71 \pm 0.83 \times 10^{-14}$), from which concentrations of ^{10}Be are derived. AMS measurement uncertainties and a 1.5% additional uncertainty were propagated in quadrature and the average total uncertainty for all samples is 2.0%.

5.4 ANALYTICAL RESULTS

5.4.1 PORTABLE OSL READER DATA

Bulk IRSL and BLSL measurements were summed, and the depth-profiles were smoothed using a 3-sample moving average through luminescence measurements (FIGURE 5.5a, TABLES 5.2–5.4). Total bulk OSL measurements at PSA-1 and PSA-2 show typical swampy meadow profiles at depth, systematically decreasing up-profile (FIGURE 5.5a) to the SM-PSA bulk OSL transition at 99 and 72 cm, respectively.

Luminescence measurements increase above the bulk OSL SM-PSA transition to a maximum 3-sample average value of 3.4×10^{6} photon counts at PSA-1 (54 cm) and 2.4×10^{6} photon counts at PSA-2 (57 cm). The preservation of laminated bedding in the PSA deposits indicates they were transported by flowing water and the increased bulk luminescence measurements are therefore interpreted as having been minimally bleached before deposition. The values of bulk OSL maxima at PSA-1 and PSA-2 thus reflect potential depths at SM-1 and REG-1 from which PSA could have been sourced.

Under the DGEM, alluvium at PSA-1 is eroded from swampy meadow sediments at SM-1. In order for the peak total luminescence value at PSA-1 to have been preserved as inherited luminescence, it could only have been sourced from depths at SM-1 between 87–39 cm, 147–102 cm, or 207–187 cm (FIGURE 5.5a). In a similar way, alluvium at PSA-2 could only have been sourced from depths at REG-1 between 18–9 cm or 99–63 cm. There is no change for PSA-2 under the SSEM; alluvium at PSA-2 could still be sourced from the same two potential depths as in the DGEM. However, if alluvium at PSA-1 was also sourced from REG-1, it could have been sourced from depths ~15 cm or 99–69 cm (FIGURE 5.5a).

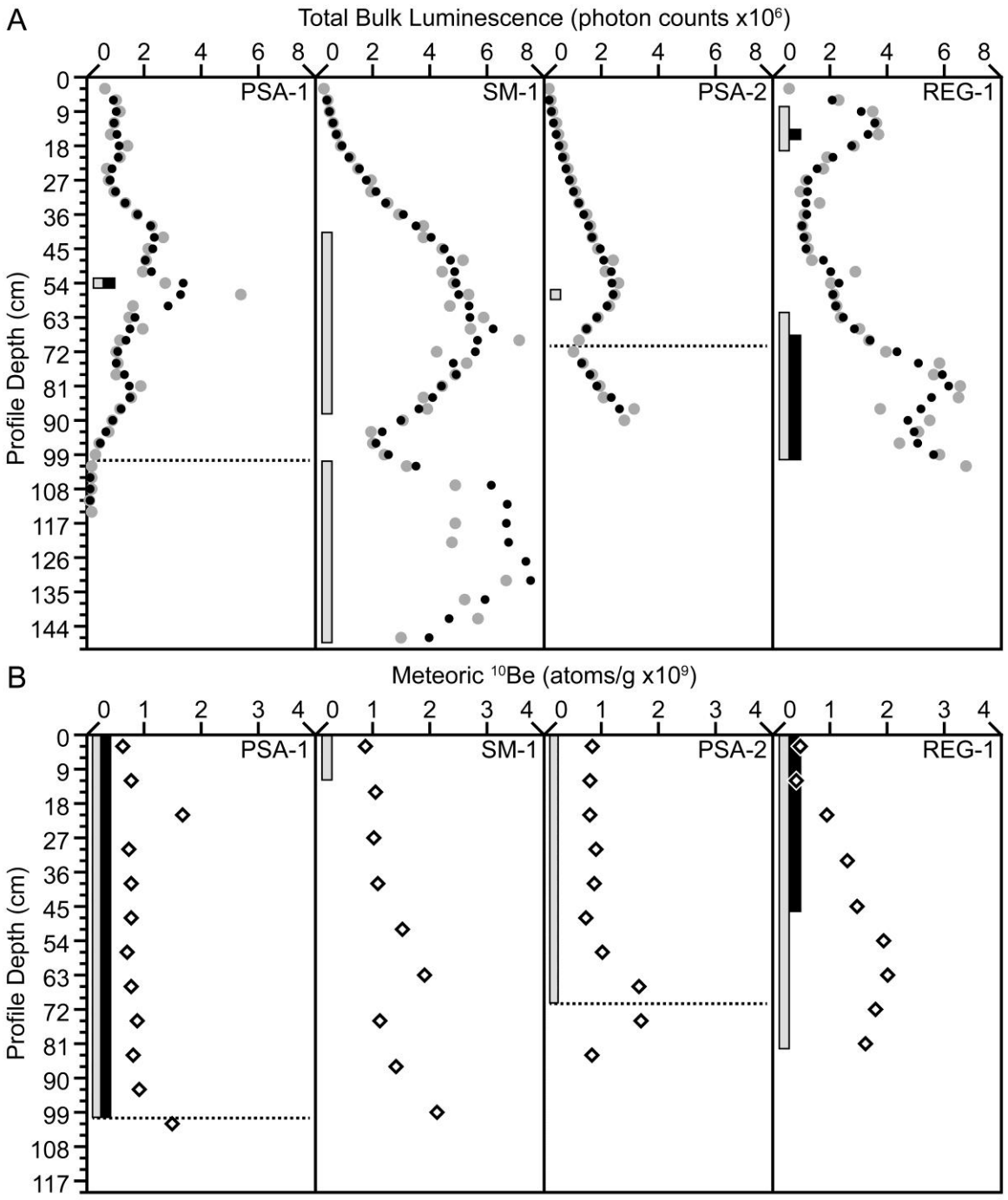

FIGURE 5.5

A. *Total luminescence (sum of IRSL and BLSL, grey dots) measured from bulk sediment samples at each profile site (PSA-1, SM-1, PSA-2, REG-1) and the 3-sample average luminescence used for analyses in this study (black dots). Dashed black lines represent the transition in bulk OSL measurements from swampy meadow sediments to post-European settlement alluvium. Grey boxes at PSA-1 and PSA-2 show the peak luminescence measurement depth and at SM-1 and REG-1 indicate the potential source depths from which alluvium at PSA-1 and PSA-2, respectively, could have originated under the discontinuous gully erosion model. The black box in PSA-1 shows the peak luminescence measurement depth and at REG-1 the black boxes indicate the potential source depths from which alluvium could have originated under the single site erosion model.* ***B.*** *Concentrations of meteoric ^{10}Be at each profile site (white diamonds). Grey boxes at PSA-1 and PSA-2 indicate the depths over which meteoric ^{10}Be concentrations are averaged in post-European settlement alluvium; the grey boxes at SM-1 and REG-1 indicate the respective source depths from which alluvium at PSA-1 and PSA-2 could have originated under the discontinuous gully erosion model. The black box at PSA-1 shows the depth over which meteoric ^{10}Be concentrations are averaged in alluvium, and in REG-1 the black box represents the source depth from which alluvium at PSA-1 could have originated under the single site erosion model.*

Table 5.2: PSA-1 Bulk OSL and Meteoric ^{10}Be Data			
Depth (cm)	Total OSL (photon counts)	3-Sample Average (photon counts)	Meteoric ^{10}Be (atoms/g) x10^{8}
3	578,932 ± 58		5.813 ± 0.146
6	1,003,848 ± 63	898,654 ± 62	
9	1,113,181 ± 64	1,005,846 ± 64	
12	900,508 ± 63	929,010 ± 63	7.410 ± 0.170
15	773,340 ± 62	1,028,667 ± 64	
18	1,412,153 ± 68	1,101,455 ± 65	
21	1,118,872 ± 65	1,068,936 ± 65	16.245 ± 0.293
24	675,782 ± 62	845,585 ± 63	
27	742,100 ± 62	779,677 ± 63	
30	921,148 ± 64	987,508 ± 65	6.941 ± 0.127
33	1,299,277 ± 68	1,310,350 ± 68	
36	1,710,625 ± 72	1,745,322 ± 71	
39	2,226,063 ± 74	2,199,601 ± 74	7.225 ± 0.139
42	2,662,114 ± 76	2,333,946 ± 74	
45	2,113,662 ± 73	2,273,124 ± 74	
48	2,043,596 ± 72	2,022,710 ± 73	7.153 ± 0.132
51	1,910,871 ± 74	2,224,281 ± 75	
54	2,718,376 ± 78	3,354,347 ± 80	
57	5,433,795 ± 87	3,252,642 ± 79	6.699 ± 0.127
60	1,605,754 ± 71	2,826,357 ± 76	
63	1,439,522 ± 69	1,647,537 ± 71	
66	1,897,335 ± 72	1,484,843 ± 69	7.391 ± 0.116
69	1,117,672 ± 67	1,336,615 ± 68	
72	994,838 ± 66	1,044,802 ± 66	
75	1,021,897 ± 66	1,006,191 ± 66	8.494 ± 0.183
78	1,001,838 ± 66	1,283,545 ± 68	
81	1,826,899 ± 72	1,455,527 ± 69	
84	1,537,843 ± 70	1,493,671 ± 70	7.659 ± 0.141
87	1,116,272 ± 67	1,167,100 ± 67	
90	847,186 ± 64	885,090 ± 65	
93	691,812 ± 63	635,046 ± 62	8.776 ± 0.189
96	366,141 ± 58	434,553 ± 59	
99	245,705 ± 56		
102	85,574 ± 52		14.432 ± 0.282
105	83,811 ± 52	83,371 ± 52	
108	80,729 ± 52	81,483 ± 44	
111	79,910 ± 28	92,341 ± 36	
114	116,385 ± 29		

Table 5.3: SM-1 Bulk OSL and Meteoric ^{10}Be Data

Depth (cm)	Total OSL (photon counts)	3-Sample Average (photon counts)	Meteoric ^{10}Be (atoms/g) x10^8
3	254,639 ± 40		8.281 ± 0.161
6	378,682 ± 43	358,412 ± 42	
9	441,916 ± 44	464,224 ± 45	
12	572,075 ± 47	565,515 ± 46	
15	682,555 ± 48	685,256 ± 48	9.947 ± 0.195
18	801,138 ± 50	890,643 ± 51	
21	1,188,235 ± 54	1,142,763 ± 53	
24	1,438,917 ± 56	1,498,743 ± 56	
27	1,869,078 ± 59	1,729,101 ± 58	9.756 ± 0.230
30	1,879,308 ± 59	2,078,653 ± 61	
33	2,487,574 ± 63	2,415,927 ± 63	
36	2,880,900 ± 65	3,055,835 ± 66	
39	3,799,032 ± 69	3,487,550 ± 68	10.468 ± 0.173
42	3,782,717 ± 69	4,006,329 ± 70	
45	4,437,237 ± 72	4,463,738 ± 72	
48	5,171,260 ± 75	4,682,535 ± 73	
51	4,439,107 ± 72	4,822,907 ± 74	14.912 ± 0.383
54	4,858,354 ± 74	4,892,649 ± 74	
57	5,380,487 ± 76	4,990,950 ± 75	
60	4,734,009 ± 74	5,344,508 ± 76	18.588 ± 0.442
63[a]	5,919,028 ± 78	5,372,840 ± 76	18.846 ± 0.338
66	5,465,484 ± 76	6,191,100 ± 78	**18.717 ± 0.390**
69	7,188,788 ± 81	5,621,415 ± 77	
72	4,209,972 ± 73	5,561,133 ± 77	
75	5,284,638 ± 76	4,797,484 ± 75	10.953 ± 0.219
78	4,897,841 ± 75	4,882,019 ± 75	
81	4,463,579 ± 74	4,370,101 ± 73	
84	3,748,884 ± 71	4,049,767 ± 72	
87	3,936,837 ± 73	3,567,193 ± 71	13.849 ± 0.250
90	3,015,857 ± 68	2,954,175 ± 68	
93	1,909,832 ± 62	2,296,902 ± 64	
96	1,965,017 ± 63	2,082,117 ± 63	
99	2,371,501 ± 65	2,506,803 ± 66	20.864 ± 0.394
102	3,183,890 ± 70	3,482,438 ± 71	
107	4,891,923 ± 77	6,106,938 ± 79	
112	10,245,001 ± 91	6,683,831 ± 81	
117	4,914,570 ± 76	6,642,445 ± 81	
122	4,767,763 ± 75	6,729,538 ± 81	
127	10506281 ± 91	7,335,048 ± 82	
132	6731101 ± 82	7,492,639 ± 83	
137	5240535 ± 77	5,888,722 ± 79	
142	5694530 ± 79	4,632,269 ± 74	
147	2961742 ± 68	3,938,846 ± 72	
152	3160266 ± 69	3,058,446 ± 69	
157	3053330 ± 69	3,158,938 ± 69	
162	3263219 ± 70	2,852,667 ± 68	
167	2241451 ± 65	2,983,033 ± 68	
172	3444429 ± 69	2,490,333 ± 66	
177	1785120 ± 63	2,111,758 ± 63	
182	1105725 ± 59	2,299,331 ± 65	
187	4007147 ± 74	3,859,264 ± 72	
192	6464921 ± 83	6,133,273 ± 81	
197	7927752 ± 87	5,601,439 ± 78	
202	2411645 ± 65	4,545,685 ± 74	
207	3297657 ± 71	3,589,417 ± 72	
212	5058948 ± 82		

[a] Replicate measurements of meteoric ^{10}Be from two samples (plain text) are averaged (bold text). The average value is used in analyses for this study.

Table 5.4: PSA-2 Bulk OSL and Meteoric ^{10}Be Data			
Depth (cm)	Total OSL (photon counts)	3-Sample Average (photon counts)	Meteoric ^{10}Be (atoms/g) x10^{8}
3	113,712 ± 49		7.967 ± 0.157
6	168,758 ± 51	172,972 ± 51	
9	236,445 ± 53	239,993 ± 53	
12	314,775 ± 55	314,173 ± 54	7.822 ± 0.152
15	391,298 ± 56	407,923 ± 56	
18	517,696 ± 58	507,310 ± 58	
21	612,937 ± 59	619,035 ± 60	7.700 ± 0.157
24	726,473 ± 61	731,267 ± 61	
27	854,392 ± 62	866,232 ± 63	
30	1,017,830 ± 64	1,012,444 ± 64	8.621 ± 0.188
33	1,165,110 ± 65	1,204,281 ± 66	
36	1,429,903 ± 68	1,381,280 ± 67	
39	1,548,828 ± 69	1,542,667 ± 69	8.553 ± 0.144
42	1,649,270 ± 69	1,669,009 ± 70	
45	1,808,929 ± 71	1,940,160 ± 71	
48	2,362,282 ± 74	2,083,818 ± 72	6.948 ± 0.127
51	2,080,243 ± 72	2,332,102 ± 74	
54	2,553,781 ± 75	2,363,944 ± 74	
57	2,457,807 ± 75	2,420,016 ± 75	9.726 ± 0.198
60	2,248,459 ± 74	2,181,690 ± 73	
63	1,838,805 ± 72	1,830,859 ± 71	
66	1,405,314 ± 69	1,467,496 ± 69	16.462 ± 0.343
69	1,158,369 ± 67		
72	980,832 ± 65		
75	1,273,241 ± 68	1,287,557 ± 68	16.849 ± 0.302
78	1,608,599 ± 71	1,587,681 ± 71	
81	1,881,203 ± 73	1,833,507 ± 72	
84	2,010,718 ± 73	2,339,450 ± 75	
87	3,126,428 ± 79	2,628,183 ± 77	
90	2,747,404 ± 78		

Table 5.5: REG-1 Bulk OSL and Meteoric ^{10}Be Data			
Depth (cm)	Total OSL (photon counts)	3-Sample Average (photon counts)	Meteoric ^{10}Be (atoms/g) x10^8
3	510,195 ± 55		4.286 ± 0.126
6	2,206,785 ± 70	2,050,685 ± 67	
9	3,435,076 ± 76	3,067,651 ± 74	
12	3,561,093 ± 77	3,550,664 ± 77	3.603 ± 0.088
15	3,655,824 ± 77	3,316,084 ± 76	
18	2,731,334 ± 73	2,736,882 ± 73	
21	1,823,489 ± 68	2,072,869 ± 69	8.896 ± 0.188
24	1,663,784 ± 67	1,532,843 ± 66	
27	1,111,256 ± 63	1,212,736 ± 64	
30	863,167 ± 61	1,178,951 ± 64	
33	1,562,429 ± 67	1,138,425 ± 64	12.823 ± 0.232
36	989,680 ± 63	1,176,086 ± 64	
39	976,149 ± 63	1,007,848 ± 63	
42	1,057,716 ± 64	1,060,247 ± 64	
45	1,146,875 ± 65	1,151,358 ± 65	14.523 ± 0.361
48	1,249,482 ± 66	1,740,209 ± 69	
51	2,824,269 ± 75	2,014,687 ± 71	
54	1,970,309 ± 71	2,303,909 ± 73	19.319 ± 0.494
57	2,117,148 ± 72	2,081,502 ± 71	
60	2,157,049 ± 72	2,182,135 ± 72	
63	2,272,208 ± 73	2,453,019 ± 74	19.717 ± 0.354
66	2,929,799 ± 76	2,831,613 ± 76	
69	3,292,833 ± 78	3,381,699 ± 78	
72	3,922,464 ± 81	4,333,658 ± 82	17.656 ± 0.304
75	5,785,677 ± 87	5,087,083 ± 85	
78	5,553,107 ± 87	5,940,740 ± 88	
81	6,483,436 ± 89	6,151,005 ± 88	15.904 ± 0.330
84	6,416,472 ± 89	5,541,100 ± 86	
87	3,723,392 ± 80	5,187,303 ± 85	
90	5,422,046 ± 86	4,715,536 ± 84	
93	5,001,169 ± 85	4,934,885 ± 85	
96	4,381,441 ± 84	5,049,600 ± 86	
99	5,766,190 ± 88	5,616,544 ± 87	
102	6,702,000 ± 91		

5.4.2 MEASURED METEORIC ^{10}BE CONCENTRATIONS

Concentrations of meteoric ^{10}Be at each profile come from point samples rather than amalgamations of sediment from various depths, so therefore each measurement represents the isotopic content of the profile from one sample depth to the next. Sample material from BIRC-X63 was processed twice, yielding meteoric ^{10}Be concentrations of $1.86 \pm 0.04 \times 10^9$ and $1.88 \pm 0.03 \times 10^9$, a difference of 1.4%, which demonstrates the reproducibility and consistency of the methods used and results. Meteoric ^{10}Be measurements are reasonably constant throughout PSA profiles and average $8.2 \pm 0.16 \times 10^8$ atoms/g at both

PSA-1 and PSA-2 (FIGURE 5.5b). The main difference between the profiles is that a horizon of coarse gravels is exposed in PSA-1 at a depth of 30 cm (TABLE 5.1); no such horizon exists at PSA-2. At $1.6 \pm 0.029 \times 10^9$ atoms/g, the meteoric ^{10}Be content of the gravel horizon at PSA-1 corresponds to an isolated major increase in meteoric ^{10}Be well above the average.

Measurements of meteoric ^{10}Be at SM-1 exhibit an increase in concentration from $8.3 \pm 0.16 \times 10^8$ atoms/g at the surface to $1.9 \pm 0.039 \times 10^9$ atoms/g at 63 cm. Below 63 cm, meteoric ^{10}Be decreases, but increases once more with depth to $2.1 \pm 0.039 \times 10^9$ atoms/g at 99 cm depth. Concentrations of meteoric ^{10}Be at REG-1 show a general increase from $4.3 \pm 0.13 \times 10^8$ atoms/g at the surface to $2.0 \pm 0.035 \times 10^9$ atoms/g at a depth of 63 cm.

The relatively uniform content of meteoric ^{10}Be in PSA deposits is an indication that the sediment was well mixed in transport prior to deposition. Thus, using meteoric ^{10}Be to identify the depth from which it was eroded at its source requires averaging meteoric ^{10}Be concentrations from SM-1 or REG-1 one depth at a time until the average concentration exceeds that of the PSA. In the DGEM, sediment at PSA-1 could have only been derived from shallow erosion of the uppermost 12 cm of SM-1; erosion any deeper than this would result in higher than observed average meteoric ^{10}Be concentrations at PSA-1. Sediment at PSA-2 could be the result of erosion into sediment at REG-1 as deep as 81 cm. In the SSEM, sediment at PSA-1 could be sourced from erosion to a depth of 45 cm at REG-1, but no deeper (FIGURE 5.5b).

5.5 DISCUSSION OF RESULTS

5.5.1 SOURCE OF PSA IN BIRCHAMS CREEK

Only one of the four potential PSA source and depth combinations, as indicated by bulk OSL and meteoric ^{10}Be analyses, is consistent with PSA at profile PSA-1: shallow erosion of weathered regolith at and upstream from profile REG-1. Given that sediment at profiles PSA-1 and PSA-2 exhibit the same meteoric ^{10}Be concentrations and that PSA-2 could only have come from REG-1 further supports this inference. Furthermore, the sediment textures of PSA-1, PSA-2, and shallow sediment at REG-1 range from fine sandy clay

loam to sandy loam; clay loam and medium clay are much more prevalent at SM-1, an indication that SM-1 is not the source of alluvium at PSA-1.

Estimates of sediment eroded upstream must balance estimates of sediment deposited downstream, volumetrically and isotopically, if erosion at and up-valley from REG-1 is the source of sediment at both PSA-1 and PSA-2. In this estimation, all PSA is assumed to be stored within the basin and that all channels and ponds have flat bottoms and vertical walls.

The volume of existing ponds in AD 1880 is determined from data given by Eyles (1977a) and the depths are estimated from surface area/depth relationships derived from field evidence in AD 1977. From this, the volume of ponds existing in AD 1880 was estimated to be 2,511 m^3. Using the measured meteoric ^{10}Be concentrations from PSA-1, and an average of PSA density measurements (1.379 g/cm^3; n = 4), the total estimated meteoric ^{10}Be inventory that filled the ponds existing in AD 1880 is $3.8 \pm 0.073 \times 10^{18}$ atoms, assuming the valley bottom surface in AD 1880 is represented by the depth of the gravel horizon at PSA-1 (30 cm). As indicated by bulk OSL measurements and meteoric ^{10}Be concentrations at profile REG-1, initial erosion is estimated to have been to a depth of only 0.15 m along the course of Birchams Creek. The eroded surface area required to produce the estimated meteoric ^{10}Be inventory filling ponds downstream is derived from the following:

$$Surface\ Area = \frac{I}{\left(\left(C_{REG-1-3} \times d_{C_{REG-1-3}}\right) + \left(C_{REG-1-12} \times d_{C_{REG-1-12}}\right)\right)}$$

where I is the isotopic inventory of meteoric ^{10}Be atoms in PSA-filled ponds, $C_{REG\text{-}1\text{–}3}$ is the meteoric ^{10}Be concentration of REG-1 at 3 cm depth (atoms/m^3), $d_{C_{REG-1-3}}$ = 0.09 m (the depth over which this concentration is assumed), $C_{REG\text{-}1\text{–}12}$ is the meteoric ^{10}Be concentration of profile REG-1 at 12 cm depth (atoms/m^3), and $d_{C_{REG-1-12}}$ = 0.06 m (the remainder of the 0.15 m erosion depth estimate). Dividing the calculated surface area of erosion (45,747 m^2) by 11.9 m – the average *b*-axis (i.e. width) of ponds in AD 1941 – determines the length of channel erosion required to supply enough sediment and meteoric ^{10}Be to the AD 1880 ponds to be 3,844 m. The total stream length of Birchams Creek upstream from the AD 1880 ponds, as mapped in AD 1941, is 3,732 m, or 97% of the stream length required to fill the ponds.

Once the AD 1880 ponds were filled, any remaining deposition of PSA would have spread out over the valley bottom. The current areal extent of PSA deposits in Birchams Creek – basin slopes with ≤1° (30 m SRTM elevation data) – covers 570 m^2 at PSA-1 and 270 m^2 at PSA-2; these PSA volumes and their associated meteoric ^{10}Be inventories must also be balanced. PSA deposits are 30 cm at PSA-1 (its lower limits being defined by the observed gravel layer) and 63 cm deep at PSA-2, yielding sediment volumes of 171 m^3 and 170 m^3, respectively. The total meteoric ^{10}Be inventory for the valley bottom PSA is $4.1 \pm 0.083 \times 10^{17}$ atoms. A further 9 cm of erosion of only ponds mapped in AD 1941 (5,281 m^2) produces 475 m^3 of sediment and $4.7 \pm 0.10 \times 10^{17}$ atoms of meteoric ^{10}Be, enough to supply more sediment and meteoric ^{10}Be (139% and 114%, respectively) than is estimated at PSA deposits at profile PSA-1 and PSA-2. Excess sediment and meteoric ^{10}Be in this estimate is due to generalisations in working with 9 cm depth-intervals or PSA volume estimations, or perhaps a small amount of sediment and meteoric ^{10}Be is transported out of the creek catchment. The flux of meteoric ^{10}Be to the PSA deposits after deposition (i.e. from AD 1914–2013, or 1932–2013) is $7.96–9.81 \times 10^{14}$ atoms determined by Eqn. 2 in Graly et al. (2011) using a 100-year annual rainfall rate of 68–69 cm yr^{-1} (Australian Bureau of Meteorology stations 070-030, -056, -232, and -233) at 35.2°S. This post-PSA depositional flux accounts for 0.019–0.024% of the total measured meteoric ^{10}Be inventory and does not have an effect on results or interpretations of the data presented here.

5.5.2 GULLY INITIATION IN BIRCHAMS CREEK

A single-grain OSL age of PSA at the base of PSA-1 (see CHAPTER 6.0) yields a depositional age between AD 1914–1932. This burial age is consistent with the headward advancement of the gully observed by landowners in AD 1910 mapped by Eyles (1977a). Though the valley substrate that was initially incised to supply PSA was identified and though the capability for sediment and isotopic budgets to balance from erosional sources to deposition areas was demonstrated, the mechanism for triggering erosion is not yet known.

Topographic thresholds related to upstream catchment area must be crossed in order for the shear stress of flowing water to overcome the shear resistance of the valley bottom sediment to trigger gully incision (Melville and Erskine, 1986; Patton and Schumm, 1975;

Prosser and Abernethy, 1996; Prosser and Slade, 1994; Schumm, 1979). Relationships between the critical slope threshold (S_{cr}, given as % gradient) and upstream catchment area (A, in hectares) provided by (Vandaele et al., 1996)

$$S_{cr} = aA^{-b}$$

where a and b are site specific constants that account for local climate and erodibility. Since initial gully incision sites are largely unknown in the Tablelands, S_{cr} and A of gullied creeks are unmeasurable; thus a and b cannot be derived empirically and so I substitute a range of values derived for valley-bottom gullies in Europe that have similar soil textures and mean annual rainfall as Birchams Creek (a = 0.025–0.09; b = -0.25– -0.4) (Vandaele et al., 1996). The upstream area of Birchams Creek at REG-1 is 306 ha and the slope of the Birchams Creek valley bottom at PSA-2 is ~1°, which requires S_{cr} > 1.75 for incision to occur by means of crossing a topographic threshold. Using substituted values of a and b, S_{cr} in Birchams Creek ranges from 0.105–0.888 (or 4.7°–40°); thus, valley bottom slopes at REG-1, where discontinuous gullies initially incised, would have to be ~5–40× steeper before a topographic threshold is crossed. Moreover, scour ponds in Birchams Creek all occur on valley bottom surfaces with the shallowest gradients (Eyles, 1977a), suggesting that no topographic thresholds have been crossed, yet erosion still occurred.

Land use between AD 1914–1932 changed from natural open eucalypt woodlands to cleared grazing pastures (Eyles, 1977a, b) and the first 15 years of the 20th century were affected by drought (Erskine and Warner, 1988; Erskine and Warner, 1998). Eyles (1977a) noted that feral pigs had been observed disturbing the Birchams Creek valley bottom during periods of drought; elsewhere in the Tablelands, cattle congregated in wallows in valley bottoms during these droughts, and those wallows eventually developed into a deep gullies, such as at Waterhole Creek (Eyles, 1977b). Livestock grazing has the dual affect of compacting surficial soils (Trimble and Mendel, 1995) and breaking apart sediment aggregates, which can fill in pore space, both of which decreases infiltration and has the overall effect of increasing a stream's capacity to transport large sediment grains and erode (Warren et al., 1986). A combination of decreased native vegetation, drought conditions, and trampling by congregating livestock in Birchams Creek most likely created extremely localised slopes >S_{cr}, which served as foci for overland flow and subsequently triggered discontinuous gullying along valley bottoms. Following the incision of discontinuous gullying, the AD 1910 gully (Eyles, 1977a) propagated beyond the upstream extent of the

ponds that existed in AD 1880, forming the continuous gully shown on Eyles' AD 1941 map. The establishment of connectivity between discontinuous gullies thus formed a conduit through which any subsequently eroded sediment could be carried out of the Birchams Creek catchment.

5.6 CHAPTER CONCLUSIONS

Bulk OSL measurements and concentrations of meteoric ^{10}Be were used together, for the first time, to identify the source location and source depth of gully-derived alluvium in the Tablelands of New South Wales, Australia. The initial erosion of scour ponds along Birchams Creek, and eventual development of gullies, started by shallow erosion (~15 cm depth) of a weathered regolith valley bottom substrate and not of swampy meadow sediments as suggested by previous studies (Prosser, 1990, 1991; Prosser et al., 1994). Sediment volumes and isotopic inventories of meteoric ^{10}Be between upstream erosional sources and downstream depositional locations are balanced, further supporting the notion that erosion of weathered regolith is the source of PSA. This finding is similar to Muñoz-Salinas et al.'s (2014) conclusions from further north in the Tablelands, though this study is the first to determine original gully incision depths.

The processes that drove incision in Birchams Creek, namely forest clearing and grazing following European arrival to the Tablelands, are the likely causes of gully erosion and PSA deposition throughout the region. Revegetating non-swampy meadow valley bottom substrates and encouraging protection of swampy meadow wetlands on the Australian Tablelands may hold a solution for preventing continued growth of existing gullies and preventing new erosional gullies from developing. These methods may also prove to be useful in landscapes worldwide where gully erosion actively erodes the landscape, whether triggered by anthropogenic land use changes or natural processes.

Gully incision into non-swampy meadow valley bottoms
and PSA deposition seem to have been caused by
European grazing practices.
Do the ages of PSA deposition confirm this?

CHAPTER

WHEN WAS PSA DEPOSITED IN THE TABLELANDS?

6.1 A POORLY CONSTRAINED CHRONOLOGY OF PSA DEPOSITION

European exploration and settlement in Australia were initially focused within the Sydney area, but surveyors and explorers soon ventured from Sydney and returned with detailed descriptions, meteorological data, illustrations, and anecdotes from the pre-European southeastern Tablelands (hereafter "Tablelands") and of the challenges their exploration teams faced (Blaxland, 1870; Evans, 1916; Lawson, 1813; Mitchell, 1839a, b; Oxley, 1820; Scott, 2001; Wentworth, 1813). Further descriptions of the Tablelands shortly after European settlement and grazing began were kept in diaries and journals of early graziers (Meredith, 1844).

The surveyors and graziers described the pre-European Tablelands landscape as one of forested hillslopes and hilltops with open valley bottoms where sedges and grasses grew in water-saturated wetlands called swampy meadows (Eyles, 1977b; Mactaggart et al., 2008). Water flowing through these valley bottoms was typically not channelised. Rather, it filtered through the swampy meadows and sometimes collected in ponds – chains of ponds – which proved to be an invaluable source of water for grazing livestock (see Eyles, 1977b; Scott, 2001).

The modern Tablelands landscape is vastly different. The most notable changes include the deforestation of hillslopes to provide more grazing land for livestock and agriculture, the

absence of nearly all swampy meadows and chains of ponds, and the near-total ubiquity of stream incision forming amphitheatre gullies in hillslopes and deep stream gullies along the length of every valley bottom throughout the region (Butzer and Helgren, 2005; Eyles, 1977a, b, c; Hughes and Prosser, 2003; Scott, 2001). Gully incision deposited mantles of alluvium (see CHAPTERS 4.0 and 5.0) in valley bottoms, burying swampy meadows. Questions regarding the ages of post swampy-meadow alluvium (PSA) remain unanswered.

Though widespread gully erosion in the Tablelands occurred numerous times throughout the Holocene (Eriksson et al., 2006), PSA deposition and the gullies from which alluvium was derived seem to be inextricably linked to the impact of European land use change in the early- to mid- AD 1800s. Therefore, the exact cause and timing of gully erosion in the Tablelands remains at the heart of decades of debate. There are only a few observations of European land use practices directly causing the development of gully systems in the Tablelands (Gillespie, 1981; Johnston and Brierley, 2006; Starr, 1989), though there is anecdotal evidence that suggests widespread gullying began after Europeans arrived, most notably in the form of European artefacts being preserved at the base of PSA deposits (Gore et al., 2000; Rustomji and Pietsch, 2007; Starr, 1989; Wasson et al., 1998). OSL data connect the timing of PSA deposition to European land use change in the Mulwaree River basin near Tarago, NSW (AD 1833–1919) and the Wollondilly River basin east of Goulburn, NSW (AD 1800–1978) (Rustomji and Pietsch, 2007). Radiocarbon ages of 10 ± 115 yr BP in Birchams Creek (Eyles, 1977a) and 255 ± 60 yr BP in Groves Creek (Coventry and Walker, 1977) hint at post-European sediment deposition; however, the exact locations or depths of radiocarbon samples in neither creek are provided or shown on a map. Missing detail of radiocarbon samples precludes reassessing ^{14}C determinations, not to mention issues of a flat ^{14}C calibration curve over the last few centuries (Reimer et al., 2004), reduction of ^{14}C available in the atmosphere from burning fossil fuels (Tans et al., 1979), and the possibility of fluvial recycling of charcoal resulting in ^{14}C ages being related to earlier depositional episodes (Blong and Gillespie, 1978).

The cause and effect relationship between changed land use practices and gully erosion is seemingly straightforward; however, the discussion is compounded by the disagreement in results derived from studies that quantify the timing of swampy meadow accumulation and PSA deposition. Swampy meadow growth initiated ~3 ka in Gooromon Ponds Creek (Wasson et al., 1998), ~1 ka in Grabben Gullen Creek (Muñoz-Salinas et al., 2014), and

~3.7 ka in Mulloon Creek (Johnston and Brierley, 2006) and seems to have accumulated continuously in many valleys over the last few thousands of years. However, some researchers conclude that PSA deposition may have begun before Europeans arrived to Australia, inferring that some gully erosion had been initiated by mechanisms other than European land use change (e.g. Butzer and Helgren, 2005; Johnston and Brierley, 2006; Muñoz-Salinas et al., 2014).

The triggering mechanisms for gully incision remain elusive. The climate around Lake George in southeastern New South Wales became warmer and drier after the late Pleistocene and has not changed much over the last few thousand years (Bowler et al., 1976; Coventry, 1976). A lack of coincidence between climatic factors and known gully ages throughout the Tablelands seems to suggest that regional climate change is not an extrinsic driving mechanism of gully erosion (Prosser, 1991) and that some other intrinsic landscape modifier drives erosion. However, if climate change is implicit in triggering gully erosion, its visible effects on a landscape seem to be manifested by a non-uniform lag after the driving climatic event.

Landscape modification was certainly administered by Aboriginal Australians (see CHAPTER 3.0) (Gammage, 2011), and bushfires started by Aboriginal Australians have increased since the mid-Holocene (Hughes and Sullivan, 1981; Mooney et al., 2011). Other than low intensity, controlled fires (Gammage, 2011), there is little anecdotal evidence to support any link between Aboriginal land use and gully incision on the modern Tablelands landscape despite claims to the contrary (Butzer and Helgren, 2005), and there is no evidence to support more frequent or intense burning as a cause of widespread gully erosion (Hughes and Sullivan, 1981; Prosser, 1990; Prosser and Slade, 1994).

Movement of Europeans into the Tablelands closely followed the early years of exploration by government surveyors. Much of the Bathurst and Goulburn Plains were occupied by graziers who sought to “improve” the land by encouraging grass growth, which often involved ringbarking trees, draining swampy meadows, and starting fires to clear the native vegetation. The overall result of these actions is the focus of the remainder of this paper. Scott (2001) contains a comprehensive and detailed history of European arrival to the Tablelands. While the official dates of legal settlement in the Tablelands provide useful benchmarks for the timing of landscape change and erosion events, the presence of squatters who grazed well beyond the limits of the established counties before

land beyond these limits was legally opened is recognised. These squatters had the potential to have caused landscape degradation before the official onset of legal occupation (Bayley, 1975; Gale and Haworth, 2002), though this claim is contested (Woodward et al., 2011).

The causes and timing of gully erosion in the Tablelands remain to be fully explained, and the mismatch between anecdotal evidence and quantitative data on the timing of gullying can only be rectified by increasing the number of locations for which high-precision dates of either gully erosion or PSA deposition are determined (Prosser and Soufi, 1998; Prosser and Winchester, 1996). This study tests the notion that PSA deposition is in fact a geomorphic artefact of European land use changes in the early AD 19th century by presenting single grain OSL ages for swampy meadow sediments and PSA depositional ages from six sites throughout the central southeastern Tablelands (hereafter, the "Goulburn Plains"). To avoid unconscious pre-judgement of the ages and origins of sandy sediments, PSA continues to be defined as post swampy-meadow alluvium due to its stratigraphically-younger position overlying the swampy meadow sediments.

6.2 METHODS

6.2.1 SEDIMENT BURIAL AGES DETERMINED USING OSL

The amount of optically stimulated luminescence in sediment is directly related to the duration of time it has been buried and the rate of incoming radiation from surrounding sediment (Aitken, 1998). If the natural sediment radiation dosimetry is known, the burial age of sediment can be determined by measuring the luminescence emitted from sediment grains in a controlled setting, effectively determining the equivalent dose (D_e, Wintle, 2008a) according to the following relationship:

$$Burial\ Age\ (years) = \frac{Equivalent\ Dose, D_e\ (Gy)}{Dose\ Rate\ \left(\frac{Gy}{years}\right)}$$

where radiation levels and dose rates are given in units of Grays (*Gy*). Quartz is often the mineral of choice for OSL studies because it retains its luminescence in the absence of stimulation unlike feldspars whose luminescence signals may fade over time (Wintle,

1973), though recent efforts to overcome the limitations presented by anomalous fading in feldspars have been successful (Li et al., 2014, and references therein).

OSL has many archaeological applications such as deriving burial ages of sediment, which contain human bones (Roberts et al., 2005), anthropological artefacts (Fanning et al., 2008), or fossilised animals (Roberts et al., 2001). The geomorphic applications for OSL are numerous as well, including dating aeolian, fluvial, and glacial deposits (Duller, 2004; Olley et al., 1998; Olley et al., 2004; Wintle, 2008b). However, these geomorphic settings often do not allow for quartz to be completely bleached, and if unaccounted for, inherited luminescence leads to overestimates of the true burial age. Galbraith et al. (1999) demonstrate the ability to measure luminescence from individual grains of quartz, allowing for the bleaching history of individual quartz grains to be assessed, greatly increasing the method's usefulness in geomorphic settings where bleaching is often incomplete.

Various age models have been derived to determine the appropriate burial ages of sediment in different geomorphic settings. The central age model (CAM) is best suited for populations of quartz grains that have been bleached, more or less, to the same degree producing a log-normal distribution, such as aeolian sand and thus yielding a single age (Galbraith et al., 1999). The minimum age model (MAM) is best suited for a mixture of sediment that has been mostly incompletely bleached, thus containing inherited luminescence; MAMs are best applied to fluvial and glacial sediment that contain many quartz grains with inherited luminescence but a few grains that were completely bleached before deposition (Galbraith et al., 1999). The MAM considers luminescence measurements from all quartz grains, but more strongly weights those that were most completely bleached before burial.

6.2.2 SAMPLE SITE SELECTION AND COLLECTION

Testing the notion that PSA was eroded and deposited as a direct result of European land use in the early 19th century requires burial ages from PSA deposits from a wide geographical area within the Tablelands region. Previous studies provided OSL ages from swampy meadow (SM) sediment in Grabben Gullen Creek (2014; Muñoz-Salinas et al., 2011) and from two locations on the eastern margin of the Tablelands: Mulwaree and

Wollondilly Rivers (FIGURE 6.1) (Rustomji and Pietsch, 2007). The field area for this study is focused on the central southeastern Tablelands, the Goulburn Plains, since the area is geographically and climatically similar, separated from the Bathurst Plains by the Abercrombie Mountains, and separated from the Monaro Plains by the Brindabella and Tinderry Mountains (see FIGURE 2.1 in CHAPTER 2.0). The Goulburn Plains have also had a similar land use history having been opened for legal settlement by the NSW government at different times than the Bathurst or Monaro Plains. Moreover, previous studies of OSL burial ages (Eriksson et al., 2006; 2014; Muñoz-Salinas et al., 2011; Rustomji and Pietsch, 2007), gully erosion (Coventry and Walker, 1977; Eriksson et al., 2006; Eyles, 1977a, b, c; Prosser, 1991; Prosser et al., 1994; Starr, 1989), and radiocarbon studies (Coventry and Walker, 1977; Eyles, 1977a) are located in the Goulburn Plains, thus making results from this study directly comparable to results from previous work.

A total of eleven gully exposure profiles were collected for portable OSL measurement from the Goulburn Plains, from which twelve OSL burial age samples were to be distributed. All eleven profiles from the Goulburn Plains clearly exhibit visually distinct SM and PSA sedimentary units that are confirmed by the portable OSL reader data (see CHAPTER 3.0). Six sites were chosen that vary in size and underlying lithology (TABLE 6.1) for OSL burial age analysis, with two ages being determined from each site: Birchams Creek (BIRC), Fenwick Creek (FENW), Gooromon Ponds Creek (GOOR), Groves Creek (GROV), Phils River (PHIL), and Ryries Creek (RYRI) (FIGURE 6.1). Sediment profile descriptions of the six study sites were completed in detail (TABLE 6.2), and I collected two samples from each for OSL burial age dating. The transition in the bulk luminescence profile depth-trends where upwardly-decreasing luminescence of SM sediments changes into deposition of incompletely bleached sediment of the PSA was used to guide the burial age sample collection strategy (TABLE 6.3). The first burial age sample at each site (e.g. BIRC-A at Birchams Creek) was collected at the base of PSA, the depth of which is confirmed by portable OSL data, providing an age for the initial onset of upstream gully erosion. The second burial age sample (e.g. BIRC-B at Birchams Creek) was collected below the SM-PSA luminescence transition to provide the age of SM sediment before it was buried by PSA. Collecting samples in pairs not only provides SM and PSA ages but also an estimate either of any depositional hiatuses between the two stratigraphic units or of the amount of SM sediment eroded during PSA deposition.

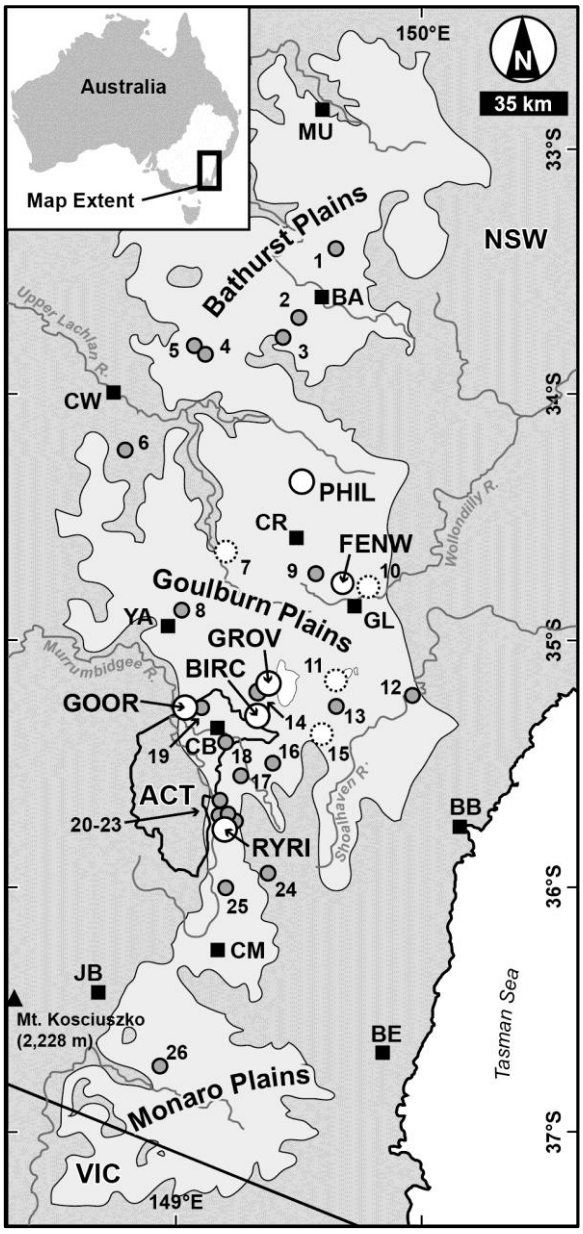

FIGURE 6.1

Reference map of Australia (inset) showing the extent of the southeastern Australian Tablelands, situated on the eastern headwaters of the Murray-Darling River basin (light grey shaded area in inset map), the largest ocean-draining river system in Australia. Main FIGURE shows the Tablelands field area (light grey region), which largely occupies elevations between 500–1,000 m, halfway between sea level (Tasman Sea) and Australia's highest point, Mt. Kosciuszko (black triangle). Cities (black squares) and state boundaries are shown for geographic reference: MU: Mudgee; BA: Bathurst; CW: Cowra; CR: Crookwell; GL: Goulburn; YA: Yass; CB: Canberra; BB: Batemans Bay; CM: Cooma; JB: Jindabyne; BE: Bega; NSW: New South Wales; ACT: Australian Capital Territory; VIC: Victoria. Sites where burial ages of swampy meadow sediments or alluvial deposits are determined from this study (solid white circles) or other studies (dashed white circles, see main text for references), sites of gullies where incision ages are anecdotal or unknown (grey circles): PHIL: Phils River; FENW: Fenwick Creek; GROV: Groves Creek; BIRC: Birchams Creek; GOOR: Gooromon Ponds Creek; RYRI: Ryries Creek; 1: Wyagnon Creek; 2: Georges Plains Creek; 3: Queen Charlotte's Creek; 4: Mandurama Ponds Creek; 5: Grubbenbun Creek; 6: Breakfast Creek; 7: Grabben Gullen Creek; 8: Bango Creek; 9: Whiteheads Creek; 10: Wollondilly River; 11: Mulwaree River; 12: Shoalhaven River; 13: Boro Creek; 14: Brooks Creek; 15: Mulloon Creek; 16: Primrose Valley Creek; 17: Burra Creek; 18: Jerrabomberra Creek; 19: Ginninderra Creek; 20: Waterhole Creek; 21: Michelago Creek; 22: Margarets Creek; 23: Teatree Creek; 24: Wangrah Creek; 25: Gungoandra Creek; 26: Matong Creek.

Table 6.1. Bedrock Geology of Sampled Sites[a]	
BIRC	Primarily Ordovician sandstone, but part of a turbidic sequence including mudstone and shale. Some metamorphic quartzite, phyllite, and slate. Geologic unit is extensive and not all lithologies may be found within Birchams Creek. Basin area = 4.3 km^2
FENW	Ordovician quartz and feldspar sandstone interbedded with siltstone and mudstone. Minor chert throughout. Devonian leucogranite with some rhyolite dykes that underly a small portion of the drainage divide. Basin area = 22.6 km^2
GOOR	Silurian rhyodacitic ignimbrites and volcaniclastic sediments underly the majority of the catchment. Rhyodacitic porphyry underlies a small portion of the basin as do mixed mudstone, siltstone, limestone and hornfels. Basin area = 81.7 km^2
GROV	Ordovician sandstone (same as Birchams Creek), but part of a turbidic sequence including mudstone and shale. Some metamorphic quartzite, phyllite, and slate. Geologic unit is extensive and not all lithologies may be found within Groves Creek. Early Devonian granitoids underly a very small fraction of the catchment. Tertiary quartz pebble conglomerates underly portions of the headwater divides. Basin area = 6.3 km^2
PHIL	Silurian siltstone, sandstone, volcaniclastic sediments, and quartzite and schist underly much of the basin while smaller portions of the basin are underlain by carbonaceous siltstones and sandstones, and rhyolitic volcaniclastic sandstone - in some places overlain by Quaternary colluvial gravels. Quartz veins also prevalent. Early Miocene basalts occupy small portions of the headwater drainage divides. Unconsolidated sands and gravels of the same age cover some of the Silurian siltstones. Basin area = 68.5 km^2 (upstream from Peelwood Rd.)
RYRI	Ordovician band of adamellite batholith underlies the central portion of the catchment. Adjacent to the batholith are the same sandstone-rich turbiditic sequences found at Birchams and Groves Creeks. Silurian rhyodacitic tuff with minor mixed sedimentary lithologies are found at the mouth of the creek, below the profile sample site. Basin area = 69.1 km^2

[a] Geologic data comes from the 1:100,000 scale geologic maps from the New South Wales Department of Resources and Energy: http://www.resourcesandenergy.nsw.gov.au/miners-and-explorers/geoscience-information/products-and-data/maps/geological-maps/1-100-002

Table 6.2: Sediment Profile Descriptions (part 1)

Site	Depth (cm)	Description
BIRC	0-3	Fine sandy loam with sandy structure. Dark, loose incipient A-horizon with many roots. pH = 5.5. Munsell Colour = 10YR 3/3 (m).
	3-21	Fine sandy clay loam with earthy structure. <2% charcoal. No bedding features. Roots growing throughout. pH = 6. Munsell Colour = 10YR 6/4 (m).
	21-27	Sand with loose gravel layer consisting of clasts ranging from 12-40 mm (avg. = 20.9 mm; n = 10). Larger roots growing throughout with ~2% charcoal. pH = 7. Munsell Colour = 7.5YR 6/6 (m).
	27-30	Loam, fine sandy with earthy structure. Individual coherent and platy fine-laminae preserved. ~2% charcoal. pH = 6.5. Munsell Colour = 2.5Y 5/6 (m).
	30-33	Sandy clay loam, similar to above but without platy structure. ~5% charcoal. pH = 6. Munsell Colour = 10YR 5/6 (m).
	33-39	Sandy loam with earthy structure with no coherence. Sandy throughout with no bedding features. ~5% charcoal. pH = 6. Munsell Colour = 10YR 5/6 (m).
	39-48	Sandy clay loam. Homogeneous unit with earthy structure and no bedding features. Mottled gray and orange colouring. 10% charcoal. pH = 6.5. Munsell Colour = 10YR 5/8 (m).
	48-54	Sandy loam with earthy structure and alternating horizons of fine-medium sand though distinct bedding not observed. 10% charcoal. pH = 7. Munsell Colour = 10YR 5/6 (m).
	54-96	Fine sandy clay loam with earthy structure and no bedding features though there is banding/mottling due to iron-staining. 15% charcoal. pH = 7. 10YR 5/4 (m).
	96-102	Medium clay unit with angular blocky pedal structure. Bottom of post-swampy meadow sediments. 10% charcoal. pH = 7. Munsell Colour = 10YR 2/2 (m).
	102-114+	Medium clay with angular blocky pedal structure and reddish-gray mottling. Top of swampy meadow sediments. Base of unit was not determined. ~15% charcoal. pH = 7. Munsell Colour = 7.5YR 2.5/2 (m).
FENW	0-9	Fine sandy loam with earthy structure. Roots quite thick for ~9 cm. Wavy boundary with underlying unit. pH = 6. Munsell Colour = 10YR 4/3 (m).
	9-20	Fine sandy clay loam with earthy structure. Fewer roots and bedding structures faintly preserved. <2% charcoal. pH = 6.5. Munsell Colour = 2.5Y 4/3 (m).
	20-24	Sandy loam with earthy structure mostly consisting of a coarse-grained sand lens with pebbles. Gravels range from 5-14 mm (avg. = 9.6 mm; n = 5). Distorted bedding structures. 2% charcoal. pH = 6.5. Munsell Colour = 2.5Y 4/3 (m).
	24-36	Sandy clay loam with earthy structure. Very clear trough-bedding or cut/fill structures. Very few roots throughout. Typically coarse-grained in bottom of troughs, fining upward with ~20% charcoal. pH = 6. Munsell Colour = 2.5Y 3/3 (m).
	36-42	Sandy loam with sandy structure preserving a lens of sandy material, fining upwards with some bedding preserved in upper-most fine grains. ~30% charcoal. pH = 7. Munsell Colour = 2.5Y 4/2 (m).
	42-42.5	Sandy clay loam with earthy structure of a thin layer of sandy clay that makes up the bottom of the lens above. pH = 6.5. Munsell Colour = 2.5Y 4/3 (m).
	42.5-57	Sandy loam with sandy structure that preserves well-defined cross-bedding and cut/fill strucutres. 10% charcoal. pH = 6. Munsell Colour = 2.5Y 4/2 (m).
	57-72	Medium clay with earthy structure. Bedding features less defined but still present. Contains optical transition from swampy meadow to post-swampy meadow sediments. 5% charcoal. pH = 6. Munsell Colour = 2.5Y 4/3 (m).
	72-90+	Medium clay unit with earthy structure and homogeneous black-gray clay with orange mottling. No bedding features. <2% charcoal. pH = 6.5. Munsell Colour = 10YR 2/2 (m).
GOOR	25-73	Fine sandy loam with earthy structure and limited root growth though ant colonies are continually present. pH = 7. Munsell Colour = 10YR 4/4 (m).
	73-77	Fine sandy clay loam with earthy structure containing the transition from swampy meadow sediments into post-swampy meadow sediments. Ant activity observed but no roots. pH = 7. Munsell Colour = 10YR 3/4 (m).
	77-99+	Sandy clay unit with angular blocky pedal structure of clays of swampy meadow sediments. No ant activity or root growth. pH = 7. Munsell Colour = 2.5Y 3/2 (m).

Table 6.2: Sediment Profile Descriptions (part 2)

Site	Depth (cm)	Description
GROV	0-6	Loam, fine sandy unit with sandy structure and bioturbation from plant roots. 20% charcoal. pH = 7. Munsell Colour = 10YR 3/3 (m).
	6-12	Fine sandy clay loam with sandy structure. Gravel at base of unit ranging from 7-102 mm (avg. = 33.5 mm; n = 15). No bedding features preserved. 5% charcoal. pH = 6.5. Munsell Colour = 10YR 3/3 (m).
	12-48	Loam, fine sandy unit with earthy structure. Plant and insect bioturbation throughout, including live scorpion. Some small gravels found in lenses. Lowest depth marks onset of post-swampy meadow sediment deposition. 10% charcoal. pH = 6.5. Munsell Colour = 10YR 3/3 (m).
	48-70	Light clay unit. Apedal with earthy structure. Roots and 5% charcoal throughout. Gravels throughout unit ranging from 5-32 mm (avg. = 12.7 mm; n = 11). Upper portion of swampy meadow sediments. pH = 7. Munsell Colour = 2.5YR 2.5/1 (m).
	70-72+	Medium clay unit with angular blocky pedal structure. <2% charcoal. pH = 7. Munsell Colour = 5YR 2.5/1 (m).
PHIL	0-3	Loam, fine sandy unit with sandy structure. Grass roots are prevalent. Very loose and distinctly different from unit below. pH = 6. Munsell Colour = 10YR 4/3 (m).
	3-30	Fine sandy clay loam with earthy structure. 2% charcoal. pH = 6.5. Munsell Colour = 10YR 5/3 (m).
	30-42	Sandy unit with loose sandy structure. Considerable amounts of gravel and pebbles ranging from 5-23 mm (avg. = 14 mm; n = 11). pH = 6. Munsell Colour = 10YR 4/3 (m).
	42-52	Sandy loam unit with earthy structure. Lenses of iron-stained clay and appears speckled with light and dark sediment, possibly preserving some bedding features more visible in lower units. 2-5% charcoal. pH = 7. Munsell Colour = 7.5YR 3/2 (m).
	52-59	Fine sandy loam with earthy structure preserving small bedding features throughout unit which seem continuous into the unit above. <2% charcoal. Bottm of post-swampy meadow sediments. pH = 7. Munsell Colour = 2.5Y 4/3 (m).
	59-63	Sandy clay unit that is the top of swampy meadow sediments. Gray clays with bedding features continuous into layer above. ~2% charcoal. pH = 7. Munsell Colour = 10YR 3/2 (m).
	63-69	Medium clay with apedal structure and the darkest of the swampy meadow units. No bedding features preserved. pH = 7. Munsell Colour = 10YR 2/1 (m).
	69-84+	Medium clay with apedal structure. Base of unit was not measured though seems to go at least to stream-level. Gravels found within unit range from 5-14 mm (avg. = 8.1 mm; n = 13). pH = 7 . Munsell Colour = 10YR 2/2 (m).
RYRI	5-18	Sandy loam unit with earthy structure. Roots continuously thick. Large gravels fining upward throughout unit ranging from 5-20 mm with a layer of gravel at the top of the unit. pH = 6. Munsell Colour = 10YR 5/4 (m).
	18-25	Fine sandy clay loam with earthy structure. Roots are fewer but still present. Fine, cross-bedded laminae are visible. pH = 6.5. Munsell Colour = 2.5Y 4/2 (m).
	25-32	Sandy clay unit with earthy structure and a few roots. Gravels present, ~5 mm. pH = 6.5. Munsell Colour = 2.5Y 3/3 (m).
	32-38	Sandy clay unit with earthy structure. Gravels still present though larger than above ~10 mm, though sorting is poor. Ambiguous laminations. ~5% charcoal. pH = 7. Munsell Colour = 2.5Y 4/2 (m).
	38-48	Silty clay loam unit with roots continuing through. Earthy structure making up base of post-swampy meadow sediments. pH = 7. Munsell Colour = 2.5Y 3/2 (m).
	48-90	Silty clay unit with angular blocky pedal structure. Roots do not extend far into this unit. Top of swampy meadow sediments. pH = 7. Munsell Colour = Gley1 3/N (m).
	90-90+	Silty clay unit with pedal structure. Angular blocky peds are more compact and coherent. Still some roots, but not many. Bottom of swampy meadow unit not measured. pH = 7. Munsell Colour = Gley1 3/N (m).

Table 6.3: Portable OSL Data

	Bulk OSL Transition Depth (cm)	Maximum IRSL (photons)	Maximum BLSL (photons)	Swampy Meadow IRSL:BLSL	Post European Settlement Alluvium IRSL:BLSL	Swampy Meadow Texture[a]	Post European Settlement Alluvium Texture[a]
BIRC	99	70,689	5,363,106	0.005 ± 0.002	0.016 ± 0.007	MC	S, SL, FSL, SCL, Lfsy, FSCL, MC
FENW	70	50,671	1,374,938	0.004 ± 0.002	0.014 ± 0.011	MC	SL, FSL, SCL, FSCL, MC
GOOR	75	29,753	3,764,842	0.004 ± 0.001	0.006 ± 0.001	SC	FSL, FSCL
GROV	48	21,808	768,638	0.016 ± 0.003	0.025 ± 0.003	LC, MC	Lfsy, FSCL
PHIL	60	140,714	2,888,350	0.025 ± 0.010	0.055 ± 0.019	SC, MC	S, SL, FSL, Lfsy, FSCL
RYRI	45	261,834	1,637,431	0.038 ± 0.007	0.127 ± 0.036	SiC	SL, SiCL, FSCL, SC

[a] Australian soil classifications from Northcote (1971). In order of texture grade: S = Sand, SL = Sandy loam, FSL = Fine sandy loam, SCL = Light sandy clay loam, Lfsy = Loam (fine sandy), SCL = Sandy clay loam, SiCL = Silty clay loam, FSCL Fine sandy clay loam, SC = Sandy clay, SiC = Silty clay, LC = Light clay, MC = Medium clay.

6.2.3 FIELD GAMMA DOSIMETRY

In situ gamma radiation was measured at each site to estimate the level of ionising radiation each sample receives from surrounding sediment using an Ortec digiDART portable HPGe multichannel analyser spectrometer with a 3-inch diameter crystal iodide measurement probe. The probe was fully inserted into the gully wall using the holes dug out by OSL sample collection tubes. At Gooromon Ponds Creek, the measurement probe could not be fully buried, and the measurement only recorded 50% of the full gamma-dosimetry; however, dosimetry data for Gooromon Ponds Creek were adjusted in subsequent analyses and this adjustment is assessed by comparing high and low resolution dosimetry measurements for all PSA samples.

6.2.4 BURIAL AGE OSL SAMPLE PROCESSING

Burial age OSL samples were removed from their light-proof tubes at Macquarie University, Australia, in the laboratory under light-safe conditions. Tube-end sediment likely experienced some bleaching during collection and are thus not used for sediment dating analyses. Water content of tube-end sediment was used as a proxy for sample moisture and was subsequently pulverised in a shaker mill and the powdered sample was used for beta-radiation measurement.

The 90–212 µm fraction of unbleached sediment was treated with 10% hydrochloric acid to remove carbonates and 10% sodium peroxide to remove organics. Quartz and feldspars

were isolated from remaining heavy minerals by a sodium polytungstate density separation (2.7 g/cm^3) and then quartz was separated from feldspars by a second density separation (2.62 g/cm^3). Quartz separates were etched in 40% hydrofluoric acid for 45 minutes to remove the outermost layer of quartz grains that were subject to alpha irradiation, leaving purified quartz. The dry quartz was then sieved into three datable grain size fractions (90–125 µm, 125–180 µm, and 180–212 µm).

6.2.5 DOSE RECOVERY

Pre-heat temperatures for single grain analysis were determined using dose recovery analyses on three SM samples (BIRC-B, PHIL-B, RYRI-B) and three PSA samples (FENW-A, GOOR-A, GROV-A). This procedure determines the temperature that most effectively removes thermally unstable luminescence derived from artificial dosing, which is luminescence not present in natural samples. Four aliquots of the 180–212 µm purified quartz grain size fraction of each sample were mounted using silkospray adhesive onto a 3 mm-diameter area of aluminium discs. To remove the natural luminescence signal, each aliquot was bleached under blue-light LEDs for 100 s after temperatures were ramped from room temperature to 50°C. Bleached aliquots were given an artificial radiation dose of 10 Gy to provide a surrogate natural luminescence, and one aliquot from each sample was subjected to a series of increasing pre-heat temperatures of 220°C, 240°C, 260°C, or 280°C for each single-aliquot regenerative-dose (SAR) (Murray and Wintle, 2000) cycle doses of 10 Gy, 5 Gy, 20 Gy, 0 Gy, and another 10 Gy. Each natural-dose OSL measurement was normalized by a test-dose of 5 Gy and a dose-recovery curve was constructed. Preheats of 240°C returned the most consistent recycling ratios of the surrogate natural 10 Gy dose (average = 1.00, ranging from 0.98–1.02; n = 6) and a recovered palaeodose that was closest to the surrogate natural dose; thus 240°C was used as the pre-heat temperature for single grain analyses.

6.2.6 LUMINESCENCE MEASUREMENT

Individual quartz grains of the 180–212 μm grain size fraction were loaded onto aluminium single-grain discs with a grid of 10 × 10 precision drilled pits, 300 μm in diameter. Luminescence measurements were conducted on a Risø OSL/TL-DA-20 model luminescence reader, fitted with an Electron Tubes Ltd 9235QA photomultiplier and 7.5 mm Hoya U-340 filter. The stimulation source is a 10 mW, 532 nm Nd:YVO_4 solid-state diode pumped green laser. I followed a modified SAR protocol, measuring the natural luminescence stored in each quartz grain. Following natural luminescence measurements, each grain was subjected to regeneration doses of 4 Gy, 8 Gy, 2 Gy, 0 Gy, and another 4 Gy, each and normalized by a test dose measurement of 2 Gy. Each quartz grain was subjected to 2 s of laser stimulation for natural, regeneration-dose, and test dose luminescence, with infrared stimulation at the end of each SAR cycle. The use of test-dose normalization corrects for grain-specific changes in sensitivity, or the ability to store luminescence and release it when stimulated (Duller, 2008). The normalized doses are then plotted against the given dose and a curve is fitted through the data to determine an equivalent dose (D_e) for the measured natural luminescence. This process is repeated on a grain-by-grain basis for at least 1,000 grains of each sample until 100 useable grains were identified or until the useable quartz stock was depleted (i.e. RYRI-A and RYRI-B).

6.2.7 GRAIN REJECTION CRITERIA

Not all quartz grains yield reliable luminescence signals for dating purposes or emit luminescence. Acceptable luminescence data should only be used from quartz grains that satisfy certain criteria (Roberts, 2008). I used Jacobs et al.'s (2006) grain rejection criteria as a guideline to remove poor-quality data from further analyses in the burial age determinations. Grains were rejected if

(1) the natural luminescence signal was not at least three times greater than the background signal,
(2) the recycling ratio (the reproducibility of the repeated 4 Gy dose), including its 2-sigma uncertainties, was <1 or >1,
(3) the infrared-stimulated luminescence recycling ratio was <1,

(4) the values of the repeated 4 Gy doses for each grain were more than 10% different,

(5) there was no signal, or the signal did not decay during optical stimulation,

(6) regeneration dose curves did not fit within the uncertainties of the normalised regeneration dose luminescence measurements or their uncertainties (including a 2% measurement uncertainty) according to an exponential fit, or a combination of an exponential fit with a linear component,

(7) the natural dose exceeded that of the regeneration dose fit curve (supersaturation), or

(8) the 0 Gy regeneration dose generated a recuperated luminescence value that was >5% of the natural luminescence. Grains that passed these criteria were accepted and the D_e calculated on a grain-by-grain basis.

6.2.8 EQUIVALENT DOSE DETERMINATION

Individual D_e measurements from accepted grains of quartz provide the raw data from which burial ages are determined using various mathematical models, each one appropriate for a different bleaching history or depositional setting. Radial plots have become the standard method of plotting the D_e values of luminescence data as they not only display the D_e associated with the luminescence measurement of each grain, but also show the precision with which that measurement was made (Galbraith, 1988). Radial plots also clearly convey which data fall within the 2σ standard estimate of the calculated D_e for the entire population of measured grains.

Fluvial sediment is often not completely bleached before being redeposited and the resultant D_e distribution from individual grains of quartz will be skewed by an additional residual dose, the distribution of which is referred to as overdispersion. Samples with high overdispersion will not be centralized on a common D_e value as they exhibit a distribution of D_e values that is greater than that predicted by a normal Gaussian population. Overdispersion of D_e values in fluvial sediment suggest that most measured grains incorporate inherited luminescence. The D_e value for each sample is modelled on all quartz grains but quartz grains that are the most-completely bleached are given more significance

and weighting because they represent the luminescence associated with the true burial age. Thus, based on field observations of partial bleaching, the MAM is chosen to determine the overall D_e value for fluvial sediment (Galbraith, 2005; Galbraith et al., 1999; Jacobs et al., 2006).

6.2.9 DOSE RATE CALCULATIONS

Powdered sample from the PSA was used for high resolution gamma- and beta-spectrometry measurement at the Environmental Radioactivity Laboratories at ERISS run by the Australian Government Department of the Environment in Darwin, Northern Territory. High resolution gamma- and beta- spectrometry aid in assessing the precision of *in situ* field gamma spectrometry and beta spectrometry at Macquarie University. SM samples were not analysed because erosion during deposition of PSA sediment potentially removed unknown amounts of SM sediment and high resolution radiation-spectrometry would not be able to detect dosimetry from missing sediment. Alpha-irradiated rinds of quartz sediment were etched away during sample processing, but an assumed internal dose rate of 0.032 ± 0.011 Gy/kyr is factored in to total dose rate calculations. Cosmic-ray dosimetry is determined using equations and factors derived in Prescott and Hutton (1994) and factored into total dose rate calculations with a 10% uncertainty.

6.3 RESULTS

6.3.1 PORTABLE OSL READER DATA

The majority of portable OSL reader profiles from the Goulburn Plains yield bulk IRSL and BLSL depth-trends similar to those observed in SM and PSA sediments at Grabben Gullen Creek profile GGC-P3 (Muñoz-Salinas et al., 2014) and elsewhere in the Tablelands (see CHAPTER 4.0) (FIGURE 6.2). The IRSL:BLSL ratio at nearly every site also changes significantly from SM sediments to PSA sediments (with the exception of Fenwick Creek where there is overlap of 1σ uncertainties), though the uncertainties on the IRSL:BLSL ratios in SM sediment at Fenwick Creek are much smaller than those of PSA.

The portable OSL reader results are thus used to guide collection of OSL burial age samples at the six chosen sites.

6.3.2 DOSIMETRY MEASUREMENTS

High resolution gamma-spectrometry measurements (TABLE 6.4) yield dose rates identical to those measured in the field within 1σ uncertainties with the exception of Gooromon Ponds Creek where the high resolution dosimetry is less than the *in situ* field dosimetry (FIGURE 6.3a). High resolution beta dosimetry and beta dosimetry measurements made in the laboratory at Macquarie University all replicate within 1σ uncertainties (FIGURE 6.3b), even at Gooromon Ponds Creek. Whether the ^{238}U and ^{232}Th radioactive decay series are in secular equilibrium were assessed by calculating the ^{210}Pb/^{226}Ra and ^{228}Th/^{228}Ra ratios of radionuclide activities of PSA sediment. ^{210}Pb/^{226}Ra ratios (n = 6) range from 0.765 to 1.169 and average 1.035 ± 0.058 (standard error); ^{228}Th/^{228}Ra ratios (n = 6) range from 0.950 to 1.073 and average 1.021 ± 0.018 (standard error) (TABLE 6.4). Radionuclides in both ratios are equal; thus, all sampled sediment is in equilibrium and no corrections will need to be made.

In Chapter 4.0, I show that tens of centimetres of PSA can be deposited during one flood; thus, SM sediments are buried under >0.5 m of PSA almost immediately, which attenuates the cosmic-ray dose, greatly diminishing its ability to irradiate quartz at the PSA-SM transition. Because of the strong replication of lab- and field-based dosimetry measurements to high resolution dosimetry measurements, total dosimetries for PSA samples (TABLE 6.5) are given as the sums of high resolution gamma-, beta-, and cosmic-ray dose rates. Total dosimetry for SM samples is the sum of field gamma-, laboratory beta-, and cosmic-ray dose rates.

6.3.3 QUARTZ ACCEPTION AND REJECTION

Between 1,341 and 5,663 quartz grains were analysed per sample in order to satisfy a preferred total of ~100 accepted grains to represent a dose population of grains, as fewer than 100 grains will not adequately represent the population (TABLE 6.5). Only 6% of total grains measured were accepted. The majority of rejected quartz, 59%, had luminescence less than three-times that of the background, which is considered grounds for automatic rejection (Jacobs et al., 2006); 11% were rejected for poorly replicating the duplicated 4 Gy regeneration dose; and 10% of grains emitted luminescence, even when there should have been no luminescence to emit after the 0 Gy regeneration dose stimulation, a phenomenon called recuperation (Aitken, 1998). Quartz from Gooromon Ponds Creek had the smallest percentage of accepted grains from the overall population of analysed sediment, and though all quartz grains from Ryries Creek samples were analysed, the 100-grain threshold was not met.

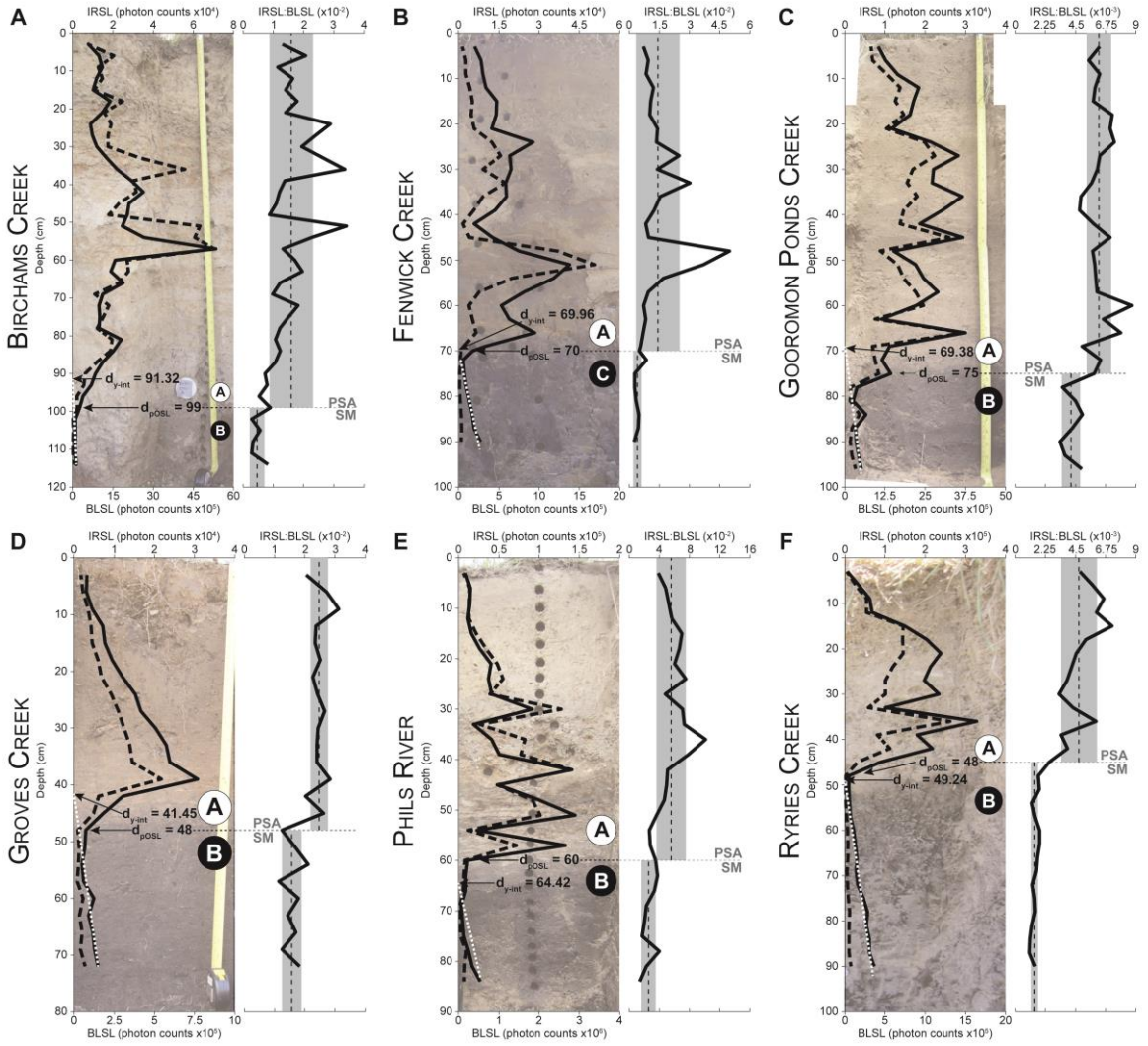

FIGURE 6.2

Bulk luminescence measurements of sediment through swampy meadow (SM) and post-European settlement alluvium (PSA) at ***A.*** *Birchams Creek,* ***B.*** *Fenwick Creek,* ***C.*** *Gooromon Ponds Creek,* ***D.*** *Groves Creek,* ***E.*** *Phils River, and* ***F.*** *Ryries Creek. Bulk IRSL and BLSL measurements (dashed and solid black lines, respectively) are plotted with depth. The white stippled lines in SM BLSL measurements show regression to $d_{y\text{-}int}$, the former valley bottom surface before erosion and deposition of PSA sediments. White circles (A) and black circles (B/C) show depth range of PSA and SM samples used for burial age OSL analysis, respectively; both circles are drawn to scale with the depth axes. Ratios of IRSL:BLSL (solid black line) are shown in the second panel; average ratio of SM or PSA samples indicated by dashed black line with 1σ uncertainties represented by the grey box. Dashed grey lines indicate the bulk OSL transition from SM to PSA sediments. Photographs of each SM-PSA profile are shown behind portable OSL reader data.*

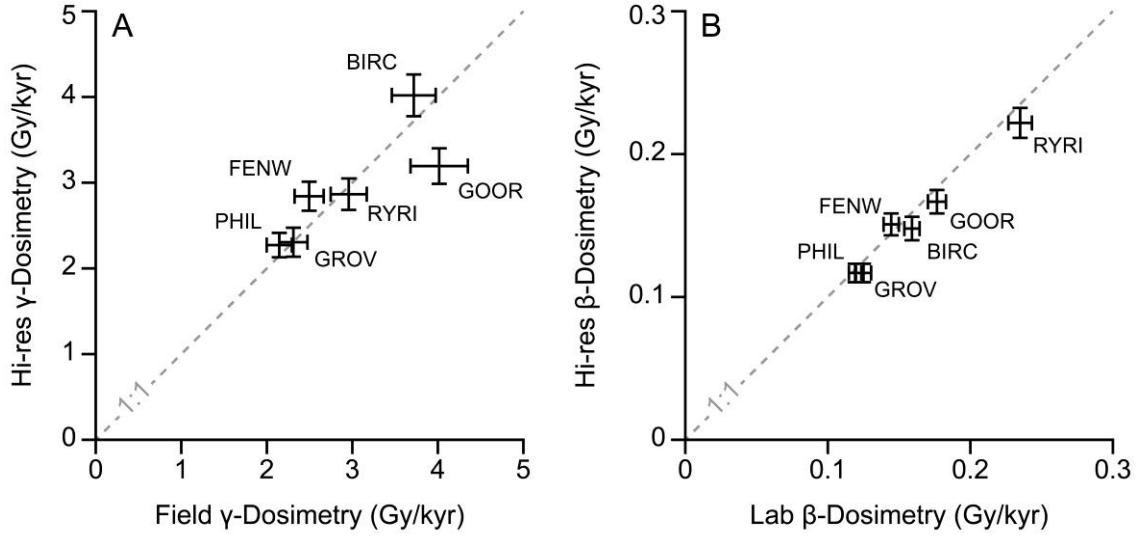

FIGURE 6.3

A. *High resolution dosimetry measurements PSA samples are plotted against field dosimetry measurements. That Birchams Creek), Fenwick Creek), Groves Creek, Phils River, and Ryries Creek all lie on the 1:1 line indicate that field dosimetries are reliable measures of gamma spectrometry; however, there is disagreement between field and high resolution gamma-dosimetries for Gooromon Ponds Creek. Uncertainties are 1σ.* ***B.*** *Within 1σ uncertainties, laboratory-based and high resolution beta-dose rates demonstrate close agreement.*

6.3.4 EQUIVALENT DOSES AND BURIAL AGES

Equivalent dose (D_e) determinations from accepted quartz grains from each of the twelve samples are plotted in FIGURE 6.4 and exhibit large amounts of scatter, or overdispersion (69–166%, TABLE 5.5). Minimum age model derived D_e estimates, combined with high resolution dosimetry measurements, yield SM burial ages ranging from 340.8 ± 28.4 a to 106.5 ± 9.9 a, where the benchmark year (0 a) is AD 2013, the year all samples were collected and measured. PSA burial ages range from 195.1 ± 17.8 to 90.4 ± 8.9 a, and all PSA ages post-date the arrival of Europeans to the Tablelands (FIGURE 6.5). There are no signs of stratigraphic inversion of the OSL ages at most sites, and the ages of the uppermost SM horizons are older than PSA deposits (TABLE 6.4). The exception is at Ryries Creek where SM sediments are 146.6 ± 58.4 a, which correspond to SM accumulation until between AD 1834–1937 and PSA deposition between AD 1801–1834.

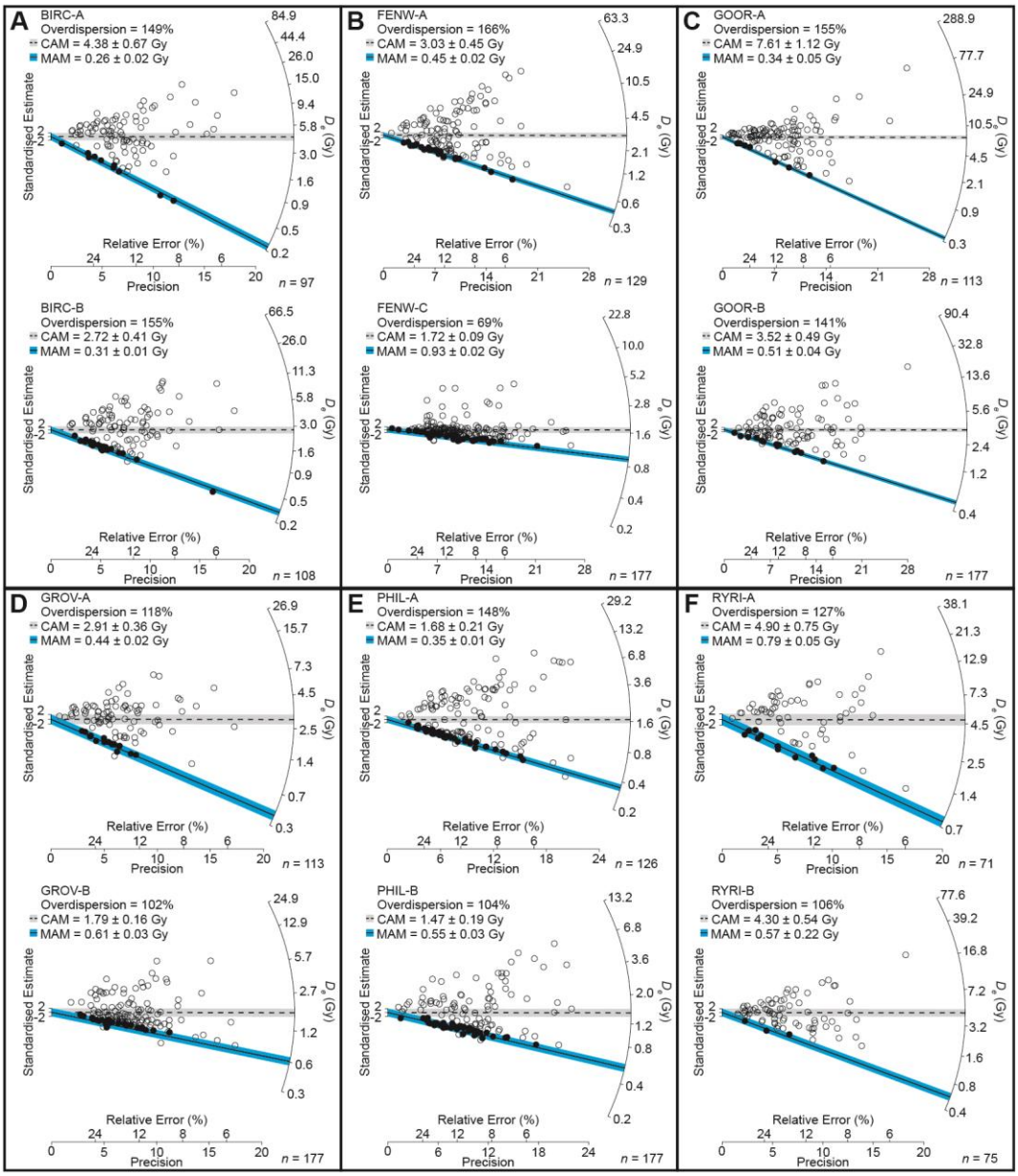

FIGURE 6.4

*Radial plots showing equivalent dose (D_e) distributions from luminescence measurements on single grains of quartz from **A.** Birchams Creek, **B.** Fenwick Creek, **C.** Gooromon Ponds Creek, **D.** Groves Creek, **E.** Phils River, and **F.** Ryries Creek. D_e estimates at each site show high levels of scatter and overdispersion; thus, the central age model (CAM) D_e estimates, shown by the dashed line and light grey bar, are not proper estimates of the burial age. Samples included in the minimum age model (MAM) estimates of D_e are shown by filled black circles and the MAM-derived D_e value is shown by the solid black line and dark grey bar. Corresponding MAM burial ages are displayed in TABLE 6.4.*

Table 6.4: Sample Dosimetry and OSL Ages

	Water	Radionuclide activities (Bq/kg)[b]						γ-ray Dose	β-Dosimetry	Cosmic-ray Dose	Total Dose	MAM D_e	Sediment Age	
	Content (%)[a]	^{238}U	^{226}Ra	^{210}Pb	^{228}Ra	^{228}Th	^{40}K	Rate (Gy/kyr)[c]	Rate (Gy/kyr)[d]	Rate (Gy/kyr)[e]	Rate (Gy/kyr)[b,f]	(Gy)[f,g]	(yrs)[h]	Calendar (AD)
BIRC-A	6.9 ± 4.0	48 ± 5	35.3 ± 1.2	27 ± 5	54.6 ± 2.5	58.0 ± 1.7	408 ± 19	**1.151 ± 0.048**	**1.477 ± 0.078**	0.211 ± 0.021	2.872 ± 0.180	0.260 ± 0.019	90.4 ± 8.9	1914 - 1932
BIRC-B	13.0 ± 5.0							1.204 ± 0.120	1.498 ± 0.054	0.197 ± 0.020	2.931 ± 0.232	0.312 ± 0.014	106.5 ± 9.9	1897 - 1916
FENW-A	15.5 ± 4.0	54 ± 5	31.2 ± 1.0	33 ± 5	55.7 ± 2.3	56.3 ± 1.6	468 ± 19	**1.124 ± 0.044**	**1.503 ± 0.078**	0.191 ± 0.019	2.850 ± 0.168	0.448 ± 0.015	157.2 ± 11.1	1845 - 1867
FENW-C	17.4 ± 5.0							0.968 ± 0.097	1.539 ± 0.063	0.186 ± 0.019	2.726 ± 0.210	0.929 ± 0.023	340.8 ± 28.4	1644 - 1701
GOOR-A	8.2 ± 4.0	52 ± 5	30.8 ± 1.0	36 ± 5	59.1 ± 2.3	59.6 ± 1.6	474 ± 19	**1.273 ± 0.047**	**1.665 ± 0.082**	0.205 ± 0.021	3.175 ± 0.190	0.342 ± 0.046	107.7 ± 16.0	1889 - 1921
GOOR-B	12.0 ± 5.0							2.020 ± 0.202	1.765 ± 0.064	0.196 ± 0.020	4.012 ± 0.339	0.512 ± 0.036	127.6 ± 14.3	1871 - 1900
GROV-A	12.9 ± 5.0	41 ± 5	24.1 ± 1.1	27 ± 5	48.4 ± 2.5	46.0 ± 1.5	339 ± 18	**0.913 ± 0.044**	**1.166 ± 0.070**	0.201 ± 0.020	2.311 ± 0.166	0.444 ± 0.021	192.1 ± 17.0	1804 - 1838
GROV-B	17.7 ± 6.0							0.907 ± 0.091	1.301 ± 0.054	0.191 ± 0.019	2.430 ± 0.205	0.614 ± 0.033	252.7 ± 25.8	1735 - 1786
PHIL-A	15.7 ± 4.0	42 ± 5	28.1 ± 1.0	30 ± 5	40.9 ± 2.1	41.7 ± 1.3	357 ± 17	**0.880 ± 0.042**	**1.166 ± 0.068**	0.195 ± 0.020	2.273 ± 0.144	0.349 ± 0.011	153.5 ± 11.3	1848 - 1871
PHIL-B	21.2 ± 5.0							0.933 ± 0.093	1.280 ± 0.056	0.184 ± 0.018	2.430 ± 0.190	0.545 ± 0.030	224.3 ± 21.9	1767 - 1811
RYRI-A	7.3 ± 4.0	135 ± 7	41.8 ± 1.3	43 ± 6	71.4 ± 2.9	76.6 ± 2.0	521 ± 22	**1.573 ± 0.057**	**2.209 ± 0.105**	0.213 ± 0.021	4.028 ± 0.241	0.786 ± 0.052	195.1 ± 17.8	1800 - 1836
RYRI-B	10.7 ± 5.0							1.194 ± 0.119	2.478 ± 0.086	0.205 ± 0.020	3.909 ± 0.294	0.573 ± 0.224	146.6 ± 58.4	1808 - 1925

[a] Water content as a percentage of water mass to wet-sample mass. Uncertainties are estimations based on field observations and environmental site conditions. Values used to determine total dose rate and ages.

[b] Uncertainties are 1σ

[c] Total seidment gamma-ray dosimetry. All samples were meausred in the field, but PSA samples (bold) were sent to the Environmental Radioactivity Laboratories at ERISS in Darwin, NT, Australia, for high resolution gamma ray spectrometry. Reported high resolution doses are corrected for water content.

[d] All measurements are corrected for sample water content. High-resolution beta dosimetry for PSA samples (bold) was measured at the Environmental Radioactivity Laboratories at ERISS in Darwin, NT, Australia.

[e] Cosmic-ray dosimetry from Prescott and Hutton (1994); all samples are adjusted for water content. Uncertainties are 10%.

[f] Total dose rate incorporates high-resolution dosimetries (if applicable) and an assumed internal dose rate of 0.032 ± 0.011 Gy/kyr. Uncertainties are calculated as the quadratic sum of random and systematic uncertainties

[g] An additional 2% uncertainty associated with laboratory beta source calibration.

[h] Burial ages presented in year before present, where present is AD 2013, the year all samples were collected and analysed.

Table 6.4: Grain Acception and Rejection Table

	BIRC-A		BIRC-B		FENW-A		FENW-C		GOOR-A		GOOR-B		GROV-A		GROV-B		PHL-A		PHIL-B		RYRI-A		RYRI-B	
	n=	%	*n*=	%	*n*=	%	*n*=	%	*n*=	%	*n*=	%	*n*=	%	*n*=	%	*n*=	%	*n*=	%	*n*=	%	*n*=	%
Grains Measured	*1,588*	100	*1,434*	100	*1,515*	100	*941*	100	*3,613*	100	*5,663*	100	*1,341*	100	*957*	100	*1,408*	100	*1,399*	100	*1,390*	100	*1,389*	100
Accepted	*97*	6	*108*	8	*129*	9	*177*	19	*113*	3	*106*	2	*98*	7	*136*	14	*139*	10	*126*	9	*71*	5	*75*	5
Rejected[a]	*1,491*	94	*1,326*	92	*1,386*	91	*764*	81	*3,500*	97	*5,557*	98	*1,243*	93	*821*	86	*1,269*	90	*1,273*	91	*1,319*	95	*1,314*	95
BG	*865*	54	*706*	49	*847*	56	*425*	45	*2,041*	56	*3,321*	59	*653*	49	*382*	40	*834*	59	*792*	57	*817*	59	*824*	59
IR2sig	*93*	6	*84*	6	*61*	4	*36*	4	*235*	7	*321*	6	*69*	5	*47*	5	*52*	4	*64*	5	*69*	5	*80*	6
RR2sig	*132*	8	*120*	8	*158*	10	*85*	9	*432*	12	*663*	12	*101*	8	*88*	9	*116*	8	*114*	8	*138*	10	*145*	10
RRR	*37*	2	*42*	3	*26*	2	*35*	4	*69*	2	*125*	2	*48*	4	*30*	3	*16*	1	*26*	2	*29*	2	*34*	2
RS	*115*	7	*94*	7	*71*	5	*30*	3	*214*	6	*389*	7	*87*	6	*55*	6	*66*	5	*66*	5	*53*	4	*36*	3
RG	*50*	3	*56*	4	*33*	2	*19*	2	*93*	3	*132*	2	*50*	4	*29*	3	*28*	2	*35*	3	*15*	1	*24*	2
RF	*28*	2	*18*	1	*26*	2	*27*	3	*62*	2	*106*	2	*33*	2	*34*	4	*10*	1	*24*	2	*18*	1	*38*	3
RT	*29*	2	*15*	1	*26*	2	*4*	0	*71*	2	*30*	1	*29*	2	*14*	1	*9*	1	*6*	0	*65*	5	*32*	2
RE	*142*	9	*191*	13	*138*	9	*103*	11	*283*	8	*470*	8	*173*	13	*142*	15	*138*	10	*146*	10	*115*	8	*101*	7

[a] Grain rejection criteria are as follows: BG - Luminescence signal <3x background; IR2sig - Infrared (IR) 2σ <1; Recycling ratio (RR) 2σ <1 or >1; RRR - RR > 10%; RS - No or poor luminescence signal; RG - Background >50% of the luminsence signal; RF - Dose response curve does not fit exponential models with or without a linear component; RT - Saturation limit reached; RE - 0 Gy regeneration dose >5% of the natural luminescence signal.

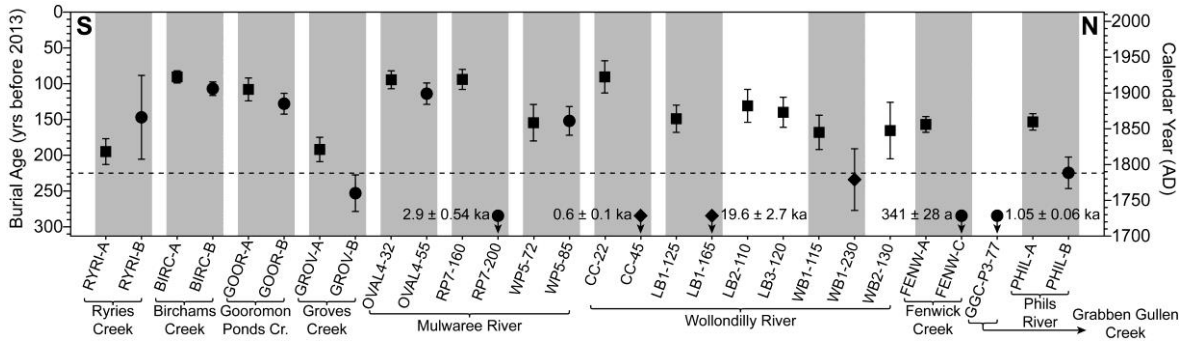

FIGURE 6.5
Burial ages of Tablelands SM and PSA samples (circles and squares, respectively) from this study, Rustomji and Pietsch (2007), and Muñoz-Salinas et al. (2014), generally arranged from south (S) to north (N). Black diamonds are samples from non-SM alluvium underlying PSA samples. Samples from the same sediment profile are grouped by grey boxes – only the two samples closest to the SM-PSA transition are included here. Dashed black line marks the calendar year AD 1788 when Europeans arrived in Port Jackson, present-day Sydney, NSW.

6.4 DISCUSSION OF BURIAL AGE RESULTS

6.4.1 INTEGRITY OF BURIAL AGES

The minimum age model is more appropriate in interpreting burial ages from PSA data rather than the central age model largely because of the fluvial setting of PSA in valley bottoms. The preservation of bedding structures at some sample sites (see CHAPTER 4.0) and the increase in inherited luminescence across the SM-PSA transition are indications that PSA is not well-bleached and likely includes a mixture of sediment with various bleaching histories. Overdispersion of D_e estimates at each sample site (FIGURE 6.4) support the interpretation that PSA sediment is a mixture of sediment with different bleaching histories. Thus, only the minimum age model can reveal the timing of initial PSA and SM deposition in these fluvial settings.

Two samples is not enough to give a detailed depositional history at any of the sample sites; however, the chronologic agreement in ages and lack of stratigraphic inversion builds confidence that SM environments were present throughout the Tablelands into the 19th century and that all sampled PSA deposits are post-European in age. The one exception from the dataset is Ryries Creek. The burial age of SM sediment at Ryries Creek, 146.6 ± 58.4 a, corresponds the years AD 1808–1925 and includes large 1σ uncertainties while PSA at Ryries Creek was buried at 195.1 ± 17.8 a or AD 1800–1836. While both SM and PSA age at Ryries Creek are derived from substantially fewer quartz grains than all other sites (n = 75 and 71, respectively), the PSA's age estimate is weighted by a similar number

of accepted quartz grains as other PSA sites whereas the SM age model is weighted only on 3 of the 75 accepted quartz grains. There is no reason to doubt the PSA burial age, and it is plausible that had one more tube of sediment from RYRI-B been collected, the number of accepted quartz grains would increase, the precision on the burial ages would increase, and the large uncertainties on its age be dramatically reduced.

Burial ages indicate large time gaps between SM and PSA sediment corresponding to 144 a at Fenwick Creek, 18 a at Groves Creek, and 37 a at Phils River. Time gaps either indicate that there was no SM accumulation before PSA deposition or an unknown amount of younger SM sediments was eroded and transported away before PSA deposition began, or there was significant accumulation of luminescence in SM sediments after PSA deposition. Bulk OSL data at the oldest site in the Goulburn Plains, Ryries Creek (195 a) likely represents the palaeo-valley bottom (see CHAPTER 5.0); thus, there has been minimal post-depositional accumulation of luminescence at Ryries Creek because bulk OSL at the SM-PSA transition still exhibits zero luminescence (FIGURE 6.2). There is no evidence that swampy meadows ever stopped accumulating sediment anywhere else in the Tablelands prior to incision (Muñoz-Salinas et al., 2014; Rustomji and Pietsch, 2007), so the observed time gaps in these data must result from swampy meadow erosion during PSA deposition.

6.4.2 POST-EUROPEAN SETTLEMENT ALLUVIUM

The coincidence of all PSA depositional ages with the post-European era of settlement in the Tablelands strongly supports the traditional geomorphic interpretation and corroborates Rustomji and Pietsch's (2007) conclusions that these sediments were deposited after the arrival of Europeans to the region. The Tablelands had been settled by Aboriginal Australians for tens of thousands of years, however (Stockton and Holland, 1974), so PSA should be redefined in Australia as post-*European* settlement alluvium. Outside of Australia, redefining PSA in the Tablelands may seem trivial, but in the Australian vernacular, this redefinition importantly acknowledges the presence of Aboriginal Australians in the Tablelands prior to European arrival. The use of the acronym PSA is maintained as it is widely used to refer to post-European settlement and its effects in other European-colonised lands (Booth et al., 2009; Brannstrom and Oliveira, 2000; Kreznor et al., 1990; Merritts et al., 2011; Wilkinson and McElroy, 2007).

6.4.3 CHRONOLOGY OF GULLY EROSION IN THE TABLELANDS

The PSA ages presented in this study are not the first to come from the Tablelands region of New South Wales; however, they do provide the first regional examination of PSA deposition. All six study sites lie within the portion of the Tablelands settled by Europeans by the AD 1830s (see FIGURE 7 in Scott, 2001), and the oldest PSA deposit dated in this study is in the southernmost part of the European-settled area at Ryries Creek, which is the area first occupied by Europeans.

Ages derived from this study are compared to other ages of PSA deposits or gully activity known from oral or anecdotal evidence and by quantitative dating methods, but some of these methods are liable to substantial uncertainty and misunderstanding. For instance, radiocarbon ages from fluvial settings are potentially unreliable (Blong and Gillespie, 1978) and young radiocarbon ages are not easily calibrated to calendar years (Reimer et al., 2013). Also, oral and anecdotal evidence rely on consistent recollection of erosional events and land use changes, and exact ages or dates may not be valid unless the source of information was documented at the time of the event or independently collected memories corroborate each other (Lane, 1997; Starr, 1989).

With an OSL burial age of 195 ± 18 a, RYRI-A corresponds to AD 1800–1836, meaning that if gullying associated with deposition of Ryries Creek PSA resulted from land use change, it came very early in the history of European settlement in the Tablelands. Drainage basins in the Tinderry Mountains that are currently covered by native forests show no signs of incision (Neil and Fogarty, 1991), implying that incision is likely associated with changes in catchment vegetation, perhaps as a result of European land use change. According to Starr's (1989) interviews with European settlers, the first graziers at Michelago, NSW arrived in 1828 and Starr concluded that gullying in Michelago Creek and its tributaries, Margarets and Teatree Creeks, which neighbour Ryries Creek, began within the first 30–40 years of settlement. Sandsheets deposited over SM units in Wangrah Creek on the opposite side of the Tinderry Mountains (Gillespie et al., 1992) were radiocarbon-dated, though no ages are given – only that they are "modern" and continued to be deposited into the mid-AD 1800s (Prosser, 1991). Gullying was activated in Gungoandra Creek south of Michelago around the same time (Prosser and Abernethy, 1996). Given the evidence of regional erosion dates from this and other studies, and considering that gully development may occur within five years of landscape disturbance

(Prosser and Soufi, 1998), the timing of gully erosion in Ryries Creek can be narrowed to the period AD ~1828–1834.

GROV-A in Groves Creek in the middle of the Goulburn Plains returns a burial age corresponding to AD 1804–1838. Cattle grazing was present in this region by AD 1825 (Scott, 2001) and Groves Creek is near Mulwaree River, where one of Rustomji and Pietsch's (2007) single grain OSL age profiles (WP5) shows that some PSA deposition occurred between AD 1833–1884 (FIGURE 6.5), concurrent with the approximate onset of gullying in the Burra Creek catchment 40 km south of Groves Creek (Eyles, 1977c). A radiocarbon age (255 ± 64 yrs BP) from cross-bedded sand within Groves Creek (Coventry and Walker, 1977) cannot be satisfactorily calibrated using CALIB Radiocarbon Calibration software (vers. 5.0, Stuiver and Reimer, 1993) and the 2013 INTCAL13 calibration curves (Reimer et al., 2013) to yield a meaningful calendar age. As with Ryries Creek to the south, the likely timing of gully incision and PSA deposition at Groves Creek was shortly after European arrival, around AD 1825–1835 based on historical records of settlement and OSL burial ages at Groves Creek and Mulwaree River.

European squatters arrived in the Goulburn and Crookwell regions of NSW by AD 1828 and deforestation began in the late AD 1830s for grazing and crop-based agriculture (Bayley, 1975). PSA ages from Fenwick Creek near Goulburn correspond to AD 1845–1867, closely agreeing with five of the six profiles along the nearby Wollondilly River showing PSA deposition between AD 1808–1905 (FIGURE 6.5) (Rustomji and Pietsch, 2007). Local gullying is extensive, but no other dates are available and historical data are scarce, even for the nearby gullies that were studied at Whiteheads Creek (Olley et al., 1993). PSA deposition ages at Phils River (AD 1848–1871) north of Crookwell, NSW, are nearly identical to those at Fenwick Creek. West of Crookwell, PSA has been examined along Grabben Gullen Creek (Muñoz-Salinas et al., 2011, 2014), and a trend line through an OSL age-depth plot of SM sediments suggests a pre-European age for PSA deposition. Due to its geographic proximity, PSA at Grabben Gullen Creek may have been deposited contemporaneously with that at Phils River and Fenwick Creek, and if so, Muñoz-Salinas et al.'s (2014) suggested age of Grabben Gullen Creek PSA is an overestimate resulting from undetected erosion of SM sediment prior to PSA deposition.

Birchams Creek, the youngest site of this dataset, shows PSA deposition between AD 1914–1932, well after the start of PSA deposition at Groves Creek or Mulwaree River, but

nonetheless coinciding with continued deposition at Mulwaree River – profiles OVAL4 and RP7 – into the AD 1900s (Rustomji and Pietsch, 2007). Eyles's (1977a) time-series pond and gully locations along Birchams Creek (see CHAPTER 5.0) conceptualises the transition from a valley bottom chain of ponds to a continuous gully. The absence of gullying in Birchams Creek in AD 1880 and its presence by AD 1941 are consistent with the time constraints provided here for PSA deposition at BIRC-A. A radiocarbon age of 10 ± 115 yrs BP from an unspecified locality in Birchams Creek (Eyles, 1977a) cannot be calibrated to calendar years (Reimer et al., 2013; Stuiver and Reimer, 1993) and is essentially meaningless. The current owners of the land Birchams Creek flows through, which has been in the same family for ~100 years, noted that a gully was present in the lower reaches since at least AD 1910 (Eyles, 1977a). This gully age, if trustworthy, must mean that either PSA deposition occurred slightly before the time indicated by the BIRC-A OSL age, or that the AD 1910 gully had not yet reached the sampling site. Considering that of all PSA samples presented here, BIRC-A exhibits the smallest uncertainty ($1\sigma = \pm 9$ a), the second option is more likely and thus initial incision occurred in the mid AD 1910s followed very shortly after by headward erosion of the AD 1910 gully, which formed the continuous gully present at the site today.

The OSL ages reported here indicate that PSA deposition at Gooromon Ponds Creek began between calendar years AD 1889–1921. The earlier part of this period coincides with settlement history in the Canberra region as evidenced at Jerrabomberra Creek where gullying had initiated by AD 1878 and PSA deposits within the creek contain pieces of livestock carcasses, ceramics, and fencing wire (Wasson et al., 1998). Landowners in the western region of settled territory began clearing land by the AD 1850s (Gillespie, 1981) and initial gully incision likely occurred shortly thereafter. PSA at Gooromon Ponds Creek extends beyond its confluence with its neighbour, Ginninderra Creek, which was gullied after the mid AD 1900s (Eyles, 1977b). Gullying in Ginninderra Creek deposited PSA at its confluence with Gooromon Ponds Creek in the mid- AD 1900s, but because PSA along Ginninderra Creek is exposed at a lower elevation than along Gooromon Ponds Creek, it must have been deposited after PSA at Gooromon Ponds Creek had been deposited. This chronologic interpretation is supported by the GOOR-A age, which shows that PSA along Gooromon Ponds Creek occurred in the early AD 1900s.

Since the Gooromon Ponds Creek and Birchams Creek sites are only ~20 km apart, and since the uncertainties of their deposition ages overlap during the calendar years AD 1914–

1921, it is likely that gully incision was initiated during this period, just as it had at nearby Bango Creek in AD 1915 (Gillespie, 1981) and Waterhole Creek (Eyles, 1977b). Further investigations at Boro Creek (Erskine and Melville, 1984), south of Tarago, NSW found fence lines and other European artefacts within sandy overbank deposits. Wire fences were not available in this region until the AD 1860s and not widely used until the AD 1880s (Hancock, 1972; Pickard, 2007, 2010), meaning gully erosion and PSA deposition at Boro and Jerrabomberra Creeks could not have occurred at the same time as at Ryries Creek, Groves Creek, or WP5 from Mulwaree River in the early AD 1800s, but rather was contemporaneous with deposition at Gooromon Ponds Creek and Birchams Creek in the early AD 1900s.

6.4.4 EUROPEAN LAND USE CHANGE IN A CHANGING CLIMATE

While settlement and land use change were nearly continuous after the early AD 1800s, the quantitative ages and historical accounts provided here suggest three periods of gully incision and PSA deposition: AD ~1825–1835, ~1850–1870, and ~1890–1920 in the southern, northern, and central Goulburn plains, respectively. A cumulative distribution plot of all OSL ages from this study and Rustomji and Pietsch's (2007) supports the coincidence of PSA deposition with these time periods, as it shows two prominent peaks and one lesser peak corresponding to gully incision at ~185 a, ~158 a, and ~94 a, which translate to AD 1818, AD 1855, and AD 1919 (FIGURE 6.6) The first and last of these periods coincide with a drought-dominated climate regime along coastal NSW and the middle period coincides with a flood-dominated regime (Erskine and Warner, 1988). Assuming European land use changes during the era of settlement in the Tablelands predisposed the landscape to erosion, gully incision associated with a duration of flood-dominated climatic events (the AD ~1850–1870 period) is easily understood with notably large floods having been documented in AD 1851 (Eyles, 1977c; Scott, 2001; Starr, 1989), 1852 (Olley and Wasson, 2003), 1853 (Scott, 2001; Starr, 1989), and 1864 (Eyles, 1977c), each serving as a potential gully-triggering event for Fenwick and Grabben Gullen Creeks and Phils River.

The periods of gully incision associated with long durations of drought presumably relate to the importance of vegetation in stabilising valley bottoms and stream beds, protecting

them from erosion (e.g. Erskine and Melville, 1984; Eyles, 1977a, b, c; Gale and Haworth, 2002; Gillespie, 1981; Johnston and Brierley, 2006; Muñoz-Salinas et al., 2014; Neil and Fogarty, 1991; Olley and Wasson, 2003; Page and Carden, 1998; Prosser, 1990; Prosser and Slade, 1994; Prosser and Soufi, 1998; Rustomji and Pietsch, 2007; Starr, 1989; Warner, 1984; Zierholz et al., 2001). Undoubtedly, prolonged droughts had serious consequences for the durability of vegetation ground-cover, and overgrazing in the Tablelands exacerbated natural vegetation decline from drought during both the early and latter drought-dominated climate periods (AD ~1825–1835 and ~1890–1920). The second drought-dominated regime was even more affected by the plague of rabbits that ravaged the Tablelands at the end of the AD 1800s (Scott, 2001). Gullying at Bango, Birchams, and Gooromon Ponds Creeks, OVAL4 at Mulwaree River, and CC-22 at Wollondilly River all span the period from AD 1914–1921. Toward the end of this drought-dominated period, the central Goulburn Plains saw annual average rainfall levels higher than the previous 15 years (FIGURE 6.7). Rainfall data show that during these high-rainfall years, the maximum monthly rainfall was <20% that of the year's total rainfall, indicating that the whole year was wet rather than rainfall being concentrated in a few extreme storms. This period of higher rainfall immediately following prolonged drought likely triggered gully incision in the central Goulburn Plains, including Birchams and Gooromon Ponds Creeks.

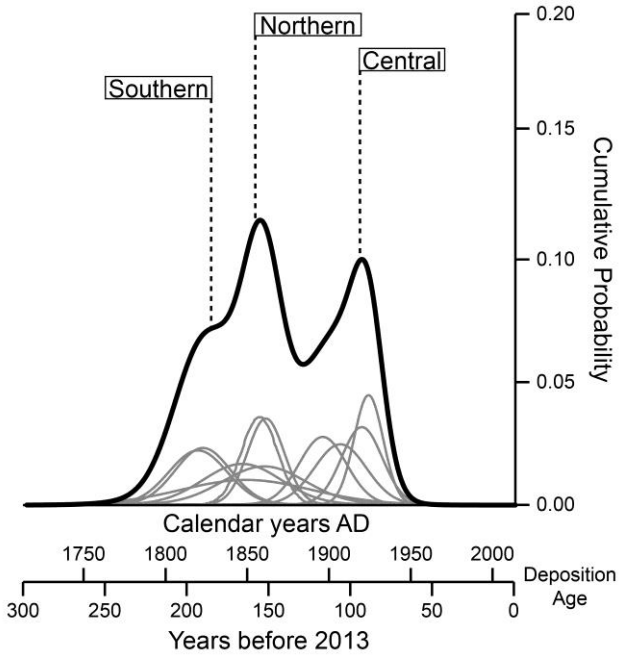

FIGURE 6.6

Cumulative probability plot of PSA OSL burial ages (n = 15) throughout the Goulburn Plains and their 1σ uncertainties from this study and from Rustomji and Pietsch (2007); see FIGURE 6.5 for a list of included samples. Three periods of gully incision and PSA deposition are observed, largely agreeing with anecdotal accounts of erosion and PSA deposition.

Because rainfall measurements are not available for the southern Goulburn Plains for the first drought-dominated regime and period of gully erosion (AD ~1825–1835), the connection between erosion and higher rainfall is less certain. However, climate data from both historical documents and early measured data within the Tablelands region and coastal NSW show that the early drought-dominated regime ended with higher rainfall in the AD 1830s (Fenby and Gergis, 2012; Gergis and Ashcroft, 2013). Though rabbits had not yet been introduced to Australia, grazing was already regionally well-developed, which on top of naturally decreased vegetation, likely primed the landscape for erosion prior to higher rainfalls in the AD 1830s. These periods of higher rainfall in the AD 1830s likely caused gully erosion at Groves and Ryries Creeks.

Historical accounts of land use change and overgrazing livestock certainly demonstrate the potential for European clearing of vegetation and increased agricultural activity to lessen the landscape's capacity to recover from disturbance (Eyles, 1977b; Gillespie, 1981; Johnston and Brierley, 2006; Prosser, 1991; Scott, 2001; Starr, 1989). However, as this study shows, increasing the number of quantitative ages for gully incision or deposition of PSA across a region begins to reveal multiple scenarios in which erosion events were limited in time to short periods of high rainfall, even mimicking patterns of European settlement in the Tablelands. Findings from this chapter contradict the long-held notion that the onset of initial gully incision is regionally asynchronous throughout the Tablelands (Prosser, 1991), and any asynchroneity is only apparent. Rather, initial incision of multiple streams from one portion of the greater Tablelands is locally synchronous and coincides with shifting climatic patterns.

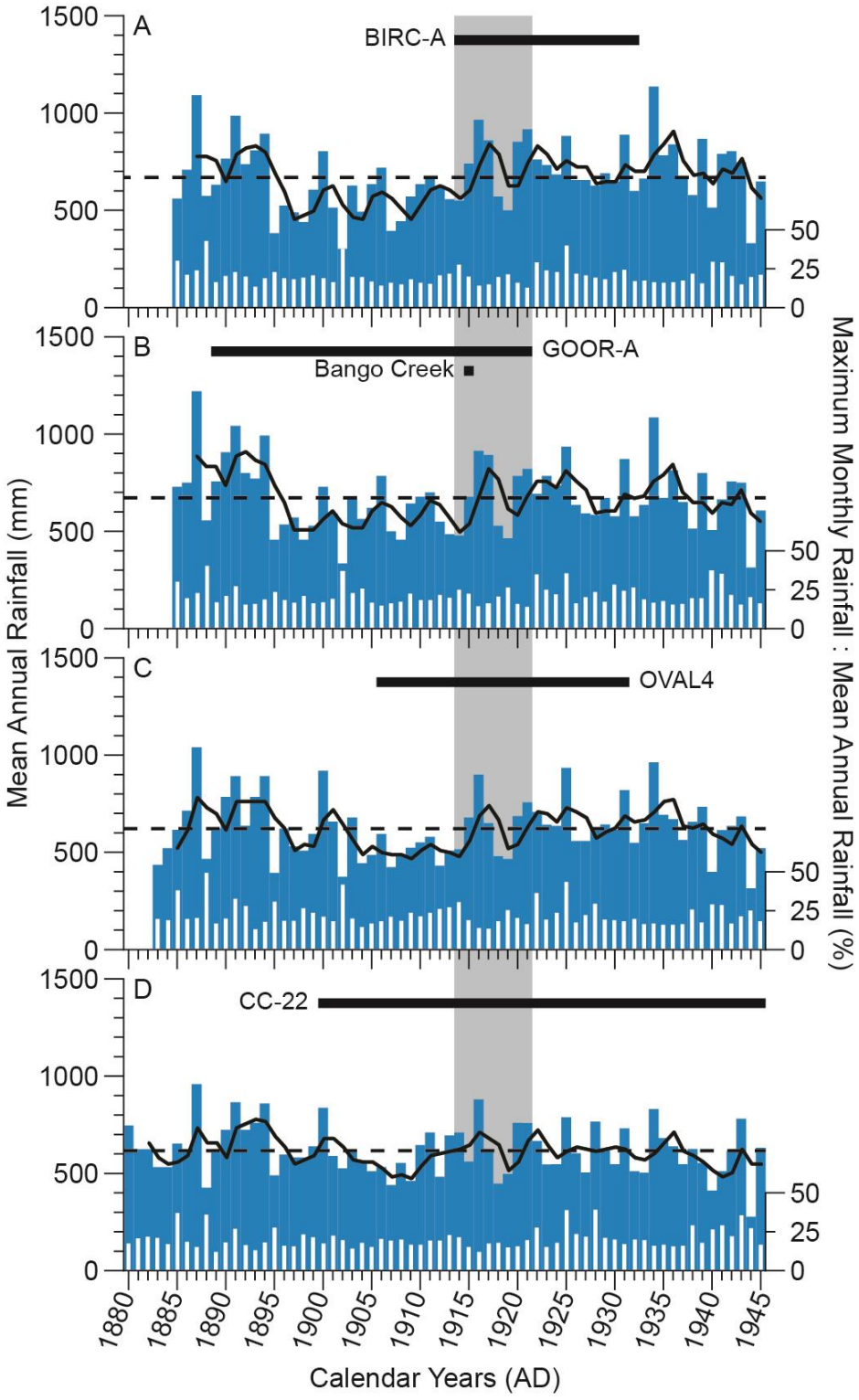

FIGURE 6.7

*Measured rainfall data from weather stations near **A.** Birchams Creek, **B.** Gooromon Ponds Creek, **C.** Mulwaree River, and **D.** Wollondilly River. Dark grey bars show mean annual rainfall in millimetres for each year of measurement. Increased rainfall beginning ~1914 marks the onset of transition from a drought-dominated climate regime to a flood-dominated regime, coinciding with those of Erskine and Walker (1988). All rainfall data comes from the Australian Bureau of Meteorology (http://www.bom.gov.au/climate/data/). Rainfall at Birchams Creek is provided by weather stations 070030, 070194, 070196, and 070227. Rainfall data for Gooromon Ponds Creek comes from weather stations 070032, 070045, 070049, and 070059. Rainfall data for Mulwaree River comes from weather stations 070079, 070086, 070102, and 070105. Rainfall data for Wollondilly River comes from weather stations 070012, 070055, 070063, and 070131.*

6.5 CHAPTER CONCLUSION

Gully erosion in the Goulburn Plains of the southeastern Australian Tablelands increased since the onset of European exploration and settlement of the region in the early AD 1800s. Single grain OSL data from six sites throughout the Goulburn Plains demonstrate that:

- Swampy meadow growth and accumulation continued into the AD 1800s;
- Alluvial deposits overlying swampy meadow sediments are indeed post-European in age and since they are likely the result of land use change after European arrival, I redefine the term PSA in Australia to mean post-European settlement alluvium;
- Significant amounts of swampy meadow sediments can be eroded during PSA deposition;
- European-induced vegetation degradation coincides with the flood- and drought-dominated regimes of southeastern Australia over the past two centuries, leading to the establishment of three periods of regional erosion. The spatial patterns of erosion – first in the southern, then the northern, and finally in the central Goulburn Plains – follow the spread of European agricultural and pastoral land use changes throughout the region, showing that gully erosion and PSA deposition in the post-European era are synchronous across localised areas within the overall Tablelands region.

Increased high-precision, quantitative data from this region are likely to expand upon the conclusions I draw here, that the extent of gullying is regional and that the incision of individual gullies occurred during limited synchronous events corresponding to periods of high rainfall, especially following droughts in areas disturbed by the introduction of European land use practices.

SYNTHESIS & CONCLUSIONS

7.1 SUMMARY OF MAIN CONCLUSIONS AND FUTURE WORK

7.1.1 CHAPTER 3.0: *WHAT IS THE BACKGROUND EROSION RATE IN THE TABLELANDS?*

The background erosion rate of the Goulburn Plains within the southeastern Australian Tablelands, inferred from measurements of *in situ* ^{10}Be, is 7.5 mm/kyr, integrating over hundreds of thousands of years. Erosion of bedrock outcrops (5.3 mm/kyr) and of whole stream catchments (8.7 mm/kyr) are statistically indistinguishable, suggesting that no relief has been generated in the Tablelands since ~600 ka. Average measurements of ^{10}Be from outcrops and fluvial sediment do not agree with ^{10}Be concentrations modelled incorporating low impact Aboriginal fire regimes currently presumed to have begun ~50 ka, implicit in the extinction of Australian megafauna. Rather, fire regimes, of the type and style seen by the first Europeans to Australia, began ~5.5 ka, corresponding to the same time that increased charcoal is observed in the sedimentary record.

This is the first study to compare measured *in situ* ^{10}Be concentrations to those expected from land use models to assess alleged anthropogenic landscape disturbance over any substantial period of time, and its success in this thesis opens the door for similar studies to be applied to landscapes around the world occupied even longer than Australia. For instance, the oldest human-made hunting tools were found from the granitic Olduvai Gorge in Tanzania (Blumenschine et al., 2003), potentially an ideal location to assess human land use change in the oldest landscape occupied by modern humans – an assessment that could expand our knowledge of the effects the earliest humans had on their surroundings, beyond

making and using hunting tools. In theory, this type of model could be applied to any landscape as long as the long-term (tens of millions of years) denudation rates are independently constrained and constant through time.

7.1.2 CHAPTER 4.0: *THE "A" OF PSA: WHAT IS IT?*

Sixteen profiles of swampy meadow-PSA stratigraphies were analysed for bulk sediment luminescence. Swampy meadow sediment exposed in gully walls exhibits similar luminescence depth trends to that of modern swampy meadows, confirming that prior to PSA deposition, nearly all valley bottoms in the Tablelands were occupied by wetland environments. PSA exposed in gully walls preserves fluvial structures and closely resembles flood alluvial deposits of known ages and not uneroded soil profiles, from which I conclude they are alluvium deposited during large floods, and not weathered granitic soil profiles. There are no observed relationships between bulk sediment OSL and mineralogy or grain size, and thus neither can be inferred from bulk OSL measurements. Adjacent sample replicates record a history of sediment bleaching effectiveness during and after large floods, indicating that the erosion and deposition processes resulting in the observed bulk OSL depth profiles are regional and not unique to one particular basin.

The possible extensions of portable OSL applications are numerous. Portable OSL was only used in this thesis to enhance field-based understanding of PSA deposition. However, systematic laboratory experiments with monomineralic, or single grain size fractions could test many of the assumptions guiding portable OSL reader users in the field. For instance, exposing pure mineral separates (e.g. quartz, feldspar, muscovite, etc.) in a laboratory to known amounts of radiation could disentangle the complex relationships between mineral phase abundance and the measured emitted IRSL and/or BLSL. Laboratory flume-experiments could also test the bleaching effectiveness under varying turbidity levels or stream flow velocities, for example. Any combination of mineralogy, grain size, and sediment transport conditions, and permutations thereof, might provide insight into the sediment bleaching and transport history of samples that are hundreds or thousands of years old. In the field, bulk OSL profiles of PSA, or any observable unit of sediment, collected at evenly spaced intervals along gully walls might provide a sense of how PSA is

being deposited after transport, whether swampy meadows were eroded during PSA deposition, or whether the pre-PSA landform is preserved under the sandy sediment.

7.1.3 CHAPTER 5.0: *HOW DO GULLIES IN THE TABLELANDS FORM? BIRCHAMS CREEK: A CASE STUDY*

Concentrations of meteoric ^{10}Be and bulk sediment OSL, both of which have characteristic profiles with depth in sediment, were used in tandem for the first time to retrospectively identify the valley bottom substrate most likely to have formed the first gullies in the Tablelands landscape. Weathered valley bottom regolith, upstream of pre-existing swampy meadows, were negatively affected by tree clearance for grazing and trampling by livestock during periods of drought, which oversteepened localised segments of Birchams Creek, creating the nucleating sites for incipient gully incision in the Tablelands. PSA is not derived from erosion of swampy meadow sediments as previously thought.

Subsurface imaging techniques, such as ground penetrating radar (GPR), could have been used to ground-truth the conclusions drawn at Birchams Creek, that PSA in the catchment was deposited down the centre of the valley. Portable OSL reader profiling and GPR could be used at a number of field sites in the Tablelands to explore the question of whether PSA buried and preserved swampy meadow landforms or significantly scoured and eroded valley bottoms during deposition. Birchams Creek would be an ideal field site for this type of work because of its small size and well constrained erosion history; similarly, Grubbenbun Creek would be suitable since the creek meanders and exposes numerous swampy meadow-PSA exposures in a wide, flat floodplain that could be used to ground-truth the GPR data.

PSA deposition at Birchams Creek demonstrated how bulk OSL and meteoric ^{10}Be can successfully be paired to assess gully initiation scenarios; however, this was carried out in a simple catchment with limited possible PSA source material and depositional areas. This work could be expanded by moving into more complex river basins, for example, a complex stream network draining a monolithologic basin, or a simple stream network draining a multilithologic basin. Results from these types of expansions could be used to develop erosion and sediment mixing models and histories for already-gullied catchments,

which would benefit watershed conservationists by pin-pointing erosion prone lithologies or valley bottom substrates in ungullied catchments. Part of the initial research plan for this thesis was to expand the sediment tracing abilities of portable OSL readers in the Tablelands. At the outset of this thesis, PSA ages were presumably AD 19th century and as such, meteoric ^{10}Be was chosen to be paired with bulk OSL to trace sediment *in lieu* of other short-lived radionuclides commonly used in sediment provenance studies whose half-lives are too short (e.g. ^{7}Be, ^{137}Cs), or would not have been present in surface sediment eroded before atom bomb testing began (e.g. ^{137}Cs). There is no reason to believe that pairing bulk sediment OSL with either ^{7}Be or ^{137}Cs to identify erosion hotspots would not work just as well in landscapes affected by erosion and sediment deposition within the last few months or decades.

7.1.4 CHAPTER 6.0: *WHEN WAS PSA DEPOSITED IN THE TABLELANDS?*

Burial ages for six PSA sediment samples, determined using OSL dating techniques, are used alongside quantitative and anecdotal evidence of gully erosion and PSA deposition throughout the Goulburn Plains to show that erosion mimicked European migration into the region. Episodes of gully incision followed European land use changes, mostly tree removal for livestock grazing, first in the southern Goulburn Plains between AD 1825–1835, in the northern Goulburn Plains between AD 1850–1870, and in the central Goulburn Plains between AD 1890–1920. This is the first study to demonstrate the local contemporaneity of gully incision, and its close relationship to shifting climate patterns over the last 200 years. That is, gully erosion, widespread PSA deposition, and swampy meadow burial are all the result of European land clearance upon arrival in the Tablelands in the early AD 19th century.

Further ages determined for PSA deposits in the Goulburn Plains are likely to reveal an even more detailed chronology than provided in CHAPTER 6.0. Research efforts were focused on the Goulburn Plains in order to have enough data to produce a coherent and robust research project. The data that was collected from the Bathurst and Monaro Plains show that continued efforts in those regions are likely to corroborate the conclusions drawn in this thesis and create chronological "bookends" in that the Bathurst Plains were explored before the Goulburn Plains, and the Monaro Plains were only accessible via and thus

occupied by Europeans after the Goulburn Plains. Exposures of PSA in the Bathurst Plains were difficult to find, unless exceedingly obvious and even gullies were not as apparent on the landscape, suggesting that the Bathurst Plains have begun to recover from gully incision. The Monaro Plains are quite the opposite in that they are still nearly completely treeless and there are many thick mantles of PSA blanketing valley bottoms. A time-series of studies from all three regions of the southeastern Australian Tablelands could prove to be a natural chronosequence of landscape recovery (e.g. Bathurst Plains), recent landscape adjustment (e.g. Goulburn Plains), and ongoing landscape perturbation (e.g. Monaro Plains) following the arrival of Europeans. Focusing this thesis on only one region of the southeastern Australian Tablelands only tells one part of the whole Australian land use history, though its proximity to Sydney, the entrance for Europeans to the continent, makes it arguably one of the most important. One could go further and farther by studying European-induced landscape degradation of the Arnhem Land in the Northern Territory or the Atherton Tablelands in Queensland, for example, where background erosion rates using *in situ* ^{10}Be have already been constrained.

7.2 THE IMPORTANCE OF EROSION AND SEDIMENTATION STUDIES

This thesis demonstrates that post-European settlement alluvium in southeastern New South Wales is widespread and a consequence of land clearance and livestock grazing after the arrival of Europeans to Australia. However, the sequence of events leading to PSA deposition in the Tablelands is not unique to the Tablelands. Gully erosion occurs throughout New South Wales (Beavis, 2000; Crighton and Gore, 2001; Gore et al., 2000; Hughes and Prosser, 2003; Hughes and Prosser, 2012; Lane, 1997), Victoria (Erskine, 1994; Whitford et al., 2010) (especially where rivers were hydraulically mined for gold (Scott, 2001)), Queensland (Brooks et al., 2009; Hughes et al., 2009; Wallbrink, 2004), Tasmania (Pemberton, 1988), and in general across the agricultural regions of Australia (Hughes et al., 2001). In most cases, such gully erosion has been accompanied by increased sedimentation rates or alluviation downstream, but soil and gully erosion are also the sources of increased sedimentation of agricultural lands and offshore. Though this thesis focused on sedimentation of agricultural land, increased offshore sedimentation also has severe consequences for coastal and marine environments (Wallbrink, 2004), including the Great Barrier Reef, which carries UNESCO World Heritage status and is under threat

by increased sedimentation from erosion in tropical northern Queensland (Hughes et al., 2009), and may continue to be under threat once anthropogenic sediment stored in catchments (Nichols et al., 2014) is delivered to the Reef.

7.3 PSA REMOVAL AND STREAM REMEDIATION

Trends of land use change through time show that the percentage of land for pasture and cropland may soon decline, yet urban areas are increasing due to the drastic rate of global population growth, a rate which shows no indication of slowing (FIGURE 7.1) (Hooke et al., 2012). If for no other reason, research and work must continue to understand conditions that make a landscape prone to gully erosion, what factors drive incision, what happens to the sediment eroded from gullies, and what the inadvertent consequences are for the communities and environments downstream of eroded land. Steps must be taken to inform and educate community leaders in agricultural areas about erosion mitigation strategies that are both environmentally protective and cost effective. For instance, CHAPTER 5.0 demonstrates the ability to identify the valley bottom substrate where gully incision in Birchams Creek occurred, showing that swampy meadow wetlands were not susceptible to incision but weathered regolith upstream was. This conclusion supports Prosser and Slade's (1994) findings that swampy meadows were not likely to be affected by grazing or fire and Zierholz et al.'s (2001) finding that even newly established wetlands on gully beds can withstand the forces of large magnitude floods. Policy makers, land managers, and graziers can thus use these corroborative findings to focus erosion remediation efforts and finances on restabilising non-wetland valley bottoms, the success of which will have positive implications for pastures (e.g. decreased soil loss) and the wetlands (e.g. decreased sedimentation, increased biodiversity)

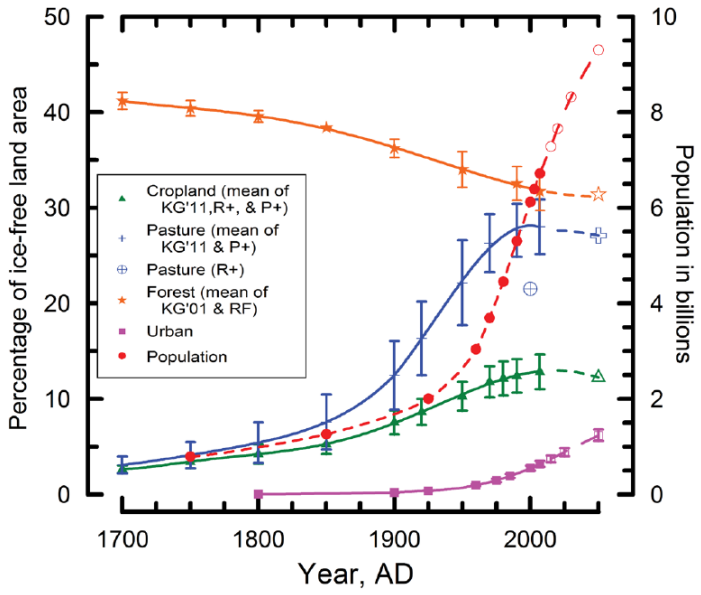

FIGURE 7.1
Land use trends of cropland, pasture, forest, and urban settings since AD 1700 compared to the global population growth trend (Hooke et al., 2012).

Remediation efforts are expensive; however, remediation, specifically revegetation, of disturbed catchments have been shown to return erosion and sedimentation rates to pre-disturbance levels (Molina et al., 2009; Reusser et al., 2015; Vanacker et al., 2007). In the midwestern United States, Booth et al. (2009) removed PSA from two small catchments in Wisconsin, which has led to the overall increase of wetlands cover and an increase in wetland biodiversity throughout the catchments (Booth and Loheide II, 2012). However, large earthmovers were used to dig trenches into the valley bottoms in order to determine the depth of PSA throughout the basin, a very invasive process. Less-invasive trench digging has been cited as the trigger for gully erosion in some Australian case studies (Johnston and Brierley, 2006; Starr, 1989), so perhaps digging trenches with earthmoving equipment is counterintuitive to restoration efforts. The effectiveness of using bulk OSL data to identify the sedimentary contact between swampy meadow sediment and PSA was demonstrated in CHAPTER 4.0, which could easily become a much less invasive and more cost effective approach for conservation organisations as samples could be collected by a few people with simple coring devices rather than large construction equipment. Merritts et al. (2011) provide an example of a similar restoration strategy in Pennsylvania that removed PSA from valley bottoms and show that native vegetation communities returned, growing from seed banks buried under PSA (FIGURE 7.2). The importance of gully restoration efforts using buried seed banks is becoming more widely recognised, and researchers in southeastern Australia are trying to increase awareness of this natural

restoration technique (O'Donnell et al., 2014), which may provide a solution to the financial concerns of more intensive restoration projects in Australia (Dobes et al., 2013). PSA has not only buried wetland ecosystems, but downstream sedimentation caused by land clearing has likely preserved significant prehistoric archaeological sites (Stafford and Creasman, 2002) and so removing PSA from floodplains may also reveal insights to our collective human history.

FIGURE 7.2
*Before (**left**) and after (**right**) photos from Lititz Run in Pennsylvania, from Merritts et al. (2011). The dashed white line indicates the depth extent of PSA deposited behind mill dams, which was removed during restoration. Native vegetation was restored from buried seed banks that had been trapped under PSA.*

7.4 THE ANTHROPOCENE

Zalasiewicz et al. (2011; 2008) believe sufficient geological, biological, and archaeological evidence is available to define a new era in the geological timescale, the Anthropocene. Exactly when this era was to have begun continues to be discussed. While some believe the Anthropocene started with the Industrial Revolution (Crutzen, 2002; Zalasiewicz et al., 2008), stratigraphers are frustrated at the Anthropocene's increased popularity and use even though there is no distinct and globally distributed boundary in the stratigraphic record to separate it from the Holocene (Autin and Holbrook, 2012). Indeed, there are some (e.g. Visconti, 2014) who believe claims of human disturbance of the geosphere are greatly exaggerated and that human activity is not sufficiently pronounced to be identifiable in the geological record millions of years in the future.

Crutzen (2002) proposed that the onset of the Anthropocene coincides with the invention of the steam engine in 1784 and the ushering in of the Industrial Revolution that altered atmospheric chemistry and climate conditions. There is no doubt that humans have become the dominant movers of Earth material for construction, infrastructure, and agricultural

purposes (Hooke, 1994, 2000; Hooke et al., 2012; Montgomery, 2007b; Wilkinson and McElroy, 2007), and Zalasiewicz et al. (2008) build on this suggestion, positing that sediment infill behind dams, for instance, will be preserved over geological timescales, thus marking the onset of the Anthropocene. More recently, the definition of a new rock type, the plastiglomerate (Corcoran et al., 2014), has been suggested as a potential identifiable marker of human activity in the geological record. And still more recently, the date of 16 July 1945 – when the first atomic bomb was tested in New Mexico – was selected as fallout radionuclides only produced in nuclear testing had never been identified in soils, but are now commonly used to monitor erosion and sediment movement (Ritchie and McHenry, 1990).

Howard (2014) has suggested that a requirement of defining a stratigraphic marker for Anthropocene sediments should be that the sediments bury or enclose human artefacts. Corcoran et al. (2014) responded to Howard's suggestion by noting that plastic debris can be found on land, along coastlines, and in the open ocean (Derraik, 2002; Kaiser, 2010). However, plastiglomerates are too recent a sedimentological marker to be used as a basal identifier of the human era. In a similar way, Zalasiewicz et al.'s (2015) proposal that fallout radionuclides from atomic testing may be the most prominent evidence of the human impact on the geologic record, but nuclear testing is still too recent to mark the onset of the Anthropocene. Perhaps the entrainment of European artefacts derived from the mass production of materials following technological advances of the Industrial Revolution (e.g. metal cans, glass bottles, wire, etc.), such as those identified in Post-European settlement alluvium in Australia (Wasson et al., 1998), would be more age-appropriate features for the Anthropocene. After all, PSA is frequently found throughout New and Old World lands (CHAPTERS 4.0, 6.0) (Beach et al., 2006; Booth et al., 2009; Brannstrom and Oliveira, 2000; Coltorti et al., 2010; Foulds et al., 2013; García-Rodríguez et al., 2002; Knox, 1977, 2006; Kreznor et al., 1990; Passmore and Macklin, 1994; Turkelboom et al., 2008; Wilkinson and McElroy, 2007), and artefacts of these types are common even in Antarctica (Camenzuli et al., 2013).

As demonstrated in CHAPTER 6.0, however, not all PSA deposits contain industrial artefacts. Rather, it seems that the most abundant record of human impact on the environment is not what is encapsulated within the sediment, but the sediment itself. Human failure to learn from the past to understand how to manage soil erosion and sedimentation in agricultural landscapes is not new, and Australian PSA, being the result

of European land clearance in the AD 1800s, is simply one of the most recent examples of the cause-and-effect relationships between human land use and landscape degradation (e.g. Beach et al., 2006; Fuchs et al., 2004; Knox, 2006; Lang et al., 1999; Montgomery, 2007a; Nyssen et al., 2004). If PSA in Australia was caused by European land use changes, surely land use changes triggered by any civilisation should result in similar PSA-type sediments being preserved around the world, providing numerous examples of the human effect on the Geological record.

Montgomery (2007b) compiled numerous examples of land use mismanagement, and the failure to conserve crop land around the world and through time. Recent reviews of radiocarbon data in European river systems (Macklin et al., 2006; Starkel et al., 2006; Thorndycraft and Benito, 2006a, b) demonstrate that the history of geomorphic activity in Europe was closely linked to climate variation until the Roman period when land clearance is associated with increased alluviation; the same studies also show similar increased geomorphic activity in the Middle Ages. While climate change may have been the driver behind increased geomorphic activity, human land use certainly primed the landscape for erosion, exacerbating natural climatic effects (Macklin et al., 2006). River aggradation associated with human land use change in Greece (Fuchs et al., 2004; Lespez, 2003), Germany (2006; Lang et al., 2003b), South Africa (Damm and Hagedorn, 2010), New Zealand (Richardson et al., 2014; Richardson et al., 2013), Central America (Anselmetti et al., 2007; Beach et al., 2006; Beach et al., 2009) North America (Stinchcomb et al., 2011; Waters, 1988), and China (Kidder et al., 2012) in the last 2–3 kyr has also been observed.

This chronological pattern continues back in time into the Bronze and Neolithic Ages as human populations cleared land for agricultural purposes, allowing hillslope sediment to be eroded and deposited in valley bottoms in Belgium (Rommens et al., 2005), Germany (Hoffmann et al., 2008), the British Isles (Foulds and Macklin, 2006), Greece (Fuchs et al., 2004; Lespez, 2003; Pope and van Andel, 1984), Ethiopia (Nyssen et al., 2004), China (Kidder et al., 2012; Rosen, 2008), and Bolivia (Coltorti et al., 2010). Australia's geomorphic record, even in the absence of known physical sedimentary deposits thousands of years old, has been altered by Aboriginal land use since ~5.5 ka, as was demonstrated in CHAPTER 3.0. I argue, and strongly agree with a recent publication by Edgeworth et al. (2015), that these 4–7 ka aggradational sequences and deposits of PSA-type sediments are the first to record widespread human-induced influence in the geological record and that they satisfy Zalasiewicz et al.'s (2015) suggestions of being diachronous, identifiable in the

sedimentary record, representative of a sudden pulse in human activity, and having geological longevity. Furthermore, these sedimentary deposits are contemporaneous with Ruddiman's (2003) observed increase of CO_2 and CH_4 in ice core records ~6 ka, giving credence to Crutzen and Steffan's (2003) suggestion that the Anthropocene may have had a stepped history since ~6 ka.

7.5 CONCLUDING REMARKS

The relationships between humans, land use, and landscape change in Australia are no less complex upon the completion of this Thesis than at the outset, and they will always be. What was gained in this Thesis is a greater knowledge and understanding of how even the most seemingly mundane of actions, such as clearing trees from a hillside or allowing animals to roam freely across a plot of land, can lead to widespread landscape degradation. These actions are not limited to southeastern Australia, nor are they limited to the last few centuries since the Industrial Revolution, but are actions that have been part of humankind for millennia around the world. The evidence provided in this Thesis continues to build upon and adds to a growing body of knowledge that demonstrates that humans have had a consistent and long-lasting effect on our environments wherever we go, permanent enough to be preserved in the geological record. If we proceed to the future thoughtfully, having learned lessons of past civilisations, perhaps we might one day be debating an appropriate date that signifies a geological period of human induced environmental and landscape recovery, rather than one of heightened erosion, degradation, and exploitation.

APPENDIX

PHOTOGRAPHS OF PORTABLE OSL FIELD SITES

A.1 BIRCHAMS CREEK 1

FIGURE A.1
Looking upstream at Birchams Creek, site 1, the location of profile, PSA-1 (see CHAPTER 5.0), and samples, BIRC-A and BIRC-B (see CHAPTER 6.0). Note that PSA deposits are not of uniform thickness; the forms of former-ponds, now filled with PSA, can be seen above the field assistant's head.

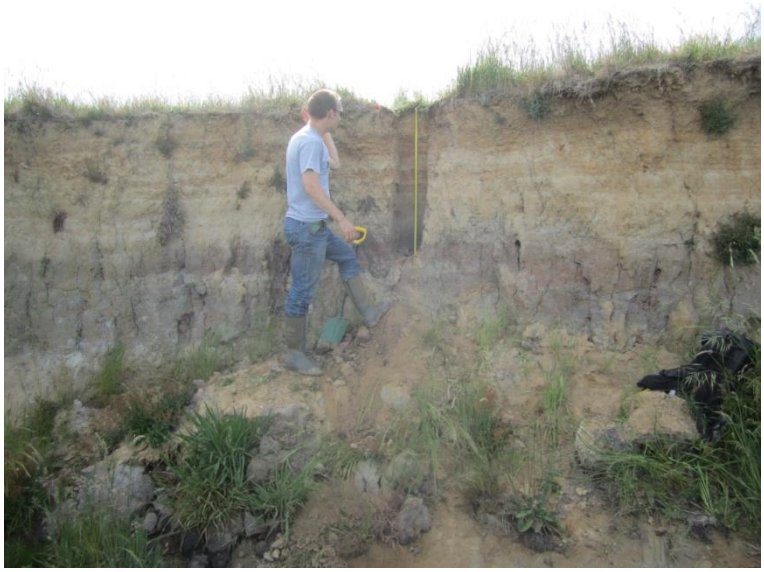

FIGURE A.2
Profile PSA-1 (see CHAPTER 5.0).

A.2 BIRCHAMS CREEK 2

FIGURE A.3
Looking downstream at Birchams Creek, site 2. Bedrock is exposed across the gully in the bottom of the frame. Profile site PSA-2 (see CHAPTER 5.0) was collected along the gully wall exposure in the background (white arrow).

FIGURE A.4
PSA and swampy meadow sediments exposed along Birchams Creek gully at site of PSA-2 (see CHAPTER 5.0).

A.3 BIRCHAMS CREEK SWAMPY MEADOW

FIGURE A.5
Exposure of swampy meadow clays at profile at Birchams Creek, site SM-1 (see CHAPTER 5.0).

FIGURE A.6
Gully exposure of swampy meadow sediments in Birchams Creek.

A.4 BIRCHAMS CREEK SANDSTONE REGOLITH

FIGURE A.7
Looking down at the profile site, REG-1 (see CHAPTER 5.0) in Birchams Creek. Profile is sampled through sandstone regolith. No swampy meadows were originally exposed here, though some ponds now exist upstream.

FIGURE A.8
Side photograph of profile REG-1 (see CHAPTER 5.0).

A.5 BREAKFAST CREEK

FIGURE A.9
Upper rim of ~6 m gully where profile samples were collected.

FIGURE A.10
Breakfast Creek gully exposure. Solid white arrow points to location of bulk OSL profile. Dashed white arrow points to Breakfast Creek Flood Deposit profile site. Much of the point bar sediment was deposited in a flood in 2012. No dates are given for the original gully, though it must be quite old, judging by the size of eucalyptus trees growing opposite.

A.6 BREAKFAST CREEK FLOOD DEPOSIT

FIGURE A.11
Hole being dug to collect bulk OSL samples.

FIGURE A.12
Breakfast Creek Flood Deposit sample pit.

A.7 TRIBUTARY TO BROOKS CREEK

FIGURE A.13
PSA at the mouth of a small tributary to Brooks Creek. Brooks Creek is seen to the left.

FIGURE A.14
Brooks Creek. PSA is exposed on opposite bank of creek, but I did not have access to it. I saw a platypus at this site.

A.8 FENWICK CREEK

FIGURE A.15
Gully along the length of Fenwick Creek, right next to Crookwell Road, which is out of the photo to the right. Field assistant (blue shirt) is pointing to the location of portable OSL profile and where samples FENW-A and FENW-B (see CHAPTER 6.0) were collected.

FIGURE A.16
PSA and swampy meadow sediments exposed in the Fenwick Creek gully wall clearly visible from Crookwell Road. In situ ^{10}Be sample, TLO-03, was collected from the bedrock ridge above this site (though TLO-03 was lost during sample processing).

A.9 GEORGES PLAINS CREEK

FIGURE A.17
Photo taken from creek bank. Horses are ~10m away from gully rim.

FIGURE A.18
Looking across Georges Plains Creek from profile location to PSA exposure on opposite bank. Power lines are along Trunkey Road, west of Georges Plains, NSW.

A.10 GOOROMON PONDS CREEK

FIGURE A.19
Looking up at swampy meadow sediment and PSA exposed at Gooromon Ponds Creek. Field assistant is at profile location, also where GOOR-A and GOOR-B (see CHAPTER 6.0) were collected.

FIGURE A.20
PSA exposed along Gooromon Ponds Creek. Photo taken from inset bars in the modern creek channel.

A.11 GRABBEN GULLEN CREEK

FIGURE A.21
PSA exposures seen in gully bank were sampled in Muñoz-Salinas et al.'s (2014) original portable OSL study at Grabben Gullen Creek, but washed away during flood in 2010.

FIGURE A.22
Location of new portable OSL reader profile at Grabben Gullen Creek (see CHAPTER 4.0).

A.12 GRABBEN GULLEN FLOOD DEPOSIT

FIGURE A.23
Collecting samples from flood alluvium deposited in 2010. Grabben Gullen Creek is seen in the background.

FIGURE A.24
Photograph of Grabben Gullen Creek flood deposit gives a better depiction of flood height above current stream levels.

A.13 GROVES CREEK

FIGURE A.25
Photo of gully taken from creek bed. White arrow points to profile where GROV-A and GROV-B (see CHAPTER 6.0) were collected.

FIGURE A.26
Great depth and width of Groves Creek gully, taken from the rim of the gully. Bedrock is exposed along many reaches of the modern creek.

A.14 GRUBBENBUN CREEK

FIGURE A.27
PSA seen at sample site in foreground, but also along meanders of modern Grubbenbun Creek at left of photo frame.

FIGURE A.28
Looking downstream along Grubbenbun Creek from same site as FIGURE A.27.

A.15 MANDURAMA PONDS CREEK

FIGURE A.29
Flood debris caught in branches of willow growing in bed of Mandurama Ponds Creek. Gully wall exposure of swampy meadow sediments seen across the creek.

FIGURE A.30
Swampy meadow sediments exposed in gully wall along Mandurama Ponds Creek. Upper horizon only appear lighter in colour because grass roots are holding sediment in place, but under the root-held horizon, the clays have recessed away from the creek, making them appear darker. White arrow points to profile location.

A.16 MATONG CREEK

FIGURE A.31
Looking downstream along Matong Creek from Matong Road bridge, east of the locality of Jimenbuen, NSW. This is the only site visited in the Monaro Plains. Creek gully is so wide here, the gully wall on left side of the photo is not visible. White arrow points to sample collection location.

FIGURE A.32
PSA exposed along Matong Creek. Gullying must have occurred decades ago, judging by the size of tree growing within eroded river channel. PSA from left bank of creek is seen in background of photo.

A.17 MATONG CREEK GRANITE HILLSLOPE

FIGURE A.33
Site of profile sampled for bulk OSL in weathered granite soil (white arrow), located on upstream side of Matong Road bridge, east of Jimenbuen, NSW.

A.18 MULWAREE RIVER

FIGURE A.34
Looking upstream from rim of Mulwaree River gully, immediately above bulk OSL profile site, which is the same as Rustomji and Pietsch's (2007) profile, WP-5.

FIGURE A.35
Portable OSL reader sample profile, immediately adjacent to Rustomji and Pietsch's (2007) profile, WP-5. PSA exposures can be seen in background along the length of the River.

A.19 PHILS RIVER

FIGURE A.36
Photo taken from rim of gully along Phils River. White arrow points to profile site, also where PHIL-A and PHIL-B (see CHAPTER 6.0) were collected.

FIGURE A.37
Looking up at swampy meadow sediments and PSA from modern creek.

A.20 PRIMROSE VALLEY CREEK

FIGURE A.38
Clearing away the profile site at Primrose Valley Creek. PSA and swampy meadow sediments are clearly visible.

FIGURE A.39
Example of livestock trampling depression that has progressed into discontinuous gully, about to connect through to the main creek. Photo taken from rim of gully directly above profile site shown in FIGURE A.38.

A.21 QUEEN CHARLOTTE'S CREEK

FIGURE A.40
Wide gully at Queen Charlotte Creek, west of Caloola, NSW. Caloola Road is seen in left of photo. Headward erosion along modern creek has bifurcated in places, creating low-lying mesas of PSA.

FIGURE A.41
PSA exposed above swampy meadow sediments on one of the PSA mesas in Queen Charlotte Creek.

A.22 RYRIES CREEK

FIGURE A.42
Revegetated valley bottom of Ryries Creek. Photo taken from bank of the creek. Profile location to the left of photographer's position.

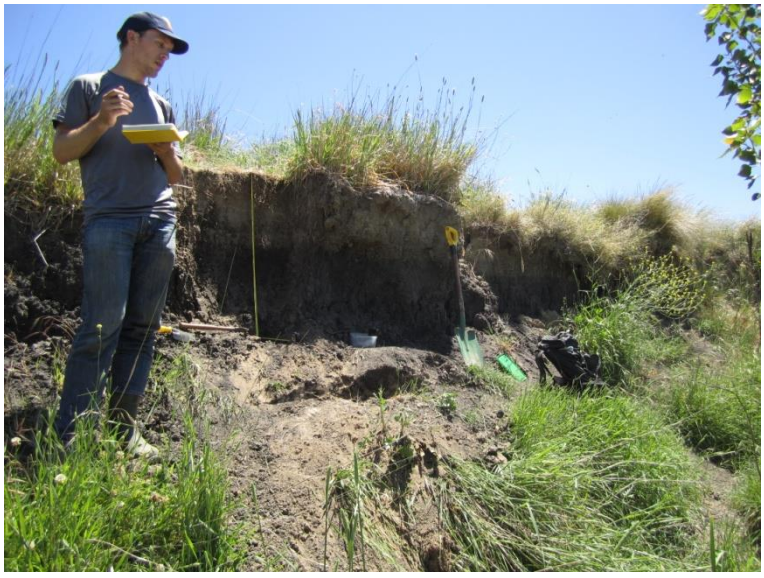

FIGURE A.43
Profile location where RYRI-A and RYRI-B (see CHAPTER 6.0) were collected.

A.23 WANGRAH CREEK CORE SITES

FIGURE A.44
Modern swampy meadow with water filtering through the grasses and sedges. Ground is nearly water-saturated. Photo shows field assistant pointing to short core used to extract modern swampy meadow sediments (see CHAPTER 4.0).

FIGURE A.45
Wangrah Creek swampy meadows as seen from Jerangle Road, south of Jerangle, NSW.

A.24 WYAGNON CREEK

FIGURE A.46
Sequence of flood deposits exposed in modern gully wall at Wyagnon Creek, north of Bathurst, NSW.

FIGURE A.47
Looking upstream from rim of gully at Wyagnon Creek. During floods, the entire valley bottom on the right hand side of photo is inundated with water.

APPENDIX

BULK OSL, MINERALOGY, & GRAIN SIZE DATA FOR CHAPTER 4.0

TABLE B.1 BIRCHAMS CREEK 1 BULK OSL DATA

Depth (cm)	IRSL (photon counts)	BLSL (photon counts)
3	7,418 ± 21	571,514 ± 36
6	20,398 ± 23	983,450 ± 41
9	12,661 ± 23	1,100,520 ± 42
12	14,660 ± 23	885,848 ± 40
15	10,739 ± 23	762,601 ± 39
18	24,826 ± 24	1,387,327 ± 44
21	15,590 ± 23	1,103,282 ± 42
24	19,032 ± 24	656,750 ± 38
27	17,483 ± 24	724,617 ± 39
30	17,520 ± 24	903,628 ± 41
33	33,687 ± 25	1,265,590 ± 44
36	55,792 ± 26	1,654,833 ± 46
39	30,238 ± 25	2,195,825 ± 49
42	31,722 ± 25	2,630,392 ± 51
45	22,999 ± 24	2,090,663 ± 49
48	17,796 ± 24	2,025,800 ± 48
51	63,445 ± 27	1,847,426 ± 47
54	60,843 ± 27	2,657,533 ± 51
57	70,689 ± 27	5,363,106 ± 60
60	27,010 ± 25	1,578,744 ± 46
63	27,721 ± 25	1,411,801 ± 45
66	23,067 ± 25	1,874,268 ± 48
69	10,944 ± 24	1,106,728 ± 43
72	17,855 ± 24	976,983 ± 42
75	15,171 ± 24	1,006,726 ± 42
78	12,100 ± 24	989,738 ± 42
81	19,410 ± 25	1,807,489 ± 47
84	18,745 ± 25	1,519,098 ± 45
87	11,803 ± 24	1,104,469 ± 43
90	6,138 ± 24	841,048 ± 40
93	5,454 ± 24	686,358 ± 39
96	1,926 ± 24	364,215 ± 35
99	2,189 ± 24	243,516 ± 33
102	239 ± 24	85,335 ± 28
105	468 ± 24	83,343 ± 28
108	263 ± 24	80,466 ± 28
111	225 ± 24	79,685 ± 28
114	955 ± 24	115,430 ± 29

TABLE B.2 BIRCHAMS CREEK 2 BULK OSL DATA

Depth (cm)	IRSL (photon counts)	BLSL (photon counts)
3	1,047 ± 21	112,665 ± 28
6	1,425 ± 21	167,333 ± 29
9	2,158 ± 22	234,287 ± 31
12	2,825 ± 22	311,950 ± 33
15	2,959 ± 22	388,339 ± 34
18	4,515 ± 22	513,181 ± 36
21	5,286 ± 22	607,651 ± 37
24	5,736 ± 22	720,737 ± 39
27	5,483 ± 22	848,909 ± 40
30	9,088 ± 23	1,008,742 ± 41
33	7,769 ± 23	1,157,341 ± 43
36	12,321 ± 23	1,417,582 ± 44
39	14,652 ± 24	1,534,176 ± 45
42	15,135 ± 24	1,634,135 ± 46
45	17,593 ± 24	1,791,336 ± 47
48	23,080 ± 24	2,339,202 ± 50
51	20,046 ± 24	2,060,197 ± 48
54	24,188 ± 25	2,529,593 ± 51
57	23,672 ± 25	2,434,135 ± 50
60	23,268 ± 25	2,225,191 ± 49
63	19,438 ± 24	1,819,367 ± 47
66	13,718 ± 24	1,391,596 ± 45
69	13,038 ± 24	1,145,331 ± 43
72	11,175 ± 24	969,657 ± 42
75	16,472 ± 24	1,256,769 ± 44
78	22,070 ± 25	1,586,529 ± 46
81	24,955 ± 25	1,856,248 ± 48
84	26,393 ± 25	1,984,325 ± 48
87	40,218 ± 26	3,086,210 ± 53
90	46,334 ± 26	2,701,070 ± 52

TABLE B.3 BIRCHAMS CREEK SWAMPY MEADOW BULK OSL DATA

Depth (cm)	IRSL (photon counts)	BLSL (photon counts)
3	812 ± 12	253,827 ± 28
6	1,326 ± 12	377,356 ± 31
9	1,252 ± 12	440,664 ± 32
12	2,178 ± 13	569,897 ± 34
15	2,623 ± 13	679,932 ± 35
18	3,290 ± 13	797,848 ± 37
21	4,797 ± 14	1,183,438 ± 40
24	5,628 ± 14	1,433,289 ± 42
27	7,037 ± 15	1,862,041 ± 45
30	7,975 ± 15	1,871,333 ± 44
33	9,615 ± 15	2,477,959 ± 48
36	12,729 ± 16	2,868,171 ± 49
39	15,876 ± 16	3,783,156 ± 53
42	15,491 ± 16	3,767,226 ± 53
45	19,555 ± 17	4,417,682 ± 55
48	23,031 ± 17	5,148,229 ± 57
51	21,404 ± 17	4,417,703 ± 55
54	24,384 ± 18	4,833,970 ± 56
57	27,660 ± 18	5,352,827 ± 58
60	28,862 ± 18	4,705,147 ± 56
63	37,299 ± 19	5,881,729 ± 59
66	28,635 ± 18	5,436,849 ± 58
69	42,967 ± 20	7,145,821 ± 62
72	31,720 ± 19	4,178,252 ± 55
75	35,639 ± 19	5,248,999 ± 57
78	32,404 ± 19	4,865,437 ± 56
81	30,988 ± 18	4,432,591 ± 55
84	29,016 ± 18	3,719,868 ± 53
87	37,843 ± 19	3,898,994 ± 53
90	27,037 ± 18	2,988,820 ± 50
93	19,440 ± 17	1,890,392 ± 45
96	23,555 ± 17	1,941,462 ± 45
99	21,596 ± 17	2,349,905 ± 47
102	36,137 ± 19	3,147,753 ± 51
107	53,716 ± 21	4,838,207 ± 56
112	93,032 ± 23	10,151,969 ± 68
117	46,819 ± 20	4,867,751 ± 56
122	38,752 ± 19	4,729,011 ± 56
127	91,979 ± 23	10,414,302 ± 68
132	56,006 ± 21	6,675,095 ± 61
137	42,210 ± 20	5,198,325 ± 57
142	47,459 ± 20	5,647,071 ± 59
147	27,396 ± 18	2,934,346 ± 50
152	29,489 ± 18	3,130,777 ± 51
157	33,723 ± 19	3,019,607 ± 50
162	36,355 ± 19	3,226,864 ± 51
167	33,379 ± 19	2,208,072 ± 47
172	19,742 ± 17	3,424,687 ± 52
177	29,280 ± 18	1,755,840 ± 44
182	38,521 ± 19	1,067,204 ± 39
187	45,527 ± 20	3,961,620 ± 54
192	84,942 ± 23	6,379,979 ± 61
197	103,666 ± 24	7,824,086 ± 64
202	24,636 ± 17	2,387,009 ± 48
207	43,806 ± 20	3,253,851 ± 51
212	112,940 ± 24	4,946,008 ± 57

TABLE B.4 BIRCHAMS CREEK SANDSTONE SOIL BULK OSL DATA

Depth (cm)	IRSL (photon counts)	BLSL (photon counts)
3	4,765 ± 20	505,430 ± 35
6	19,920 ± 22	2,186,865 ± 48
9	34,664 ± 23	3,400,412 ± 53
12	34,966 ± 23	3,526,127 ± 54
15	36,624 ± 23	3,619,200 ± 54
18	25,950 ± 22	2,705,384 ± 51
21	24,594 ± 22	1,798,895 ± 46
24	17,870 ± 22	1,645,914 ± 45
27	14,482 ± 22	1,096,774 ± 42
30	11,638 ± 21	851,529 ± 39
33	22,904 ± 23	1,539,525 ± 45
36	20,865 ± 22	968,815 ± 41
39	18,641 ± 22	957,508 ± 40
42	23,975 ± 23	1,033,741 ± 41
45	28,014 ± 23	1,118,861 ± 42
48	20,361 ± 23	1,229,121 ± 43
51	39,514 ± 24	2,784,755 ± 51
54	26,765 ± 23	1,943,544 ± 47
57	28,794 ± 24	2,088,354 ± 48
60	27,471 ± 24	2,129,578 ± 48
63	31,436 ± 24	2,240,772 ± 49
66	39,273 ± 24	2,890,526 ± 52
69	45,779 ± 25	3,247,054 ± 53
72	54,638 ± 25	3,867,826 ± 55
75	81,166 ± 27	5,704,511 ± 61
78	74,338 ± 26	5,478,769 ± 60
81	87,751 ± 27	6,395,685 ± 62
84	79,039 ± 27	6,337,433 ± 62
87	51,011 ± 26	3,672,381 ± 55
90	68,040 ± 26	5,354,006 ± 60
93	74,222 ± 27	4,926,947 ± 59
96	65,077 ± 26	4,316,364 ± 57
99	85,151 ± 27	5,681,039 ± 61
102	99,808 ± 28	6,602,192 ± 63

TABLE B.5 BREAKFAST CREEK BULK OSL DATA

Depth (cm)	IRSL (photon counts)	BLSL (photon counts)
3	645 ± 20	141,668 ± 28
6	871 ± 21	202,093 ± 30
9	1,795 ± 21	270,523 ± 32
12	1,294 ± 21	317,328 ± 33
15	1,690 ± 21	377,370 ± 34
18	2,414 ± 21	617,133 ± 37
21	4,871 ± 21	962,652 ± 41
24	5,593 ± 21	1,108,437 ± 42
27	6,389 ± 22	1,427,016 ± 44
30	7,654 ± 22	1,703,786 ± 46
33	7,296 ± 22	1,740,339 ± 46
36	8,245 ± 22	1,844,543 ± 47
39	7,741 ± 22	1,909,117 ± 47
42	5,218 ± 22	1,555,363 ± 45
45	6,135 ± 22	1,686,918 ± 46
48	6,003 ± 22	1,634,031 ± 46
51	7,532 ± 22	1,932,784 ± 47
54	6,755 ± 22	1,828,827 ± 47
57	7,074 ± 22	1,733,965 ± 46
60	7,310 ± 22	1,792,838 ± 47

TABLE B.6 BREAKFAST CREEK FLOOD DEPOSIT BULK OSL DATA

Depth (cm)	IRSL (photon counts)	BLSL (photon counts)
3	38,685 ± 24	354,950 ± 34
6	33,925 ± 24	541,188 ± 36
9	584,040 ± 37	2,995,890 ± 53
12	44,374 ± 25	490,517 ± 36
15	4,947 ± 22	246,110 ± 32
18	18,370 ± 23	294,354 ± 33
21	6,967 ± 22	294,010 ± 33
24	100,455 ± 28	713,609 ± 39
27	2,903 ± 22	289,827 ± 32
30	20,579 ± 23	697,163 ± 38
33	9,895 ± 22	255,572 ± 32
36	2,998 ± 22	213,067 ± 31
39	4,042 ± 22	253,333 ± 32
42	103,354 ± 28	508,631 ± 36
45	2,302 ± 22	275,012 ± 32
48	2,165 ± 22	131,458 ± 29
51	5,086 ± 22	225,312 ± 31
54	9,478 ± 23	223,828 ± 31
57	10,075 ± 23	289,696 ± 33
60	3,036 ± 22	358,665 ± 34
63	28,959 ± 24	487,893 ± 36
66	56,189 ± 26	450,451 ± 35
69	1,057,071 ± 42	2,123,550 ± 50
72	257,496 ± 32	1,871,714 ± 48
75	628,861 ± 38	1,516,654 ± 46
78	259,205 ± 32	1,417,920 ± 45
81	3,363,162 ± 54	1,765,191 ± 48

TABLE B.7 TRIBUTARY TO BROOK CREEK BULK OSL DATA

Depth (cm)	IRSL (photon counts)	BLSL (photon counts)
3	2,604 ± 21	190,183 ± 30
6	6,337 ± 21	224,474 ± 30
9	8,071 ± 21	211,197 ± 30
12	7,154 ± 21	310,187 ± 32
15	9,329 ± 22	311,327 ± 32
18	22,594 ± 23	336,175 ± 33
21	26,671 ± 23	446,639 ± 35
24	84,624 ± 26	869,669 ± 40
27	171,429 ± 29	1,060,069 ± 42
30	251,177 ± 31	1,081,066 ± 42
33	53,766 ± 25	617,662 ± 37
36	17,035 ± 22	284,380 ± 32
39	9,938 ± 22	279,002 ± 32
42	13,556 ± 22	394,451 ± 34
45	8,707 ± 22	310,362 ± 33
48	8,895 ± 22	275,848 ± 32
51	4,338 ± 21	169,039 ± 29
54	9,186 ± 22	397,318 ± 34
57	12,245 ± 22	411,655 ± 34
60	12,023 ± 22	414,847 ± 34
63	13,344 ± 22	533,588 ± 36
66	15,382 ± 23	561,309 ± 36
69	8,981 ± 22	483,671 ± 35
72	7,141 ± 22	298,423 ± 32
75	11,660 ± 22	601,539 ± 37
78	6,254 ± 22	277,104 ± 32
81	9,530 ± 22	316,244 ± 33
84	17,087 ± 23	323,694 ± 33
87	25,392 ± 23	300,767 ± 33

TABLE B.8 FENWICK CREEK BULK OSL, XRD, AND GRAIN SIZE DATA

Depth	IRSL	BLSL	Mineral %[b]								Grain-size %[c]					
(cm)[a]	(photon counts)	(photon counts)	Alb	Anrt	Ancl	Mus	Orth	Phil	Qtz	Zeo	Clay	Silt	FSa	MSa	CSa	D_{50} (μm)
3	1,270 ± 22	184,078 ± 30	7	0	0	14	0	1	78	0	4	54	27	10	5	48
3	*1,732 ± 20*	*204,460 ± 30*														
3	*2,643 ± 20*	*240,433 ± 31*														
6	2,450 ± 22	265,521 ± 32														
9	2,389 ± 22	293,218 ± 32														
12	3,802 ± 22	325,527 ± 33	7	0	0	9	0	0	84	0	4	58	24	10	4	38
12	*7,951 ± 21*	*367,800 ± 33*														
15	4,844 ± 22	466,771 ± 35														
18	4,577 ± 22	459,548 ± 35														
21	5,600 ± 22	402,107 ± 34	5	0	2	11	0	0	82	0	5	63	19	7	5	32
21	*5,033 ± 21*	*342,902 ± 33*														
24	12,204 ± 23	914,721 ± 40														
27	15,411 ± 23	628,645 ± 38														
30	8,830 ± 22	645,070 ± 38	3	0	0	9	0	2	86	0	4	45	19	20	12	68
30	*14,753 ± 22*	*871,801 ± 40*														
30	*30,360 ± 23*	*1,381,582 ± 44*														
33	17,186 ± 23	572,587 ± 37														
36	8,824 ± 22	583,464 ± 37														
39	5,314 ± 22	439,515 ± 35	3	0	0	17	0	2	78	0	6	72	7	8	7	21
39	*6,263 ± 21*	*797,701 ± 39*														
39	*5,587 ± 21*	*529,350 ± 36*														
42	1,421 ± 22	178,879 ± 30														
45	3,866 ± 22	412,435 ± 35														
48	36,843 ± 25	740,707 ± 39	2	0	0	8	0	1	89	0	3	33	32	27	5	153
48	*27,262 ± 23*	*1,339,074 ± 43*														
48	*20,084 ± 22*	*934,852 ± 40*														
51	50,671 ± 25	1,374,938 ± 44														
54	19,818 ± 23	1,178,054 ± 43														
57	7,393 ± 22	804,656 ± 39	6	0	0	22	0	0	72	0	7	83	9	1	1	20
57	*9,707 ± 21*	*922,428 ± 40*														
57	*10,779 ± 22*	*733,059 ± 38*														
60	3,681 ± 22	521,513 ± 36														
63	4,920 ± 22	619,956 ± 37														
66	6,194 ± 22	938,787 ± 41	7	0	0	19	0	0	74	0	6	73	17	3	0	24
66	*8,802 ± 21*	*1,008,812 ± 41*														
66	*8,931 ± 21*	*963,535 ± 40*														
69	1,751 ± 22	319,218 ± 33														
70	772 ± 21	160,341 ± 29														
70	*2,515 ± 21*	*324,758 ± 33*														
70	*1,715 ± 21*	*232,991 ± 31*														
72	383 ± 22	46,051 ± 25	5	0	0	30	0	0	65	0	7	84	8	1	0	20
72	*472 ± 20*	*144,748 ± 28*														
72	*762 ± 20*	*111,240 ± 27*														
75	157 ± 21	63,104 ± 26														
78	218 ± 21	87,811 ± 27														
81	378 ± 22	118,897 ± 28	0	2	0	29	0	0	68	0	8	84	7	1	1	17
81	*562 ± 20*	*161,051 ± 29*														
81	*168 ± 20*	*123,826 ± 28*														
84	738 ± 21	154,994 ± 29														
87	770 ± 21	181,918 ± 30														
90	605 ± 21	259,007 ± 32														
90	*417 ± 20*	*228,724 ± 31*														
90	*524 ± 20*	*222,767 ± 30*														

[a] Samples in italics are proximal replicates (~10-15 cm from main profile samples)

[b] Mineral percentages were determined using general Rietveld refinement in Highscore Plus. Alb = albite, Anrt = Anorthite, Ancl = Anorthoclase, Mus = Muscovite, Orth = Orthoclase, Phil = Philipsite, Qtz = Quartz, Zeo = Zeolite

[c] Clay = 0.01-2 μm, Silt = 2-63 μm, F.Sa = Fine Sand = 63-250 μm, M.Sa = Medium Sand = 250-500 μm, C.Sa = Coarse Sand = 500-2000 μm. No samples contained any grain-size larger than coarse sand.

TABLE B.9 GEORGES PLAINS CREEK BULK OSL DATA

Depth (cm)	IRSL (photon counts)	BLSL (photon counts)
3	5,964 ± 21	336,067 ± 33
6	13,359 ± 22	540,413 ± 36
9	11,502 ± 21	671,187 ± 37
12	16,391 ± 22	855,589 ± 39
15	26,436 ± 23	1,153,275 ± 42
18	38,676 ± 24	1,680,961 ± 46
21	30,238 ± 23	1,398,553 ± 44
24	40,046 ± 24	1,744,507 ± 46
27	102,539 ± 27	3,870,592 ± 55
30	125,570 ± 28	5,046,893 ± 59
33	372,585 ± 34	14,052,882 ± 75
36	217,854 ± 30	8,329,209 ± 66
39	40,851 ± 24	1,617,461 ± 45
42	71,577 ± 26	2,959,153 ± 52
45	38,427 ± 24	1,033,494 ± 41
48	12,757 ± 22	598,485 ± 37
51	5,045 ± 21	153,564 ± 29
54	4,915 ± 21	298,648 ± 32
57	8,870 ± 22	392,971 ± 34
60	7,291 ± 21	406,544 ± 34

TABLE B.10 GOOROMON PONDS CREEK BULK OSL DATA

Depth (cm)	IRSL (photon counts)	BLSL (photon counts)
3	6,435 ± 20	1,025,764 ± 41
6	6,885 ± 20	1,261,650 ± 43
9	10,233 ± 21	1,625,804 ± 45
12	13,599 ± 21	2,295,263 ± 49
15	12,487 ± 21	2,132,132 ± 48
18	14,583 ± 22	2,017,738 ± 47
21	10,283 ± 21	1,451,790 ± 44
24	19,805 ± 22	2,683,493 ± 51
27	22,269 ± 23	3,527,860 ± 54
30	16,839 ± 22	2,759,732 ± 51
33	15,397 ± 22	2,716,145 ± 51
36	17,940 ± 22	3,655,907 ± 54
39	14,561 ± 22	3,045,293 ± 52
42	13,640 ± 22	2,328,976 ± 49
45	25,900 ± 23	3,677,379 ± 54
48	8,696 ± 22	1,507,920 ± 45
51	12,971 ± 23	2,201,893 ± 49
54	14,616 ± 23	2,436,473 ± 50
57	17,524 ± 23	2,896,499 ± 52
60	19,310 ± 23	2,220,578 ± 49
63	7,360 ± 22	1,123,117 ± 42
66	29,753 ± 24	3,764,842 ± 55
69	6,922 ± 22	1,393,942 ± 44
72	7,357 ± 22	1,156,934 ± 42
75	8,360 ± 22	1,427,163 ± 44
78	1,204 ± 22	347,289 ± 34
81	996 ± 22	222,557 ± 31
84	3,158 ± 22	632,663 ± 38
87	1,416 ± 22	333,192 ± 33
90	1,121 ± 22	337,176 ± 33
93	1,530 ± 22	418,172 ± 35
96	2,435 ± 22	493,888 ± 36

TABLE B.11 GRABBEN GULLEN CREEK BULK OSL, XRD, AND GRAIN SIZE DATA

Depth	IRSL	BLSL	Mineral %[a]									Grain-size %[b]				
(cm)	(photon counts)	(photon counts)	Alb	Anrt	Ancl	Mus	Orth	Phil	Qtz	Zeo	Clay	Silt	FSa	MSa	CSa	D_{50} (µm)
3	12,181,352 ± 73	26,739,426 ± 90														
6	12,396,327 ± 74	29,828,338 ± 92	3	18	0	0	2	1	75	0	0	15	40	34	10	225
9	20,738,643 ± 84	44,447,196 ± 103														
12	4,063,150 ± 57	9,640,665 ± 70														
15	2,888,296 ± 52	5,620,632 ± 62	0	19	0	0	4	0	76	0	0	14	30	37	18	275
18	1,792,053 ± 47	5,219,581 ± 60														
21	215,872 ± 31	827,341 ± 40														
24	328,394 ± 33	1,044,758 ± 42	9	18	0	0	0	0	72	0	1	30	33	23	12	163
27	1,267,988 ± 44	3,007,174 ± 53														
30	847,326 ± 40	2,078,416 ± 49														
33	2,104,620 ± 49	5,150,200 ± 60	0	21	0	0	5	0	75	0	0	10	18	33	39	425
36	2,917,337 ± 52	6,299,416 ± 63														
39	655,675 ± 38	1,792,254 ± 47														
42	1,032,784 ± 42	4,021,385 ± 57	0	16	0	16	0	3	65	0	1	38	45	8	8	89
45	1,129,292 ± 42	3,770,182 ± 56														
48	345,552 ± 34	1,001,246 ± 41														
51	1,338,036 ± 44	3,724,443 ± 56	0	19	0	0	7	3	71	0	0	14	34	38	14	258
54	165,896 ± 30	463,992 ± 35														
57	640,729 ± 38	2,108,512 ± 49														
60	2,851,079 ± 52	8,032,240 ± 67	0	21	0	0	4	2	73	2	1	24	55	10	11	128
63	483,192 ± 36	1,373,969 ± 44														
66	141,175 ± 29	416,600 ± 35														
69	180,410 ± 30	612,169 ± 38	0	19	0	1	13	5	62	0	1	17	41	23	18	205
72	5,672,593 ± 61	10,598,907 ± 72														
75	6,913,539 ± 64	16,170,018 ± 80														
78	6,375,620 ± 63	13,984,952 ± 77	0	21	0	0	3	0	75	0	0	4	18	44	34	401
81	740,652 ± 39	2,487,701 ± 51														
84	422,801 ± 35	1,391,861 ± 45														
87	54,306 ± 26	245,166 ± 32	7	10	0	2	8	0	73	0	2	37	28	17	15	122
90	205,059 ± 31	651,728 ± 38														
93	156,384 ± 30	543,819 ± 37														
96	107,877 ± 28	450,204 ± 35														
99	84,185 ± 27	364,358 ± 34														
102	127,903 ± 29	503,965 ± 36														
105	182,059 ± 30	664,702 ± 38														
108	189,291 ± 30	673,140 ± 38														
111	166,625 ± 30	690,256 ± 38														
114	188,428 ± 30	713,696 ± 39														
117	294,295 ± 33	960,421 ± 41														
120	298,232 ± 33	1,017,479 ± 42														

[a] Alb = albite, Anrt = Anorthite, Ancl = Anorthoclase, Mus = Muscovite, Orth = Orthoclase, Phil = Philipsite, Qtz = Quartz, Zeo = Zeolite

[b] Clay = 0.01-2 µm, Silt = 2-63 µm, F.Sa = Fine Sand = 63-250 µm, M.Sa = Medium Sand = 250-500 µm, C.Sa = Coarse Sand = 500-2000 µm. No samples contained any grain-size larger than coarse sand.

TABLE B.12 GRABBEN GULLEN CREEK FLOOD DEPOSIT BULK OSL DATA

Depth (cm)	IRSL (photon counts)	BLSL (photon counts)
3	17,753,010 ± 81	38,805,567 ± 99
6	14,252,389 ± 77	27,801,600 ± 92
9	13,033,720 ± 75	27,527,699 ± 91
12	14,802,248 ± 77	29,618,966 ± 93
15	11,243,886 ± 72	24,972,585 ± 89
18	10,053,549 ± 70	21,125,911 ± 85
21	11,454,080 ± 73	25,144,740 ± 89
24	9,952,926 ± 70	23,125,538 ± 87
27	9,611,574 ± 70	20,041,215 ± 84
30	8,232,610 ± 67	16,859,422 ± 81
33	5,996,833 ± 62	14,475,439 ± 78
36	6,494,065 ± 64	14,477,338 ± 78
39	5,877,712 ± 62	13,973,744 ± 77
42	4,762,925 ± 59	11,070,116 ± 73
45	4,845,017 ± 59	11,130,362 ± 73
48	3,982,214 ± 57	10,517,977 ± 72
51	1,514,323 ± 45	3,780,685 ± 56
54	1,258,219 ± 44	4,365,061 ± 58
57	1,309,451 ± 44	3,571,946 ± 55
60	490,272 ± 36	1,584,101 ± 46
63	82,192 ± 27	268,319 ± 32
66	74,801 ± 27	279,937 ± 33
69	166,447 ± 30	557,485 ± 37
72	177,349 ± 30	558,319 ± 37

TABLE B.13 GROVES CREEK BULK OSL DATA

Depth (cm)	IRSL (photon counts)	BLSL (photon counts)
3	1,585 ± 20	77,527 ± 26
6	2,044 ± 20	75,109 ± 26
9	3,440 ± 21	109,918 ± 27
12	4,201 ± 21	176,988 ± 29
15	4,469 ± 21	191,296 ± 30
18	5,896 ± 21	234,766 ± 31
21	6,768 ± 21	300,966 ± 32
24	9,222 ± 22	380,921 ± 34
27	10,931 ± 22	414,065 ± 34
30	12,322 ± 22	505,883 ± 36
33	13,811 ± 22	572,799 ± 36
36	14,396 ± 22	596,458 ± 37
39	21,808 ± 23	768,638 ± 39
42	6,089 ± 21	302,926 ± 32
45	4,786 ± 21	182,149 ± 30
48	839 ± 21	68,874 ± 26
51	1,050 ± 21	62,568 ± 25
54	992 ± 21	47,285 ± 25
57	636 ± 21	56,593 ± 25
60	2,129 ± 21	119,580 ± 28
63	1,273 ± 21	88,798 ± 27
66	1,899 ± 21	112,225 ± 27
69	1,522 ± 21	122,898 ± 28
72	2,630 ± 21	144,766 ± 29

TABLE B.14 GRUBBENBUN CREEK BULK OSL DATA

Depth (cm)	IRSL (photon counts)	BLSL (photon counts)
3	4,745 ± 20	714,325 ± 38
6	3,940 ± 20	855,800 ± 39
9	9,313 ± 21	1,258,684 ± 43
12	7,406 ± 21	1,033,457 ± 41
15	6,734 ± 21	894,992 ± 40
18	5,111 ± 21	839,681 ± 39
21	5,978 ± 21	922,053 ± 40
24	4,697 ± 21	766,421 ± 38
27	3,797 ± 21	686,461 ± 38
30	3,046 ± 21	485,799 ± 35
33	3,488 ± 21	567,951 ± 36
36	2,671 ± 21	463,177 ± 35
39	1,354 ± 20	339,500 ± 33
42	1,915 ± 21	488,722 ± 35
45	2,187 ± 21	479,554 ± 35
48	1,759 ± 21	615,400 ± 37
51	2,510 ± 21	624,001 ± 37
54	2,442 ± 21	617,310 ± 37
57	2,950 ± 21	692,232 ± 38
60	2,910 ± 21	700,400 ± 38

TABLE B.15 MANDURAMA PONDS CREEK BULK OSL DATA

Depth (cm)	IRSL (photon counts)	BLSL (photon counts)
3	1,481 ± 21	168,427 ± 29
6	1,451 ± 21	167,614 ± 29
9	1,773 ± 21	184,768 ± 30
12	6,245 ± 22	506,111 ± 36
15	2,792 ± 22	275,330 ± 32
18	3,361 ± 22	334,709 ± 33
21	2,181 ± 22	257,681 ± 32
24	1,884 ± 22	238,750 ± 31
27	4,871 ± 22	337,042 ± 33
30	2,200 ± 22	399,613 ± 34
33	3,625 ± 22	664,038 ± 38
36	5,618 ± 22	849,036 ± 40
39	6,814 ± 22	986,159 ± 41
42	6,543 ± 22	1,089,564 ± 42
45	7,469 ± 22	1,234,660 ± 43
48	6,787 ± 22	1,229,030 ± 43
51	8,817 ± 22	1,436,248 ± 44
54	10,824 ± 22	1,888,638 ± 47
57	8,959 ± 22	1,542,919 ± 45
60	8,851 ± 22	1,528,477 ± 45
63	10,760 ± 22	1,685,532 ± 46
66	10,672 ± 22	1,659,487 ± 46
69	12,982 ± 23	2,212,703 ± 49
72	16,589 ± 23	2,419,258 ± 50
75	19,420 ± 23	2,685,765 ± 51
78	21,397 ± 24	3,264,765 ± 53
81	26,828 ± 24	3,565,263 ± 54
84	26,053 ± 24	3,430,590 ± 54
87	47,703 ± 25	6,113,243 ± 61
90	44,438 ± 25	5,474,647 ± 60

TABLE B.16 MATONG CREEK BULK OSL DATA

Depth (cm)	IRSL (photon counts)	BLSL (photon counts)
3	29,875 ± 24	1,651,008 ± 46
6	45,102 ± 25	2,042,794 ± 48
9	46,699 ± 25	2,186,102 ± 49
12	72,986 ± 27	3,094,537 ± 53
15	78,742 ± 27	2,957,196 ± 52
18	81,663 ± 27	3,412,484 ± 54
21	97,501 ± 28	4,235,861 ± 57
24	192,344 ± 31	7,590,084 ± 65
27	128,002 ± 29	4,730,322 ± 58
30	157,580 ± 30	6,282,043 ± 62
33	168,147 ± 30	7,697,898 ± 65
36	64,702 ± 27	2,975,481 ± 52
39	87,123 ± 28	4,154,805 ± 57
42	100,474 ± 28	4,947,510 ± 59
45	95,925 ± 28	4,610,062 ± 58
48	78,902 ± 28	4,092,030 ± 56
51	237,284 ± 32	10,222,031 ± 70
54	318,007 ± 34	18,006,633 ± 80
57	269,852 ± 33	15,728,993 ± 77
60	308,557 ± 34	15,800,334 ± 77
63	196,373 ± 31	9,984,028 ± 69
66	226,030 ± 32	11,491,799 ± 72
69	350,360 ± 34	18,708,708 ± 81
72	116,886 ± 29	6,234,814 ± 62
75	9,630 ± 24	707,181 ± 39
78	9,548 ± 24	619,674 ± 38
81	5,333 ± 24	314,419 ± 34
84	5,337 ± 24	413,587 ± 35
87	3,375 ± 24	208,485 ± 32
90	2,191 ± 24	118,229 ± 29
93	2,802 ± 24	181,317 ± 31
96	1,758 ± 24	104,605 ± 29
99	2,435 ± 24	116,745 ± 29
102	2,014 ± 24	134,560 ± 30
105	1,979 ± 24	134,305 ± 30
108	1,646 ± 24	146,417 ± 30
111	2,090 ± 24	157,164 ± 30

TABLE B.17 MATONG CREEK GRANITE HILLSLOPE BULK OSL DATA

Depth (cm)	IRSL (photon counts)	BLSL (photon counts)
3	3,932 ± 23	155,052 ± 30
6	3,962 ± 23	174,451 ± 31
9	5,087 ± 23	211,262 ± 32
12	5,730 ± 24	303,212 ± 34
15	7,788 ± 24	339,113 ± 34
18	8,393 ± 24	388,006 ± 35
21	8,970 ± 24	396,435 ± 35
24	8,876 ± 24	438,403 ± 36
27	12,091 ± 25	497,901 ± 37
30	14,873 ± 25	578,761 ± 38
33	14,105 ± 25	630,353 ± 38
36	15,373 ± 25	639,819 ± 39
39	24,298 ± 25	797,594 ± 40
42	25,737 ± 26	869,791 ± 41
45	30,645 ± 26	1,012,285 ± 42
48	35,302 ± 26	1,093,076 ± 43
51	40,336 ± 27	1,239,162 ± 44
54	46,805 ± 27	1,388,055 ± 45
57	48,689 ± 27	1,394,265 ± 45
60	63,046 ± 26	1,600,665 ± 46
63	60,194 ± 28	1,685,492 ± 47
66	66,042 ± 28	1,717,050 ± 47
69	62,261 ± 28	1,790,007 ± 48
72	88,278 ± 29	2,308,844 ± 50
75	82,836 ± 29	2,119,175 ± 49
78	79,517 ± 29	2,049,248 ± 49

TABLE B.18 MULWAREE RIVER BULK OSL, XRD, AND GRAIN SIZE DATA

Depth	IRSL	BLSL	Mineral %[b]								Grain-size %[c]					
(cm)[a]	(photon counts)	(photon counts)	Alb	Anrt	Ancl	Mus	Orth	Phil	Qtz	Zeo	Clay	Silt	FSa	MSa	CSa	D_{50} (µm)
3	631 ± 22	130,494 ± 29	5	0	0	10	0	0	85	0	2	28	30	26	14	180
3	*443 ± 21*	*135,480 ± 28*														
3	*1,301 ± 21*	*125,052 ± 28*														
6	902 ± 22	172,208 ± 30														
9	1,358 ± 22	217,534 ± 31														
12	1,134 ± 22	228,451 ± 31	8	0	0	2	0	0	90	0	3	33	25	27	13	175
12	*578 ± 21*	*190,653 ± 30*														
12	*1,662 ± 21*	*202,969 ± 30*														
15	1,348 ± 22	199,236 ± 31														
18	1,677 ± 22	174,026 ± 30														
21	1,267 ± 22	199,161 ± 31	3	0	0	12	0	2	83	0	3	25	23	34	16	250
21	*732 ± 21*	*195,521 ± 30*														
21	*1,072 ± 21*	*176,334 ± 30*														
24	1,106 ± 22	224,519 ± 31														
27	794 ± 22	210,778 ± 31														
30	1,778 ± 22	275,520 ± 33	7	0	0	2	0	0	91	0	3	32	31	25	9	151
30	*2,279 ± 21*	*357,864 ± 33*														
30	*2,674 ± 21*	*315,296 ± 33*														
33	4,669 ± 23	576,696 ± 37														
36	3,381 ± 23	680,964 ± 38														
39	3,287 ± 23	735,965 ± 39	3	0	0	10	0	0	86	0	3	27	29	29	12	196
39	*5,937 ± 22*	*551,852 ± 36*														
39	*3,170 ± 21*	*481,447 ± 35*														
42	2,480 ± 23	514,520 ± 36														
45	3,626 ± 23	408,853 ± 35														
48	1,721 ± 23	385,422 ± 34	2	0	0	10	0	1	87	0	2	23	21	28	26	279
48	*2,828 ± 21*	*411,436 ± 34*														
48	*552 ± 21*	*252,990 ± 31*														
51	3,895 ± 23	504,074 ± 36														
54	6,006 ± 23	617,732 ± 38														
57	2,466 ± 23	368,335 ± 34	3	0	0	9	0	0	88	0	2	21	26	37	15	259
57	*2,647 ± 22*	*527,833 ± 36*														
57	*2,109 ± 21*	*474,407 ± 35*														
60	3,213 ± 23	769,489 ± 39														
63	4,924 ± 23	714,501 ± 39														
66	4,257 ± 23	636,925 ± 38	2	0	0	15	0	1	82	0	3	23	31	29	14	215
66	*4,811 ± 22*	*1,050,643 ± 41*														
66	*4,109 ± 22*	*756,332 ± 39*														
69	2,897 ± 23	607,570 ± 38														
72	4,293 ± 23	805,600 ± 40														
75	393 ± 23	253,649 ± 32	4	0	0	23	0	0	72	0	6	67	20	6	1	30
75	*857 ± 21*	*203,092 ± 30*														
75	*921 ± 21*	*292,623 ± 32*														
78	-613 ± 22	274,809 ± 33														
81	651 ± 22	216,332 ± 31														
84	2,877 ± 23	656,382 ± 38	2	1	0	15	0	0	81	0	6	66	19	8	2	32
84	*1,499 ± 21*	*361,656 ± 34*														
84	*689 ± 21*	*233,545 ± 31*														
87	2,326 ± 23	342,704 ± 34														
90	1,607 ± 23	410,957 ± 35														

[a] Samples in italics are proximal replicates (~10-15 cm from main profile samples)

[b] Alb = albite, Anrt = Anorthite, Ancl = Anorthoclase, Mus = Muscovite, Orth = Orthoclase, Phil = Philipsite, Qtz = Quartz, Zeo = Zeolite

[c] Clay = 0.01-2 µm, Silt = 2-63 µm, F.Sa = Fine Sand = 63-250 µm, M.Sa = Medium Sand = 250-500 µm, C.Sa = Coarse Sand = 500-2000 µm. No samples contained any grain-size larger than coarse sand.

TABLE B.19 PHILS RIVER BULK OSL DATA

Depth (cm)	IRSL (photon counts)	BLSL (photon counts)
3	5,926 ± 20	155,052 ± 28
6	13,257 ± 21	275,333 ± 31
9	- 6,234 ± 24	269,471 ± 31
12	12,050 ± 21	216,677 ± 30
15	21,117 ± 22	306,743 ± 32
18	33,835 ± 23	510,788 ± 35
21	47,351 ± 24	796,670 ± 39
24	54,517 ± 24	735,790 ± 38
27	38,653 ± 23	813,769 ± 39
30	127,431 ± 27	1,822,185 ± 46
33	25,687 ± 22	357,115 ± 33
36	82,232 ± 26	816,709 ± 39
39	76,905 ± 26	993,732 ± 41
42	140,714 ± 28	2,796,506 ± 51
45	47,429 ± 24	963,725 ± 40
48	91,305 ± 26	1,996,973 ± 47
51	101,273 ± 26	2,888,350 ± 51
54	11,431 ± 21	440,786 ± 34
57	71,298 ± 25	2,650,285 ± 50
60	7,477 ± 21	214,930 ± 30
63	6,150 ± 21	166,832 ± 29
66	5,608 ± 21	173,339 ± 30
69	1,341 ± 20	61,655 ± 25
72	1,720 ± 20	89,108 ± 26
75	2,020 ± 20	125,088 ± 28
78	9,202 ± 19	237,400 ± 30
81	7,060 ± 21	326,344 ± 33
84	6,762 ± 21	529,310 ± 36

TABLE B.20 PRIMROSE VALLEY CREEK BULK OSL, XRD, AND GRAIN SIZE DATA

Depth	IRSL	BLSL	Mineral %[a]									Grain-size %[b]				
(cm)	(photon counts)	(photon counts)	Alb	Anrt	Ancl	Mus	Orth	Phil	Qtz	Zeo	Clay	Silt	Fsa	Msa	Csa	D_{50} (µm)
3	3,359 ± 21	186,807 ± 30	7	0	0	23	0	2	68	0	5	76	15	4	1	22
6	6,250 ± 21	258,401 ± 31														
9	5,398 ± 21	233,939 ± 31														
12	5,639 ± 21	250,594 ± 31	7	0	0	28	0	2	63	0	5	89	6	0	0	17
15	6,635 ± 22	258,211 ± 32														
18	4,183 ± 21	292,242 ± 32														
21	10,393 ± 22	405,460 ± 34	7	0	0	27	0	2	64	0	5	78	3	0	14	20
24	11,048 ± 22	368,356 ± 34														
27	10,975 ± 22	352,371 ± 33														
30	17,790 ± 23	525,836 ± 36	9	0	0	26	0	2	63	0	5	76	4	0	15	22
33	25,625 ± 23	793,307 ± 39														
36	42,990 ± 25	766,881 ± 39														
39	9,622 ± 22	344,047 ± 33	8	0	0	33	0	3	56	0	5	83	3	0	9	19
42	20,418 ± 23	617,295 ± 37														
45	15,917 ± 23	480,532 ± 35														
48	36,323 ± 24	773,551 ± 39	12	0	0	22	0	1	65	0	5	86	8	0	0	20
51	11,480 ± 22	385,909 ± 34														
54	9,332 ± 22	343,476 ± 33														
57	17,651 ± 23	685,566 ± 38	8	0	0	21	0	0	70	0	5	85	6	0	4	20
60	7,760 ± 22	267,219 ± 32														
63	8,440 ± 22	361,401 ± 34														
66	8,698 ± 22	399,475 ± 34	7	0	0	26	0	1	66	0	5	84	3	0	7	18
69	1,505 ± 21	133,390 ± 29														
72	3,558 ± 21	251,976 ± 31														
75	4,557 ± 21	312,906 ± 33	7	0	0	35	0	1	57	0	6	81	5	0	8	18
78	1,707 ± 21	84,202 ± 27														
81	713 ± 21	47,816 ± 25														
84	4,174 ± 22	205,233 ± 30	7	0	0	28	0	0	64	0	6	67	5	4	19	22
87	7,292 ± 22	319,692 ± 33														
90	10,357 ± 22	389,469 ± 34														

[a] Alb = albite, Anrt = Anorthite, Ancl = Anorthoclase, Mus = Muscovite, Orth = Orthoclase, Phil = Philipsite, Qtz = Quartz, Zeo = Zeolite

[b] Clay = 0.01-2 µm, Silt = 2-63 µm, F.Sa = Fine Sand = 63-250 µm, M.Sa = Medium Sand = 250-500 µm, C.Sa = Coarse Sand = 500-2000 µm. No samples contained any grain-size larger than coarse sand.

TABLE B.21 QUEEN CHARLOTTE'S CREEK BULK OSL DATA

Depth (cm)	IRSL (photon counts)	BLSL (photon counts)
3	8,817 ± 21	2,511,157 ± 50
6	7,721 ± 21	2,810,503 ± 51
9	9,582 ± 22	3,176,915 ± 53
12	20,121 ± 23	5,867,303 ± 61
15	5,189 ± 21	2,571,857 ± 50
18	10,905 ± 22	5,340,025 ± 59
21	4,886 ± 21	2,876,215 ± 52
24	5,198 ± 21	3,134,195 ± 53
27	5,001 ± 21	1,413,080 ± 44
30	1,341 ± 21	856,324 ± 40
33	3,728 ± 21	830,070 ± 39
36	3,620 ± 21	930,025 ± 40
39	6,487 ± 21	1,848,340 ± 47
42	7,430 ± 22	2,076,416 ± 48
45	9,639 ± 22	2,651,500 ± 51
48	12,962 ± 22	3,285,557 ± 53
51	14,692 ± 22	3,934,375 ± 55
54	20,198 ± 23	4,882,676 ± 58
57	22,243 ± 23	6,922,821 ± 63
60	15,189 ± 22	5,167,435 ± 59

TABLE B.22 RYRIES CREEK BULK OSL DATA

Depth (cm)	IRSL (photon counts)	BLSL (photon counts)
3	2,553 ± 22	19,985 ± 23
6	25,140 ± 24	164,670 ± 30
9	52,346 ± 26	298,109 ± 33
12	53,545 ± 26	335,096 ± 34
15	143,519 ± 29	746,548 ± 39
18	141,999 ± 29	1,017,577 ± 42
21	144,563 ± 29	1,195,301 ± 43
24	118,549 ± 28	1,062,162 ± 42
27	100,230 ± 28	987,844 ± 42
30	100,779 ± 28	1,167,478 ± 43
33	56,901 ± 26	499,907 ± 37
36	261,834 ± 33	1,637,431 ± 46
39	80,461 ± 28	894,178 ± 41
42	110,792 ± 29	1,083,550 ± 42
45	29,445 ± 25	442,190 ± 36
48	1,390 ± 23	31,525 ± 25
51	1,537 ± 23	33,209 ± 25
54	1,159 ± 23	36,960 ± 26
57	2,087 ± 23	55,543 ± 27
60	4,341 ± 24	91,482 ± 28
63	5,539 ± 24	116,422 ± 29
66	5,677 ± 24	131,065 ± 30
69	4,953 ± 24	121,472 ± 29
72	4,758 ± 24	142,220 ± 30
75	7,879 ± 24	211,876 ± 32
78	10,299 ± 24	267,027 ± 33
81	8,014 ± 24	253,189 ± 33
84	8,328 ± 24	287,792 ± 33
87	8,019 ± 24	291,268 ± 34
90	13,318 ± 25	351,287 ± 35

TABLE B.23 WANGRAH CREEK SWAMPY MEADOW BULK OSL DATA

Core 1		
Depth (cm)	IRSL (photon counts)	BLSL (photon counts)
0	25 ± 25	11,724 ± 26
3	689 ± 25	78,701 ± 29
6	889 ± 25	100,366 ± 30
9	254 ± 25	89,719 ± 29
12	413 ± 25	114,347 ± 30
15	887 ± 25	102,854 ± 30
18	1,394 ± 25	130,027 ± 30
21	2,107 ± 25	209,067 ± 32
Core 2		
Depth (cm)	IRSL (photon counts)	BLSL (photon counts)
1	169 ± 24	50,137 ± 27
4	1,611 ± 25	225,405 ± 33
7	1,823 ± 25	252,488 ± 33
10	3,375 ± 25	560,588 ± 38
13	3,143 ± 25	727,885 ± 40
16	2,062 ± 24	754,040 ± 40
19	5,970 ± 25	1,773,846 ± 47
Core 3		
Depth (cm)	IRSL (photon counts)	BLSL (photon counts)
1	0 ± 24	9,349 ± 25
4	675 ± 24	103,533 ± 29
7	945 ± 24	180,966 ± 31
10	1,233 ± 24	251,072 ± 33
13	2,105 ± 24	399,071 ± 36
16	5,180 ± 25	887,908 ± 41
19	10,132 ± 25	1,398,161 ± 45

TABLE B.24 WYAGNON CREEK BULK OSL DATA

Depth (cm)	IRSL (photon counts)	BLSL (photon counts)
3	70,825 ± 27	2,205,571 ± 49
6	76,019 ± 27	2,787,919 ± 51
9	48,489 ± 26	1,898,572 ± 47
12	42,974 ± 25	1,672,849 ± 46
15	49,317 ± 25	1,961,194 ± 48
18	67,298 ± 26	2,481,791 ± 50
21	50,089 ± 26	2,088,097 ± 48
24	67,561 ± 26	2,636,634 ± 51
27	37,660 ± 25	1,895,774 ± 47
30	41,632 ± 25	2,217,728 ± 49
33	45,445 ± 25	2,519,058 ± 50
36	44,909 ± 25	2,441,153 ± 50
39	41,744 ± 25	1,786,988 ± 47
42	28,207 ± 24	1,481,302 ± 45
45	30,685 ± 24	1,546,636 ± 45
48	18,344 ± 24	698,538 ± 39
51	15,347 ± 23	855,496 ± 40

REFERENCES

Adamson, C. M., Effects of soil conservation treatment on runoff and sediment loss from a catchment in southwestern New South Wales, Australia, *in* Proceedings Effects of Man on the Interface of the Hydrological Cycle with the Physical Environment, Paris, 1974, Volume IAHS-AISH Publication No. 113, International Association of Hydrological Sciences, p. 3–14.

Agusti, J., and Lordkipanidze, D., 2011, How "African" was the early human dispersal out of Africa?: Quaternary Science Reviews, v. 30, no. 11–12, p. 1338–1342.

Aitken, M. J., 1998, An Introduction to Optical Dating: The Dating of Quaternary Sediments by the Use of Photon-stimulated Luminescence, Oxford, UK, Oxford University Press, 267 p.:

Anderson, A., 1989, Mechanics of overkill in the extinction of New Zealand moas: Journal of Archaeological Science, v. 16, p. 137–151.

Anselmetti, F. S., Hodell, D. A., Ariztegui, D., Brenner, M., and Rosenmeier, M. F., 2007, Quantification of soil erosion rates related to ancient Maya deforestation: Geology, v. 35, no. 10, p. 915–918.

Armesto, J. J., Manuschevich, D., Mora, A., Smith-Ramirez, C., Rozzi, R., Abarzúa, A. M., and Marquet, P. A., 2010, From the Holocene to the Anthropocene: A historical framework for land cover change in southwestern South America in the past 15,000 years: Land Use Policy, v. 27, p. 148–160.

Atkinson, G., 1984, Erosion damage following bushfires: Journal of the Soil Conservation Service of New South Wales, v. 40, p. 4–9.

Autin, W. J., and Holbrook, J. M., 2012, Is the Anthropocene an issue of stratigraphy of pop culture?: GSA Today, v. 22, no. 7, p. 60–61.

Balco, G., Stone, J. O., Lifton, N. A., and Dunai, T. J., 2008, A complete and easily accessible means of calculating surface exposure ages or erosion rates from ^{10}Be and ^{26}Al measurements: Quaternary Geochronology, v. 3, no. 3, p. 174–195.

Barnosky, A. D., Koch, P. L., Feranec, R. S., Wing, S. L., and Shabel, A. B., 2004, Assessing the causes of Late Pleistocene extinctions on the continents: Science, v. 306, p. 70–75.

Barnosky, A. D., and Lindsey, E. L., 2010, Timing of Quaternary megafaunal extinction in South America in relation to human arrival and climate change: Quaternary International, v. 217, no. 1–2, p. 10–29.

Barrows, T. T., Stone, J. O., and Fifield, L. K., 2004, Exposure ages for Pleistocene periglacial deposits in Australia: Quaternary Science Reviews, v. 23, no. 5–6, p. 697–708.

Barrows, T. T., Stone, J. O., Fifield, L. K., and Cresswell, R. G., 2001, Late Pleistocene glaciation of the Kosciuszko Massif, Snowy Mountains, Australia: Quaternary Research, v. 55, p. 179–189.

Barrows, T. T., Stone, J. O., Fifield, L. K., and Cresswell, R. G., 2002, The timing of the Last Glacial Maximum in Australia: Quaternary Science Reviews, v. 21, p. 159–173.

Bayley, W. A., 1975, Uplands Pastures: History of Crookwell Shire New South Wales, Crookwell, NSW, Australia, Crookwell Shire Council, 207 p.:

Beach, T., Dunning, N., Luzzadder-Beach, S., Cook, D. E., and Lohse, J., 2006, Impacts of the ancient Maya on soils and soil erosion in the central Maya Lowlands: Catena, v. 65, no. 2, p. 166–178.

Beach, T., Luzzadder-Beach, S., Dunning, N., Jones, J., Lohse, J., Guderjan, T., Bozarth, S., Millspaugh, S., and Bhattacharya, T., 2009, A review of human and natural changes in Maya Lowland wetlands over the Holocene: Quaternary Science Reviews, v. 28, no. 17–18, p. 1710–1724.

Beavis, S. G., 2000, Structural controls on the orientation of erosion gullies in mid-western New South Wales, Australia: Geomorphology, v. 33, no. 1–2, p. 59–72.

Bierman, P., and Steig, E. J., 1996, Estimating rates of denudation using cosmogenic isotope abundances in sediment: Earth Surface Processes and Landforms, v. 21, p. 125–139.

Bierman, P. R., Coppersmith, R., Hanson, K., Neveling, J., Portenga, E. W., and Rood, D. H., 2014, A cosmogenic view of erosion, relief generation, and the age of faulting in southern Africa: Geological Society of America Today, v. 24, no. 9, p. 4–11.

Bird, M. I., Hutley, L. B., Lawes, M. J., Lloyd, J., Luly, J. G., Ridd, P. V., Roberts, R. G., Ulm, S., and Wurster, C. M., 2013, Humans, megafauna and environmental change in tropical Australia: Journal of Quaternary Science, v. 28, no. 5, p. 439–452.

Bishop, P., 1985, Southeast Australian late Mesozoic and Cenozoic denudation rates: A test for late Tertiary increases in continental denudation: Geology, v. 13, no. 7, p. 479–482.

Bishop, P., 1986, Horizontal stability of the Australian continental drainage divide in south central New South Wales during the Cainozoic: Australian Journal of Earth Sciences, v. 33, p. 205–307.

Bishop, P., Muñoz-Salinas, E., MacKenzie, A. B., Pulford, I., and McKibbin, J., 2011, The character, volume and implications of sediment impounded in mill dams in Scotland: The case of the Baldernock Mill dam in East Dunbartonshire: Earth and Environmental Science Transactions of the Royal Society of Edinburgh, v. 101, p. 97–110.

Bishop, P., Sanderson, D., Hansom, J., and Chaimanee, N., 2005, Age-dating of tsunami deposits: Lessons from the 26 December 20114 tsunami in Thailand: The Geographical Journal, v. 171, no. 4, p. 379–384.

Bishop, P., Young, R. W., and McDougall, I., 1985, Stream profile change and longterm landscape evolution: Early Miocene and modern rivers of the east Australian highland crest, central New South Wales, Australia: The Journal of Geology, v. 93, p. 455–474.

Black, M. P., and Mooney, S. D., 2006, Holocene fire history from the Greater Blue Mountains World Heritage Area, New South Wales, Australia: The climate, humans and fire nexus: Regional Environmental Change, v. 6, p. 41–51.

Black, M. P., Mooney, S. D., and Attenbrow, V., 2008, Implications of a 14 200 year contiguous fire record for understanding human-climate relationships at Goochs Swamp, New South Wales, Australia: The Holocene, v. 18, no. 3, p. 437–447.

Black, M. P., Mooney, S. D., and Martin, H. A., 2006, A >43,000-year vegetation and fire history from Lake Baraba, New South Wales, Australia: Quaternary Science Reviews, v. 25, p. 3003–3016.

Blaxland, G., 1870, Journal of a Tour of Discovery Across the Blue Mountains, New South Wales, in the Year 1813, S. T. Leigh and Co.

Blong, R. J., and Gillespie, R., 1978, Fluvially transported charcoal gives erroneous 14C ages for recent deposits: Nature, v. 271, no. 5647, p. 739–741.

Blong, R. J., Riley, S. J., and Crozier, P. J., 1982, Sediment yield from runoff plots following bushfire near Narrabeen Lagoon, NSW: Search (Sydney, N.S.W.), v. 13, no. 1–2, p. 36–38.

Blumenschine, R. J., Peters, C. R., Masao, F. T., Clarke, R. J., Deino, A. L., Hay, R. L., Swisher, C. C., Stanistreet, I. G., Ashley, G. M., McHenry, L. J., Sikes, N. E., van der Merwe, N. J., Tactikos, J. C., Cushing, A. E., Deocampo, D. M., Njau, J. K., and Ebert, J. I., 2003, Late Pliocene *Homo* and hominid land use from western Olduvai Gorge, Tanzania: Science, v. 299, no. 5610, p. 1217–1221.

BOM, Bureau of Meteorology, 2015, Climate and Past Weather, Commonwealth of Australia.

Booth, E. G., and Loheide II, S. P., 2012, Hydroecological model predicitons indicate wetter and more diverse soil water regimes and vegetation types following floodplain restoration: Journal of Geophysical Research, v. 117, no. G02011.

Booth, E. G., Loheide II, S. P., and Hansis, R. D., 2009, Postsettlement alluvium removal: a novel floodplain restoration technique (Wisconsin): Ecological Restoration, v. 27, no. 2, p. 136–139.

Bowler, J. M., Hope, G. S., Jennings, J. N., Singh, G., and Walker, D., 1976, Late Quaternary climates of Australia and New Guinea: Quaternary Research, v. 6, p. 359–394.

Bowler, J. M., Johnston, H., Olley, J. M., Prescott, J. R., Roberts, R. G., Wilfred, S., and Spooner, N. A., 2003, New ages for human occupation and climatic change at Lake Mungo, Australia: Nature, v. 421, p. 837–840.

Bowler, J. M., Jones, R., Allen, H., and Thorne, A. G., 1970, Pleistocene human remains from Australia: A living site and human cremation from Lake Mungo, western New South Wales: World Archaeology, v. 2, no. 1, p. 39–60.

Brannstrom, C., and Oliveira, A. M. S., 2000, Human modification of stream valleys in the western plateau of São Paulo, Brazil: implications for environmental narratives and management: Land Degradation & Development, v. 11, no. 6, p. 535–548.

Brooks, A. P., Shellberg, J. G., Knight, J., and Spencer, J., 2009, Alluvial gully erosion: An example from the Mitchell fluvial megafan, Queensland, Australia: Earth Surface Processes and Landforms, v. 34, no. 14, p. 1951–1969.

Brown, E. T., Stallard, R. F., Larsen, M. C., Bourlès, D. L., Raisbeck, G. M., and Yiou, F., 1998, Determination of predevelopment denudation rates of an agricultural watershed (Cayaguás River, Puerto Rico) using in-situ-produced ^{10}Be in river-borne quartz: Earth and Planetary Science Letters, v. 160, p. 723–728.

Brown, E. T., Stallard, R. F., Larsen, M. C., Raisbeck, G. M., and Yiou, F., 1995, Denudation rates determined from the accumulation of in situ-produced ^{10}Be in the Luquillo Experimental Forest, Puerto Rico: Earth and Planetary Science Letters, v. 129, p. 193–202.

Brown, J. A. H., 1972, Hydrologic effects of a bushfire in a catchment in south-eastern New South Wales: Journal of Hydrology, v. 15, no. 1, p. 77–96.

Brown, L., Pavich, M. J., Hickman, R. E., Klein, J., and Middleton, R., 1988, Erosion of the eastern United States observed with 10Be: Earth Surface Processes and Landforms, v. 13, no. 5, p. 441–457.

Burbidge, C. I., Sanderson, D. C. W., Housley, R. A., and Allsworth Jones, P., 2007, Survey of Palaeolithic sites by luminescence profiling, a case study from Eastern Europe: Quaternary Geochronology, v. 2, p. 296–302.

Burney, D. A., Burney, L. P., Godfrey, L. R., Jungers, W. L., Goodman, S. M., Wright, H. T., and Jull, A. J. T., 2004, A chronology for late prehistoric Madagascar: Journal of Human Evolution, v. 47, p. 25–63.

Burney, D. A., and Flannery, T. F., 2005, Fifty millennia of catastrophic extinctions after human contact: Trends in Ecology and Evolution, v. 20, no. 7, p. 395–401.

Butzer, K. W., and Helgren, D. M., 2005, Livestock, land cover, and environmental history: the Tablelands of New South Wales, Australia, 1820-1920: Annals of the Association of American Geographers, v. 95, no. 1, p. 80–111.

Camenzuli, D., Freidman, B. L., Statham, T. M., Mumford, K. A., and Gore, D. B., 2013, On-site and in situ remediation technologies applicable to metal-contaminated sites in Antarctica and the Arctic: A review: Polar Research, v. 32, p. 1–15.

Carbonell, E., Bermudez de Castro, J. M., Arsuaga, J. L., Diez, J. C., Rosas, A., Cuenca-Bescos, G., Sala, R., Mosquera, M., and Rodriguez, X. P., 1995, Lower Pleistocene hominids and artifacts from Atapuerca-TD6 (Spain): Science, v. 269, no. 5225, p. 826–830.

Carbonell, E., Bermúdez de Castro, J. M., Parés, J. M., Pérez-González, A., Cuenca-Bescos, G., Ollé, A., Mosquera, M., Huguet, R., van der Made, J., Rosas, A., Sala, R., Vallverdú, J., García, N., Granger, D. E., Martinón-Torres, M., Rodríguez, X. P., Stock, G. M., Vergès, J. M., Allué, E., Burjachs, F., Cáceres, I., Canals, A., Benito, A., Díez, C., Lozano, M., Mateos, A., Navazo, M., Rodríguez, J., Rosell, J., and Arsuaga, J. L., 2008, The first hominin of Europe: Nature, v. 452, p. 465–469.

Cawson, J. G., Sheridan, G. J., Smith, H. G., and Lane, P. N. J., 2013, Effects of fire severity and burn patchiness on hillslope-scale surface runoff, erosion and hydrologic connectivity in a prescribed burn: Forest Ecology and Management, v. 310, p. 219–233.

Christie-Blick, N., 2012, Geological Time Conventions and Symbols: GSA Today, v. 22, no. 2, p. 29–29.

Clark, R. J., and Sanderson, D. C. W., 1994, Photostimulated luminescence excitation spectroscopy of feldspars and micas: Radiation Measurements, v. 23, no. 2–3, p. 641–646.

Colhoun, E. A., Hannan, D., and Kiernan, K., 1996, Late Wisconsin glaciation of Tasmania: Papers and Proceedings of the Royal Society of Tasmania, v. 130, no. 2, p. 33–45.

Coltorti, M., Fazia, J. d., Rios, F. P., and Tito, G., 2010, The Ñuagapua alluvial fan sequence: Early and Late Holocene human-induced changes in the Bolivian Chaco: Proceedings of the Geologists' Association, v. 121, no. 2, p. 218–228.

Corbett, L. B., Young, N. E., Bierman, P. R., Briner, J. P., Neumann, T. A., Rood, D. H., and Graly, J. A., 2011, Paired bedrock and boulder ^{10}Be concentrations resulting from early Holocene ice retreat near Jakobshavn Isfjord, western Greenland: Quaternary Science Reviews, v. 30, no. 13–14, p. 1739–1749.

Corcoran, P. L., Moore, C. J., and Jazvac, K., 2014, An anthropogenic marker horizon in the future rock record: GSA Today, v. 24, no. 6, p. 4–8.

Cosgrove, R., 1999, Forty-two degrees south: The archaeology of Late Pleistocene Tasmania: Journal of World Prehistory, v. 13, no. 4, p. 357–402.

Costin, A. B., 1972, Carbon-14 Dates from the Snowy Mountains area, southeastern Australia, and their interpretation: Quaternary Research, v. 2, no. 4, p. 579–590.

Coventry, R. J., 1976, Abandoned shorelines and the Late Quaternary history of Lake George, New South Wales: Journal of the Geological Society of Australia, v. 23, no. 3, p. 249–273.

Coventry, R. J., and Walker, P. H., 1977, Geomorphological significance of late quaternary deposits of the Lake George Area, N.S.W: Australian Geographer, v. 13, no. 6, p. 369–376.

Cox, R., Zentner, D. B., Rakotondrazafy, A. F. M., and Rasoazanamparany, C. F., 2010, Shakedown in Madagascar: Occurrence of lavakas (erosional gullies) associated with seismic activity: Geology, v. 38, no. 2, p. 179–182.

Crighton, P., and Gore, D., 2001, Wannara Creek, *in* Marutani, T., Brierley, G. J., Trustrum, N. A., and Page, M., eds., Source-to-Sink Sedimentary Cascades in Pacific Rim Geo-Systems: Matsumoto, Japan, Ministry of Land, Infrastructure and Transport, p. 154–161.

Crouch, R. J., 1987, The relationship of gully sidewall shape to sediment production: Australian Journal of Soil Research, v. 25, no. 4, p. 531–539.

Crutzen, P. J., 2002, Geology of mankind: Nature, v. 415, p. 23.

Crutzen, P. J., and Steffen, W., 2003, How long have we been in the Anthropocene Era?: Climatic Change, v. 61, no. 3, p. 251–257.

Cupper, M. L., and Duncan, J., 2006, Last glacial megafaunal death assemblage and early human occupation at Lake Menindee, southeastern Australia: Quaternary Research, v. 66, no. 2, p. 332–341.

Dalrymple, G. B., 2001, The age of the Earth in the twentieth century: A problem (mostly) solved, *in* Lewis, C. L. E., and Knell, S. J., eds., The Age of the Earth: from 4004 BC to AD 2002, Volume 190: London, UK, Geological Society of London, p. 205–221.

Damm, B., and Hagedorn, J., 2010, Holocene floodplain formation in the southern Cape region, South Africa: Geomorphology, v. 122, no. 3–4, p. 213–222.

Delcourt, H. R., and Delcourt, P. A., 1997, Pre-Columbian Native American use of fire on southern Appalachian landscapes: Conservation Biology, v. 11, no. 4, p. 1010–1014.

Delcourt, P. A., Delcourt, H. R., Ison, C. R., Sharp, W. E., and Gremillion, K. J., 1998, Prehistoric human use of fire, the Eastern Agricultural Complex, and Appalachian oak-chestnut forests: Paleoecology of Cliff Palace Pond, Kentucky: American Antiquity, v. 63, no. 2, p. 263–278.

Denevan, W. M., 1992, The pristine myth: The landscape of the Americas in 1492: Annals of the Association of American Geographers, v. 82, no. 3, p. 369–385.

Derraik, J. G. B., 2002, The pollution of the marine environment by plastic deris: A review: Marine Pollution Bulletin, v. 44, no. 9, p. 842–852.

Dethier, D. P., Ouimet, W., Bierman, P. R., Rood, D. H., and Balco, G., 2014, Basins and bedrock: Spatial variation in ^{10}Be erosion rates and increasing relief in the southern Rocky Mountains, USA: Geology, v. 42, no. 2, p. 167–170.

Dillehay, T. D., Bonavia, D., Goodbred Jr., S. L., Pino, M., Vásquez, V., and Tham, T. R., 2012, A late Pleistocene human presence at Huaca Prieta, Peru, and early Pacific Coastal adaptations: Quaternary Research, v. 77, no. 3, p. 418–423.

Dillehay, T. D., Ramírez, C., Pino, M., Collins, M. B., Rossen, J., and Pino-Navarro, J. D., 2008, Monte Verde: Seaweed, food, medicine, and the peopling of South America: Science, v. 320, no. 5877, p. 784–786.

Dlapa, P., Chrenková, K., Mataix-Solera, J., and Šimkovic, I., 2012, Soil profile improvement as a by-product of gully stabilization measures: Catena, v. 92, p. 155–161.

Dobes, L., Weber, N., Bennett, J., and Ogilvy, S., 2013, Stream-bed and flood-plain rehabilitation at Mulloon Creek, Australia: A financial and economic perspective: The Rangeland Journal, v. 35, no. 3, p. 339–348.

Dodson, J., Fullagar, R., Furby, J., Jones, R., and Prosser, I., 1993, Humans and megafauna in a Late Pleistocene environment from Cuddie Springs, north western New South Wales: Archaeology in Oceania, v. 28, p. 94–99.

Duller, G. A. T., 1994, Luminescence dating of poorly bleached sediments from Scotland: Quaternary Geochronology (Quaternary Science Reviews), v. 13, no. 5–7, p. 521–524.

Duller, G. A. T., 2004, Luminescence dating of quaternary sediments: recent advances: Journal of Quaternary Science, v. 19, no. 2, p. 183–192.

Duller, G. A. T., 2008, Single-grain optical dating of Quaternary sediments: why aliquot size matters in luminescence dating: Boreas, v. 37, p. 589–612.

Duller, G. A. T., and Bøtter-Jensen, L., 1993, Luminescence from potassium feldspars stimulated by infrared and green light: Radiation Protection Dosimetry, v. 47, no. 114, p. 683–688.

Dunne, J., Elmore, D., and Muzikar, P., 1999, Scaling factors for the rates of production of cosmogenic nuclides for geometric shielding and attenuation at depth on sloped surfaces: Geomorphology, v. 27, no. 1–2, p. 3–11.

Edgeworth, M., Richter, D. d., Waters, C., Haff, P., Neal, C., and Price, S. J., 2015, Diachronous beginnings of the Anthropocene: The lower bounding surface of anthropogenic deposits: The Anthropocene Review, p. 1–26.

Eriksson, M. G., Olley, J. M., Kilham, D. R., Pietsch, T., and Wasson, R. J., 2006, Aggradation and incision since the very late Pleistocene in the Naas River, south-eastern Australia: Geomorphology, v. 81, no. 1–2, p. 66–88.

Erskine, W., and Melville, M. D., 1984, Sediment movement in a discontinuous gully system at Boro Creek, southern Tablelands, N.S.W., Drainage Basin Erosion and Sedimentation: A Conference on Erosion, Transportation, and Sedimentation in Australian Drainage Basins: Newcastle, N.S.W., Australia, Soil Conservation Service of N.S.W., p. 197–204.

Erskine, W. D., 1994, River response to accelerated soil erosion in the Glenelg River catchment, Victoria: Australian Journal of Soil and Water Conservation, v. 7, no. 2, p. 39–47.

Erskine, W. D., and Warner, R. F., 1988, Geomorphic Effects of Alternating Flood- and Drought-Dominated Regimes on NSW Coastal Rivers, *in* Warner, R. F., ed., Fluvial Geomorphology of Australia: Sydney, Australia, Academic Press, p. 223–242.

Erskine, W. D., and Warner, R. F., 1998, Futher assessment of flood- and drought-dominated regimes in south-eastern Australia: Australian Geographer, v. 29, no. 2, p. 257–261.

Evans, G. W., 1916, Two Journals of Early Exploration in New South Wales, Sydney, Australia, The Library Committee of the Commonwealth Parliament, Series I. Governors' Despatches to and from England.

Eyles, R. J., 1977a, Birchams Creek: the transition from a chain of ponds to a gully: Australian Geographical Studies, v. 15, no. 2, p. 146–157.

Eyles, R. J., 1977b, Changes in drainage networks since 1820, Southern Tablelands, N.S.W: Australian Geographer, v. 13, no. 6, p. 377–386.

Eyles, R. J., 1977c, Erosion and land use in the Burra catchment, Queanbeyan: Journal of the Soil Conservation Service of New South Wales, v. 33, no. 1, p. 47–59.

Fanning, P. C., Holdaway, S. J., and Rhodes, E. J., 2008, A new geoarchaeology of Aboriginal artefact deposits in western NSW, Australia: Establishing spatial and temporal geomorphic controls on the surface archaeological record: Geomorphology, v. 101, no. 3, p. 524–532.

Fenby, C., and Gergis, J., 2012, Rainfall variations in south-eastern Australia part 1: Consolidating evidence from pre-instrumental documentary sources, 1788-1860: International Journal of Climatology, v. 33, no. 14, p. 2956–2972.

Field, J., Fillios, M., and Wroe, S., 2008, Chronological overlap between humans and megafauna in Sahul (Pleistocene Australia-New Guinea): A review of the evidence: Earth-Science Reviews, v. 89, p. 97–115.

Field, J., and Wroe, S., 2012, Aridity, faunal adaptations and Australian Late Pleistocene extinctions: World Archaeology, v. 44, no. 1, p. 56–74.

Fifield, L. K., Wasson, R. J., Pillans, B., and Stone, J. O. H., 2010, The longevity of hillslope soil in SE and NW Australia: Catena, v. 81, no. 1, p. 32–42.

Flood, J., 1974, Pleistocene man at Cloggs Cave: His tool kit and environment: Mankind, v. 9, p. 175–188.

Foulds, S. A., and Macklin, M. G., 2006, Holocene land-use change and its impact on river basin dynamics in Great Britain and Ireland: Progress in Physical Geography, v. 30, no. 5, p. 589–604.

Foulds, S. A., Macklin, M. G., and Brewer, P. A., 2013, Agro-industrial alluvium in the Swale catchment, northern England, as an event marker for the Anthropocene: The Holocene, v. 0, no. 0, p. 1–16.

Fuchs, M., Lang, A., and Wagner, G. A., 2004, The history of Holocene soil erosion in the Phlious Basin, NE Peloponnese, Greece, based on optical dating: The Holocene, v. 14, no. 3, p. 334–345.

Gabunia, L., Vekua, A., Lordkipanidze, D., Swisher III, C. C., Ferring, R., Justus, A., Nioradze, M., Tvalchrelidze, M., Antón, S. C., Bosinski, G., Jöris, O., Lumley, M.-A.-d., Majsuradze, G., and Mouskhelishvili, A., 2000, Earliest Pleistocene hominid

cranial remains from Dmanisi, Republic of Georgia: Taxonomy, geological setting, and age: Science, v. 288, no. 5468, p. 1019–1025.

Gaina, C., Müller, D. R., Royer, J.-Y., Stock, J., Hardebeck, J., and Symonds, P., 1998, The tectonic history of the Tasman Sea: A puzzle with 13 pieces: Journal of Geophysical Research: Solid Earth, v. 103, no. B6, p. 12413–12433.

Galbraith, R., 2005, Statistics for Fission Track Analysis, Boca Raton, Fl, USA, Chapman & Hall/CRC.

Galbraith, R. F., 1988, Graphical display of estimates having differing standard errors: Technometrics, v. 30, no. 3, p. 271–281.

Galbraith, R. F., Roberts, R. G., Laslett, G. M., Yoshida, H., and Olley, J. M., 1999, Optical dating of single and multiple grains of quartz from Jinmium Rock Shelter, Norther Australia: Part I, experimental design and statistical models: Archaeometry, v. 41, no. 2, p. 339–364.

Gale, S. J., and Haworth, R. J., 2002, Beyond the limits of location: human environmental disturbance prior to official European contact in early colonial Australia: Archaeology in Oceania, v. 37, p. 123–136.

Gallant, J., Wilson, N., Dowling, T., Read, A., and Inskeep, C., 2011, SRTM-derived 1 Second Digital Elevation Models Version 1.0, *in* Australia), C. o. A. G., ed.: Canberra, ACT, Australia, Geoscience Australia.

Gammage, B., 2011, The Biggest Estate on Earth: How Aborigines Made Australia, Sydney, Allen & Unwin, 384 p.:

García-Rodríguez, F., Mazzeo, N., Sprechmann, P., Metzeltin, D., Sosa, F., Treutler, H. C., Renom, M., Scharf, B., and Gaucher, C., 2002, Paleolimnological assessment of human impacts in Lake Blanca, SE Uruguay: Journal of Paleolimnology, v. 28, p. 457–468.

Gergis, J., and Ashcroft, L., 2013, Rainfall variations in south-eastern Australia part 2: A comparison of documentary, early instrumental and paleoclimate records, 1788-2008: International Journal of Climatology, v. 33, no. 14, p. 2973–2987.

Gill, J. L., Williams, J. W., Jackson, S. T., Lininger, K. B., and Robinson, G. S., 2009, Pleistocene megafaunal collapse, novel plant communities, and enhanced fire regimes in North America: Science, v. 326, no. 5956, p. 1100–1103.

Gillespie, P. D., 1981, Development of gully erosion at the head of Bango Creek near Yass, New South Wales: Journal of the Soil Conservation Service of New South Wales, v. 37, no. 1, p. 5–13.

Gillespie, R., 2008, Updating Martin's global extinction model: Quaternary Science Reviews, v. 27, p. 2522–2529.

Gillespie, R., and Brook, B. W., 2006, Is there a Pleistocene archaeological site at Cuddie Springs?: Archaeology in Oceania, v. 41, no. 1, p. 1–11.

Gillespie, R., Camens, A. B., Worthy, T. H., Rawlence, N. J., Reid, C., Bertuch, F., Levchenko, V., and Cooper, A., 2012, Man and megafauna in Tasmania: closing the gap: Quaternary Science Reviews, v. 37, p. 38–47.

Gillespie, R., Prosser, I. P., Dlugokencky, E., Sparks, R. J., Wallace, G., and Chappell, J. M. A., 1992, AMS dating of alluvial sediments on the southern Tablelands of New South Wales, Australia: Radiocarbon, v. 34, no. 1, p. 29–36.

Godfrey-Smith, D. I., Huntley, D. J., and Chen, W.-H., 1988, Optical dating studies of quartz and feldspar sediment extracts: Quaternary Science Reviews, v. 7, p. 373–380.

Gore, D. B., Brierley, G. J., Pickard, J., and Jansen, J. D., 2000, Anatomy of a floodout in semi-arid eastern Australia: Zeitschrift für Geomorphologie, v. Supplement-Band 122, p. 113–139.

Gosse, J. C., and Phillips, F. M., 2001, Terrestrial in situ cosmogenic nuclids: theory and application: Quaternary Science Reviews, v. 20, no. 14, p. 1475–1560.

Graly, J. A., Bierman, P. R., Reusser, L. J., and Pavich, M. J., 2010, Meteoric ^{10}Be in soil profiles - A global meta-analysis: Geochimica et Cosmochimica Acta, v. 74, no. 23, p. 6814–6829.

Graly, J. A., Reusser, L. J., and Bierman, P. R., 2011, Short and long-term delivery rates of meteoric ^{10}Be to terrestrial soils: Earth and Planetary Science Letters, v. 302, no. 3–4, p. 329–336.

Granger, D. E., Kirchner, J. W., and Finkel, R., 1996, Spatially averaged long-term erosion rates measured from in situ-produced cosmogenic nuclides in alluvial sediment: The Journal of Geology, v. 104, no. 3, p. 249–257.

Gray, D. R., and Foster, D. A., 2004, Tectonic evolution of the Lachlan Orogen, southeast Australia: historical review, data synthesis and modern perspectives: Australian Journal of Earth Sciences, v. 51, p. 773–817.

Grayson, D. K., and Meltzer, D. J., 2003, A requiem for North American overkill: Journal of Archaeological Science, v. 30, p. 585–593.

Grün, R., Eggins, S., Aubert, M., Spooner, N., Pike, A. W. G., and Müller, W., 2010, ESR and U-series analyses of faunal material from Cuddie Springs, NSW, Australia: Implications for the timing of the extinction of the Australian megafauna: Quaternary Science Reviews, v. 29, p. 596–610.

Grün, R., Eggins, S., Wells, R. T., Rhodes, E., Bestland, E., Spooner, N., Ayling, M., Forbes, M., and McCulloch, M., 2006, A cautionary tale from down under: Dating the Black Creek Swamp megafauna site on Kangaroo Island, South Australia: Quaternary Geochronology, v. 1, p. 142–150.

Grün, R., Wells, R., Eggins, S., Spooner, N., Aubert, M., Brown, L., and Rhodes, E., 2008, Electron spin resonance dating of South Australian megafauna sites: Australian Journal of Earth Sciences, v. 55, p. 917–935.

Guthrie, R. D., 2004, Radiocarbon evidence of mid-Holocene mammoths stranded on an Alaskan Bering Sea island: Nature, v. 429, p. 746–749.

Hancock, W. K., 1972, Discovering Monaro: A Study of Man's Impact On His Environment, Cambridge, Cambridge University Press, 209 p.:

Heckenberger, M. J., Kuikuro, A., Kuikuro, U. T., Russell, J. C., Schmidt, M., Fausto, C., and Franchetto, B., 2003, Amazonia 1492: Pristine forest or cultural parkland?: Science, v. 301, p. 1710–1715.

Heikkilä, U., Beer, J., and Alfimov, V., 2008, Beryllium-10 and beryllium-7 in precipitation in Dübendorf (440 m) and at Jungfraujoch (3580 m), Switzerland (1998-2005): Journal of Geophysical Research, v. 113, no. D11, p. D11104.

Heimsath, A. M., Chappell, J., Dietrich, W. E., Nishiizumi, K., and Finkel, R. C., 2001, Late Quaternary erosion in southeastern Australia: A field example using cosmogenic nuclides: Quaternary International, v. 83–85, p. 169–185.

Heimsath, A. M., Chappell, J., Finkel, R. C., Fifield, K., and Alimanovic, A., 2006, Escarpment erosion and landscape evolution in southeastern Australia: Geological Society of America Special Paper, v. 398, p. 173–190.

Heimsath, A. M., Chappell, J., Spooner, N. A., and Questiaux, D. G., 2002, Creeping soil: Geology, v. 30, no. 2, p. 111–114.

Heimsath, A. M., Dietrich, W. E., Nishiizumi, K., and Finkel, R. C., 1997, The soil production function and landscape equilibrium: Nature, v. 388, p. 358–361.

Heimsath, A. M., Fink, D., and Hancock, G. R., 2009, The 'humped' soil production function: Eroding Arnhem Land, Australia: Earth Surface Processes and Landforms, v. 34, p. 1674–1684.

Heisinger, B., Lal, D., Jull, A. J. T., Kubik, P., Ivy-Ochs, S., Knie, K., and Nolte, E., 2002a, Production of selected cosmogenic radionuclides by muons: 2. Capture of negative muons: Earth and Planetary Science Letters, v. 200, no. 3–4, p. 357–369.

Heisinger, B., Lal, D., Jull, A. J. T., Kubik, P., Ivy-Ochs, S., Neumaier, S., Lazarev, V., and Nolte, E., 2002b, Production of selected cosmogenic radionuclides by muons: 1. Fast muons: Earth and Planetary Science Letters, v. 200, no. 3–4, p. 345–355.

Helz, G. R., and Valette-Silver, N., 1992, Beryllium-10 in Chesapeake Bay sediments: an indicator of sediment provenance: Estuarine, Coastal and Shelf Science, v. 34, no. 5, p. 459–469.

Hijmans, R. J., Cameron, S. E., Parra, J. L., Jones, P. G., and Jarvis, A., 2005, Very high resolution interpolated climate surfaces for global land areas: International Journal of Climatology, v. 25, p. 1965–1978.

Hippolyte, J.-C., Brocard, G., Tardy, M., Nicoud, G., Bourlès, D., Braucher, R., Ménard, G., and Souffaché, B., 2006, The recent fault scarps of the Western Alps (France): Tectonic surface ruptures or gravitational sacking scarps? A combined mapping, geomorphic, levelling, and ^{10}Be dating approach: Tectonophysics, v. 418, no. 3–4, p. 255–276.

Hoffmann, T., Lang, A., and Dikau, R., 2008, Holocene river activity: analysing ^{14}C-dated fluvial and colluvial sediments from Germany: Quaternary Science Reviews, v. 27, no. 21–22, p. 2031–2040.

Holdaway, R. N., and Jacomb, C., 2000, Rapid extinction of the moas (Aves: Dinornithiformes): Model, test, and implications: Science, v. 287, p. 2250–2254.

Hooke, R. L., 1994, On the efficacy of humans as geomorphic agents: GSA Today, v. 4, no. 9, p. 217, 224–225.

Hooke, R. L., 2000, On the history of humans as geomorphic agents: Geology, v. 28, no. 9, p. 843–846.

Hooke, R. L., Martin-Duque, J. F., and Pedraza, J., 2012, Land transformation by humans: A review: GSA Today, v. 22, no. 12, p. 4–10.

Hope, J. H., Lampert, R. J., Edmondson, E., Smith, M. J., and van Tets, G. F., 1977, Late Pleistocene faunal remains from Seton Rock Shelter, Kangaroo Island, South Australia: Journal of Biogeography, v. 4, no. 4, p. 363–385.

Howard, J. L., 2014, Proposal to add anthrostratigraphic and technostratigraphic units to the code for classification of anthropogenic Holocene deposits: The Holocene, v. 24, no. 12, p. 1856–1861.

Hughes, A. O., Olley, J. M., Croke, J. C., and McKergow, L. A., 2009, Sediment source changes over the last 250 years in a dry-tropical catchment, central Queensland, Australia: Geomorphology, v. 104, no. 3–4, p. 262–275.

Hughes, A. O., and Prosser, I. P., 2003, Gully and Riverbank Erosion Mapping for the Murray-Darling Basin: CSIRO Land and Water.

Hughes, A. O., and Prosser, I. P., 2012, Gully erosion prediciton across a large region: Murray-Darling Basin, Australia: Soil Research, v. 50, p. 267–277.

Hughes, A. O., Prosser, I. P., Stevenson, J., Scott, A., Lu, H., Gallant, J., and Moran, C. J., 2001, Gully Erosion Mapping for the National Land and Water Resources Audit: CSIRO Land and Water.

Hughes, P. J., and Sullivan, M. E., 1981, Aboriginal burning and Late Holocene geomorphic events in eastern NSW: Search (Sydney, N.S.W.), v. 12, no. 8, p. 277–278.

Hunt, T. L., and Lipo, C. P., 2006, Late colonization of Easter Island: Science, v. 311, p. 1603–1607.

Huntley, D. J., and Berger, G. W., 1995, Scatter in luminescence data for optical dating - some models: Ancient TL, v. 13, no. 1, p. 5–9.

Jacobs, Z., Duller, G. A. T., and Wintle, A. G., 2006, Interpretation of single grain D_e distributions and calcuation of D_e: Radiation Measurements, v. 41, p. 264–277.

Johanson, D. C., Masao, F. T., Eck, G. G., White, T. D., Walter, R. C., Kimbel, W. H., Asfaw, B., Manega, P., Ndessokia, P., and Suwa, G., 1987, New partial skeleton of *Homo habilis* from Olduvai Gorge, Tanzania: Nature, v. 327, p. 205–209.

Johnson, C. N., 2005, What can the data on late survival of Australian megafauna tell us about the cause of their extinction?: Quaternary Science Reviews, v. 24, no. 20–21, p. 2167–2172.

Johnson, C. N., 2009, Ecological consequences of Late Quaternary extinctions of megafauna: Proceedings of the Royal Society B, v. 276, p. 2509–2519.

Johnston, P., and Brierley, G., 2006, Late Quaternary river evolution of floodplain pockets along Mulloon Creek, New South Wales, Australia: The Holocene, v. 16, no. 5, p. 661–674.

Jungers, M. C., Bierman, P. R., Matmon, A., Nichols, K., Larsen, J., and Finkel, R., 2009, Tracing hillslope sediment production and transport with in situ and meteoric 10Be: Journal of Geophysical Research, v. 114, no. F4, p. F04020.

Kaiser, J., 2010, The dirt on ocean garbage patches: Science, v. 328, no. 5985, p. 1506.

Kershaw, A. P., McKenzie, G. M., and McMinn, A., 1993, A Quaternary vegetation history of northeastern Queensland from pollen analysis of ODP Site 820: Proceedings of the Ocean Drilling Program, Scientific Results, v. 133, p. 107–114.

Kidder, T., Liu, H., Xu, Q., and Li, M., 2012, The alluvial geoarchaeology of the Sanyangzhuang Site on the Yellow River floodplain, Henan Province, China: Geoarchaeology, v. 27, no. 4, p. 324–343.

King, G. E., Sanderson, D. C. W., Robinson, R. A. J., and Finch, A. A., 2014, Understanding processes of sediment bleaching in glacial settings using a portable OSL reader: Boreas, v. 43, no. 4, p. 955–972.

Kirkup, H., Brierley, G., Brooks, A., and Pitman, A., 1998, Temporal variability of climate in south-eastern Australia: A reassessment of flood- and drought-dominated regimes: Australian Geographer, v. 29, no. 2, p. 241–255.

Knox, J. C., 1977, Human impacts on Wisconsin stream channels: Annals of the Association of American Geographers, v. 67, no. 3, p. 323–342.

Knox, J. C., 2006, Floodplain sedimentation in the Upper Mississippi Valley: Natural versus human accelerated: Geomorphology, v. 79, p. 286–310.

Kohen, J. L., Stockton, E. D., and Williams, M. A. J., 1984, Shaws Creek KII rockshelter: A prehistoric occupation site in the Blue Mountains piedmont, eastern New South Wales: Archaeology in Oceania, v. 19, no. 2, p. 57–73.

Kohl, C. P., and Nishiizumi, K., 1992, Chemical isolation of quartz for measurement of *in-situ*-produced cosmogenic nuclides: Geochimica et Cosmochimica Acta, v. 56, p. 3583–3587.

Korschinek, G., Bergmaier, A., Faestermann, T., Gerstmann, U. C., Knie, K., Rugel, G., Wallner, A., Dillmann, I., Dollinger, G., von Gostomski, C. L., Kossert, K., Maiti, M., Poutivtsev, M., and Remmert, A., 2010, A new value for the half-life of ^{10}Be by heavy-ion elastic recoil detection and liquid scintillation counting: Nuclear Instruments and Methods in Physics Research B: Beam Interactions with Materials and Atoms, v. 268, p. 187–191.

Kortekaas, M., and Murray, A. S., 2005, A method for the removal of mica from quartz separates: Ancient TL, v. 23, no. 2, p. 43–46.

Krause, A. K., Franks, S. W., Kalma, J. D., Loughran, R. J., and Rowan, J. S., 2003, Multi-parameter fingerprinting of sediment deposition in a small gullied catchment in SE Australia: Catena, v. 53, p. 327–348.

Kreznor, W. R., Olson, K. R., Jones, R. L., and Johnson, D. L., 1990, Quantification of postsettlement deposition in a northwestern Illinois sediment basin: Soil Science Society of America Journal, v. 54, no. 5, p. 1393–1401.

Lal, D., 1991, Cosmic ray labeling of erosion surfaces: *In situ* nuclide production rates and erosion models: Earth and Planetary Science Letters, v. 104, no. 2–4, p. 424–439.

Lal, D., and Peters, B., 1962, Cosmic ray produced isotopes and their application to problems in geophysics, *in* Wilson, J. G., and Wouthysen, S. A., eds., Progress in Elementary Particle and Cosmic Ray Physics: New York, Wiley, p. 1–74.

Lal, D., 1967, Cosmic ray produced radioactivity on the earth, *in* Sitte, K., ed., Handbuch der Physik: New York, Springer-Verlag, p. 551–612.

Lampert, R. J., and Hughes, P. J., 1974, Sea level change and Aboriginal coastal adaptations in southern New South Wales: Archaeology & Physical Anthropology in Oceania, v. 9, no. 3, p. 226–235.

Lane, P. N. J., Sheridan, G. J., and Noske, P. J., 2006, Changes in sediment loads and discharge from small mountain catchments following wildfire in south eastern Australia: Journal of Hydrology, v. 331, p. 495–510.

Lane, R., 1997, Oral Histories and Scientific Knowledge in Understanding Environmental Change: a case study in the Tumut Region, NSW: Australian Geographical Studies, v. 35, no. 2, p. 195–205.

Lang, A., 2003, Phases of soil erosion-derived colluviation in the loess hills of South Germany: Catena, v. 51, p. 209–221.

Lang, A., Bork, H.-R., Mäckel, R., Preston, N., Wunderlich, J., and Dikau, R., 2003a, Changes in sediment flux and storage within a fluvial system: some examples from the Rhine catchment: Hydrological Processes, v. 17, p. 3321–3334.

Lang, A., and Hönscheidt, S., 1999, Age and source of colluvial sediments at Vaihingen-Enz, Germany: Catena, v. 38, no. 2, p. 89–107.

Lang, A., Kadereit, A., Behrends, R. H., and Wagner, G. A., 1999, Optical dating of anthropogenic sediments at the archaeological site of Herrenbrunnenbuckel, Bretten-Bauerbach (Germany): Archaeometry, v. 41, no. 2, p. 397–411.

Lang, A., and Mauz, B., 2006, Towards chronologies of gully formation: Optical dating of gully fill sediments from Central Europe: Quaternary Science Reviews, v. 25, p. 2666–2675.

Lang, A., Niller, H.-P., and Rind, M. M., 2003b, Land degradation in Bronze Age Germany: Archaeological, pedological, and chronometrical evidence from a hilltop settlment on the Frauenberg, Niederbayern: Geoarchaeology, v. 18, no. 7, p. 757–778.

Lawson, W., 1813, Journal of an Expedition Across the Blue Mountains, 11 May-6 June 1813, State Library of New South Wales.

Leakey, L. S. B., Tobias, P. V., and Napier, J. R., 1964, A new species of the genus *Homo* from Olduvai Gorge: Nature, v. 202, no. 4927, p. 7–9.

Leitch, C. J., Flinn, D. W., and van de Graaff, R. H. M., 1983, Erosion and nutriend loss resulting from Ash Wednesday (February 1983) wildfires: A case study: Australian Forestry, v. 46, no. 3, p. 173–180.

Lespez, L., 2003, Geomorphic responses to long-term land use changes in Eastern Macedonia (Greece): Catena, v. 51, no. 3–4, p. 181–208.

Li, B., Jacobs, Z., Roberts, R. G., and Li, S.-H., 2014, Review and assessment of the potential of post-IR IRSL dating methods to circumvent the problem of anomalous fading in feldspar luminescence: Geochronometria, v. 41, no. 3, p. 178–201.

Li, S.-H., 1994, Optical dating: Insufficiently bleached sediments: Radiation Measurements, v. 23, no. 2–3, p. 563–567.

Liu, X., Hunt, H. V., and Jones, M. K., 2009, River valleys and foothills: Changing archaeological perceptions of North China's earliest farms: Antiquity, v. 83, no. 319, p. 82–945.

Macklin, M. G., Benito, G., Gregory, K. J., Johnstone, E., Lewin, J., Michczyńskad, D. J., Soja, R., Starkel, L., and Throndycraft, V. R., 2006, Past hydrological events reflected in the Holocene fluvial record of Europe: Catena, v. 66, no. 1–2, p. 145–154.

Mactaggart, B., Bauer, J., Goldney, D., and Rawson, A., 2008, Problems in naming and defining the swampy meadow - An Australian perspective: Journal of Environmental Management, v. 87, no. 3, p. 461–473.

Magilligan, F. J., 1985, Historical Floodplain Sedimentation in the Galena River Basin, Wisconsin and Illinois: Annals of the Association of American Geographers, v. 75, no. 4, p. 583–594.

Martin, P. S., 1973, The discovery of America: Science, v. 179, p. 969–974.

Masarik, J., and Beer, J., 2009, An updated simulation of particle fluxes and cosmogenic nuclide production in the Earth's atmosphere: Journal of Geophysical Research, v. 114, no. D11103.

Massa, C., Bichet, V., Gauthier, É., Perren, B. B., Mathieu, O., Petit, C., Monna, F., Giraudeau, J., Losno, R., and Richard, H., 2012, A 2500 year record of natural and anthropogenic soil erosion in South Greenland: Quaternary Science Reviews, v. 32, p. 119–130.

Matmon, A., Bierman, P. R., Larsen, J., Southworth, S., Pavich, M., and Caffee, M., 2003, Temporally and spatially uniform rates of erosion in the southern Appalachian Great Smoky Mountains: Geology, v. 31, no. 2, p. 155–158.

McIntosh, P. D., Price, D. M., Eberhard, R., and Slee, A. J., 2009, Late Quaternary erosion events in lowland and mid-altitude Tasmania in relation to climate change and first human arrival: Quaternary Science Reviews, v. 28, no. 9–10, p. 850–872.

McLauchlan, K., 2003, Plant cultivation and forest clearance by prehistoric North Americans: Pollen evidence from Fort Ancient, Ohio, USA: The Holocene, v. 13, no. 4, p. 557–566.

Megaw, J. V. S., 1965, Excavations in the Royal National Park, New South Wales: A first series of radiocarbon dates from the Sydney district: Oceania, v. 35, no. 3, p. 202–207.

Melville, M. D., and Erskine, W., 1986, Sediment remobilization and storage by discontinuous gullying in humid southeastern Australia, *in* Hadley, R. F., ed., Drainage Basin Sediment Delivery, International Association of Hydrological Sciences, p. 277–286.

Meredith, L. A., 1844, Notes and Sketches of New South Wales During a Residence in that Colony from 1839 to 1844, London, J. Murray.

Merritts, D., Walter, R., Rahnis, M., Hartranft, J., Cox, S., Gellis, A., Potter, N., Hilgartner, W., Langland, M., Manion, L., Lippincott, C., Siddiqui, S., Rehman, Z., Scheid, C., Kratz, L., Shilling, A., Jenschke, M., Datin, K., Cranmer, E., Reed, A., Matuszewski, D., Voli, M., Ohlson, E., Neugebauer, A., Ahamed, A., Neal, C., Winter, A., and Becker, S., 2011, Anthropocene streams and base-level controls from historic dams in the unglaciated mid-Atlantic region, USA: Philosophical Transactions of the Royal Society A: Mathematical, Physical and Engineering Sciences, v. 369, no. 1938, p. 976–1009.

Mieth, A., and Bork, H.-R., 2005, History, origin and extent of soil erosion on Easter Island (Rapa Nui): Catena, v. 63, p. 244–260.

Miller, G. H., Fogel, M. L., Magee, J. W., Gagan, M. K., Clarke, S. J., and Johnson, B. J., 2005, Ecosystem collapse in Pleistocene Australia and a human role in megafaunal extinction: Science, v. 309, no. 5732, p. 287–290.

Miller, G. H., Magee, J. W., Johnson, B. J., Fogel, M. L., Spooner, N. A., McCulloch, M. T., and Ayliffe, L. K., 1999, Pleistocene extinction of *Genyornis newtoni*: Human impact on Australian megafauna: Science, v. 283, p. 205–208.

Mitchell, M. T. L., 1839a, Three Expeditions Into the Interior of Eastern Australia with Descriptions of the Recently Explored Region of Australia Felix and of the Present Colony of New South Wales, London, T. and W. Boone.

Mitchell, M. T. L., 1839b, Three Expeditions Into the Interior of Eastern Australia With Descriptions of the Recently Explored Region of Australia Felix, and of the Present Colony of New South Wales, London, T. and W. Boone.

Molina, A., Govers, G., Cisneros, F., and Vanacker, V., 2009, Vegetation and topographic controls on sediment deposition and storage on gully beds in a degraded mountain area: Earth Surface Processes and Landforms, v. 34, p. 755–767.

Monaghan, M. C., Krishnaswami, S., and Turekian, K. K., 1986, The global-average production rate of ^{10}Be: Earth and Planetary Science Letters, v. 76, no. 3–4, p. 279–287.

Montgomery, D. R., 2007a, Dirt: The Erosion of Civilizations, Berkeley, California, USA, University of California Press, 295 p.:

Montgomery, D. R., 2007b, Is agriculture eroding civilization's foundation?: GSA Today, v. 17, no. 10, p. 4–9.

Mooney, S. D., Harrison, S. P., Bartlein, P. J., Daniau, A.-L., Stevenson, J., Brownlie, K. C., Buckman, S., Cupper, M., Luly, J., Black, M., Colhoun, E., D'Costa, D., Dodson, J., Haberle, S., Hope, G. S., Kershaw, P., Kenyon, C., McKenzie, M., and Williams, N., 2011, Late Quaternary fire regimes of Australasia: Quaternary Science Reviews, v. 30, no. 1–2, p. 28–46.

Muñoz-Salinas, E., Bishop, P., Sanderson, D., and Kinnaird, T., 2014, Using OSL to assess hypotheses related to the impacts of land-use change with the early nineteenth century arrival of Europeans in south-eastern Australia: An exploratory case study from Grabben Gullen Creek, New South Wales: Earth Surface Processes and Landforms, v. 39, no. 12, p. 1576–1586.

Muñoz-Salinas, E., Bishop, P., Sanderson, D. C. W., and Zamorano, J.-J., 2011, Interpreting luminescence data from a portable OSL reader: three case studies in fluvial settings: Earth Surface Processes and Landforms, v. 36, no. 5, p. 651–660.

Munyikwa, K., Brown, S., and Kitabwalla, Z., 2012, Delineating stratigraphic breaks at the bases of postglacial eolian dunes in central Alberta, Canada using a portable OSL reader: Earth Surface Processes and Landforms, v. 37, p. 1603–1614.

Murray, A. S., and Wintle, A. G., 2000, Luminescence dating of quartz using an improved single-aliquot regenerative-dose protocol: Radiation Measurements, v. 32, no. 1, p. 57–73.

Neil, D., and Fogarty, P., 1991, Land use and sediment yield on the southern Tablelands of New South Wales: Australian Journal of Soil and Water Conservation, v. 4, no. 2, p. 33–39.

Nichols, K. K., Bierman, P. R., and Rood, D. H., 2014, ^{10}Be constrains the sediment sources and sediment yields to the Great Barrier Reef from the tropical Barron River catchment, Queensland, Australia: Geomorphology, v. 224, p. 102–110.

Nishiizumi, K., Kohl, C. P., Arnold, J. R., Klein, J., Fink, D., and Middleton, R., 1991, Cosmic ray produced ^{10}Be and ^{26}Al in Antarctic rocks: Exposure and erosion history: Earth and Planetary Science Letters, v. 104, no. 2–4, p. 440–454.

Nishiizumi, K., Lal, D., Klein, J., Middleton, R., and Arnold, J. R., 1986, Production of ^{10}Be and ^{26}Al by cosmic rays in terrestrial quartz *in situ* and implications for erosion rates: Nature, v. 319, p. 134–136.

Noske, P. J., Lane, P. N. J., and Sheridan, G. J., 2010, Stream exports of coarse matter and phosphorus following wildfire in NE Victoria, Australia: Hydrological Processes, v. 24, p. 1514–1529.

Nyman, P., Sheridan, G. J., Smith, H. G., and Lane, P. N. J., 2011, Evidence of debris flow occurrence after wildfire in upland catchments of south-east Australia: Geomorphology, v. 125, p. 383–401.

Nyssen, J., Poesen, J., Moeyersons, J., Deckers, J., Haile, M., and Lang, A., 2004, Human impact on the environment in the Ethiopian and Eritrean highlands - a state of the art: Earth-Science Reviews, v. 64, p. 273–320.

O'Donnell, J., Fryirs, K., and Leishman, M. R., 2014, Digging deep for diversity: Riparian seed bank abundance and species richness in relation to burial depth: Freshwater Biology, v. 59, no. 1, p. 100–113.

Olley, J., Caitcheon, G., and Murray, A., 1998, The distribution of apparent dose as determined by Optically Stimulated Luminescence in small aliquots of fluvial quartz: Implications for dating young sediments: Quaternary Geochronology, v. 17, no. 11, p. 1033–1040.

Olley, J. M., Murray, A. S., Mackenzie, D. H., and Edwards, K., 1993, Identifying sediment sources in a gullied catchment using natural and anthropogenic radioactivity: Water Resources Research, v. 29, no. 4, p. 1037–1043.

Olley, J. M., Pietsch, T., and Roberts, R. G., 2004, Optical dating of Holocene sediments from a variety of geomorphic settings using single grains of quartz: Geomorphology, v. 60, no. 3–4, p. 337–358.

Olley, J. M., Roberts, R. G., Yoshida, H., and Bowler, J. M., 2006, Single-grain optical dating of grave-infill associated with human burials at Lake Mungo, Australia: Quaternary Science Reviews, v. 25, no. 19–20, p. 2469–2474.

Olley, J. M., and Wasson, R. J., 2003, Changes in the flux of sediment in the Upper Murrumbidgee catchment, Southeastern Australia, since European settlement: Hydrological Processes, v. 17, no. 16, p. 3307–3320.

Oxley, J., 1820, Journals of Two Expeditions into the Interior of New South Wales, London, John Murray, Albemarle-Street, 408 p.:

Page, K. J., and Carden, Y. R., 1998, Channel adjustment following the crossing of a threshold: Tarcutta Creek, southeastern Australia: Australian Geographical Studies, v. 36, no. 3, p. 289–311.

Pain, C., Gregory, L., Wilson, P., and McKenzie, N., 2011, The Physiographic Regions of Australia: Australian Collaborative Land Evaluation Program and National Committee on Soil and Terrain.

Passmore, D. G., and Macklin, M. G., 1994, Provenance of fine-grained alluvium and late Holocene land-use change in the Tyne basin, northern England: Geomorphology, v. 9, no. 2, p. 127–142.

Patterson, C., Tilton, G., and Inghram, M., 1955, Age of the Earth: Science, v. 121, no. 3134, p. 69–75.

Patton, P. C., and Schumm, S. A., 1975, Gully erosion, northwestern Colorado: A threshold phenomenon: Geology, v. 3, no. 2, p. 88–90.

Pauketat, T. R., 1998, Refiguring the Archaeology of Greater Cahokia: Journal of Archaeological Research, v. 6, no. 1, p. 45–89.

Peel, M. C., Finlayson, B. L., and McMahon, T. A., 2007, Updated world map of the Köppen-Geiger climate classification: Hydrology and Earth System Science, v. 4, p. 439–473.

Pemberton, M., 1988, Soil erosion between Birchs Inlet and Eliott Bay, southwestern Tasmania: Papers and Proceedings of the Royal Society of Tasmania, v. 122, no. 2, p. 109–114.

Pickard, J., 1994, Post-European changes in creeks of semi-arid rangelands, "Polpah Station", New South Wales, *in* Millington, A. C., and Pye, K., eds., Environmental Change in Drylands: Biogeographical and Geomorphological Perspectives: London, John Wiley & Sons, p. 271–283.

Pickard, J., 2007, The transition from shepherding to fencing in colonial Australia: Rural History, v. 18, no. 2, p. 143–162.

Pickard, J., 2010, Wire fences in colonial Australia: Technology transfer and adaptation, 1842-1900: Rural History, v. 21, no. 1, p. 27–58.

Pietsch, T., Olley, J. M., and Nanson, G. C., 2008, Fluvial transport as a natural luminescence sensitiser of quartz: Quaternary Geochronology, v. 3, no. 4, p. 365–376.

Pinter, N., Fiedel, S., and Keeley, J. E., 2011, Fire and vegetation shifts in the Americas at the vanguard of Paleoindian migration: Quaternary Science Reviews, v. 30, no. 3–4, p. 269–272.

Poesen, J., Nachtergaele, J., Verstraeten, G., and Valentin, C., 2003, Gully erosion and environmental change: importance and research needs: Catena, v. 50, p. 91–133.

Poesen, J., Vandekerckhove, L., Nachtergaele, J., Oostwoud Wijdenes, D., Verstraeten, G., and van Wesemael, B., 2002, Gully Erosion in Dryland Environments, *in* Bull, L. J., and Kirkby, M. J., eds., Dryland Rivers: Hydrology and Geomorphology of Semi-arid Channels: West Sussex, England, John Wiley & Sons, Ltd., p. 231–262.

Poolton, N. R. J., Bøtter-Jensen, L., Wintle, A. G., Jakobsen, J., Jørgensen, F., and Knudsen, K. L., 1994, A portable system for the measurement of sediment OSL in the field: Radiation Measurements, v. 23, no. 2/3, p. 529–532.

Pope, K. O., and van Andel, T. H., 1984, Late Quaternary alluviation and soil formation in the southern Argolid: Its history, causes and archaeological implications: Journal of Archaeological Science, v. 11, no. 4, p. 281–306.

Portenga, E. W., and Bierman, P. R., 2011, Understanding Earth's eroding surface with ^{10}Be: GSA Today, v. 21, no. 8, p. 4–10.

Portenga, E. W., Bierman, P. R., Duncan, C., Corbett, L. B., Kehrwald, N. M., and Rood, D. H., 2015, Erosion rates of the Bhutanese Himalaya determined using in situ-produced ^{10}Be: Geomorphology, v. 233, p. 112–126.

Prescott, J. R., and Hutton, J. T., 1988, Cosmic ray and gamma ray dosimetry for TL and ESR: Nuclear Tracks and Radiation Measurements, v. 14, p. 223–227.

Prescott, J. R., 1994, Cosmic ray contributions to dose rates for luminescence and ESR dating: Large depths and long-term time variations: Radiation Measurements, v. 23, no. 2/3, p. 497–500.

Price, G. J., and Webb, G. E., 2006, Late Pleistocene sedimentology, taphonomy and megafauna extinction on the Darling Downs, southeastern Queensland: Australian Journal of Earth Sciences, v. 53, no. 6, p. 947–970.

Prosser, I. P., 1990, Fire, humans, and denudation at Wangrah Creek, southern Tablelands, N.S.W.: Australian Geographical Studies, v. 28, no. 1, p. 77–95.

Prosser, I. P., 1991, A comparison of past and present episodes of gully erosion at Wangrah Creek, southern Tablelands, New South Wales: Australian Geographical Studies, v. 29, no. 1, p. 139–154.

Prosser, I. P., and Abernethy, B., 1996, Predicting the topographic limits to a gully network using a digital terrain model and process thresholds: Water Resources Research, v. 32, no. 7, p. 2289–2298.

Prosser, I. P., Chappell, J., and Gillespie, R., 1994, Holocene valley aggradation and gully erosion in headwater catchments, south-eastern highlands of Australia: Earth Surface Processes and Landforms, v. 19, no. 5, p. 465–480.

Prosser, I. P., Dietrich, W. E., and Stevenson, J., 1995, Flow resistance and sediment transport by concentrated overland flow in a grassland valley: Geomorphology, v. 13, p. 71–86.

Prosser, I. P., and Slade, C. J., 1994, Gully formation and the role of valley-floor vegetation, southeastern Australia: Geology, v. 22, no. 12, p. 1127–1130.

Prosser, I. P., and Soufi, M., 1998, Controls on gully formation following forest clearing in a humid temperate environment: Water Resources Research, v. 34, no. 12, p. 3661–3671.

Prosser, I. P., and Williams, L., 1998, The effect of wildfire on runoff and erosion in native *Eucalyptus* forest: Hydrological Processes, v. 12, p. 251–265.

Prosser, I. P., and Winchester, S. J., 1996, History and processes of gully initiation and development in eastern Australia: Zeitschrift für Geomorphologie, v. Supplementband 105, p. 91–109.

Reed, N. A., Bennett, J. W., and Porter, J. W., 1968, Solid core drilling of Monks Mound: Technique and findings: American Antiquity, v. 33, no. 2, p. 137–148.

Reeves, B. O. K., 1978, Head-Smashed-In: 5500 years of bison jumping in the Alberta Plains: Plains Anthropologist, v. 23, no. 82, p. 151–174.

Reimer, P. J., Baille, M. G. L., Bard, E., Bayliss, A., Beck, J. W., Bertrand, C. J. H., Blackwell, P. G., Buck, C. E., Burr, G. S., Cutler, K. B., Damon, P. E., Edwards, R. L., Fairbanks, R. G., Friedrich, M., Guilderson, T. P., Hogg, A. G., Hughen, K. A., Kromer, B., McCormac, G., Manning, S., Ramsey, C. B., Reimer, R. W., Remmele,

S., Southon, J. R., Stuiver, M., Talamo, S., Taylor, F. W., van der Plicht, J., and Weyhenmeyer, C. E., 2004, IntCal04 terrestrial radiocarbon age calibration, 0-26 cal kyr BP: Radiocarbon, v. 46, no. 3, p. 1029–1058.

Reimer, P. J., Bard, E., Bayliss, A., Beck, J. W., Blackwell, P. G., Ramsey, C. B., Buck, C. E., Cheng, H., Edwards, R. L., Friedrich, M., Grootes, P. M., Guilderson, T. P., Haflidason, H., Hajdas, I., Hatté, C., Heaton, T. J., Hoffmann, D. L., Hogg, A. G., Hughen, K. A., Kaiser, K. F., Kromer, B., Manning, S. W., Niu, M., Reimer, R. W., Richards, D. A., Scott, E. M., Southon, J. R., Staff, R. A., Turney, C. S. M., and van der Plicht, J., 2013, INTCAL13 and MARINE13 radiocarbon age calibration curves 0-50,000 years cal BP: Radiocarbon, v. 55, no. 4, p. 1869–1887.

Reusser, L., Bierman, P., and Rood, D., 2015, Quantifying human impacts on rates of erosion and sediment transport at a landscape scale: Geology, v. 43, no. 2, p. 171–174.

Reusser, L., Graly, J., Bierman, P., and Rood, D., 2010, Calibrating a long-term meteoric ^{10}Be accumulation rate in soil: Geophysical Research Letters, v. 37, no. 19, p. L19403.

Reusser, L. J., and Bierman, P. R., 2010, Using meteoric ^{10}Be to track fluvial sand through the Waipaoa River basin, New Zealand: Geology, v. 38, no. 1, p. 47–50.

Richardson, J. M., Fuller, I. C., Holt, K. A., Litchfield, N. J., and Macklin, M. G., 2014, Rapid post-settlement floodplain accumulation in Northland, New Zealand: Catena, v. 113, p. 292–305.

Richardson, J. M., Fuller, I. C., Macklin, M. G., Jones, A. F., Holt, K. A., Litchfield, N. J., and Bebbington, M., 2013, Holocene river behaviour in New Zealand: response to regional centennial-scale climate forcing: Quaternary Science Reviews, v. 60, p. 8–27.

Ritchie, J. C., and McHenry, J. R., 1990, Application of radioactive fallout cesium-137 for measuring soil erosion and sediment accumulation rates and patterns: A review: Journal of Environmental Quality, v. 19, no. 2, p. 215–233.

Roberts, H. M., 2008, The development and application of luminescence dating to loess deposits: a perspective on the past, present, and future: Boreas, v. 37, no. 4, p. 483–507.

Roberts, R. G., Flannery, T. F., Ayliffe, L. K., Yoshida, H., Olley, J. M., Prideaux, G. J., Laslett, G. M., Baynes, A., Smith, M. A., Jones, R., and Smith, B. L., 2001, New ages for the last Australian megafauna: Continent-wide extinction about 46,000 years ago: Science, v. 292, p. 1888–1892.

Roberts, R. G., Jones, R., and Smith, M. A., 1990, Thermoluminescence dating of a 50,000-year-old human occupation site in northern Australia: Nature, v. 345, p. 153–156.

Roberts, R. G., Jones, R., Spooner, N. A., Head, M. J., Murray, A. S., and Smith, M. A., 1994, The human colonisation of Australia: Optical dates of 53,000 and 60,000 years bracket human arrival at Deaf Adder Gorge, Northern Territory: Quaternary Geochronology (Quaternary Science Reviews), v. 13, p. 575–583.

Roberts, R. G., Morwood, M. J., and Westaway, K. E., 2005, Illuminating southeast Asian prehistory: new archaeological and paleoanthropological frontiers for luminescence dating: Asian Perspectives, v. 44, no. 2, p. 293–319.

Rolett, B., and Diamond, J., 2004, Environmental predictors of pre-European deforestation on Pacific islands: Nature, v. 431, p. 443–446.

Rommens, T., Verstraeten, G., Lang, A., Poesen, J., Govers, G., Van Rompaey, A., and Peeters, I., 2005, Soil erosion and sediment deposition in the Belgian loess belt during the Holocene: establishing a sediment budget for a small agricultural catchment: The Holocene, v. 15, no. 7, p. 1032-1043.

Rosen, A. M., 2008, The impact of environmental change and human land use on the alluvial valleys in the Loess Plateau of China during the Middle Holocene: Geomorphology, v. 101, no. 1–2, p. 298–307.

Rowe, R. K., 1994, The influence of Quaternary aridity on soils of non-arid regions: A case-study of soils in the Tallangatta area of southeastern Australia [PhD: Monash University, 238 p.

Ruddiman, W. F., 2003, The Anthropocene greenhouse era began thousands of years ago: Climatic Change, v. 61, no. 3, p. 261–293.

Rule, S., Brook, B. W., Haberle, S. G., Turney, C. S. M., Kershaw, A. P., and Johnson, C. N., 2012, The aftermath of megafaunal extinction: Ecosystem transformation in Pleistocene Australia: Science, v. 335, p. 1483–1487.

Rustomji, P., and Pietsch, T., 2007, Alluvial sedimentation rates from southeastern Australia indicate post-European settlement landscape recovery: Geomorphology, v. 90, no. 1–2, p. 73–90.

Sanderson, D. C. W., Bishop, P., Stark, M. T., and Spencer, J. Q., 2003, Luminescence dating of anthropogenically reset canal sediments from Angkor Borei, Mekong Delta, Cambodia: Quaternary Science Reviews, v. 22, p. 1111–1121.

Sanderson, D. C. W., and Murphy, S., 2010, Using simple portable OSL measurements and laboratory characterisation to help understand complex and heterogeneous sediment sequences for luminescence dating: Quaternary Geochronology, v. 5, no. 2-3, p. 299–305.

Sandgren, P., and Fredskild, B., 2008, Magnetic measurements recording Late Holocene man-induced erosion in S. Greenland: Boreas, v. 20, no. 4, p. 315–331.

Sandiford, M., 2003, Neotectonics of southeastern Australia: Linking the Quaternary faulting record with seismicity and *in situ* stress: Geological Society of Australia Special Publication, v. 22, p. 101–113.

Schumm, S. A., 1979, Geomorphic thresholds: The concept and its applications: Transactions of the Institute of British Geographers, v. 4, no. 4, p. 485–515.

Scott, A., 2001, Water erosion in the Murray-Darling Basin: Learning from the past: CSIRO Land & Water, 43/01.

Shaw, J. M., 2003, Climate change and deforestation: Implications for the Maya collapse: Ancient Mesoamerica, v. 14, no. 1, p. 157–167.

Sheridan, G. J., Lane, P. N. J., and Noske, P. J., 2007, Quantification of hillslope runoff and erosion processes before and after wildfire in a wet *Eucalyptus* forest: Journal of Hydrology, v. 343, p. 12–28.

Smith, B. D., 1997, The initial domestication of *Cucurbita pepo* in the Americas 10,000 years ago: Science, v. 276, no. 5314, p. 932–934.

Smith, H. G., Sheridan, G. J., Lane, P. N. J., Noske, P. J., and Heijnis, H., 2011, Changes to sediment sources following wildfire in a forested upland catchment, southeastern Australia: Hydrological Processes, v. 25, p. 2878–2889.

Sokal, R. R., Oden, N. L., and Wilson, C., 1991, Genetic evidence for the spread of agriculture in Europe by demic diffusion: Nature, v. 351, p. 143–145.

Stafford, C. R., and Creasman, S. D., 2002, The hidden record: Late Holocene landscapes and settlement archaeology in the lower Ohio River valley: Geoarchaeology, v. 17, no. 2, p. 117–140.

Stankoviansky, M., 2003, Historical evolution of permanent gullies in the Myjava Hill Land, Slovakia: Catena, v. 51, p. 223–239.

Starkel, L., Soja, R., and Michczyńskad, D. J., 2006, Past hydrological events reflected in Holocene history of Polish rivers: Catena, v. 66, no. 1–2, p. 24–33.

Starr, B., 1989, Anecdotal and relic evidence of the history of gully erosion and sediment movement in the Michelago Creek catchment area, NSW: Australian Journal of Soil and Water Conservation, v. 2, no. 3, p. 26–31.

Stinchcomb, G. E., Messner, T. C., Driese, S. G., Nordt, L. C., and Stewart, R. M., 2011, Pre-colonial (A.D. 1100-1600) sedimentation related to prehistoric maize agriculture and climate change in eastern North America: Geology, v. 39, no. 4, p. 363–366.

Stockton, E. D., and Holland, W., 1974, Cultural sites and their environment in the Blue Mountains: Archaeology & Physical Anthropology in Oceania, v. 9, no. 1, p. 36–65.

Stone, J., 1998, A rapid fusion method for separation of beryllium-10 from soils and silicates: Geochimica et Cosmochimica Acta, v. 62, no. 3, p. 555–561.

Stone, J. O., 2000, Air pressure and cosmogenic isotope production: Journal of Geophysical Research, v. 105, no. B10, p. 23,753–723,759.

Stuart, A. J., Kosinktev, P. A., Higham, T. F. G., and Lister, A. M., 2004, Pleistocene to Holocene extincion dynamcs in giant deerand wooly mammoth: Nature, v. 431, p. 684–689.

Stuiver, M., and Reimer, P. J., 1993, Extended ^{14}C data base and revised CALIB 3.0 ^{14}C age calibration program: Radiocarbon, v. 35, no. 1, p. 215–230.

Suppiah, R., and Hennessy, K. J., 1998, Trends in total rainfall, heavy rain events and number of dry days in Australia, 1910-1990: International Journal of Climatology, v. 10, p. 1141–1164.

Tans, P. P., De Jong, A. F. M., and Mook, W. G., 1979, Natural atmospheric ^{14}C variation and the Suess effect: Nature, v. 280, no. 5725, p. 826–828.

Thorndycraft, V. R., and Benito, G., 2006a, The Holocene fluvial chronology of Spain: evidence from a newly compiled radiocarbon database: Quaternary Science Reviews, v. 25, no. 3–4, p. 223–234.

Thorndycraft, V. R., and Benito, G., 2006b, Late Holocene fluvial chronology of Spain: The role of climatic variability and human impact: Catena, v. 66, no. 1–2, p. 34–41.

Tomkins, K. M., Humphreys, G. S., Wilkinson, M. T., Fink, D., Hesse, P. P., Doerr, S. H., Shakesby, R. A., Wallbrink, P. J., and Blake, W. H., 2006, Contemporary versus long-term denudation along a passive margin: the role of extreme events: Earth Surface Processes and Landforms, v. 32, p. 1013–1031.

Toy, T. J., Foster, G. R., and Renard, K. G., 2002, Soil Erosion: Processes, Prediction, Measurement, and Control, New York, John Wiley & Sons, Inc.

Trimble, S. W., 1983, A sediment budget for Coon Creek basin in the Driftless Area, Wisconsin, 1853-1977: American Journal of Science, v. 283, p. 454–474.

Trimble, S. W., and Mendel, A. C., 1995, The cow as a geomorphic agent – A critical review: Geomorphology, v. 13, p. 233–253.

Turkelboom, F., Poesen, J., and Trébuil, G., 2008, The multiple land degradation effects caused by land-use intensification in tropical steeplands: A catchment study from northern Thailand: Catena, v. 75, p. 102–116.

Turney, C. S. M., Bird, M. I., Fifield, L. K., Roberts, R. G., Smith, M., Dortch, C. E., Grün, R., Lawson, E., Ayliffe, L. K., Miller, G. H., Dortch, J., and Cresswell, R. G., 2001, Early human occupation at Devil's Lair, southwestern Australia 50,000 years ago: Quaternary Research, v. 55, no. 1, p. 3–13.

Valentin, C., Poesen, J., and Li, Y., 2005, Gully erosion: Impacts, factors and control: Catena, v. 63, p. 132–153.

Valette-Silver, J. N., Brown, L., Pavich, M., Klein, J., and Middleton, R., 1986, Detection of erosion events using ^{10}Be profiles: example of the impact of agriculture on soil erosion in the Chesapeake Bay area (U.S.A.): Earth and Planetary Science Letters, v. 80, no. 1–2, p. 82–90.

van Geen, A., Valette-Silver, N. J., Luoma, S. N., Fuller, C. C., Baskaran, M., Tera, F., and Klein, J., 1999, Constraints on the sedimentation history of San Francisco Bay from ^{14}C and ^{10}Be: Marine Chemistry, v. 64, no. 1–2, p. 28–38.

Vanacker, V., von Blanckenburg, F., Govers, G., Molina, A., Poesen, J., Deckers, J., and Kubik, P., 2007, Restoring dense vegetation can slow mountain erosion to near natural benchmark levels: Geology, v. 35, no. 4, p. 303–306.

Vandaele, K., Poesen, J., Govers, G., and van Wesemael, B., 1996, Geomorphic threshold conditions for ephemeral gully incision: Geomorphology, v. 16, p. 161–173.

Veevers, J. J., 2006, Updated Gondwana (Permian-Cretaceous) earth history of Australia: Gondwana Research, v. 9, p. 231–260.

Vekua, A., Lordkipanidze, D., Rightmire, G. P., Agusti, J., Ferring, R., Maisuradze, G., Mouskhelishvili, A., Nioradze, M., Ponce de Leon, M., Tappen, M., Tvalchrelidze, M., and Zollikofer, C., 2002, A new skull of early *Homo* from Dmanisi, Georgia: Science, v. 297, no. 5578, p. 85–89.

Visconti, G., 2014, Anthropocene: Another academic invention?: Rendiconti Lincei, v. 25, no. 3, p. 381–392.

Voarintsoa, N. R. G., Cox, R., Razanatseheno, M. O. M., and Rakotondrazafy, A. F. M., 2012, Relation between bedrock geology, topography and lavaka distribution in Madagascar: South African Journal of Geology, v. 115, no. 2, p. 225–250.

Wallbrink, P. J., 2004, Quantifying the erosion processes and land-uses which dominate fine sediment supply to Moreton Bay, Southeast Queensland, Australia: Journal of Environmental Radioactivity, v. 76, no. 1–2, p. 67–80.

Walter, R. C., and Merritts, D. J., 2008, Natural Streams and the Legacy of Water-Powered Mills: Science, v. 319, no. 5861, p. 299–304.

Warner, R. F., 1984, Man's impacts on Australian drainage systems: Australian Geographer, v. 16, no. 2, p. 133–141.

Warren, B. E., 1969, X-Ray Diffraction, Reading, Massachusetts, Courier Dover Publications.

Warren, S. D., Thurow, T. L., Blackburn, W. H., and Garza, N. E., 1986, The influence of livestock trampling under intensive rotation grazing on soil hydrologic characteristics: Journal of Range Management, v. 39, no. 6, p. 491–495.

Wasson, R. J., Annual and decadal variation of sediment yield in Australia, and some global comparisons, *in* Proceedings Canberra Symposium, Canberra, 1994, Volume no. 224, IAHS, p. 269–279.

Wasson, R. J., Mazari, R. K., Starr, B., and Clifton, G., 1998, The recent history of erosion and sedimentation on the Southern Tablelands of southeastern Australia: sediment flux dominated by channel incision: Geomorphology, v. 24, no. 4, p. 291–308.

Waters, M. R., 1988, Holocene alluvial geology and geoarchaeology of the San Xavier reach of the Santa Cruz River, Arizona: Geological Society of America Bulletin, v. 100, no. 4, p. 479–491.

Waters, M. R., Forman, S. L., Jennings, T. A., Nordt, L. C., Driese, S. G., Feinberg, J. M., Keene, J. L., Halligan, J., Lindquist, A., Pierson, J., Hallmark, C. T., Collins, M. B., and Wiederhold, J. E., 2011a, The Buttermilk Creek Complex and the origins of Clovis at the Debra L. Friedkin Site, Texas: Science, v. 331, no. 6024, p. 1599–1603.

Waters, M. R., Stafford Jr., T. W., McDonald, H. G., Gustafson, C., Rasmussen, M., Cappellini, E., Olsen, J. V., Szklarczyk, D., Jensen, L. J., Gilbert, M. T. P., and Willerslev, E., 2011b, Pre-Clovis mastodon hunting 13,800 years ago at the Manis Site, Washington: Science, v. 334, no. 6054, p. 351–353.

Weissel, J. K., and Hayes, D. E., 1978, Magnetic Anomalies in the Southeast Indian Ocean, *in* Hayes, D. E., ed., Antarctica Oceanology II: The Australian-New Zealand Sector: Washington, D. C., American Geophysical Union, p. 165–196.

Wentworth, C. K., 1922, A scale of grade and class terms for clastic sediments: The Journal of Geology, v. 30, no. 5, p. 377–392.

Wentworth, W. C., 1813, Journal of an Expedition Across the Blue Mountains, 11 May-6 June 1813, Volume Safe 1/22a, State Library of New South Wales, p. 14.

Whitford, J. A., Newham, L. T. H., Vigiak, O., Melland, A. R., and Roberts, A. M., 2010, Rapid assessment of gully sidewall erosion rates in data-poor catchments: A case study in Australia: Geomorphology, v. 118, p. 330–338.

Wilkinson, B. H., and McElroy, B. J., 2007, The impact of humans on continental erosion and sedimentation: Geological Society of America Bulletin, v. 119, no. 1–2, p. 140–156.

Wilkinson, M. T., and Humphreys, G. S., 2005, Exploring pedogenesis via nuclide-based soil production rates and OSL-based bioturbation rates: Australian Journal of Soil Research, v. 43, no. 6, p. 767–779.

Wilkinson, S. N., Wallbrink, P. J., Hancock, G. J., Blake, W. H., Shakesby, R. A., and Doerr, S. H., 2009, Fallout radionuclide tracers identify a switch in sediment sources and transport-limited sediment yield following wildfire in a eucalypt forest: Geomorphology, v. 110, p. 140–151.

Willenbring, J. K., and von Blanckenburg, F., 2010, Meteoric cosmogenic Beryllium-10 adsorbed to river sediment and soil: Applications for Earth-surface dynamics: Earth-Science Reviews, v. 98, no. 1–2, p. 105–122.

Williams, M., Cook, E., van der Kaars, S., Barrows, T., Shulmeister, J., and Kershaw, P., 2009, Glacial and deglacial climatic patterns in Australia and sourrounding regions from 35 000 to 10 000 years ago reconstructed from terrestrial and near-shore proxy data: Quaternary Science Reviews, v. 28, no. 23–24, p. 2398–2419.

Wills, W. H., Drake, B. L., and Dorshow, W. B., 2014, Prehistoric deforestation at Chaco Canyon?: Proceedings of the National Academy of Sciences, v. 111, no. 32, p. 11584–11591.

Wintle, A. G., 1973, Anomalous fading of thermo-luminescence in mineral samples: Nature, v. 245, p. 143–144.

Wintle, A. G., 2008a, Fifty years of luminescence dating: Archaeometry, v. 50, no. 2, p. 276–312.

Wintle, A. G., 2008b, Luminescence dating: where it has been and where it is going: Boreas, v. 37, no. 4, p. 471–482.

Woodward, C., Chang, J., Zawadzki, A., Shulmeister, J., Haworth, R., Collecutt, S., and Jacobsen, G., 2011, Evidence against early nineteenth century major European induced environmental impacts by illegal settlers in the New England Tablelands, south eastern Australia: Quaternary Science Reviews, v. 30, no. 27–28, p. 3743–3747.

Wroe, S., and Field, J., 2006, A review of the evidence for a human role in the extinction of Australian megafauna and an alternative interpretation: Quaternary Science Reviews, v. 25, no. 21–22, p. 2692–2703.

Wroe, S., Field, J., Fullagar, R., and Jermin, L. S., 2004, Megafaunal extinction in the Late Quaternary and the global overkill hypothesis: Alcheringa: An Australiasian Journal of Palaeontology, v. 28, no. 1, p. 291–331.

Wroe, S., Field, J. H., Archer, M., Grayson, D. K., Price, G. J., Louys, J., Faith, J. T., Webb, G. E., Davidson, I., and Mooney, S. D., 2013, Climate change frames debate over the extinction of megafauna in Sahul (Pleistocene Australia-New Guinea): Proceedings of the National Academy of Sciences, v. 110, no. 22, p. 8777–8781.

Wyshnytzky, C. E., Ouimet, W. B., McCarthy, J., Dethier, D. P., Shroba, R. R., Bierman, P. R., and Rood, D. H., 2015, Meteoric ^{10}Be, clay, and extractable iron depth profiles in the Colorado Front Range: Implications for understanding soil mixing and erosion: Catena, v. 127, p. 32–45.

Xu, S., Dougans, A. B., Freemn, S. P. H. T., Schnabel, C., and Wilcken, K. M., 2010, Improved ^{10}Be and ^{26}Al-AMS with a 5 MV spectrometer: Nuclear Instruments and Methods in Physics Research B: Beam Interactions with Materials and Atoms, v. 268, no. 7–8, p. 736–738.

Yan, B., Tomer, M. D., and James, D. E., 1988, Historical channel movement and sediment accretion along the South Fork of the Iowa River: Journal of Soil and Water Conservation, v. 65, no. 1, p. 1–8.

Yen, D. E., 1995, The development of Sahul agriculture with Australia as a bystander: Antiquity, v. 69, no. 265, p. 831–847.

Young, R., and McDougall, I., 1993, Long-term landscape evolution: Early Miocene and modern rivers in southern New South Wales, Australia: The Journal of Geology, v. 101, p. 35–49.

Zalasiewicz, J., Waters, C. N., Williams, M., Barnosky, A. D., Cearreta, A., Crutzen, P., Ellis, E., Ellis, M. A., Fairchild, I. J., Grinevald, J., Haff, P. K., Hajdas, I., Leinfelder, R., McNeill, J., Odada, E. O., Poirier, C., Richter, D., Steffen, W., Summerhayes, C., Syvitski, J. P. M., Vidas, D., Wagreich, M., Wing, S. L., Wolfe, A. P., An, Z., and Oreskes, N., 2015, When did the Anthropocene begin? A mid-twentieth century boundary level is stratigraphically optimal: Quaternary International, v. In Press.

Zalasiewicz, J., Williams, M., Fortey, R., Smith, A., Barry, T. L., Coe, A. L., Bown, P. R., Rawson, P. F., Gale, A., Gibbard, P., Gregory, F. J., Hounslow, M. W., Kerr, A. C., Pearson, P., Knox, R., Powell, J., Waters, C., Marshall, J., Oates, M., and Stone, P., 2011, Stratigraphy of the Anthropocene: Philosophical Transactions of the Royal Society A, v. 373, no. 2035, p. 1036–1055.

Zalasiewicz, J., Williams, M., Smith, A., Barry, T. L., Coe, A. L., Brown, P. R., Brenchley, P., Cantrill, D., Gale, A., Gibbard, P., Gregory, F. J., Hounslow, M. W., Kerr, A. C., Pearson, P., Knox, R., Powell, J., Waters, C., Marshall, J., Oates, M., Rawson, P., and Stone, P., 2008, Are we now living in the Anthropocene?: GSA Today, v. 18, no. 2, p. 4–8.

Zhao, Z., 2010, New data and new issues for the study of origin of rice agriculture in China: Archaeological and Anthropological Sciences, v. 2, no. 2, p. 99–105.

Zhou, Z.-y., 2013, Agriculture in Australia, Beijing, China, China Agriculture Press.

Zierholz, C., Prosser, I. P., Fogarty, P. J., and Rustomji, P., 2001, In-stream wetlands and their significance for channel filling and the catchment sediment budget, Jugiong Creek, New South Wales: Geomorphology, v. 38, no. 3–4, p. 221–235.